AN X-RAY PREIONISED MERCURY BROMIDE DISCHARGE LASER

Andrew J.W. Brown

A Thesis Submitted for the Degree of PhD
at the
University of St Andrews

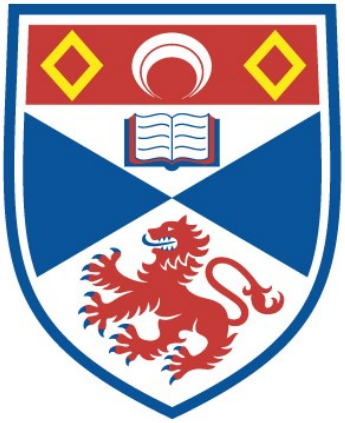

1988

AN X-RAY PREIONISED MERCURY BROMIDE DISCHARGE LASER

A thesis presented by

ANDREW J.W. BROWN, B.Sc., M.Sc.

to the

University of St. Andrews

in application for the degree of

Doctor of Philosophy

February 1988

ProQuest LLC.
789 East Eisenhower Parkway
P.O. Box 1346
Ann Arbor, MI 48106 – 1346

Th
A 76.8

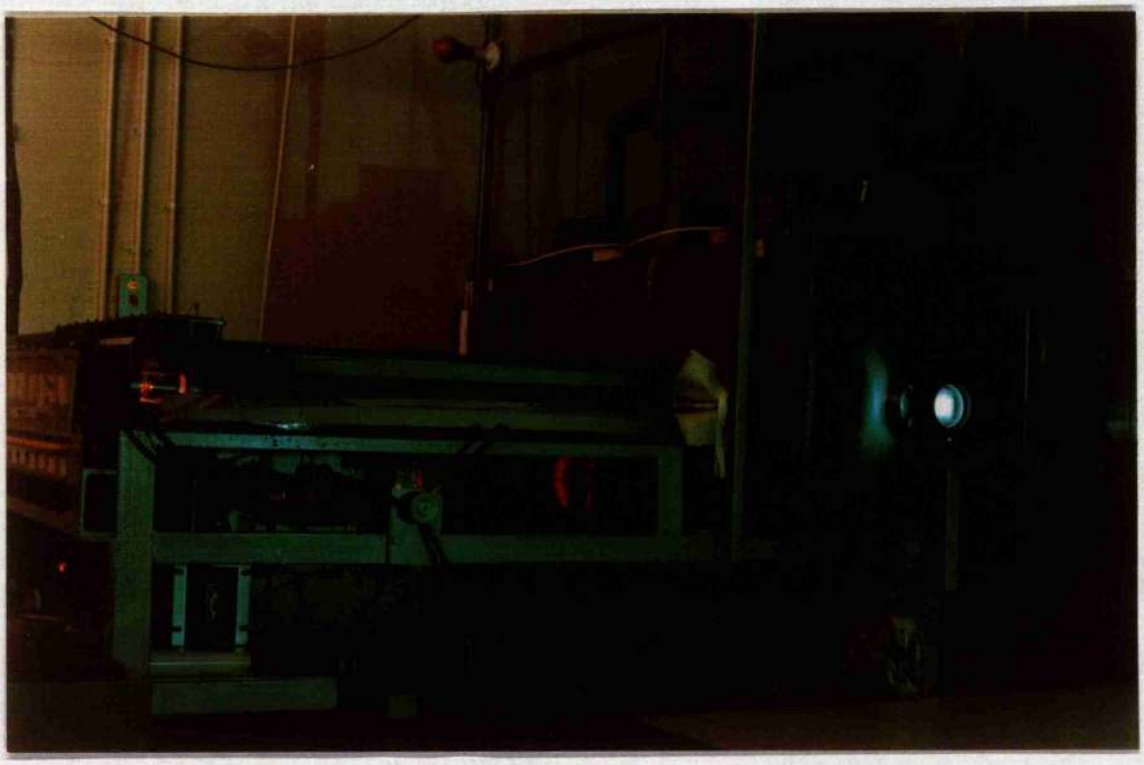

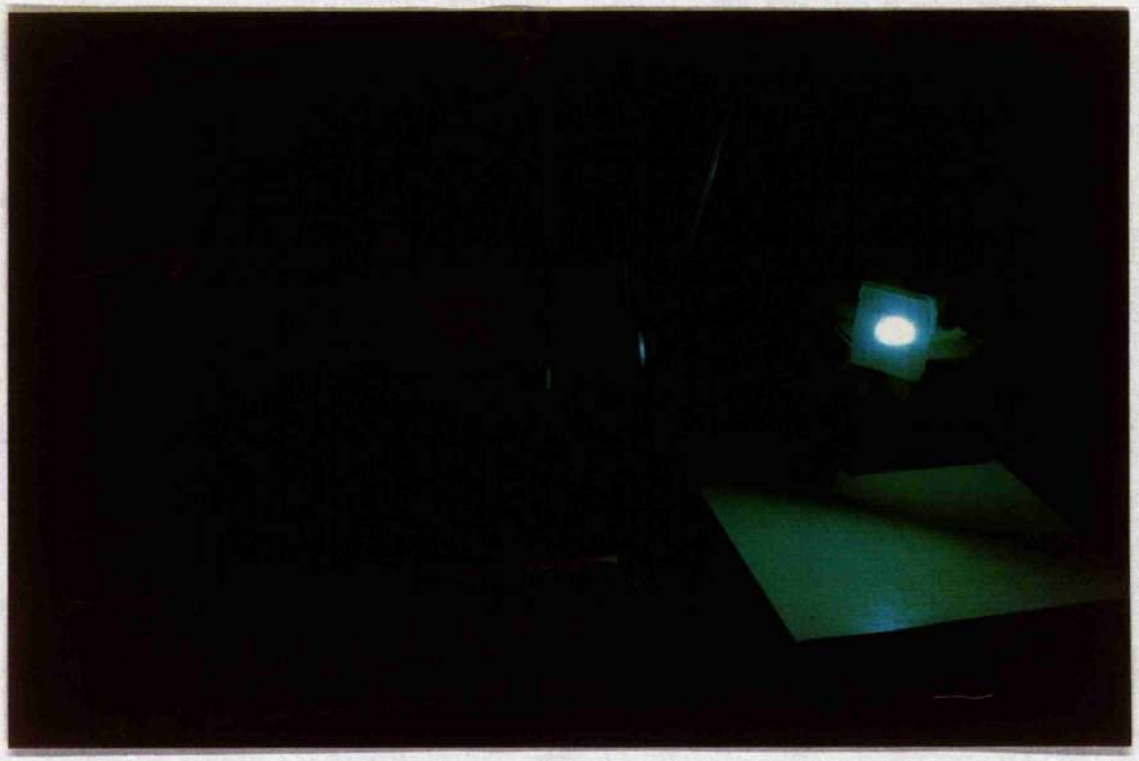

Photograph of the mercury bromide laser during operation and the resulting output beam.

DECLARATIONS

I ANDREW J.W. BROWN hereby certify that this thesis has been composed by myself, that it is a record of my own work, and that it has not been accepted in partial or complete fulfilment of any other degree of professional qualification.

I was admitted to the Faculty of Science of the University of St. Andrews under Ordinance General No. 12 on 1 October 1984 and as a candidate for the degree of Ph.D. on 1 October 1985.

Signed: .....

I hereby certify that the candidate has fulfilled the conditions of the Resolution and Regulations appropriate to the Degree of Ph.D.

Signature of Supervisor: ..... Date: 9th Feb 1988

COPYRIGHT

AUTHOR'S CAREER

The author was born in Fife, Scotland in 1961. He received his pre-university education at Methilhill Primary School and Buckhaven High School. He attended St. Andrews University and received a first class, Bachelor of Science, honours degree in Physics in 1983. In 1984 he was awarded the degree of Master of Science in Optoelectronic and Laser Devices with distinction from Heriot-Watt University. He returned to St. Andrews in October 1984 to begin research on the work described in this thesis, following the award of a Science and Engineering Research Council studentship in co-operation with the Royal Signals and Radar Establishment, Malvern.

ACKNOWLEDGEMENTS

Firstly, I would like to acknowledge the help and support of my supervisor, Dr. Paul Smith, during the last few years in St. Andrews. Without his considerable expertise in laser physics and enthusiasm for his subject the successful completion of this project would not have been possible. I must also acknowledge the Science and Engineering Research Council, EEV Ltd and the Royal and Signals Radar Establishment for financial support.

It gives me great pleasure to acknowledge the technical skills of the mechanical and electrical workshops in the Physics Department, especially Ron McCraw and Mike Robertson for their help throughout this project. Also to Myles, George, Jim, Bill, Lou, Ian, James and last, but by no means least, Derek who all worked on the laser.

I would like to thank the many friends I have made in St. Andrews for making the time here so memorable. Special thanks go to the other members of my group, Colin and Miles, for being 'the extra hand' on many occasions and for the numerous informative discussions I have had with them. Also to Ian and Graeme for their help and advice, Alistair and Rab for all the Guinness, Moire and Jeff for all those meals, Eileen for her exceptional kindness as a friend and to Janet - who is as much a part of this thesis as anyone. To all the others too numerous to mention - cheers!

I am also indebted to Karen Lumsden for deciphering my writing and expertly typing this thesis.

Finally, I must thank my family - who were always there.

DEDICATION

To my family

- without whose continual love, support and encouragement

I would not be who I am today

ABSTRACT

An X-ray preionised mercury bromide discharge laser (502-504 nm) has been designed, constructed and optimised. The double pulse forming line system built to drive the laser has proven to be both versatile and reliable. It utilises multiple-paralleled thyratrons and has demonstrated the characteristics required for long life operation of high average power gas discharge lasers. The supply produces a voltage pulse of 240 nsec duration and its output impedance is variable from 300 mΩ to 3.6 Ω. With twelve thyratrons in parallel current risetimes of 83 kA μsec^{-1} into a 300 mΩ matched load and 2 nsec jitter have been achieved. A voltage transient on the leading edge of the discharge pulse, to aid gas breakdown, up to $1^1/_2$ times the line charge voltage is possible through a 'spike line' incorporated in the system.

The X-ray preioniser, based on a cold cathode field emitter, produces an exposure of 5 mR in the discharge region which is adequate for effective preionisation of the laser. A full parametric study of the laser covering gas composition and pressure, X-ray source effects energy loading and other pulsed power supply effects has been carried out. The peak output energy recorded was 710 mJ with neon buffer gas at 4 atmospheres pressure. This represents an energy extraction of 0.5 JL^{-1}. Pulse lengths of 92 nsec (FWHM) and efficiencies greater than 1.5 % have been achieved.

CONTENTS

CHAPTER 1

INTRODUCTION

1.1 Introduction

In recent years there has been considerable interest in the development of lasers emitting in the blue-green region of the visible spectrum, between 450 nm and 550 nm where there exists a minimum in attenuation of electromagnetic radiation propagating in sea water (see fig 1.1). Applications of such lasers include laser depth sounding [1] to provide accurate mapping of coastal waters and military applications such as submarine communications [2], in which the laser , positioned either on a satellite or alternatively on land and aimed at a spaced based mirror, would be used to transmit signals over wide areas of the ocean. This enables submarines to remain submerged whilst receiving information, thus avoiding revealing their position. The optical receivers for such a communications system must be extremely sensitive with a wide field of view, fast response time and narrow bandwidth to discriminate between solar background noise and the weak signal some distance below the surface. Atomic vapour resonance filters based on caesium [3] and rubidium [4] have shown potential for this purpose and are the subject of a fuller discussion in chapter 6. The alternative to this optical communication system is the use of extremely low frequency (ELF) radiation where the wavelengths employed are typically several kilometres and consequently extremely large transmitting and receiving aerials must be used. Other possible uses for high power visible lasers include pumping of dye lasers and applications in medical physics and biophysics may transpire [5].

There are several laser systems capable of producing high energy outputs in the blue-green, among these are frequency conversion to 459 nm of the UV output from an XeCl laser (308 nm) by stimulated Raman scattering in lead vapour [6], frequency doubling the output from a Nd:YAG laser to 532 nm [1], lasing at ~490 nm in the broadband XeF C→A transition [7] and the mercury bromide laser [2]. In the latter approach blue-green emission at 502 nm - 504 nm is produced directly from the laser without the extra complications introduced by Raman shifting or frequency conversion which also reduce system efficiency.

The large bandwidth (~70 nm) and long upper state lifetime (~100 nsec) [8] of the XeF C→A transition result in a low cross section for stimulated emission, thus intense pumping is required to produce adequate gain and also the laser must be operated under conditions which suppress lasing on the stronger B→X transition. To date, although the XeF C→A laser has shown good promise in e-beam [8] and optically [9] pumped systems, the results achieved with discharge excited lasers have been fairly modest although future work with novel self injecting systems [10] may enhance this performance. Considerable progress has been made in the development of mercury bromide lasers since their discovery a decade ago [11] where they have shown promise for high energy, high efficiency and high repetition rate operation for lifetimes in excess of 5×10^8 shots [12].

In this thesis the design, construction and optimisation of an X-ray preionised mercury bromide discharge laser is discussed. The remainder of this first chapter introduces the spectroscopy and kinetics of this laser, followed by a discussion of the techniques used for pumping such a system. In the following chapters the design of the pulsed power supply developed for driving this laser, the flash X-ray preioniser and the laser cavity are discussed. Chapter 5 presents the results obtained with the laser and in the final chapter the possibilities for future work and further development are explored.

1.2 Spectroscopy and Kinetics

The spectroscopy of the mercury halides (HgX_2, X = Br, Cl, I) has recently achieved much attention following their recognition as candidates for efficient high power lasers operating in the visible part of the spectrum [13-17]. However, an extensive study over a period of some 30 years had previously been carried out by Wieland [18-20] of the emission produced from electric discharges in mercury halides. The emitted spectrum has been shown to arise from excited mercurous halides formed in the dissociation reaction.

$$HgX_2^* \rightarrow HgX^* + X$$

upon excitation of the parent triatomic mercuric halide* molecule. In particular the $B^2\Sigma^+_{1/2}$ $\rightarrow X^2\Sigma^+_{1/2}$ bands of the HgX^* are of great interest for laser studies.

Figure 1.2 shows the potential energy diagram for the lowest electronic states of mercurous bromide (HgBr) and indicates the laser transition, those for the chloride and iodide are similar but not discussed here. The ground state, $X^2\Sigma_{1/2}$, is bound as are the excited $B^2\Sigma^+_{1/2}$ and $C^2\Pi_{1/2}$ states as shown, whilst the $A^2\Pi_{1/2}$ and $A^2\Pi_{3/2}$ curves are dissociative. Laser emission occurs on vibrational-rotational transitions from the $B^2\Sigma^+_{1/2}$ excited state of the mercurous bromide radical to the $X^2\Sigma^+_{1/2}$ ground state. The large Frank-Condon shift between the minima of the B and X states, a consequence of their respective ionic and covalent nature [21], is such that the laser transition terminates on high lying vibrational levels of the X state. These are then rapidly de-excited by collisions with the buffer gas [22], typically neon or helium at several atmospheres pressure, preventing 'bottlenecking' of the lower laser level. The deactivated HgBr (X) molecule recombines with Bromine molecules in the fast (~10^{-5} seconds) bimolecular reaction [23].

$$HgBr\ (X) + Br_2 \rightarrow HgBr_2 + Br$$

to re-form the parent compound. Under carefully controlled conditions this reaction completely and rapidly regenerates the $HgBr_2$ molecules permitting long gas fill lifetimes and high repetition rate operation characteristic of these lasers. As discussed in chapter 4 this requires close attention to be given to the materials compatibility problems associated with these devices.

The B $\rightarrow$ X spontaneous emission spectrum in mercurous bromide extends over the range 450 nm - 515 nm and is dominated by two strong groups of lines near 502 nm and 504 nm. The structure of the spectrum has been analysed by several workers [14,15,20] and shown to consist of transitions in several $\upsilon' \rightarrow \upsilon''$ bands of the twelve isotopic molecules of significance found in 'natural' mercury bromide. The two observed lasing lines coincide with the strongest lines of the spontaneous emission and are attributed to the $\upsilon'=0 \rightarrow \upsilon''=22$ and $\upsilon'=0 \rightarrow \upsilon''= 23$ or $\upsilon'=3 \rightarrow \upsilon''= 26$ transitions [11], the higher intensity being observed at the shorter wavelength. Also observed spectroscopically is the $B^2\Sigma^+_{1/2} \rightarrow A^2\Pi_{1/2}$

transition [24] which shows a broad band spectrum characteristic of a bound to free transition centred around 685 nm and some 300 times weaker than the B→ X transition. However the $B^2\Sigma^+_{1/2} \rightarrow A^2\Pi_{3/2}$ transition which is predicted to occur ~125 nm to the blue of this transition peak has not been observed.

The mechanism by which the upper laser level HgBr ($B^2\Sigma^+_{1/2}$) is excited in a rare gas buffered electrical discharge was established by McGeoch et al. [25] as electron impact dissociation of the parent $HgBr_2$ molecule after a period of some controversy. This route was originally proposed by Schimitschek and Celto [26], however measured cross-sections [27] for the process

$$e^- + HgBr_2 \rightarrow HgBr\ (B) + Br + e^-$$

were very small and led to the conclusion that electron impact did not play a significant role in the population inversion in the active medium. This led to a number of alternative explanations including dissociative excitation of $HgBr_2$ by rare-gas metastables [28], dissociation following electron ion recombination of $HgBr_2^+$ [29] or dissociation following energy transfer from metastable atoms in the presence of N_2 and Xe [28,29,30]. Whilst the role of energy transfer from nitrogen and xenon metastable states (reviewed below) is still the subject of some discussion [30], the dominant upper laser level production mechanism in rare gas buffered discharges is currently believed to be by dissociative electron impact of $HgBr_2$. Other, less important processes, [72] such as electron ion recombination

$$e^- + HgBr_2^+ \rightarrow HgBr\ (B) + Br.$$

and dissociative attachment may also play a lesser role in HgBr(B) state formation.

A significant improvement in laser power and efficiency has been observed [32] in small scale mercury bromide discharge lasers upon the addition of nitrogen to the gas mixture, excited states of which have resonances within the manifold of bound $HgBr_2$ states as shown in figure 1.3. The typical fractional concentration of mercury bromide for optimum laser performance using electrical discharge excitation is in the 0.1-0.3% range.

This is achieved using operational temperatures of 150-180°C to produce the desired vapour pressure of the compound, as discussed in chapter 4, with neon or helium buffer gas at 1-5 atmospheres pressure. The addition of a few percent of nitrogen to such a mixture significantly alters the kinetic processes in the gas owing to the large N_2 to $HgBr_2$ fractional concentration and the electronic excitation threshold energy of nitrogen [33] which is comparable to that of mercury bromide [30,31] and much lower than that of neon [34]. The proposed kinetic process in discharges containing nitrogen for upper laser level production is that of excitation transfer from the N_2 ($A^3\Sigma_u^+$) state resulting in formation of the HgBr ($B^2\Sigma^+_{1/2}$) state. A similar energy transfer scheme involving the $^3P_2$ state of Xe [28] has not shown the improvements observed with nitrogen additive possibly due to absorption in the blue/green region resulting in lower optical extraction. The results of an investigation into the effects of these additives on the performance of the large scale X-ray preionised laser described in this thesis are presented in chapter 5.

During electrical excitation of mercuric bromide in rare gas buffered discharges a manifold of electronic states, some of which are shown in figure 1.3 labeled as regions a-d with reference to the experimentally determined absorption bands, below the ionisation potential of 10.6 eV are produced [29] although available evidence suggests that only the excited $^{3,1}\Sigma_u^+$ states of $HgBr_2$ around 6.4 eV dissociate directly to form the HgBr (B) upper laser level [35]. Nighan and Brown grouped the $HgBr_2$ excitation into three processes having threshold energies of 5.0, 6.4 and 7.9 eV [36] and presented a provisional set of cross-sections. McGeoch et al [14] also derived cross-sections in a similar manner and numerous authors [37,38,39] have experimentally measured these cross-sections in the electron energy range of interest. The 5 eV process results in the dissociation of $HgBr_2$ to form the HgBr ($X^2\Sigma_{1/2}^+$) ground state, whilst the 7.9 eV process produces higher lying C and D excited states of the radical. The 6.4 eV process results in direct production of the HgBr ($B^2\Sigma_{1/2}^+$) upper laser level following dissociation of the $^{3,1}\Sigma_u^+$ states of $HgBr_2$ and is the dominant formation route although quenching of higher lying C and D states adds another possible pumping channel.

Modified versions of these cross-sections were used by Kushner et al [31] in a multidimensional model of a mercury bromide discharge laser, in conjunction with experimental results, to predict the operation of these lasers. They found it necessary to include in their model the effects of free mercury, produced as a by-product of the discharge, to explain the experimentally observed characteristics of the laser. Their results show that electron impact ionisation collisions from the excited states of mercury produced in the discharge (some of which are shown in figure 1.3), in reactions of the form

$$e + Hg \rightarrow Hg^{*}(6^3P_{0,1}) + e$$

$$e + Hg^{*}(6^3P_{0,1}) \rightarrow Hg^{**}(6^3P_2) + e$$

$$e + Hg^{**}(6^3P_2) \rightarrow Hg^{+} + 2e$$

have the highest rate constant of any process in the discharge. Thus any reaction pathways which lead to the formation of mercury or its excited states, such as production of the dissociative HgBr ($A^2\Pi_{1/2}$) state, contribute heavily to the rate of ionisation and subsequent collapse of the discharge. The presence of mercury in significant quantities in these discharges has been observed spectroscopically [12] and also in the work presented here as will be discussed in chapter 5. Kushner's model predicts that the concentration of excited states of mercury increases during the discharge pulse and multistep ionisation processes involving mercury atoms dominate the ionisation as the discharge progresses resulting in subsequent constriction of the discharge. This rapid process has limited the pulse lengths in discharge excited lasers to below 100 nsec as found by Znotins et al. [40] and in the work discussed here.

The topics discussed in this section have received much attention in the past decade and for a more complete discussion of the kinetics and spectroscopy of mercury bromide lasers the reader is referred to the references cited.

1.3 Methods of Excitation

Following the first demonstration of laser action in mercury bromide by ultraviolet photolytic dissociation [11], a number of excitation schemes including U.V., X-ray and

e-beam preionised discharges [26,32,40,41], e-beam sustained discharges [42], e-beam pumping [43] and excitation by wide band optical radiation [44] have been used. A brief discussion of some of these techniques is now presented with attention given to the method of X-ray preionised discharge pumping pertinent to the work described in this thesis.

The optical absorption spectrum of the mercury halides was initially studied by Terenim [45] and Wieland [46,47] and more recently by Maya [48]. These studies have shown that light absorbed in the 180-400 nm range leads to the photodissociation of the HgX_2 molecule in the reaction

$$HgX_2 + h\upsilon_{pump} \rightarrow HgX^* + X$$

where HgX^* is an excited state of the radical. In mercury bromide two absorption peaks have been observed at 230 nm and 195 nm as shown in figure 1.4. The former of these, corresponding to a photon energy of 5.4 eV, has been identified with the production of the ground state HgBr (X) state whilst the latter, 6.4 eV photon energy, results in the formation of excited radicals and in particular the HgBr (B) upper laser level. Schimitschek et al. [11] utilised the output from an ArF (193 nm) laser to photodissociate $HgBr_2$ and obtained 0.25 mJ of blue-green laser output. Bazhulin et al. have utilised a plasmadynamic surface discharge as a wide-band optical source of high brightness to optically pump mercury halide [44,49,50] and other lasers [9]. With this technique an additional pumping channel becomes possible by populating the upper laser level through excitation of mercurous bromide molecules left in the ground state following photon emission. This X → B absorption in HgBr has been reported by Green et al. [51] in the afterglow of a pulsed electrical discharge in mercuric bromide. The observed absorption peak is near 350 nm leading to a quantum efficiency approaching 70%, much higher than that for pumping from the parent $HgBr_2$ molecule of 40%. This technique offers the possibility of continuously re-using the HgBr molecules in lasing to produce a highly efficient cw laser system. One further benefit offered by this method is of possible longer wavelength (~ 2 eV) absorption from the X state to the repulsive A state assisting in the depopulation of the lower laser level.

In electron beam pumping [52] a high energy (typically > 200 keV) electron beam is injected into the laser medium. High power densities can be deposited in the gas by this

technique and it is often used as a 'brute-force' method to obtain laser action. The electron beam is generated by accelerating electrons through a vacuum under the influence of a high voltage. Electron beam pumping eliminates the problem of discharge stability as found in discharge excited lasers. Large pulse energies with modest efficiencies are typical of e-beam pumped systems. However they do suffer from several drawbacks. The energy deposition profile into the gas is non-uniform and multiple beam or cylindrical geometries are used to correct this and the high voltage engineering for the pulsed power supply is bulky, complex and expensive. More importantly the thin foil window separating the high pressure gas from the diode vacuum is placed under extreme mechanical and thermal stress. Foil thicknesses on the order of 50 μm are typically used to maximise the transmission of the electron beam into the cavity. Energy deposited in this foil by the e-beam leads to heating and subsequent failure of the foil. This limits the repetition rate of these devices to less than 1 Hz in the interest of preserving the foil, catastrophic failure of which could be expensive and time consuming.

Avalanche discharge excited lasers offer the potential for high efficiency and high average power operation from devices of reasonable size. The short (~ 24 nsec) upper radiative lifetime of the upper HgBr (B) laser level and high operating pressures require the use of rapid discharge circuits and transverse electrode geometries in low inductance configurations similar to those developed for carbon dioxide [53] and excimer [54] lasers. This ensures power is delivered to the gas in as short a time as possible at reasonable values of electric field before the onset of discharge instabilities. Numerous configurations of pulsed power supply have been developed for driving these electrical discharges and basically consist of an energy storage bank and a switch. Capacitors alone or in L-C inversion circuits [55], water dielectric pulse forming lines [56], Blumlein circuits and pulse forming networks using discrete components [57] and co-axial cables have all been used for energy storage whilst thyratrons, rail gaps and low inductance spark gaps have been used as switches. More discussion of this is given in chapter 2. Following the application of a high voltage electrical pulse, the gas between the electrodes breaks down and electrons avalanche under the influence of the electric field, multiplying through ionising collisions. In high pressure gases such discharges are unstable, spatial non-uniformities grow and form arcs or streamers between the electrodes. These lead to a very non-uniform discharge which is

inefficient in exciting the gas due to the inadequate excitation rates in regions of low current density. Also the inhomogeneous nature of the discharge results in nonuniform changes in refractive index in the medium affecting the optical quality of the laser beam Such instabilities may be suppressed by using a source of preionisation and this is discussed in the next section.

1.4 Preionisation of High Pressure Discharges

There are two well known processes in gas discharge physics which can convert an initially non-conducting gas between two electrodes into a conducting plasma. For low gas pressures the process is the classical Townsend breakdown [58] whilst at higher gas pressures typical of rare gas halide and excimer lasers 'Kanal' or streamer breakdown [59] occurs. In Townsend breakdown, on application of an electric field to the electrodes primary electrons produced by external radiation (eg. cosmic rays or trace radioactive elements) begin to avalanche towards the anode multiplying through secondary ionisation. The process is sustained through secondary emission of electrons from the cathode by either photoelectric emission or positive ion bombardment. At the low gas pressures in question the mean free path of electrons and ions in the discharge is sufficient to remove any local inhomogeneities and volumetric overlap of successive avalanches originating from the secondary electrons ensures uniform breakdown occurs. After breakdown this type of discharge is known as a glow discharge. The formation of such a discharge is governed by the characteristic timescale for positive feedback from the cathode - a process which has a predicted timescale of $\sim 10^{-6}$ seconds.

In high pressure discharges initiated by large over-voltages a different 'kanal' or streamer breakdown occurs with observed formation times of $\sim 10^{-9}$ seconds, much faster than those characteristic of Townsend breakdown. The theory of this form of discharge was the subject of a study by Meek [59] and was applied by Palmer [60], and later Levatter and Lin [61], to the cases of carbon dioxide and excimer lasers. Streamer breakdown occurs as a result of the development of a large space charge field associated with a single avalanche which becomes comparable to the applied field, combined with the effect of low electronic and ionic diffusion rates in the high pressure gas. As an electron is accelerated across the electrode gap under the infleunce of the applied field, multiplication through electron

avalanche takes place as in Townsend discharges. The similarity between the two types of breakdown ends there. An avalanche head consisting mainly of free electrons propagates towards the anode leaving behind a space charge of positive ions of much lower mobility. At some critical point the space charge associated with the avalanche head becomes comparable with the applied field and streamer formation ensues. Secondary avalanches initiated by photoelectrons in the vicinity of the of the avalanche are formed, the greatest multiplication of these being directed mainly along the axis of the primary avalanche where the space charge field supplements the applied field. Anode and cathode propagating streamers develop moving at a velocity greater than that of the initial avalanche head, enhanced by the effects of the space charge, and a conducting filament eventually bridges the electrode gap. As this process does not depend on feeedback processes from the electrodes the discharge formation time is reduced compared to that of Townsend breakdown. Figure 1.5 shows the formation of such a streamer.

This filamentary discharge is a direct consequence of the absence of the homogenisation effects of electron and ion diffusion in low pressure Townsend discharges. To inhibit this streamer formation and produce a uniform high pressure glow discharge necessary for efficient pumping of rare gas halide and excimer lasers some form of preionisation is required to produce a suitable low density of electrons in the gas prior to the initiation of the main discharge. The avalanches produced by these preionisation electrons then volumetrically overlap, smoothing out the effects of the space charge and removing the tendency of the discharge to form an arc. In Palmer's simple physical model [60] he derives a minimum preionisation level based on the requirement that the individual avalanches from the preionisation electrons overlap by the critical stage when the space charge field becomes comparable to the applied field. This ensures the field gradients associated with individual avalanches are smoothed out and streamer formation is inhibited. By equating the mean separation distance between the primary electrons generated by the preionisation process $n_{eo}^{-1/3}$ (where n_{eo} is the initial electron density) to the critical radius of the avalanche head at the moment the space charge field becomes comparable to the applied field, the minimum prionisation electron density can be calculated. Although the results of this model were consistent with those found experimentally for CO_2 TEA lasers, indicating preionisation levels in excess of 10^4 electrons cm^{-3} were required for prevention of streamer formation,

Levatter and Lin [61] pointed out two deficiences of the model. The first was the neglect of finite voltage risetime on the density of preionisation electrons near the cathode and the subsequent consequences of this in relation to discharge stability. Also Palmer's model does not include any analysis of the relationship between physical parameters of the gas mixture such as the Townsend ionisation coefficient, electron mobility and discharge E/N.

Levatter and Lin used a modified version of Palmer's model including the above effects to determine the minimum preionisation electron density and voltage risetime for a typical mixture suitable for electrical discharge excitation of an XeF rare gas halide excimer laser and compared the numerically generated results with experiment. Their calculations show a minimum electron density on the order of $2x10^5$ electrons cm^{-3} is required for formation of a homogeneous and stable discharge, a value consistent with their experimental investigations. They also propose that in situations where the preionisation source is terminated before application of the electric field, extremely fast voltage risetimes (~15 nsec) are required to prevent excessive drift of electrons from the cathode area before initiation of the avalanche process and subsequent streamer formation, due to inadequate overlap of the avalanches in the depleted area. However when the preionisation source strength is maintained throughout the avalanche initiation process, as is usually arranged under normal operating conditions for X-ray preionised devices, this voltage risetime requirement is relaxed. An extensive study by Taylor [62] of discharge stability in XeCl lasers using laser induced preionisation showed a minimum preionisation density of $\sim 10^7$ electrons cm^{-3} was required to ensure the establishment of a stable discharge. However these results are pertinent to much higher gas pressures than those of Levatter and Lin (4.5 atmospheres compared to 1 atmosphere). At these higher gas pressures the extent of the avalanches discussed in the above model are reduced and so a higher initial electron density is required to ensure adequate overlap occurs to prevent streamer formation. These results suggest the pressure dependance for the preionisation threshold required to produce a uniform discharge scales as the cube of the pressure as suggested by Smith and Mellis [63]. Taylor also investigated the effect of spatial variations in the preionisation density in directions parallel and transverse to the applied electric field direction on the uniformity of the discharge. His results show that uniform preionisation is required in the direction transverse to the electric field to achieve a uniform discharge whilst large local gradients in the preionisation density

parallel to the electric field may be tolerated without affecting the quality of a large part of the discharge. This then puts certain constraints on the preionisation source which must be met to eliminate its effects on the ability to produce a uniform, streamer free, discharge. The source must be able to generate a sufficient density of preionisation electrons in the gas to ensure initiation of an arc free discharge, which is spatially uniform in the direction transverse to the applied field. The technique of X-ray preionisation satisfies these constraints as is elucidated in chapter 3.

Once a spatially uniform discharge is established it may be sustained, providing the pump pulse duration is long enough, for a period of time until hot spots on the electrodes develop or thermal instabilities or some kinetic process in the gas occurs, which promotes constriction of the discharge. For the case of mercury bromide discharge lasers the limiting factor in the ability to sustain a uniform discharge is the multistep ionisation of excited states of mercury produced as by-products of the discharge, as discussed above. The consequences of this process on the performance of the laser described in this thesis and on the design of pulsed power supplies for driving mercury bromide lasers will be discussed in chapter 5. Numerous methods have been used to produce the initial preionisation electron density in gas discharge lasers and some of these are now discussed.

The most commonly used form of preionisation is that of U.V. preionisation. Ultra violet radiation produced close to the discharge region is used to photo-ionise the gas prior to the initiation of the main discharge pulse. A series of sparks is often used for the radiation souce [64] as is found in many commercial lasers but corona or surface discharges have also been employed. A second form of U.V. preionisation, the technique of laser induced preionisation [62], uses the U.V. radiation from an excimer laser (eg. KrF, 248 nm) injected down the axis of the discharge volume. Electron beam preionisation where a beam of electrons is injected into the gas to generate the required preionisation density has also been used [65]. This technique however suffers from similar limitations in repetition rate as for e-beam pumping because of foil lifetimes. The mass penetration depths of electrons [66] and U.V. radiation [53] in high pressure gases restrict the volume these can uniformly preionise and hence limit the scalability of these techniques. Furthermore, the presence of corona or spark discharges inside the laser cavity can cause contamination of the gas and reduce the lifetime of the laser mixture. The technique of X-ray preionisation avoids many of the

limitations of these other methods.

Sumida et al. [67] first reported the use of X-rays in the preionisation of a high pressure gas discharge and the benefits of this technique were soon realised by numerous authors [68,69,70]. The large mass penetration depths [71] of moderate energy (20-100 keV) X-rays in high pressure gases compared to those of electrons or U.V. radiation enable much larger volumes to be uniformly preionised. Furthermore, the 'windows' in the cavity through which the X-rays must pass to enter the discharge region do not suffer from the same thermal and mechanical stresses as the thin foil windows in e-beam preionised systems do. They can be made structurally more robust than their e-beam counterparts because of the greater penetration ability of X-rays in the energy range of interest, thus removing repetition rate limitations. Contamination problems caused by corona or spark discharges inside the cavity are eliminated using X-rays as the source is separate from the laser cavity. This method also allows collimation of the X-rays through the use of suitable shielding with subsequent confinement of the discharge, not possible with highly diverging U.V. sources close to the electrodes. The implications of this lead to a relaxation of and possible elimination of the profiling requirements of electrodes and, as discussed in chapter 5, the ability to restrict the extent of the preionising X-rays can lead to impressive improvements in discharge uniformity . The technique of X-ray preionisation is elucidated in chapter 3 where some of these points are considered in more detail.

References

1. R.L. Cooke and P.H. Dickinson, Proc. I.O.A., Vol. 8 part 5 (1986).
2. R. Burnham and E.J. Schimitschek, Review Article, Laser Focus (June 1981).
3. J.B.Marling, J. Neilson, L.C. West and L.L. Wood, J.Appl.Phys. 50, 610 (1979).
4. Y.C. Chung, J.D. Dobbins and T.M. Shay, submitted to IEEE J. Quantum. Electron. October 1987.
5. Prof.W.Sibbett, Dept. of Physics and Astronomy, St.Andrews University, Fife, Scotland. Private Communication.
6. H. Rieger, IEEE J.Quantum.El. QE22, 405 (1986).
7. C. H.Fisher, R.E. Center, G.J. Mullaney and J.P. McDaniel, Appl.Phys.Lett. 35, 26 (1979).
8. Y.Nachshon, F.K.Tittel, W.L.Wilson Jr. and W.L. Nighan, J.Appl.Phys. 56, 36 (1984).
9. V.S.Zuev, G.N. Kashinikov, N.P. Kozlov, S.B. Mamaev, V.K. Orlov, Yu.S. Protosov and V.A. Sorokin, Sov.J.Quantum.Electron. 16, 1665 (1986).
10. R.C.Hollins, D.L.Jordan and A.Feltham, Paper 2, Eighth National Quantum Electronics Conference, Dept. of Physics, University of St. Andrews, Fife, Scotland (September, 1987).
11. E.J. Schimitschek, J.E. Celto and J.A. Trias, Appl.Phys.Lett. 31, 608 (1977).
12. Mathematical Sciences Northwest Ltd. Final Report, 200 Watt Mercury Bromide Laser (1984).
13. F. Kvasnik and T.A. King, Optics Commun. 41, 199 (1982).
14. J. Tellinghuisen and J. Gail Ashmore, Appl.Phys.Lett. 40, 867 (1982).
15. J. Tellinghuisen, P.C. Tellinghuisen, S.A. Davies, P. Berwanger and K.S. Viswanthan, Appl.Phys.Lett. 41 (9), 789 (1982).
16. M.N. Ediger, A.W. McCown and J.G. Eden, IEEE J.Quant.Elect. QE19, 263 (1983).
17. H.J. Baker, A.M. Felthem, N. Seddon, QE7, Malvern, (September 1985).

18. K. Wieland, Helv. Phys. Acta 2, 46 (1929).

19. K. Wieland, Helv. Phys. Acta 14, 420 (1941).

20. K. Wieland, Z. Elektrahem 64, 761 (1960).

21. W.R.Wadt, Appl.Phys.Lett. 34, 658 (1979).

22. H. Helvajian and C. Wittig, Appl.Phys.Lett. 38, 731 (1981).

23. A.C. Erlandson and T.A. Cool, Chem.Phys.Lett. 96, 685 (1983).

24. W.P. Lapatovich, G.R. Gibbs and J.M. Proud, Appl.Phys.Lett. 41, 786 (1982).

25. M.W. McGeoch, J.C. Hsia and D.E. Klimek, J.Chem.Phys. 78, 1180 (1983).

26. E.J. Schimitschek and J.E. Celto, Optics Lett. 2, 64 (1978).

27. J. Allison and R.N. Zare, Chem.Phys. 35, 263 (1978).

28. R.S.F. Chang and R. Burnham, Appl.Phys.Lett. 36, 397 (1980).

29. W.L. Nigham, Appl.Phys.Lett. 36, 173 (1980).

30. H.J. Baker and N. Seddon, Appl.Phys.B. 36, 171 (1985).

31. M.J. Kushner, A.L. Pindroh, C.H. Fisher, T.A. Znotins and J.J. Ewing J.Appl.Phys. 57, 2406 (1985).

32. R. Burnham, Appl.Phys.Lett. 33, 156 (1978).

33. D.C. Cartwright, S. Trajmar, A. Chutjian and W. Williams Phys. Rev. A 16, 1041 (1977).

34. N.J.Mason and W.R.Newell J. Phys. B 20, 1357 (1987).

35. W.R. Wadt, J.Chem.Phys. 72, 2469 (1980).

36. W.L. Nigham and R.T. Brown, J.Appl.Phys. 53, 7201 (1982).

37. M.W. McGeoch, J.C. Hsia and D.E. Klimek, J.Chem.Phys. 78, 1180 (1983).

38. A.N. Malinin, A.K. Shuaibov and V.S. Shevera, Sov. J. Quantum Electron. 13, 977 (1983).

39. V. Kushawaha and M. Mahmood, J.Appl.Phys. 62, 2173 (1987).

40. T.A. Znotins, C.H. Fisher, T.E. DeHart, J.P. McDaniel and J.J. Ewing, Appl.Phys.Lett. 46, 228 (1985).

41. R. Burnham and W.T. Whitney, J.Appl.Phys. 52, 3849 (1981).

42. M.W. McGeoch, J.C. Hsia and D.E. Klimek, J.Appl.Phys. 54, 3723 (1983).

43. J.H. Parks, Appl.Phys.Lett. 31, 297 (1977).

44. S.P. Bazhulin, N.G. Basov, V.S. Zuev, Yu.S. Leonov and Yu.Yu. Stoilov

Sov. J. Quantum Electron. 8, 402 (1978).

45. A. Terenin, Z.Phys. 44, 713 (1927).

46. K. Wieland, Z.Phys. 76, 801 (1932).

47. K. Wieland, Z.Phys. 77, 157 (1932).

48. J. Maya, J.Chem.Phys. 67, 4976 (1977).

49. S.P. Bazhulin, N.G. Basov, S.N. Bugrimov, V.S. Zuev, A.S. Kamrukov, G.N. Kashnikov, N.P. Kozolov, P.A. Ovchinnikov, A.G. Opekan, V.K. Orlov and Yu.S. Protosov, Sov. J. Quantum Electron.16, 663 (1986).

50. S.P. Bazhulin, N.G. Basov, S.N. Bugrimov, V.S. Zuev, A.S. Kamrukov, G.N. Kashnikov, N.P. Kozolov, P.A. Ovchinnikov, A.G. Opekan and Yu.S. Protosov, Sov. J. Quantum Electron.16, 990 (1986).

51. D.P. Green, K.P. Killeen and J.G. Eden, Appl.Phys.Lett. 48, 1175 (1986).

52. L.P. Bradley, Inst.Phys.Conf. Ser. No. 29, 59 (1978).

53. O.R. Wood, Proc. IEEE 62, 355 (1974).

54. Ch. Brau in 'Excimer Lasers' 2nd edition, Ed. Ch.K. Rhodes. Topics in Applied Physics, vol. 30, Springer-Verlag (1984).

55. See for example Questek Technical Notes Nos. 1 and 4 (1983).

56. M.R. Osborne, M.H.R. Hutchinson and P.W. Smith, Optics Commun. 52, 415 (1985).

57. A.J.W. Brown and P.W. Smith, Paper 8.1, Seventeenth Modulator Symposium, Seattle, June 1986. Also published as EEV Technical Reprint 161.

58. J.S. Townsend, Nature 62, 340 (1900).

59. J.M. Meek, Phys.Rev. 57, 722 (1940).

60. A.J. Palmer, Appl.Phys.Lett. 25, 138 (1974).

61. J.I. Levatter and S.C. Lin, J.Appl.Phys. 51, 210 (1980).

62. R.S. Taylor, Appl.Phys.B. 41, 1 (1986).

63. A.L.S. Smith and J.Mellis, Appl.Phys. B 37, 171-179 (1985).

64. For example, R. Burnham and N. Djeu, Appl.Phys.Lett. 29, 707 (1976).

65. Physical Electronics, C.L.Hemenway, R.W.Henry, M. Caulton 2nd ed. (John Wiley, 1967).

66. ICRU Report 37 - Stopping Powers for Electrons and Positrons.

67. S. Sumida, M. Obara and T. Fujioka, Appl.Phys.Lett. 33, 913 (1978).

68. S.C. Lin and J.I. Levatter, Appl.Phys.Lett. 34, 505 (1979).

69. H. Shields and A.J. Alcock, Optics Commun. 42, 128 (1982).

70. A.V. Kozyrev, Yu.D. Korolev, G.A. Mesyats, Yu.N. Novoselov, A.M. Prokhorov, V.S. Skakun, V.F. Tarasenko and S.A. Genkin, Sov. J. Quantum Electron. 14, 356 (1984).

71. Handbook of X-rays, ed. E.F. Kaelble, McGraw-Hill New York (1967).

72. T.M. Shay, D. Gookin, M.C. Jordan, F.E. Hanson and E.J. Schimitschek, IEEE J. Quantum. Electron. QE21, 1271 (1985).

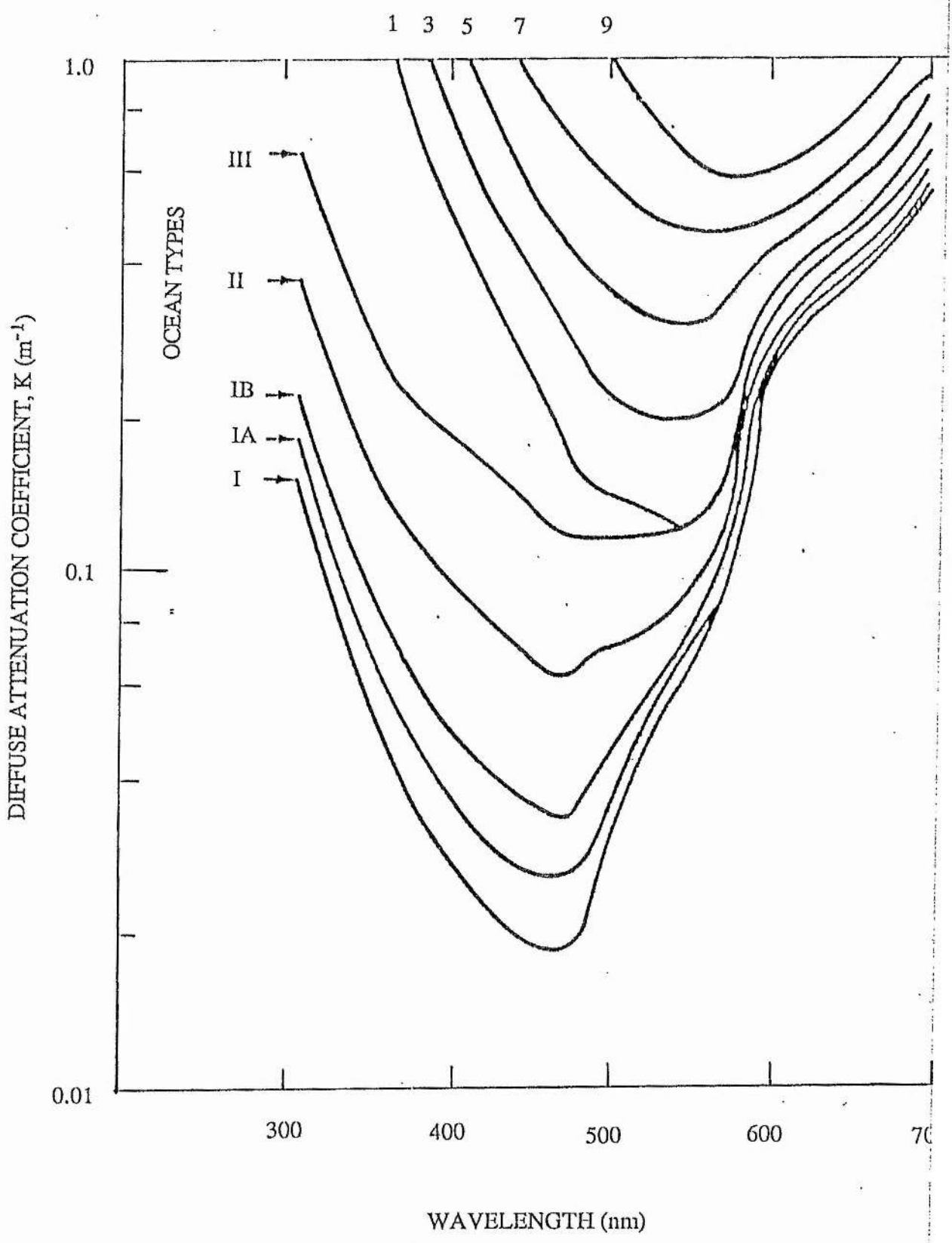

FIGURE (1.1): Diffuse attenuation coefficients for ocean waters. (from ref [1]).

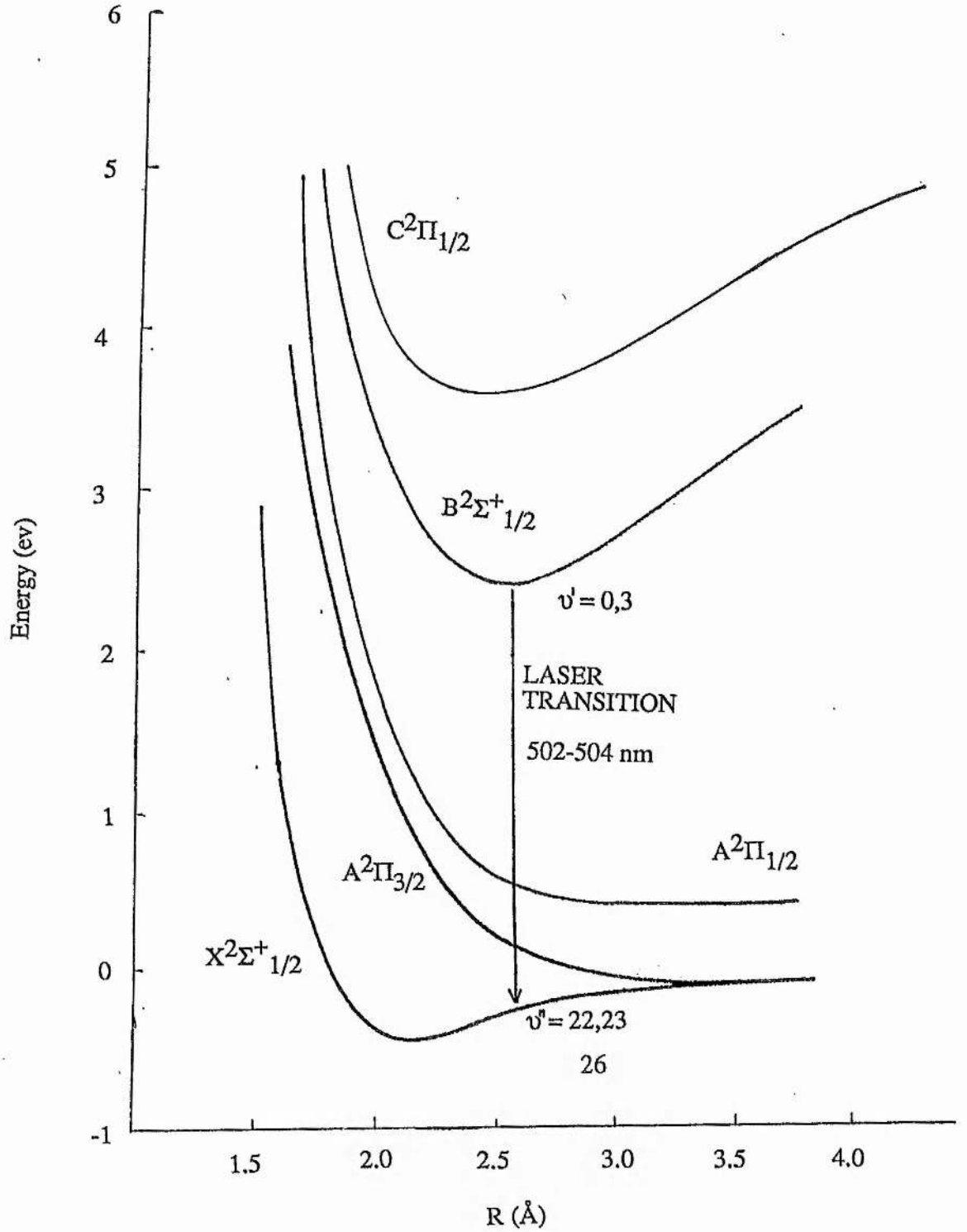

FIGURE (1.2): Potential energy diagram for the lowest electronic states of HgBr. The laser transition takes place between the vibrationally relaxed B state to high lying vibrational levels in the X state. Recombination via the fast bimolecular reaction

$$HgBr(X) + Br_2 \rightarrow HgBr_2(X) + Br$$

takes place reforming the parent molecule.

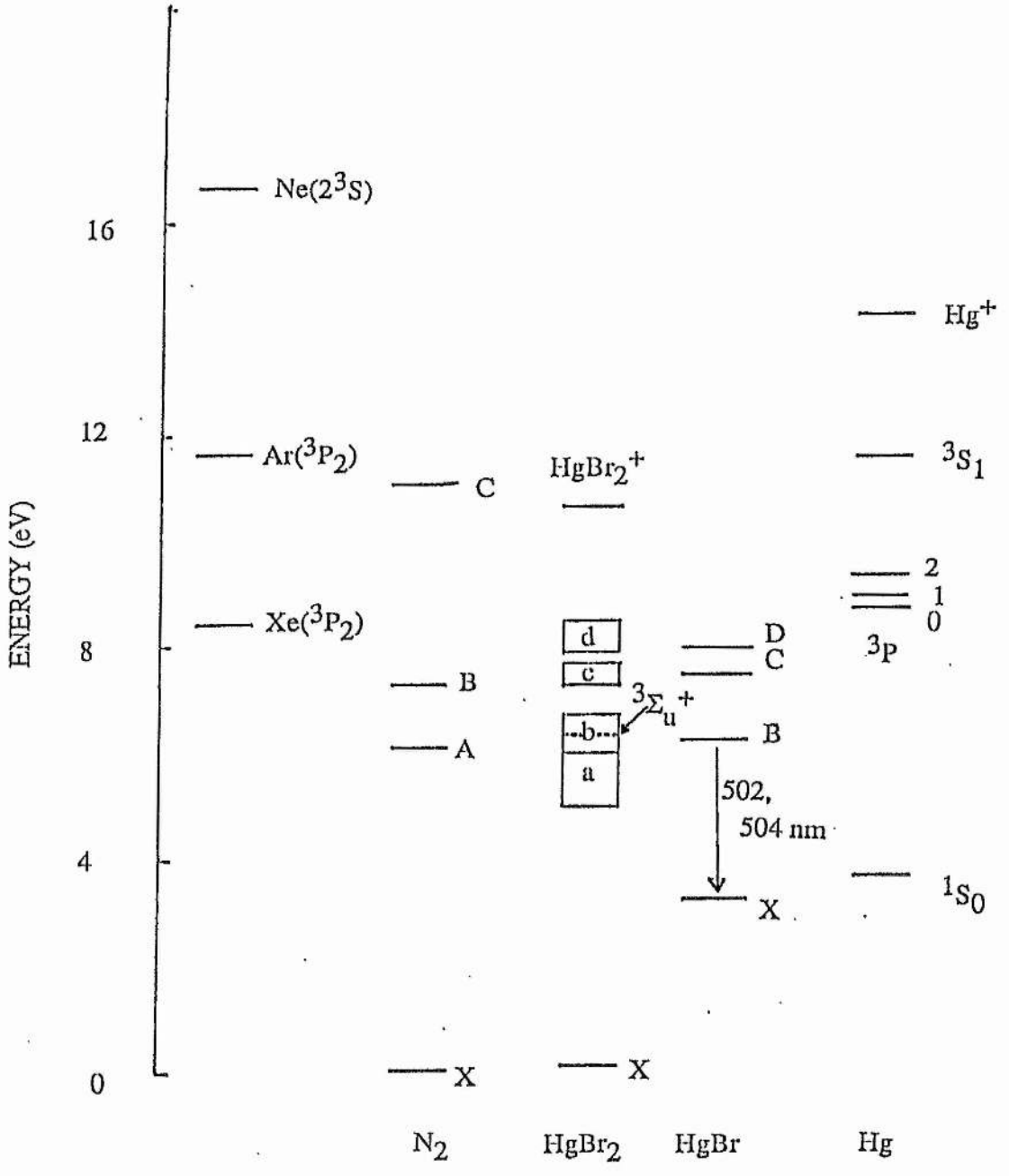

FIGURE (1.3): Energy diagram for the mercury bromide laser showing the metastable states of various gases and some of the excited states of mercury.

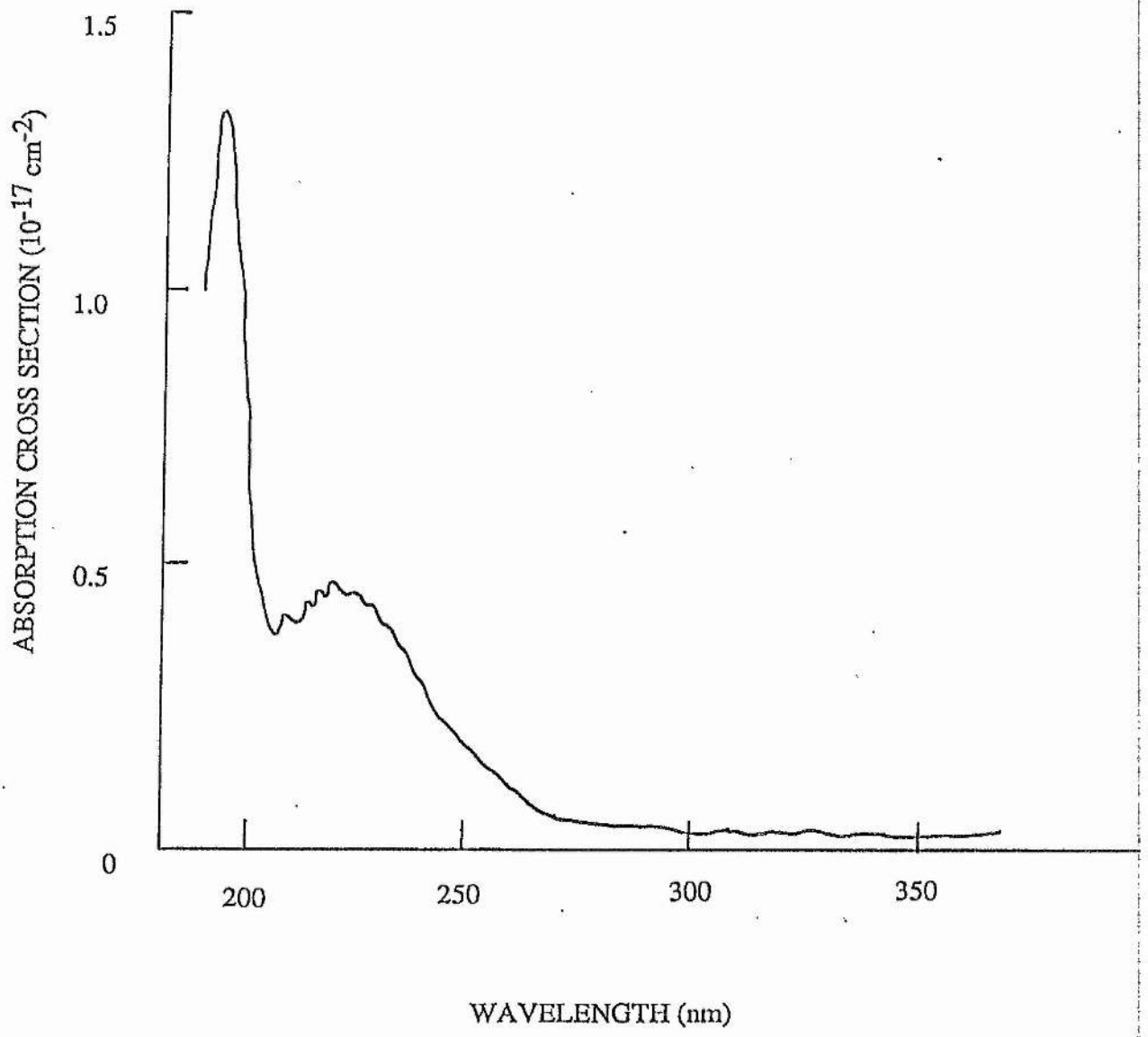

FIGURE (1.4): Ultraviolet absorption cross section for mercury bromide at 170°C. (from ref [48]).

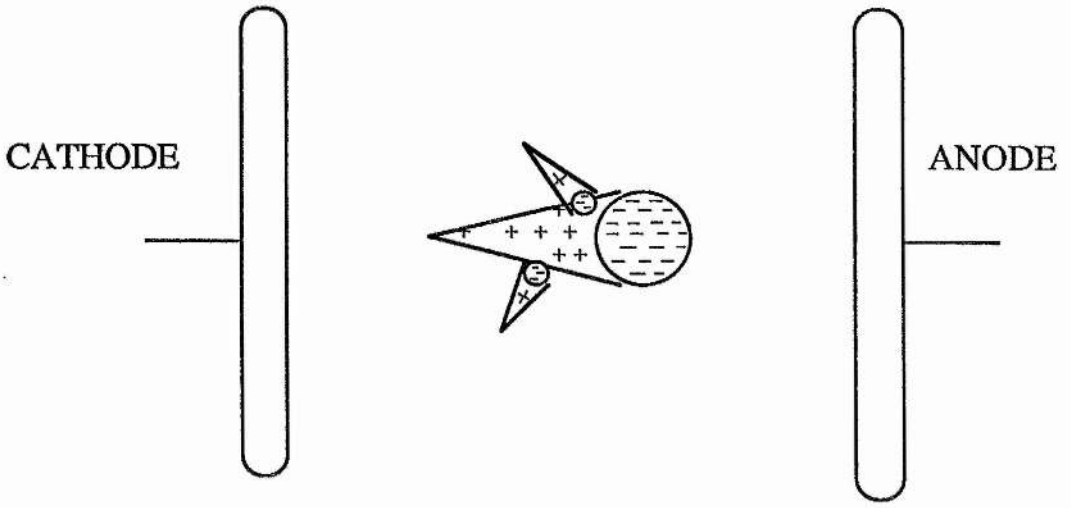

When the space charge associated with an initial avalanche becomes comparable to the applied field streamer formation ensues.

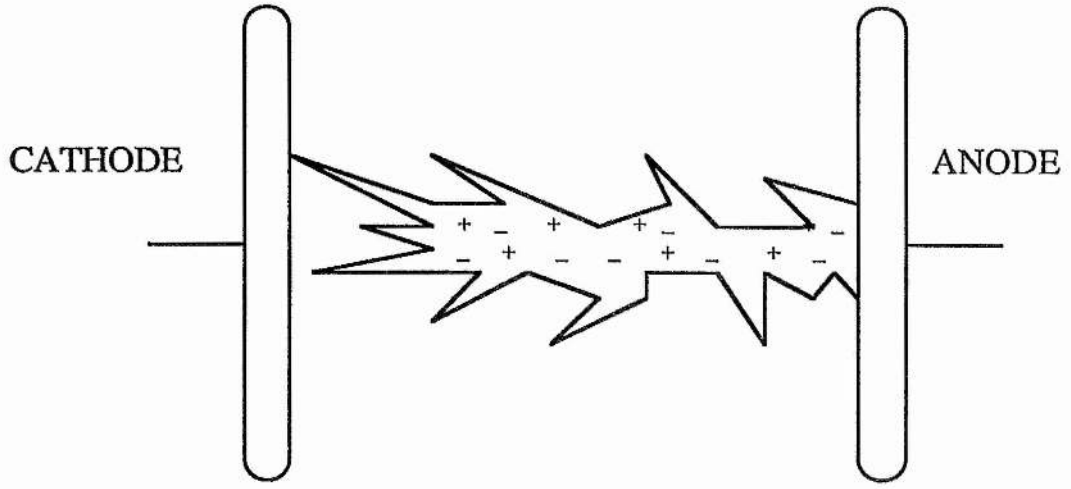

Secondary avalanches form, multiply along the direction of the applied field and a conducting filament eventually bridges the gap

FIGURE(1.5): Formation of a streamer in a high pressure gas discharge without preionisation.

CHAPTER 2

PULSED POWER SUPPLY

2.1 Requirements of Pulsed Power Supply

As discussed in Chapter 1, numerous configurations of discharge circuitry have been used as pulsed power supplies for gas discharge lasers. Prior to a discussion of the design , construction and operation of the supply developed for use with this laser system, some of the requirements of such supplies are presented. Assuming the ideal case where no absorption occurs in the windows or the gas allowing perfect optical extraction to be achieved and a gaussian lineshape near the centre of the emission band, the pump power, P, per unit volume which must be deposited in the gas to produce a gain coefficient of unity per unit length is given by [1,2]

$$P = \frac{8 \pi h c^2 \Delta \lambda}{\lambda^5 \eta \varphi}$$

where λ is the transition wavelength, $\Delta \lambda$ the linewidth, η the efficiency of populating the upper laser level and φ the quantum efficiency. For mercury bromide this leads to a required pump power density on the order of 100 $kWcm^{-3}$ to produce a gain of 10%cm^{-1}, for shorter wavelength lasers such as the rare gas halide lasers the pumping requirements are even more demanding. The stored energy in these supplies must also be deposited in the gas at a rate sufficient to maintain the population inversion and on a timescale shorter than that in which inhomogeneities can develop leading to collapse of the discharge. These demands on the pulsed power supplies are exacerbated when the lasers are required to operate at significant repetition rate. Some further requirements of such power supplies are listed below:

1. The initial amplitude of the electric field between the two discharge electrodes prior to gas breakdown must be at least three times that of the field which results when self-sustained discharge conditions have been established. The electric field required to break down the gas is always higher than the self-sustained discharge field and recent work has shown this to be necessary for establishment of a stable high pressure glow discharge in a uniform laser gas

mix [3].

2. The upper state lifetime in the mercury bromide laser is relatively short, ~24nsec [4], so the voltage and current risetimes need to be as fast as possible to ensure sufficient power is deposited in the discharge and a significant population inversion established before the process of spontaneous emission depletes this level, implying the use of low inductance, rapid discharge circuitry. This type of circuitry has been extensively used in CO_2 and excimer lasers[2]. As discussed in chapter 1, Levatter and Lin [5] proposed that slow voltage risetimes could result in streamer formation in the discharge under certain conditions. It is widely accepted that voltage risetimes of 50 nsec or faster are adequate for operation of these lasers, however it has also been noted that extended risetimes in excess of 150nsec may be used without any serious reduction in the quality of the discharge in an XeCl laser [6].

3. The glow voltage at which a discharge operates is dictated by the gas mixture and spacing of the laser electrodes. In order to efficiently operate mercury bromide lasers evidence suggested the pump power density deposited in the gas should be at as high a level as possible without overpumping the gas leading to arc formation through the development of instabilities in the discharge. This requires the output impedance of the pulsed power supply to be as low as possible, a difficult constraint to meet in practice as sub-ohm impedances are required. Care must be taken to minimise the inductance of the feeds from the pulsed power supply to the discharge cavity and the cavity inductance to prevent loss of current rise-time at these low impedance levels.

4. The components used to construct the pulsed power supply must be capable of high repetition rate operation without failure from excessive wear or heating, for high average power, long life lasers.

5. It is often necessary to synchronise the pulse from the supply to another event, for instance the output from a flash X-ray preioniser or the laser output pulse to a specific temporal occurrance. Therefore, time jitter between receipt of an external trigger command and onset of the discharge pulse must be minimised.

These requirements were applied to the design of a repetitively pulsed power supply constructed to drive the mercury bromide laser described in this thesis. The development of this supply is now elucidated.

2.2 Pulse Forming Line Theory

The design of the pulsed power supply was based on pulse forming line (PFL) techniques [7,8,9], which afford control over the rate of power deposition into the discharge and temporal control over the pulse. PFL's in the form of coaxial cables, strip transmission lines or the discrete component equivalents have been widely used for the generation of high voltage pulses. The electrical properties of these lines are determined by the capacitance and inductance per unit length (for a cable) or per section (for a discrete component network). A discrete line of capacitance C and inductance L per section has a characteristic impedance

$$Z = (L/C)^{1/2} \ \Omega$$

and will delay an electromagnetic wave launched along it by

$$\tau_{delay} = (L\,C)^{1/2} \text{ seconds per section}$$

Figure 2.1 (a,b) shows examples of such lines of impedance Z, which are charged to a voltage, V_C, and discharged by switch, S, into the terminating load R. On closure of the switch a voltage pulse of magnitude

$$V_R = V_C \frac{R}{R+Z} \text{ volts}$$

is produced across the load and simultaneously a wave of magnitude

$$V_Z = V_C \frac{Z}{R+Z} \text{ volts}$$

propagates away from the load, discharging the line. On encountering an impedance discontinuity, as at the end of the line, an electromagnetic wave is reflected with a magnitude determined by the reflection coefficient at the interface. The reflection coefficient is given by

$$\rho = \frac{Z_2 - Z_1}{Z_2 + Z_1}$$

where Z_1 is the impedance before the discontinuity and Z_2 after, see figure 2.1 (c). The reflected portion of the incident wave, V_r, is then

$$V_r = \rho V_i$$

and the transmitted portion

$$V_t = V_i + V_r$$

For the special conditions where the line impedance after the discontinuity is infinite (open circuit) or zero (short circuit) the reflection coefficients are, respectively

$$\rho_{\text{open circuit}} = +1$$

$$\rho_{\text{short circuit}} = -1$$

The wave propagating in the line is then reflected unaltered ($\rho = 1$) and returns towards the load. Under 'matched' load conditions where the load impedance equals the line impedance ($R = Z$) the voltage over the load is $V_L/2$ and lasts for a time equal to the two way transit time of a wave in the line. For a network with n sections the pulse length is

$$\tau_{\text{pulse}} = 2n\,(LC)^{1/2} \text{ seconds}$$

In networks terminated by non matched loads complete discharge of the line does not occur during the two-way propagation of the wave and the effect of the mismatch results in voltage steps ($R > Z$) or oscillations ($R < Z$) at the load. An analysis of these waveforms can be made in terms of the reflections at the end of the line terminated by the mismatched load. These reflections propagate in the line to the open circuit end where they are completely reflected, as discussed above, and return to the load end where they appear as positive or negative steps depending on the form of the mismatch. These reflections continue with a period equal to the two way transit time of the line with decreasing magnitude until the energy in the line is dissipated in the load. Figure 2.2 shows examples of voltage pulses across pulse forming line loads for these various cases.

The matched load condition is also that for which maximum energy transfer to the load takes place. The energy deposited in the load is given by

$$E_D = V_L\ I_L\ \tau_{\text{pulse}} \qquad \text{Joules}$$

where

$$I_l = \frac{V_c}{R+Z} \quad \text{Amps}$$

is the current through the load, and using the equations in the text

$$E_D = \frac{V_c^2 R\, 2\, n\, (LC)^{1/2}}{(R+Z)^2}$$

The energy stored in the line is given by

$$E_S = 1/2\ nCV_c^2 \quad \text{Joules}$$

where nC is the total line capacitance and the efficient of energy transfer,η, is

$$\eta = \frac{E_S}{E_D} = \frac{4R}{(Z+R)^2} (L/C)^{1/2}$$

hence

$$\eta = \frac{4RZ}{(Z+R)^2} = 4 \frac{R}{Z+R} \frac{Z}{Z+R}$$

and

$$\eta = 4 (V_R / V_C) (V_Z / V_C) = 4 \frac{V_R (V_C - V_R)}{V_C^2} = (1 - (\frac{2V_R - V_C}{V_C})^2)$$

which has a maximum at $2V_R = V_C$, the same condition as for matched load operation. So for an efficient system the voltage across the load should be approximately half the line charge voltage and under these conditions effective pulse forming line action will take place resulting in maximum energy transfer.

2.3 Pulsed Power Supply Design

There are numerous possible configurations of pulse forming networks that may be used in pulsed power supplies depending on the electrical characteristics required of the system. The previous section concentrated on the theory of single pulse forming lines but this is equally applicable to Blumlein pulse forming lines and double pulse forming lines (DPFL's) (effectively two single pfl's in parallel) with the appropriate modifications to take

the different configuration into account. Figure 2.3 shows schematics of these two alternative line geometries together with their electrical characteristics for matched load operation. To ensure the pulsed power supply operated at the lowest output impedance, to satisfy the requirements discussed earlier, its design was based on a double pulse forming line configuration. The matched load for this system occurs at a value of half the single line impedance in contrast to being equal to the line impedance for PFL's and twice this for Blumlein PFL's. The main advantage of the Blumlein configuration is that the load voltage under matched conditions is the same as the charge voltage, however this only occurs at the expense of the much higher operating impedance.

The design criteria for the pulsed power supply were as follows:

(1) The output impedance of the final supply was chosen to be 300 mΩ, a figure felt to be low enough to efficiently drive the laser.

(2) A pulse length on the order of 200 nsec was decided on for driving the laser upon reference to the pulsed power circuitry used in other rare gas halide lasers[10].

(3) A maximum line charge voltage of 35 kV was chosen being the peak forward anode voltage of the thyratrons used to trigger the supply, where they operate at their most efficient level, and which enabled the line to be run in air without problems associated with corona losses. Thyratrons were chosen as the switching device to be used in the pulsed power supply for their long lifetimes, high repetition rate capability and low jitter characteristics [14]. For a charge voltage of 30 kV the matched load output from the supply is 15 kV, which although is higher than the self sustaining voltage observed in XeCl lasers of similar discharge size to this [10], proved to be close to the optimum value for this laser as discussed in chapter 5. The line components have to be capable of long life operation at these high voltages and the design had to minimise problems associated with corona discharges, flash over and electrical breakdown.

(4) A voltage transient on the front edge of the pulse from the supply some 3/2 times the line charge voltage was desired to aid establishment of a glow discharge. Rapid overvolting of the electrode gap decreases the discharge formation time and hence the time for any instabilities to develope allowing a uniform plasma to dèvelope without any filamentation.

The low line impedance can be achieved by operating twelve DPFL's in parallel, each of impedance 3.6 Ω, therefore, the first line experiments had to establish how well a single

pulse forming line of impedance 7.2 Ω could be built and operated. These initial experimer were used to empirically determine the most appropriate method by which the line could be constructed and to characterise the performance of the line as accurately as possible.

The first lines tested were basically a number of ceramic 'door knob' capacitors held between two strips of aluminium, the capacitors being separated by a few centimetres to leave an inductive gap between them, in an effort to produce a line resembling the circuit in figure 2.1 (b). A copper sulphate load of resistance close to that estimated for matched operation was used to terminate the line which was switched by either a self-breaking spark gap or a glass thyratron (EEV CX 1685). The $BaTiO_3$ ceramic 'door knob' capacitors supplied by Morgan Matroc Ltd., used in this and all subsequent versions of the line, had a maximum working voltage of 40 kV and a capacitance of 1.2 nF. Capacitors with a maximum voltage rating of 40 kV were chosen not only for reasons of reliability, but also to minimise the effect of the reduction in capacitance of $BaTiO_3$ capacitors with applied voltage caused by the ferro-electric nature of the material [11,12]. At a line charge voltage of 30 kV, manufacturers data suggests that the capacitors should change their value by no more than 5% due to the dielectric stress incurred at the applied voltage. Numerous line configurations were explored varying the number of capacitors, up to a maximum of ten, and the spacing between them, however this method of introducing the required inductance into the line proved unsuccessful making estimation of the line operating parameters and characterisation of the line difficult.

The next generation of test lines used discrete inductors wound from copper wire to add the necessary inductance to the line, replacing one of the aluminium strips previously used to connect the capacitors. This technique worked well resulting in excellent pulses from the line into matched loads and enabling the characteristics of the line to be determined accurately. Development of this single pulse forming line then led to the construction of a double pulse forming line (DPFL) module, basically by running two PFL's in parallel with a common high voltage connection as shown in figure 2.4, which was to be the basis for the final modular system.

The DPFL module operates in a 'fold-back' configuration where the voltage pulse from the line is transmitted to the load by a matched transmission line section. This arrangement allows the thyratrons to be operated with their cathodes at ground potential and

keeps the size of the system to a minimum. Metallic strips fabricated from 3mm mild steel sheet, 6 cm wide connect the capacitors together and form the conductors for the transmission line; the overall length of the module, including thyratron is 80 cm. The impedance of a transmission line is given by

$$Z = \frac{377\ s}{\varepsilon^{1/2}\ w}\ \Omega$$

where s is the separation of the conductors, w their width and ε the dielectric constant of the insulating material between them. Mylar ($\varepsilon = 2.7$) was used as the dielectric in the line depicted here, hence for a matched transmission line impedance of 7.2 Ω the required separation of the conductors was 1.7 mm, achievable with seven layers of 250 μm Mylar sheet, which also provided adequate insulation between the conductors. The line capacitors, as mentioned previously, had a maximum operational voltage of 40 kV and a capacitance of 1.2 nF, however measurements using a simple RC discharge circuit showed this value decreased to approximately 1 nF at 30 kV. The line inductors were wound from 16 swg copper wire to have an inductance of 60 nH [13] so each single pfl operated at an impedance of ~ 7.2 Ω and the overall DPFL output impedance was ~ 3.6 Ω. Tests on this line again proved successful, figure 2.8 (a) shows the typical output from a DPFL module charged to 30 kV and discharged by the deuterium filled thyratron into a matched copper sulphate load, a full discussion of these results is given later.

Once the DPFL module was successfully demonstrated the next step in the development of the pulsed power supply was to operate several of the lines in parallel then to scale up from this to the required twelve lines, demonstrating the feasibility of this approach and the ability to operate numerous thyratrons in parallel. Firstly, a two module and then a four module system were built and characterised, their performance being close to that anticipated from the single module results. Details of the fabrication of these systems are similar to those of the final supply discussed later.

Concurrently, a technique to automatically produce a high voltage spike on the leading edge of the discharge pulse, to aid breakdown of the gas and satisfy the previously discussed requirements, was investigated and incorporated into the DPFL system. Peaking capacitors across the discharge electrodes are often used for this purpose, however, the system developed for this laser incorporated a 'spike line' as an integrated part of the pulsed

power supply to produce a high voltage transient. The 'spike line' consists of a short, high impedance, secondary transmission line, inserted between the primary pulse forming network and the discharge electrodes. Figure 2.5 (b) shows the lattice diagram predictions for a spike line section with a one way transit time for an electromagnetic pulse of 10 nsec, of impedance three times that of the primary line and terminated in a load of infinite impedance simulating a laser gas mix prior to break-down. Analysis of the performance of the complete line system using the reflection coefficients derived from the equations in the text shows that a high voltage transient of duration equal to the round trip time in the secondary line is produced at the start of the output pulse. Under ideal conditions this transient is $1^1/_2$ times the line charge voltage when the system is discharged into an infinite load and for a conducting load, eg. the discharge after initial breakdown, the spike line will have little effect on the pulse because of its short length.

The first attempts to produce a 'spike line' in the DPFL system were by using discrete components, constructing a line with the appropriate characteristics which was inserted between the transmission line section and the load. Although some success was achieved by this method a more convenient way was to make the spike line in the form of a strip transmission line replacing the transmission line section in the original module, keeping the whole system compact. Soda glass was chosen as a suitable dielectric material for the spike line because of its insulating properties, relatively high dielectric constant ($\varepsilon = 7.5$) and availability. For a single module the 'spike line 'impedance required is 21.5 Ω which can be achieved using 1 cm thick glass sheet. Figure 2.6 shows the final module design complete with the short transmission line section which passes through the oven wall connecting the DPFL system to the discharge electrodes.

Following the integration of the spike line into the system and successful operation of four DPFL modules in parallel a twelve module system, complete with spike line, was designed and built for driving the mercury bromide laser. Photographs 2.1 and 2.2 show the final pulsed power supply with the top cover removed and from the side with the cover in place. Each of the twelve DPFL modules is charged through its own inductor which provides isolation between the modules, and switched by its own thyratron. Initially type CX 1685 glass thyratrons were used to switch the individual modules and these were cooled using fans positioned in the top cover of the system. These tubes have a peak forward anode

voltage of 35 kV and a peak anode current of 5 kA [14]. They also have the advantage of being cheaper than comparable ceramic types, an important consideration when large numbers of tubes are to be operated in parallel. At the 15 kV output potential of the line into a matched 300 mΩ load each tube conducts a maximum of 4.2 kA, well below the peak anode current rating ensuring elongated tube lifetimes. Furthermore, the 70 kA μsec^{-1}, $^{dI}/_{dt}$ rating of these tubes, as measured by the manufacturers (EEV Ltd), suggests that a total $^{dI}/_{dt}$ = 840 kA μsec^{-1} should be achievable using 12 tubes in parallel, close to the design goal. Current sharing between tubes is automatic because each thyratron switches its own pulse forming network. Whilst it is possible to use paralleled thyratrons to switch a common energy storage system in low inductance discharge circuits [15], the modular approach was chosen because it has added advantages. The output impedance of the modular system is adjusted simply by removing or adding modules, allowing alterations to be made with the minimum of inconvenience. Also if failure of one of the line components occurs, replacement may be rapidly carried out by exchanging the module in which the failure occurred, keeping the down time to a minimum. It is also easy to alter the output pulse length from the system by reducing the number of sections in each DPFL module. The whole pulsed power supply is then very flexible allowing fairly rapid manipulation of its operating parameters and minimising down times if failures occur.

The paralleled thyratrons are triggered by a low output impedance (4 Ω) trigger generator a circuit diagram of which is shown in Appendix 2. The output circuit of this generator comprised of a 0.2 μF capacitor, charged to 8kV, which is discharged through an FX 2530 thyratron into the primary of a 4:1 turns-ratio, step down autotransformer. This produces a pulse with a maximum amplitude of 2 kV rising in 100 nsec which is superimposed on a bias of -150 V as required for effective thyratron operation [14]. Individual 50 Ω coaxial cables are run in parallel from the trigger generator to the grid drive circuits of each of the thyratrons shown in figure 2.7, the priming grid of each tube being pulsed (current driven). Since the anode delay times of each of the tubes is different and can be as long as 250 nsec for CX1685 thyratrons, the length of the trigger cables to each tube is adjusted to make certain that they all fire in synchronism. It is very important that the reservoir voltage of each tube is set just below the point of which the tube fails to hold off the maximum applied voltage. This ensures that the rate of rise of current through the tube is

maximised. The procedure for "setting up" the thyratrons begins with measuring the anode delay of each individual tube, once the maximum reservoir voltage is set. Working from the tube with the maximum delay time, extra cable is added in series with the trigger cables to the other tubes so that the effective anode delay times of all the tubes are matched to within a few nanoseconds. In practice it was found that the maximum tube-to-tube variation in anode delay time was 65 nsec and Table 2.1 shows the characterisation for twelve CX 1685 thyratrons operated in parallel. A constant voltage transformer was used to supply the heater and reservoir mains transformers powering the thyratrons to prevent any variation in the mains supply from upsetting the synchronisation of the tubes. An alternative method of adjusting the anode delay times is to vary the negative bias on the control grids of each of the thyratrons, however this is a costly method as each tube would require its own control grid bias supply.

2.4 Performance of the Pulsed Power Supply

The output pulse from an individual line module and thyratron, charged to 30 kV, is shown in figure 2.8 (a). The peak output voltage is 15 kV and the 10-90% voltage risetime is observed to be approximately 50 nsec into the matched 3.6 Ω load, which represents a dI/dt of 83 kA μsec^{-1}. Careful 'fine-tuning' of the values of the line inductors was carried out to set the line impedance as close to 3.6 Ω as possible. The absence of any significant reflection suggests that the line modules have a characteristic impedance very close to the design target. Although the peak output voltage is 15 kV, which would be expected under matched conditions the pulse duration is much longer than anticipated (~ 240 nsec FWHM), due to a long tail on the pulse. This observation is discussed in more detail later.

The output pulse from the complete line system comprising twelve modules charged to 30 kV and discharged into a matched 300 mΩ copper sulphate load is shown in figure 2.8(b). It can be seen that there is some slight degradation in pulse risetime (t_r ~ 55 nsec) and the pulse is broadened to ~ 290 nsec FWHM which is probably due to slight performance variations from tube to tube which cannot be completely removed. However, the pulse shape and amplitude are similar to that given by a single line module, showing parallelling of lines in this fashion to be an excellent way of producing a pulsed power supply with low output impedance. The rate of rise of current is calculated to be 910 kA

μsec^{-1}.

To test the 'spike-line', the pulsed power supply was discharged into a high impedance (70 Ω) load which simulates the behaviour of the laser gas mix during its formative phase. The resulting output pulse is shown in figure 2.8 (c). The amplitude of the spike line is less than anticipated (~ 40 kV), which was though to be due to the thyratron risetime being significantly longer than the spike duration. This hypothesis was subsequently tested on a line module with a 45 nsec 'spike line' and the amplitude of the voltage transient produced was found to be close to the theoretical value, ie. $1^1/_2$ times the line charge voltage. Finally, the time jitter in the firing delay of the system was measured and in figure 2.8 (d) a trace of 100 overlaid shots of the rising edge of the output pulse is displayed. The observed jitter is 2-3 nsec as might be expected knowing the 1 ns jitter characteristic of the thyratrons claimed by the manufacturer [14].

An assessment of the behaviour of the power supply when operated into non-matched loads, as would be encountered when using the supply to drive a laser discharge, was undertaken, and an important problem was discovered as a result of these tests. Undermatched loads cause a voltage reversal at the anode of the thyratrons at the end of the pulse, the size of the reversal depending on the degree of missmatch. It was observed that under low load conditions a number of the thyratrons broke down and an arc was visible in the vicinity of the anode and anode stem. On closer investigation it was found that this was caused by the anticipated anode voltage reversal. Although the CX 1685 thyratrons will withstand a peak inverse anode voltage of ~ 25 kV, this reverse voltage must not be applied too rapidly otherwise the tube breaks down and subsequent damage to the anode occurs. The measurements showed that the thyratrons were failing at relatively low reverse voltages (~ 5 kV) because of the rapid rate of rise of the reverse voltage (50 nsec). To overcome this problem the CX 1685 thyratrons were replaced by CX 1785 hollow anode thyratrons which can conduct current in the reverse direction should the polarity of the voltage at the anode reverse [16]. The performance characteristics of the system using these tubes is otherwise identical to the performance using the CX 1685 thyratrons.

As previously mentioned the output pulse from the DPFL system into a matched load gave a longer pulse than anticipated due to the long tail which is evident in figure 2.8 (a). Whilst the shape of the rising edge of the pulse is predictable on the basis of the current

risetime characteristics of the thyratrons, this long tail was not anticipated. Indeed when the line modules were tested to determine their characteristic impedance at low voltages (30 volts) this tail was observed to be very much less than at the full 30 kV working voltage of the system. This tail could be due to one of two characteristics of the capacitors and may well be a product of the combined effect of these. As discussed above the capacitors were found to have a capacitance which varied with applied voltage an effect which has been further investigated [17]. The characteristic pulse length from a pulse forming line constructed from discrete capacitors,C, and inductors, L, as discussed above is given by

$$\tau = 2n(LC)^{1/2}$$

where n is the number of sections in the line. If the capacitance varies as a function of voltage ie. C = C(V) in such a way that the value decreases with the applied voltage, consequently as the line discharges the capacitance increases and, from the above equation, so does the pulse length. This is in part thought to be one factor in the observed performance. The effect of an equivalent series resistance (ESR) associated with the capacitors was also investigated to account for the observed tail, theoretically using a computer network simulation pragramme and experimentally on a low voltage network. In both these investigations the tail on the pulse from the line was observed to increase as the value of ESR in the range 1-5Ω was increased. These investigations suggested that the capacitors used in the construction of the pulsed power supply have a sizeable ESR associated with them which affects the output pulse shape. This effect could be important at high repetition rates as it could lead to heating in the capacitors, hence introducing a loss mechanism and a reduction in component lifetime.

Shown in figure 5.6 of chapter 5 are device waveforms when the power supply was operated into a laser load. The risetime of the voltage pulse is observed to be ~40 ns (10-90%) and, in the case of the neon buffered laser gas mixture, has a peak value of ~30 kV at which point the gas breaks down between the electrodes. These traces are typical of those expected from self sustained discharges as, following the formative phase, the discharge voltage achieves the relatively constant value of the glow voltage, which is determined by the electrode spacing and the gas mixture. Eventually the discharge voltage decreases as the constriction occurs due to the effect of multistep ionisation processes in free mercury produced as a by-product of the discharge as discussed in chapter 1. A fuller discussion of

the effect of gas composition and the constriction process on the characteristics of the discharge is given in chapter 5. During operation of the DPFL power supply into a laser load no major problems were encountered and the only system downtime attributable to the supply was when a flashover problem developed in the unit which was quickly remedied by the use of mylar insulator in the appropriate area. As the results discussed in chapter 5 will show the pulsed power supply proved to be an extremely reliable and flexible part of the laser system enabling an investigation of the effect of the supply parameters on the laser characteristics to be undertaken with relative ease.

The repetition rate of the power supply was limited during the experimental period to 10 Hz only because of the size of the capacitor charging unit (Hartley Measurements Ltd 1 kJ/sec) available for charging the system. There is, however, no apparent reason why such a power supply in this form should not be operated at much greater repetition rates ($\leq$ 1 kHz) limited only by such factors as capacitor loss, thyratron recovery and anode dissipation. The use of ceramic thyratrons replacing the glass ones would enable repetition rates of several kilohertz to be achieved making this an extremely attractive device for use in high average power laser systems. A summary of the characteristics of the pulsed power supply and a list of its advantages are presented in Table 2.2.

CHAPTER 2

REFERENCES

1. M.H.R. Hutchinson, Applied Optics 19, 3883 (1980).
2. Ch. A. Brau in Excimer Lasers, Topics in Applied Physics Volume 30, Editor Ch.K. Rhodes, 2nd edition (1984).
3. D.E. Rothe, J.I. Levatter and R.L. Sandstrom, Helionetics Technical Report on ONR contract N00014-82-C-0087 (1982).
4. R.W. Wayant and J.G. Eden, Appl. Phys. Lett. 33, 708 (1978).
5. J.I. Levatter and S.C. Lin, J. Appl. Phys. 51, 210 (1980).
6. Hans Cirkel, Private Communication.
7. K.J.R. Wilkinson, Some Developments in High Power Modulators for Radar, J. Inst. Elect. Engs. Pt IIIA 93, 1090 (1946).
8. K.J. Coekin, High Speed Pulse Techniques, Chapter 5, Pergamen Press.
9. G.N. Glasoe and J.V. Lebacqz, Pulse Generators Dover Publications Inc. (New York 1948).
10. M.R. Osborne, P.W. Smith and H.R. Hutchinson, Optics Comm. 52, 415 (1985).
11. K. Matsumoto, K. Sueoka, M. Obara and T. Fujioka, Rev. Sci. Instrum. 51, 1046 (1980).
12. Manufacturers Data Graphs, Morgan Matroc Ltd.
13. D.S. Evans and G.R. Jessop, VHF-UHF manual, Section 11, Royal Society of Great Britain, 3rd edition (1976).
14. EEV Ltd. Thyratron reference manual.
15. G. McDuff, 3rd IEEE Pulsed Power Conference Proceedings, 308, Albequerque 1981.
16. G. McDuff, K. Rust, H. Menown and C. Neale, EEV Technical reprint No. 147.
17. C.R. Wilson, Private Communication.

a) Cable Line

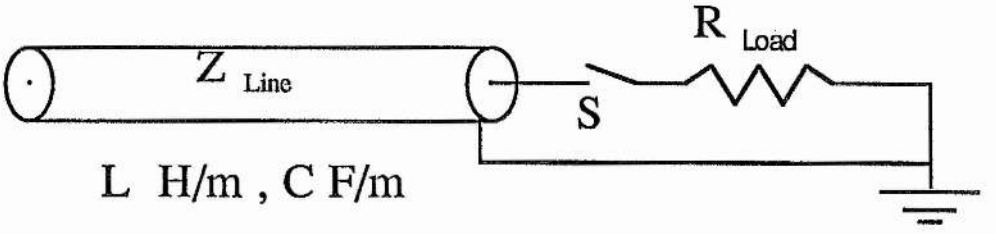

b) Discrete Components

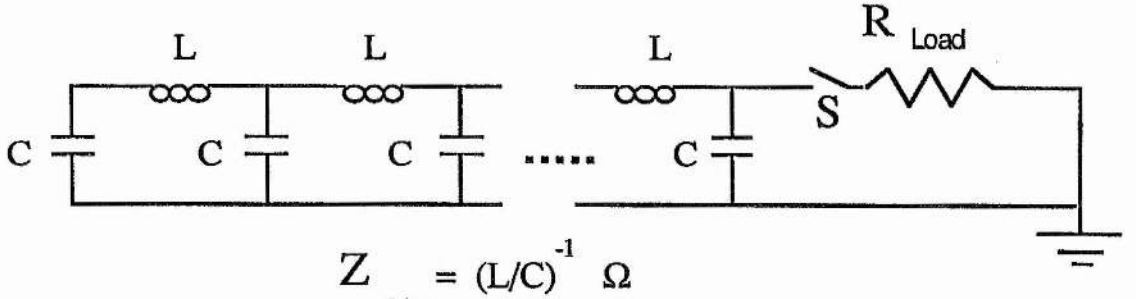

$$Z_{Line} = (L/C)^{-1} \ \Omega$$

$$\text{Delay} = (LC)^{-1} \ \text{sec/section}$$

c) Impedance Discontinuity

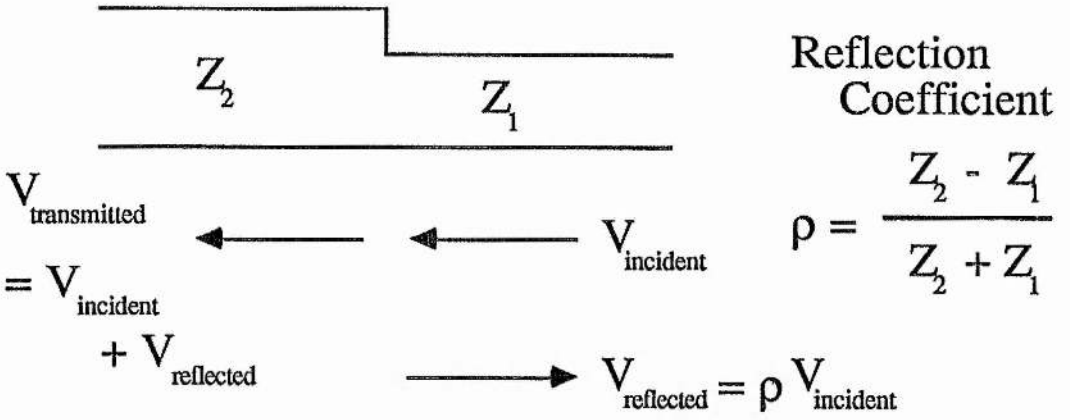

FIGURE (2.1): Characteristics of pulse forming lines constructed from a cable and discrete components.
Also shown is the effect of an impedance discontinuity on a wave propogating along the line.

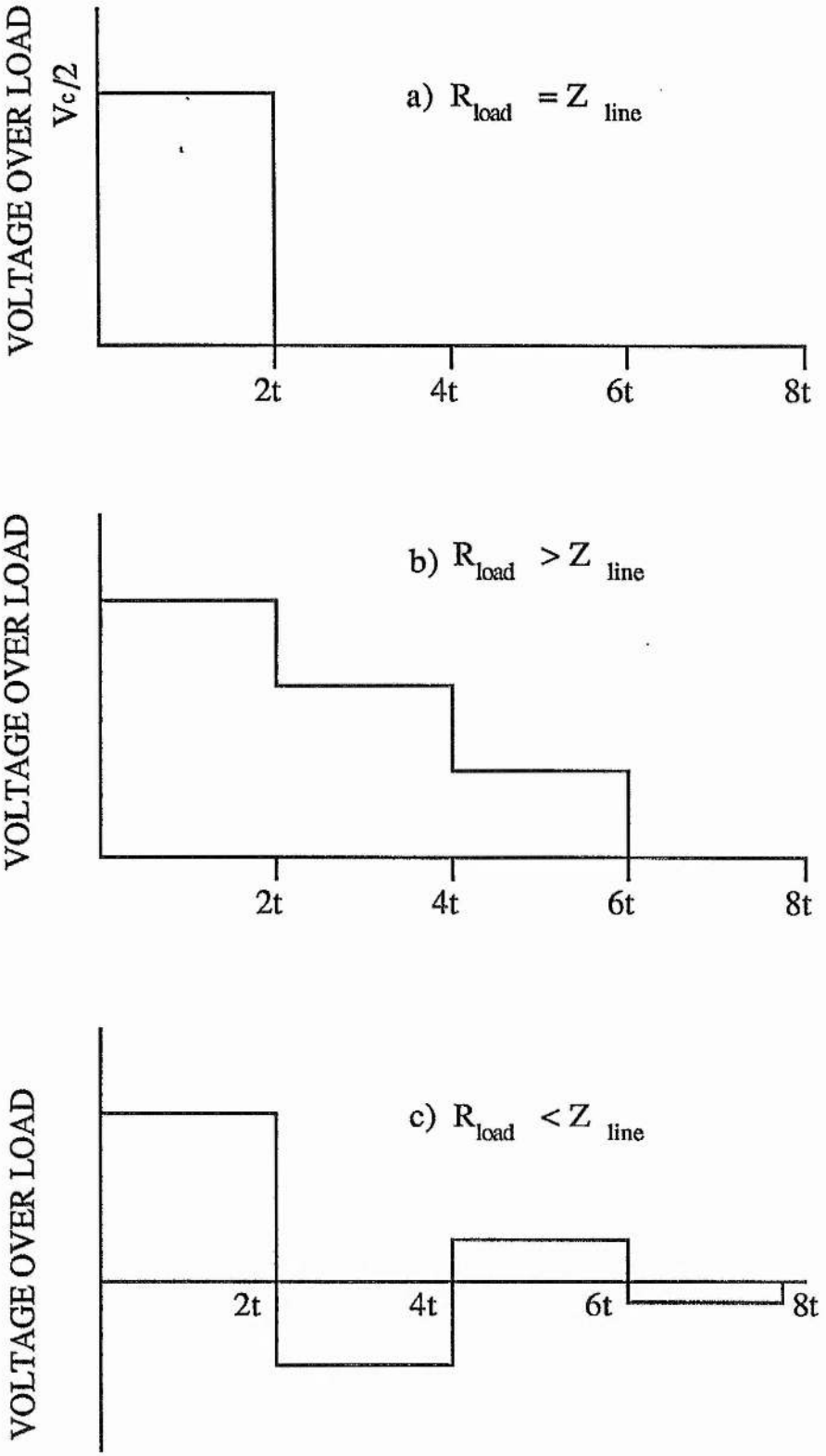

FIGURE (2.2) : Voltage over various pulse forming line loads. The ideal voltage pulse is produced under the matched load condition $R_{load} = Z_{line}$.

a) Blumlein configuration

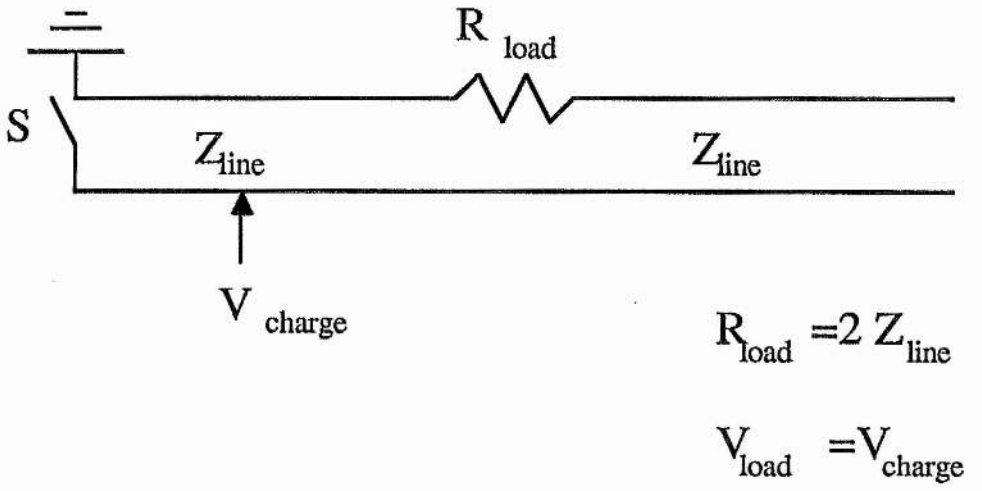

b) Double pulse forming line

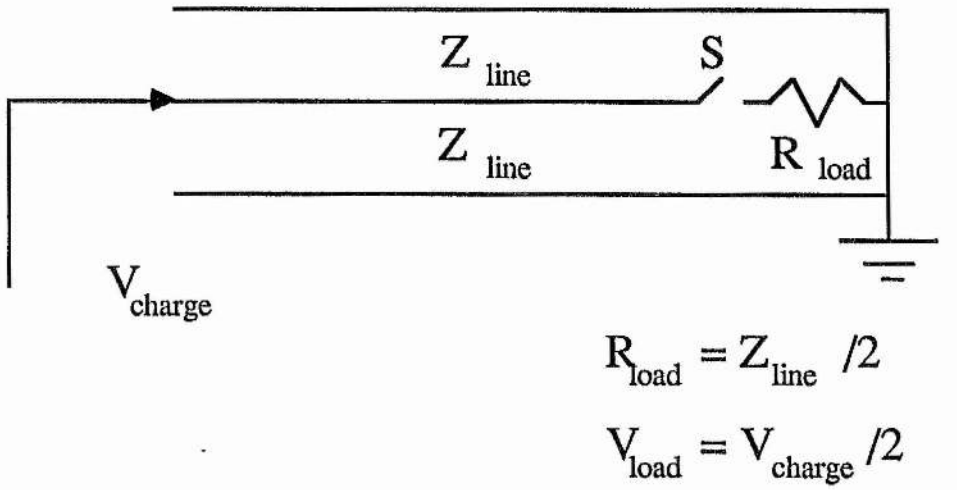

FIGURE (2.3) : Different pulse forming network configurations triggered by switch S and terminated in load R. The matched load conditions for the configurations are indicated.

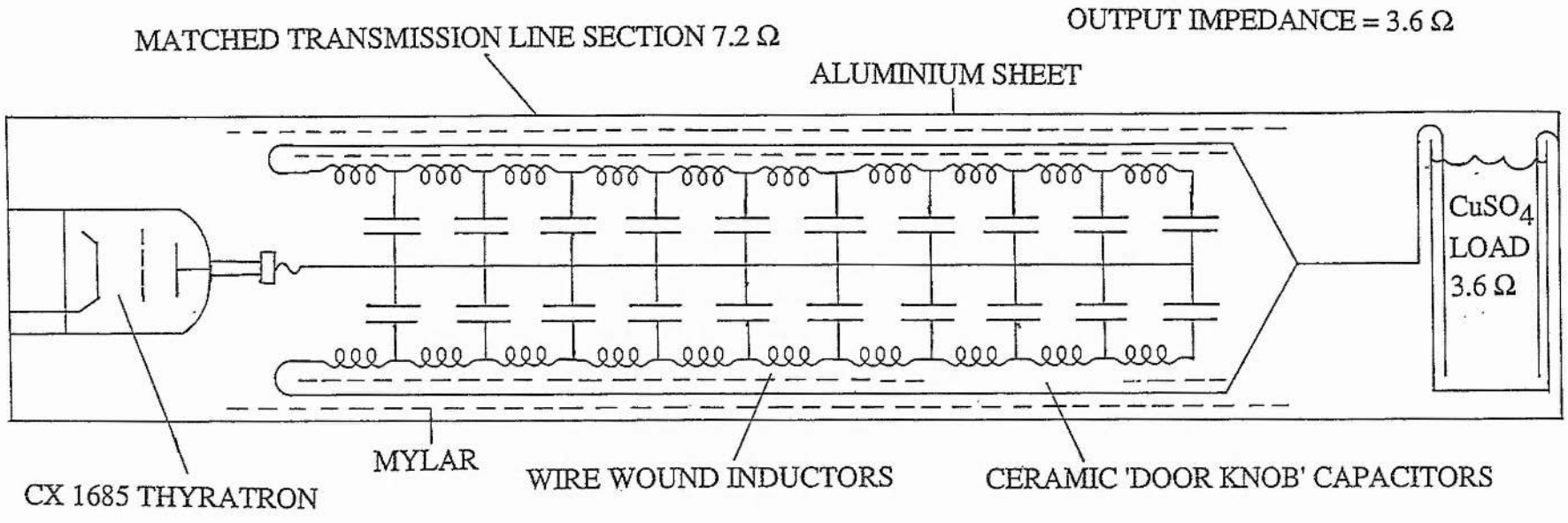

FIGURE (2.4) :Double pulse forming line module. Twelve modules to be run in parallel to produce a system impedance of 300 mΩ.

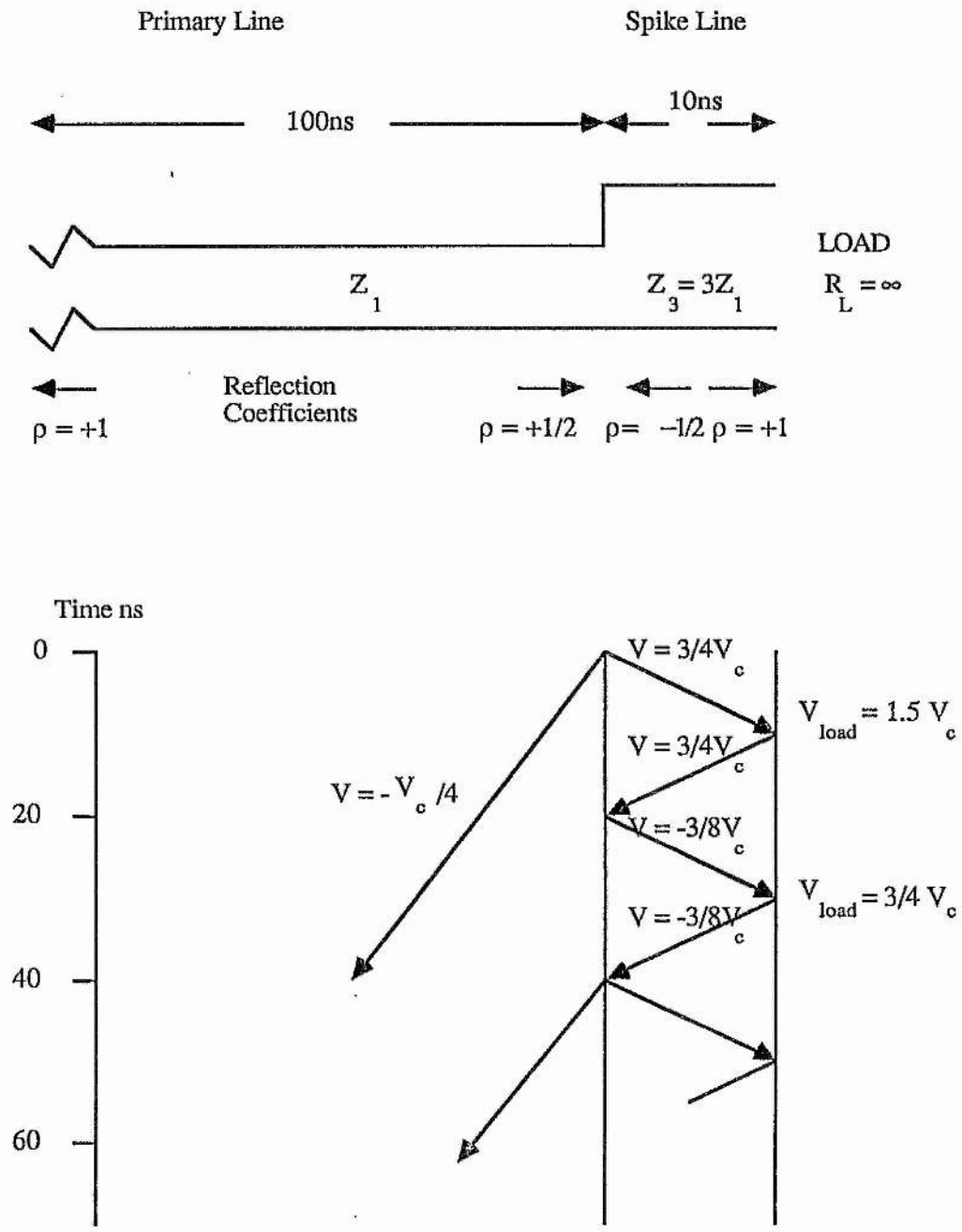

FIGURE (2.5): Lattice diagram predictions showing spike line operation into infinite load.

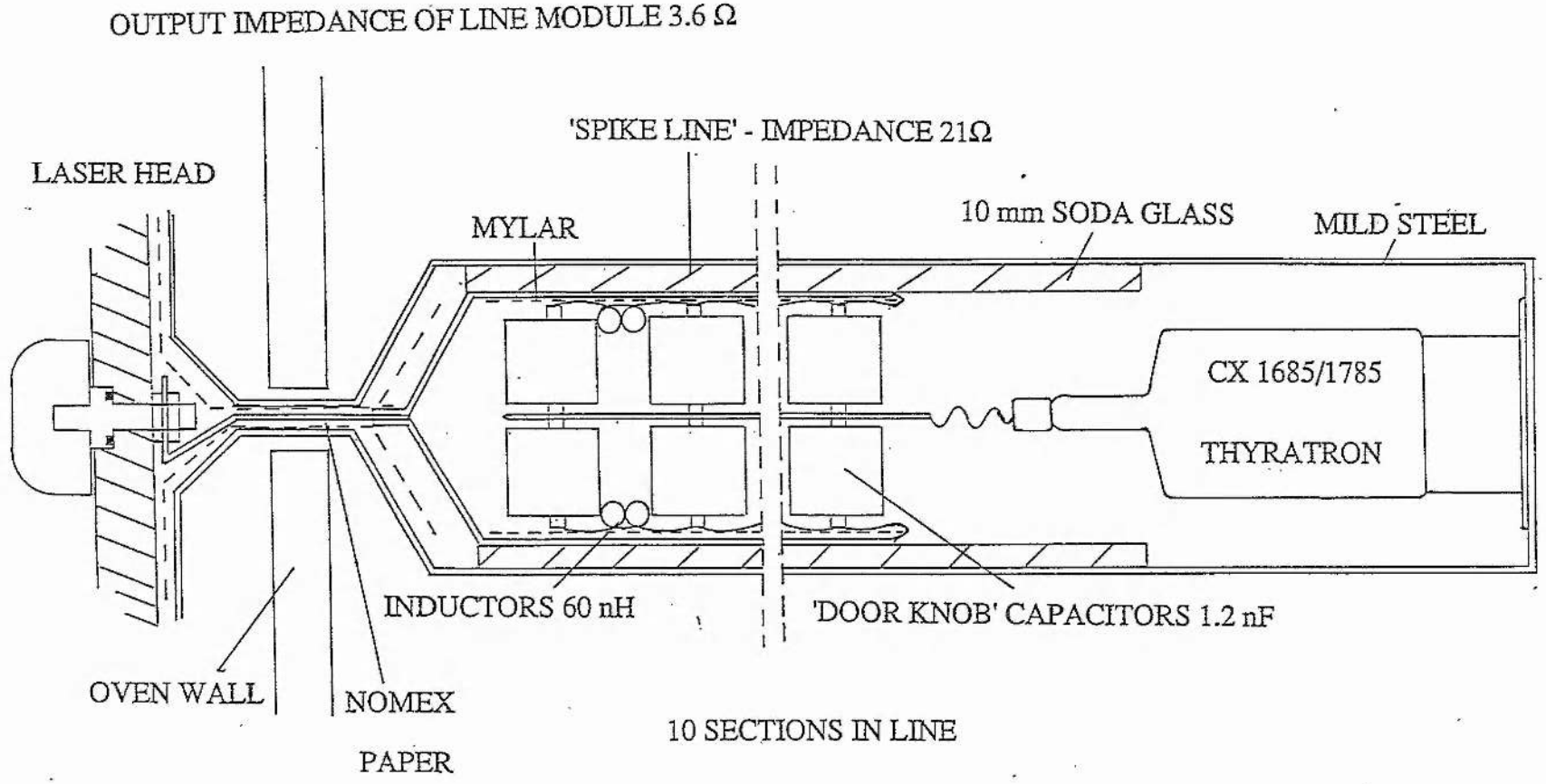

FIGURE (2.6) :Final module design with 'spike line' incorporated. Also shown are the feeds to the laser head.

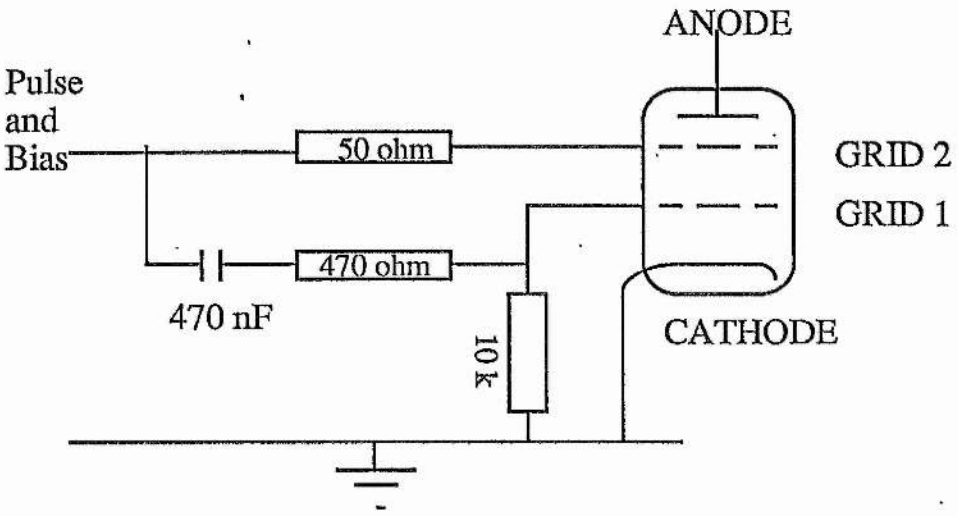

FIGURE (2.7) : Thyratron grid drive circuit

TUBE POSITION	RESERVOIR VOLTAGE (volts)	RELATIVE ANODE DELAY (nsec)
1	6.8	20
2	6.8	30
3	6.9	25
4	6.9	40
5	6.8	35
6	6.9	0
7	6.8	25
8	6.5	65
9	6.8	40
10	6.8	35
11	6.8	15
12	6.8	25

TABLE (2.1) : Maximum reservoir voltages and relative anode delay times for the twelve CX 1685 thyratrons used in the pulsed power supply.

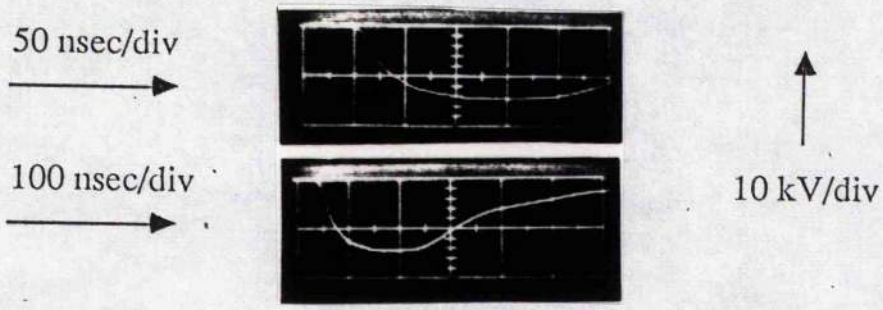

a) Output of a single line module into a matched 3.6Ω load.

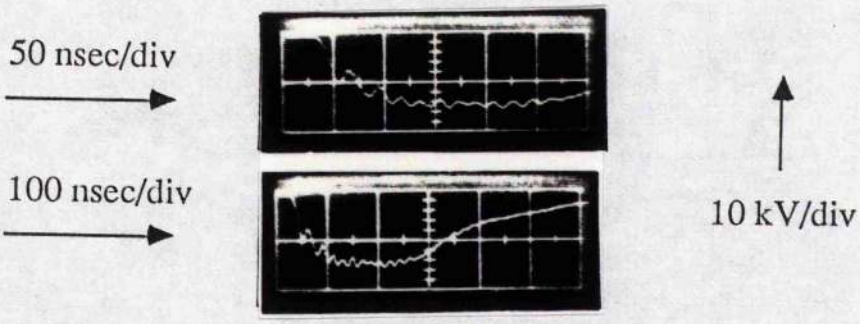

b) Output of full DPFL system (12 modules) into a matched 300mΩ load.

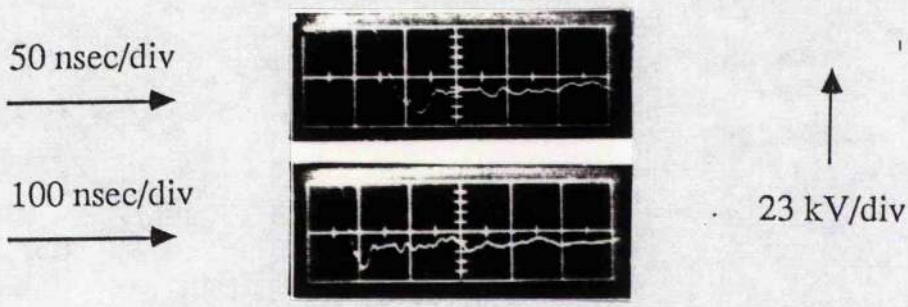

c) Output of full DPFL system into a 70 Ωload to demonstrate 'spike line' operation.

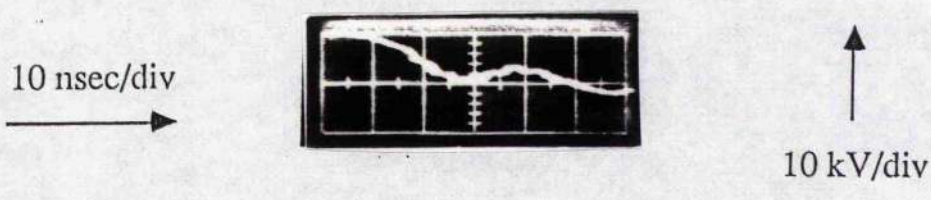

d) 100 overlaid ouput pulses from full DPFL system (rising edge) showing 2-3 nsec jitter performance.

FIGURE (2.8) : Output pulses from the pulsed power supply

SUMMARY OF DPFL PULSED POWER SUPPLY PERFORMANCE

LINE IMPEDANCE	300mΩ - 3.6Ω
MAXIMUM DC CHARGE VOLTAGE	35kV
MAXIMUM REPETITION RATE	>100 Hz present system limited to 10 Hz by available charging unit
VOLTAGE PULSE DURATION	~240 nsec
RISETIME INTO MATCHED LOAD	50 nsec equivalent to ~10^6 amps /μsec
JITTER	2 nsec command fired

ADVANTAGES OF THIS PULSED POWER SUPPLY

THYRATRON SWITCHED	Long life and reliability Command fired with low jitter
INCORPORATED SPIKE LINE	Automatic and simpler alternative to pulser sustainer type circuits. Spike voltage = 1.5 x charge voltage
MODULAR CONSTRUCTION	Line characteristics easy to alter eg variable t_p , impedance No current sharing problems with thyratrons

CLOSE MATCHING TO OPTIMUM V_{ss} THEREFORE EFFICIENT

TABLE(2.2):Characteristics of theDPFL pulsed power supply.

PHOTOGRAPH(2.1):Side view of the DPFL system showing the connections to the laser head.

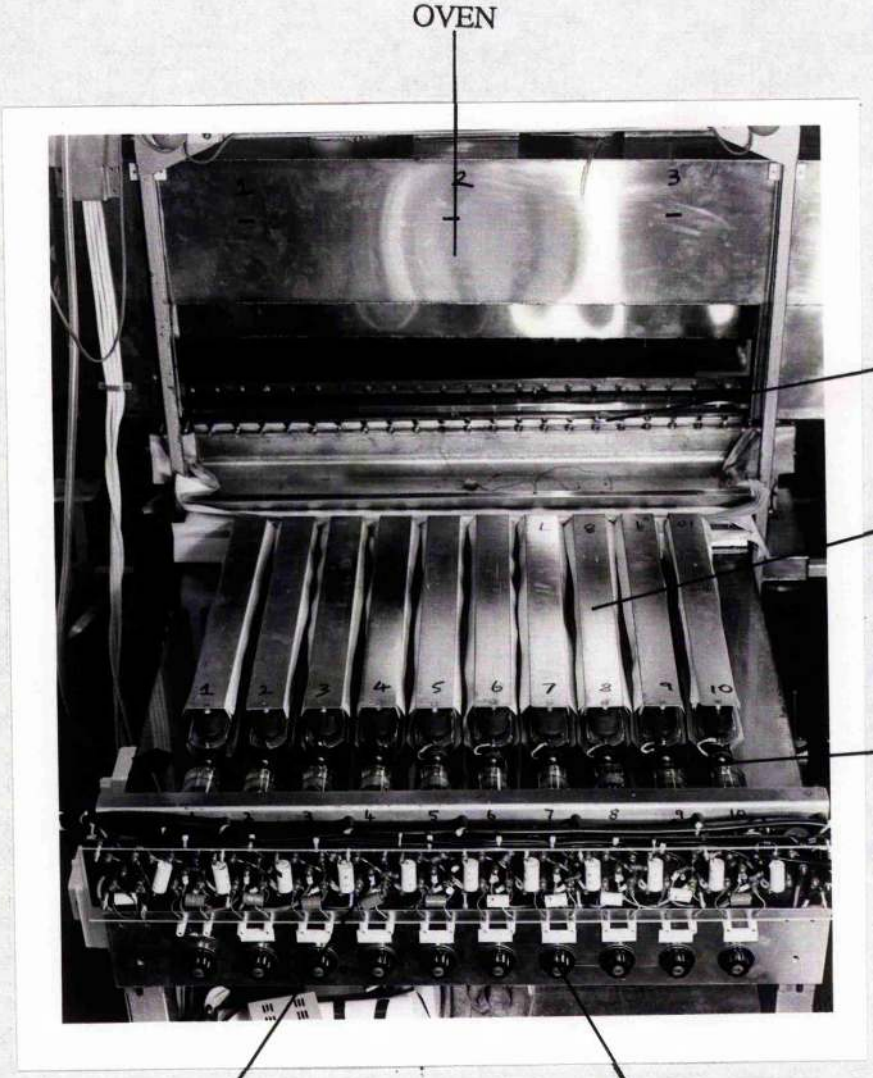

PHOTOGRAPH(2.2): View of the DPFL system with the top cover removed showing ten lines in parallel.

CHAPTER 3

THE X-RAY SOURCE

3.1 Introduction

The concept of preionisation by X-rays was introduced in chapter one and is elucidated here. Following a discussion of the requirements of the X-ray source and a brief review of X-ray production a description of the device designed and constructed for use with this laser is presented. Finally, the performance of the initial source developed and the improvements made to this source in order to achieve the required operating characteristics necessary for effective preionisation of the laser are outlined. Appendix 1 outlines some of the notation used in the text and may be useful to the reader.

As briefly mentioned in chapter 1 the technique of X-ray preionisation has proven to be an excellent method for the preionisation of large volume, high pressure laser devices for the generation of high energy and high spatial quality laser beams. This technique has several advantages over other commonly used preionisation schemes, such as the use of electron beams and uv radiation, for scaling to larger discharge dimensions. When an X-ray photon of moderate energy, typically 20-100 kV, propagates through a gas mixture the primary absorption process is by photoionisation [1], leading to the generation of high energy photoelectrons. These undergo cascade ionisation collisions until their energy is lower than that necessary to further ionise the gas (typically 30eV), a process which results in the formation of a uniform density of preionisation electrons. The mass penetration depth in high pressure gases of X-rays in this energy range [2], as compared to those of electrons [3] or UV photons [4], enables large volume discharges to be uniformly ignited without the scalability limitations of these other techniques due to their inability to produce homogeneous preionisation throughout the gap. As previously mentioned other benefits of X-ray preionisation schemes are the elimination of the fragile foil window required in e-beam systems and the removal of contamination caused by the presence of sparks used in the production of ultraviolet radiation, leading to longer gas lifetimes. The ability to externally control the spatial extent of the preionisation source has also been shown to be useful in affording control over the extent of the discharge leading to a higher degree of

uniformity by Tallman and Bigio [5] and also in the work presented in this thesis.

3.2 X-ray Source Requirements

Although the performance required of the X-ray source in terms of dose produced in the discharge volume and uniformity were not known at the time of design, a review of work performed by other authors gave an indication of what was required for effective preionisation of the laser. Tallman and Bigio [5] in experiments with an XeCl laser found as little as 0.1 mrad of 20-40 KeV X-rays measured in the cavity was sufficient to produce a highly uniform discharge although they say nothing of the uniformity of their source. Steyer and Vogues [6] have also recently shown that a dose as low as 0.2 mR produced from a source using an 85 kV voltage pulse is sufficient for preionisation of an XeCl laser, but higher doses of ~3 mR were required for their KrF laser. Levatter and Lin [7] used a low energy, 3J, low voltage, 50 kV, e-beam source with a pulse length of 150 nsec in there X-ray source developed for use with rare gas halide lasers resulting in good output uniformity but unspecified dose. They also indicate that total pulse energies as low as 1J may be sufficient to produce an effective preionisation source for large volume discharge lasers. In their high energy, high efficiency, XeCl laser, Osborne, Smith and Hutchinson [8] utilised a source producing an average dose of 55mR with spatial uniformity of $\pm$50%, the applied voltage to the diode having a peak of 110kV and a duration of 350 nanoseconds (FWHM).

Sumida et al.[9] used a source with an applied voltage of 160kV which produced a dose of 60mR at a distance of 60cm from the X-ray generator. By means of spacing the discharge volume from the preionisation source their arrangement provided extremely uniform preionisation in the discharge volume. Their experiments indicated that uniformity of preionisation was not required in a direction parallel to the electric field with respect to laser energy although spatial homogeneity of their KrF laser output was affected by this. However in the direction perpendicular to the field nonuniform preionisation can lead to the growth of discharge instabilities and rapid termination of the laser pulse. Kline and Denes [10] theoretically studied the effect of uniformity of the preionisation from a pulse of ultraviolet radiation in CO_2 lasers their model results showing that for large volume discharges uniform preionisation is not required parallel to the applied field as space charge effects distort the electric field altering the local ionisation, resulting in the formation of a

uniform discharge. Taylor [11] in an experimental study of laser induced preionisation in XeCl lasers has also observed this effect and the deterimental effect on discharge stability of nonuniform preionisation in the direction normal to the applied field. The technique of X-ray preionisation is a method by which these conditions of uniformity can be met with its proven ability to preionise uniformly the volume between two electrodes and the excellent transverse uniformities achievable with these sources [7].

Although these results are mainly pertinent to rare gas halide laser systems they can be used as a good approximation to the requirements necessary for discharge stability in mercury bromide lasers. However, in the majority of these laser systems the design is such that the X-ray source and the cavity are adjacent, so loss of dose through divergence from the source is minimal. Owing to the rather obtrusive nature of the oven surrounding the cavity of our laser as described in chapter 4, the centre of the discharge volume and X-ray source are separated by a distance of 25 cm. The X-ray dose decrease due to divergence would be expected to fall off approximately with an $r^{-1.5}$ dependence [6], where r is the distance from the source, in the design of the X-ray source it was therefore essential to ensure sufficient dose could be produced inside the cavity situated some distance away.

The optimum X-ray energy for preionisation is determined by a trade off between absorption of X-rays in the gas to produce the required initial preionisation electron density through photoionisation and the transmission of X-rays through the 'window' in the cavity into the discharge volume. A discussion of the design of the X-ray window in the cavity is given in chapter 4. As shown in figure 4.3 of chapter 4, for a typical buffer gas of neon at 5 atmospheres approximately 3% of 20 keV X-rays are absorbed in 5 centimetres. The reduction in intensity of the X-rays being minimal ensuring good uniformity of preionisation is achieved throughout the volume. Lower X-ray energies would be absorbed to a greater extent in the gas causing more photoionisation but at the expense of volume preionisation uniformity. In practice the transmission of X-rays into the cavity places a lower limit on the energy of X-rays which may effectively be used. The same figure shows only 10% of 20 keV X-rays are transmitted through 2 mm of aluminium, a material commonly used in X-ray windows for its relatively high X-ray transmission properties and a more realistic minimum useable energy is 40-50 keV.

In a theoretical analysis of the use of X-ray radiation for preionisation of high pressure gas discharges, Kozyrev et al. [12] make an estimate of the ionisation produced in a gas by this technique. They define a factor called the beam utilisation efficiency which is the ratio of the X-ray energy absorbed in the gas per unit volume to the energy of the electron beam per unit surface area of the target from which the X-rays are generated (a fuller discusion of the principles of X-ray generation are given later). As the beam voltage is decreased from ~200 kV this factor remains relatively constant as the decrease in intensity of X-rays produced is offset by an increase in their absorption coefficient in the gas so the production of photoelectrons and hence initial electron density is unaffected. However at voltages of 50 kV and below the efficiency decreases rapidly as the lower energy radiation is absorbed more strongly in the window material. The results of this analysis indicate that low accelerating voltages, ~50 kV, can be used in the production of X-ray radiation for preionisation, the lower limit being determined by the absorption of the window material as discussed above. This theoretical analysis was backed up by an experimental investigation in which the possibility of using X-rays of 30 keV photon energy to preionise discharge gaps of several tens of centimetres is demonstrated.

The X-ray preioniser described here was designed for the production of X-rays in the 50 keV region and to have a temporal duration of ~200 nsec with reference to the systems discussed above. Although the required dose in the cavity for effective preionisation was unknown for this laser it was estimated, on the basis of the above results, that a dose of several mR would suffice though this figure required experimental confirmation.

3.3 Production of X-rays

The methods and principle for generating X-rays are well understood and documented [see for example 13,14,15] and only a resume is given here. When a high energy beam of electrons, formed in a vacuum diode, strikes a target of high Z material they are decelerated resulting in the production of bremsstrahlung or breaking radiation. The spectral energy distribution of the emitted radiation is characterised by a continuous photon energy spectrum from zero to the maximum energy defined by that of the incident beam, superimposed with the characteristic spectrum of the target material. The mean

photon energy of the bremsstrahlung radiation occurs at approximately twice the minimum wavelength and the peak intensity at 1.5 times the minimum wavelength [1] where

$$\lambda min = hc/E_b$$

and h is Planks constant, c is the velocity of light and E_b is the maximum energy of the electron beam. The characteristic spectrum of the target material is produced as electrons in the inner shells of atoms, excited by the impact of high energy electrons, are replaced by an electron from a higher energy shell with the release of a photon of energy $h\upsilon = E_f - E_i$, where E_f and E_i are the final and initial enegies of the electron. The characteristic spectrum of the target anode is then discrete and peculiar to that material as it depends on the electron energy levels in the atom.

The intensity, I, of the characteristic line produced depends on the applied voltage, V, and the critical excitation voltage for the line, V_c, which is calculated from the corresponding absorption edge, through the relationship [2,15]

$$I = k(V-V_c)^n$$

where k is a constant and n lies between 1.5 and 2. This relation is valid for values of V up to $V = 6V_c$ with the greatest intensity of line emission to bremsstrahlung occuring in the region $3V_c < V < 6V_c$. Line radiation is, however, isotropic unlike the continuous bremsstrahlung spectrum as discussed below and can be absorbed in the anode material itself. The use of line spectra in preionisation has a possible advantage over bremsstrahlung radiation in that if the emitted line overlaps with the absorption edge of the gas or an additive then the effect of the source would be enhanced leading to an increase in the preionisation electron density produced. In practice achieving this overlap is difficult because the characteristic lines of elements with high atomic number (used for target materials to maximise the X-ray production process as discussed below) are at a shorter wavelength than those of the lighter gaseous elements, such as neon, used to buffer the laser mixes. For a tantalum anode (Z=73) the critical excitation votage of the k edge is ~70 kV, the longest wavelength line emitted is 0.22Å whilst the absorption edge in neon is >14Å. Also with this relatively high excitation voltage, comparable to the applied voltages

of 100 kV typical of the device described here, the intensity of the line spectrum relative to the continuous spectrum will be low.

The X-ray production efficiency for bremsstrahlung radiation is given approximately by the formula $\eta = EZ/700$ [1], where E is the incident electron energy in units of MeV and Z the atomic number of the target material. In order to maximise the electron beam to X-ray conversion efficiency high Z materials such as tungsten, tantalum or molybdenum must be used. In the case of tantalum, the material chosen for the target material in the X-ray source desgned for this laser as will be discussed, and an electron energy of 50 keV, the production efficiency is only 0.5% showing that only a small part of the incident electron beam energy is converted into radiation and the process is very inefficient.

Targets, or anodes, may be used in either the transmission or reflection geometries as depicted in Figure 3.1. In the reflection orientation the target is solid and X-rays backscattered from the target are utilised, the scattering angle of the radiation determining the device design. For a 100 keV electron beam the maximum intensity of the X-rays is at 60^{o}-80^{o} to the beam whilst for higher energy e-beams, > 0.5 MeV, the radiation is produced mainly in the direction of the incident beam [14]. In the transmission geometry, used in the X-ray source described in this thesis, the target is a thin foil and the forward scattered X-rays are used. The optimum foil thickness is determined by the electron absorption and X-ray transmission properties of the material and in general is on the order of one electron stopping range (ESR). It is obviously desirable to stop the majority of the incident electrons in the foil to make optimum use of the beam in the inefficient X-ray production process. However, the absorption of X-rays is governed by the exponential rule [2], $I = I_0 \exp(-\mu x)$ where I_0 is the incident intensity, I the transmitted intensity, μ the linear absorption coefficient and x the thickness of the absorber. The large linear absorption coefficient of the high Z target material would result in excessive self absorption of the X-rays if the foil thickness was too great. For 50 keV electrons in tantalum the optimum foil thickness determined by the ESR is ~ 5 μm [3].

Typical electron beam requirements for X-ray generators to be used as a preionisation source in discharge excited lasers are relatively modest. Accelerating voltages of 100 kV, diode current densities of several A cm^{-2} and pulse lengths around

electron beam generators which can satisfy these requirements including corona plasma cathodes [16], thermionic emitters [17] and cold cathode emitters in the form of lengths of razor blades and carbon fibre [18]. Corona plasma cathodes have received attention recently as a new type of cathode for high energy electron beam generation [19] which was subsequently developed for use as an X-ray preioniser in an excimer laser system [16]. A surface discharge at a metal-dielectric-vacuum interface creates a plasma sheath which acts as the source of electrons for the beam in these devices. The technology of these however is still in its infancy. Thermionic emitters [17] operate at temperatures of ~ 800-2000 ^{o}C where electrons emitted from the surface of the cathode produce the source for the e-beam. Cathode materials such as lanthanum hexaboride, thoriated tungsten and barium tungsten are commonly used in these devices however they are susceptible to poisoning and require large heater powers for operation. The choice of a cold cathode emitter for use in generating the electron beam in the X-ray source described here was based on the relative simplicity afforded by this technique, its proven ability in similar systems and the available expertise in our lab at the time.

Materials used as cold cathodes for electron beam generation have included stainless steel razor blades, thin foils and carbon felt [20]. The study of carbon felt emitters was driven by the desire to produce a long life electron source. After repetitive operation blade emitters suffer from erosion which affects the performance of the device. In a study by Loda and Meskan [21] they used scanning electron micrographs to predict the lifetime of blade cathodes. By estimating the material loss rate from the cathode and suggesting a lifetime of the blade based on the amount of material loss they predicted the number of shots to the end of the cathode life. Typical lifetimes for operation of these blades are limited to ~10^6 shots. However, for the relatively low repetition rates we required (~ 10 Hz), and in the first instance to produce a functional X-ray source for single shot operation a blade cathode was chosen.

The principle of operation of such cathodes has been extensively studied and documented [22,23]. When an electric field on the order of 10^7 V cm^{-1} is applied to an emitter surface there is strong field emission of electrons. To obtain such fields without the use of excessively high voltages cathodes with sharp features, such as razor blades, thin foils or arrays of spikes or pins, are used to give microscopic enhancement of the

applied electric field. The emission process begins from metallic whiskers which quickly (~ 1 nsec) heat up during a short resistive phase, explode and cover the surface of the cathode with a plasma sheath which acts as a zero work function emitter of electrons . This then becomes the source for the e-beam. In the case of an emitter with a relatively low number of shots there will be sufficient microstructure at the surface to enable the formation of this plasma to take place even at applied voltages of a few tens of kilovolts. However after several thousand shots the emission sites are eroded and consequently the required applied voltage for uniform emission increases and the blade approaches the end of its useful lifetime. The plasma formed at the surface of the emitter crosses the anode-cathode spacing at a velocity of 1 to 5 cm μsec^{-1} eventually resulting in plasma closure of the gap and collapse of the diode impedance. For pulse lengths of 300 nsec and separations of a few centimetres typical of flash X-ray sources plasma closure is not a problem.

The current density in the e-beam is space charge limited and can be approximated by the Child-Langmuir relationship[24]

$$j = 2.335 \times 10^{-6} \frac{V^{3/2}}{D^2}$$

where V is the applied voltage (volts), D the anode cathode spacing (cm) and j the current density in A cm^{-2}. For voltages of 100 kV and gap separations of a few centimetres current densities on the order of several A cm^{-2} are predictable, sufficient to produce the required X-ray dose. This space charge limited behavior of these emitters enables the prediction of current densities and the operational characteristics of various designs and scaled versions of cold cathode guns to be determined. Treatments by Forster [25] and Martin [26] have attempted to include the effects of different geometries and of the emitter support structure on the diode impedance it is, however, time varying and difficult to accurately calculate. Whilst these treatments allow an estimate of the operational conditions of the diode to be made the final optimisation of the electron beam in the preionisation source was through experimentation on the device as is discussed later.

3.4 X-ray Diode Design

The cold cathode electron gun for the X-ray generator is based on a fairly conventional design and a cross-section is shown in figure 3.2. The vacuum chamber is constructed from 321 stainless steel and has dimensions 150 cm by 30 cm by 25 cm. The front plate of the chamber is removable and houses the tantalum foil target and window through which the generated X-rays pass. To match the size of the X-ray window in the laser cavity the window in the diode is 100 cm long and 8 cm wide and sits in the same horizontal plane as that of the cavity when the two are in position for operation of the laser. For similar reasons to those to be discussed in chapter 4 of X-ray transmission and structural strength the window is constructed from 1 mm aluminium and a Hibatchi style grid provides the extra support to prevent excessive flexing of the window under the pressure differential between the room and the high vacuum in the cavity. Typically, the chamber is evacuated using an Edwards Diffusion pump (Model EO4) to pressures below 10^{-5} mbar to ensure the mean free path of electrons is greater than the anode-cathode separation and the electrons are accelerated across the full gap achieving the maximum possible energy afforded by the applied electric field. A further important benefit of high vacuum operation is that of increased breakdown potential under these conditions which means the size of the diode structure can be kept reasonable without any breakdown problems from the cathode structure to the earthed casing resulting. The vacuum seals on the X-ray window and all other parts of the chamber are by nitrile rubber O-rings. The seals for the front plate are held in place by a perspex spacer which sits between it and the rest of the diode as shown the figure. This serves to electrically isolate the front plate, when the arrangement is clamped together by nylon bolts, and allows current through the diode to be measured using an array of low impedance resistors which bridge the insulator as discussed later.

For reasons previously discussed the anode is made from a strip of 7.6μm Ta foil and is of similar dimensions to the window. The foil is backed by thin aluminium sheet (Alcan foil) to give it more rigidity for ease of handling and is physically and electrically connected to the front grounded plate by means of silver loaded epoxy adhesive covering the area of the window. The position of the foil and the other parts of the diode assembly are shown in photograph 3.1. The cathode structure is also attached to the front plate by four perspex insulators which allow accurate positioning of the cathode above the anode, a

four perspex insulators which allow accurate positioning of the cathode above the anode, a factor found experimentally to be important for uniform X-ray production. These are designed as shown in figure 3.2 and photograph 3.1 with a 'saw tooth' type appearance, made in such a way that one edge of the cut is perpendicular to the centre line of the insulator whilst the other is chamfered at 45^{o}. This has two effects; it maximises the tracking length between the cathode structure and the supports to which the insulators are attached which are at ground potential and the design is such that the breakdown strength of the insulator surface is increased. The surface breakdown process has been well studied [27] and is attributed to electron emission from the dielectric followed by multiplication along the surface in the direction of the applied field by secondary emission. This process continues until a sufficient density of electrons exists to form a conducting channel over the surface of the insulator and breakdown occurs. By designing the shape of the insulator such that electrons emitted from the surface are pevented from returning to multiply in this fashion, the surface breakdown strength can be improved. It is important to ensure that the insulator is then used in the correct orientation to the field to ensure the highest flashover strength is achieved, as is discussed later.

The whole cathode structure is situated centrally in the chamber and at suitable distances from the walls to ensure vacuum breakdown does not occur on application of the high voltage pulse. The cathode consists of a flat plate on which the 90 cm long field emitter is centrally positioned surrounded by a 'race track' structure . The 'race track' is constructed from copper tube and serves two purposes; to form an edge to the unit with sufficient radius of curvature from which unwanted field emission will not occur and to help focus the e-beam produced in the direction of the anode. Beam divergence from blade emitters can be large [28] and is an important consideration where efficient utilisation of the beam is required as for the production of X-rays from a target of finite size. By shielding the beam through use of the cathode support which is at the same potential as the emitter, the divergence is reduced and the beam propagates in the desired direction towards the foil anode. More elaborate focusing arrangements have been used in diodes for electron beam sustained lasers where efficient utilisation of the beam is of paramount importance [29], however optimisation of such a system has proven to be difficult. The form of the race track and cathode support are seen in photograph 3.1.

taken in the design of the support structure to ensure no sharp edges or curved surfaces with too small radii are present from which field enhancement and vacuum breakdown could ensue, this is one of the main functions of the 'race track' as outlined above. Also the preparation of the support structure is an important factor from this respect. The procedure for this included ensuring good cleanliness in the cavity using solvents for cleaning all the surfaces of the cathode structure to remove any contminants and possible protruding particles from the surface, and coating the race track, insulators and blade support structure in a layer of diffusion pump oil. This was applied in a 50-50 solution with acetone using a paint brush to achieve a uniform coating. Once the solvent evaporates a layer of oil is left which is effective in supressing the emission of electrons from the surface. The low vapour pressure of this type of oil ensures the cavity may still be evacuated to the low pressures necessary for operation of the diode. This treatment was routinely carried when the diode was brought up to atmosperic pressure and dismantled for inspection or modification, prior to reassembly and evacuation.

In figure 3.2 the method by which the cathode is attached to the output from the oil insulated pulsed power supply is shown. The pulsed power supply described in the following section is kept under oil (Shell Diala BG) to prevent breakdown problems from occuring at the high operating voltages of the supply. A stalk from the rear of the cathode support connects by a push fit connection to a second stalk in turn connected via a high voltage, field graded, oil to vacuum bushing, to the output from the pulsed power supply. These stalks are also treated with the oil solution as for the other parts of the structure to prevent any unwanted electron emission and possible breakdown problems. As discussed above, it is also important to ensure the radii of these surfaces are large enough to prevent field enhancement, this is especially important where the stalk passes through the transition section between the diode and the field grader where the diode neck and cathode shank are in close proximity. To keep the field enhancement factor at this point at a minimum it has been shown [30] that the optimum ratio of the radius of the diode neck to that of the cathode stalk is e, an important criteria to follow in the design of these parts.

The design of high voltage bushings such as that connecting the output of the pulsed power supply to the cathode of the diode is well established and has been proven to voltages well in excess of those used in this system [29,30]. It comprises a series of

voltages well in excess of those used in this system [29,30]. It comprises a series of perspex rings chamfered at 45° with aluminium rings fitted with O-rings inserted between them. The whole structure is clamped together by a number of nylon tie bars which compress the O-rings to form a good oil to vacuum seal. The aluminium rings serve to ensure the field across each of the perspex sections is uniform whilst the angle at which the insulators are chamfered is to maximise the breakdown strength of their surface. During operation of the X-ray diode no problems were encountered with this part of the device.

Even though these careful procedures outlined above were undertaken to prevent any problems with vacuum breakdown occuring, during the initial operation of the diode some difficulties were encountered. Little or no X-ray emission was generated on the first attempts and the 'sound' from the diode, which was accompanied by a flash of blue light observed in the perspex insulator around the outer diameter of the unit, was indicative of breakdown occuring. Upon inspection of the inside of the diode following a number of these discharges, marks where arcing had occured were observed on the front plate under the racetrack and below where the perspex insulators were positioned. These marks were very puzzleing as they were indicative of breakdown occuring from surfaces designed and treated to prevent field emission, which were further away from the grounded anode plate than the field enhancement blade cathode. One of the major causes of this problem stemmed from the perspex insulators described above. These had been inserted in the wrong orientation to the field thus rendering them less effective against surface vacuum breakdown [27]. Changing these and making a number of other small modifications to the structure, such as replacing some of the metal screws which held parts of the race track in place with nylon ones to eliminate any possible detrimental effects stemming from their sharp edges, allowed proper operation of the diode to be achieved.

3.5 The Pulsed Power Supply

The pulsed power supply used to generate the high voltage pulses to drive the X-ray source was developed by C.R. Wilson and P.W. Smith [31], and designed to meet the following specifications

Output Voltage 100 kV

Pulse Duration	≥ 200 nsec
Pulse Risetime	≤ 50 nsec
Firing Jitter	~ 2 nsec
Repetition Rate	10 Hz

The voltage requirement is that necessary to produce an X-ray source with a mean photon energy of ~50 keV which, as discussed above, is the value at which optimum utilisation of the preionisation source takes place. The output impedance of the power supply is chosen to match that of the diode impedance estimated from the equations discussed earlier and by reference to previous work on such systems [29]. Similarly the pulse duration and risetime specifications are based on those used in other devices which have proven adequate to produce the required preionisation electron densities in laser gas mixtures and also through experience with such systems [32]. In order to ensure that a sufficient electron density exists in the gas prior to initiation of the discharge it is important to be able to accurately control the timing of the preionisation pulse to that of the discharge pulse, hence the low jitter requirement of the supply. This should also enable accurate kinetic studies to be undertaken investigating the effect of temporal overlap of the X-ray pulse with the discharge pulse.

A supply based on the use of a stacked transmission line transformer (TLT) system was developed and integrated into the X-ray generator. Figure 3.3 shows the circuit diagram of the supply, the detailed operation of which is given in the reference and only the main features are highlighted here. A low impedance Blumlein pulse forming network is discharged into a stack of transmission lines connected in parallel. The transmission lines are made from lengths of standard 50Ω URM 67 co-axial cable whist the Blumlein is constructed from discrete capacitors and inductors. The output impedance of the Blumlein is matched to that of the parallelled cables resulting in a voltage pulse at the input ends of the cable equal to the Blumlein charge voltage. The output ends of the cables are connected in series producing voltage gain, the maximum theoretical value of the gain being equal to the number of stacked cables. The actual design however is more complicated than merely connecting cables in the appropriate fashion in order to prevent voltage droop on the output

pulse caused by the propagation of a secondary mode in the system. This entails the introduction of an inductive factor to the design of the supply which supresses the effect of the secondary mode and the reader is referred to the reference for the full details. By using voltage gain with this method to produce the final output voltage pulse, thyratrons may be used to switch the lower Blumlein charge voltage (~ 30 kV) ensuring the specifications of repetition rate and jitter are met. The circuit diagram of the trigger generator used to supply the thyratron grids with the appropriate bias and drive pulse is shown in Appendix 3.

Excellent results were achieved with the pulsed power supply when tested into copper sulphate loads showing gains of ~3.5, slightly below the theoretical maximum, but with remarkable similarities between the input pulse to the TLT and the output pulse. In practice the pulsed power supply performed well when used to drive the X-ray source and a typical pulse from the supply on the cathode of the e-beam source is shown in figure 3.4 in which the pulse generated across the diode is ~90kV with a risetime of 50 nsec and a duration of 320 nsec (FWHM). The reslting performance of the source is discussed below.

3.6 Measurement Techniques

In order to parameterise the performance of the X-ray generator a number of different measurement techniques were used. Diode voltage was measured at the output from the TLT using a copper sulphate potential divider and current was monitored by a parallel array of low impedance carbon composite resistors placed in the earth return. The perspex insulator between the front plate of the diode and the rest of the body providing electrical insulation between the anode and the earth return. Nylon bolts were then used to secure the front plate and also to hold the array of resistors in place bridging the insulator forming a low impedance, low inductance, known resistance in the earth return which enabled current measurements to be made. However the current traces obtained by this technique were badly affected by pick up noise and so none are included in this thesis.

Quartz fibre dosimeters (R.A. Stephen 0-200 mR) and an ionisation chamber (Vinten Instruments Model 37D3 with a 35cc chamber) were used to monitor the dose produced by the source and its uniformity. In order to prevent confusion and present results in the units used by other workers a conversion factor derived in Appendix 1 was

used to convert the dose measured in Sieverts by the ionisation chamber to Roentgens, a more commonly used unit. These were positioned at various points along the front of the X-ray window in the diode to allow the spatial uniformity to be determined as well as the dose produced and shot to shot variation although this proved rather tedious as these needed to be 'reset' following every shot. A second qualitative technique for observing the uniformity and shot to shot variation was employed in which an X-ray fluorescent screen was used. This screen (type HSF from Cuthbert Andrews Ltd) which is based on rare earth phosphors (gadolinium and yttrium oxysulfides, activated with terbium) fluoresces in the visible part of the spectrum under irradiation by X-rays giving an excellent visual display of the quality of the and shot to shot stability of the source. A piece of this screen of similar dimensions to the X-ray window was exposed to the output and a television camera protected by lead shielding was used to monitor the fluorescence patterns which were then recorded on video to allow closer scrutiny. This technique proved extremely useful in experiments on the X-ray source providing a direct means by which its performance could be observed, even at repitition rate and the ability to compare the effect of different cathode spacings and materials through use of the video. Also the screen gave a full spatial analysis of the X-ray output whereas using the ionisation chamber or dosemeters only the local output in the region of the probe could be monitered, a factor that was found to be very susceptible to small position changes and shot to shot variations. The screen then provided a means wherby a qualitative analysis of the diode performance could be achieved, even at repetition rate, whilst the other measurement techniques provided quantitative information on the source. Figure 3.5 shows the resulting patterns from the screen for two different cathodes in the source as discussed below.

3.7 X-ray Source Performance

The initial cathode employed in the X-ray diode was a length of uncoated razor blade, this however produced a very non-uniform emission. Measurements with the quartz fibre dosimeters backed up by visual evidence using the X-ray fluorescent screen, showed that the emission was constrained to a few "hot-spots" across the source as shown in figure 3.5. Attempts to improve the uniformity with this cathode, whilst maintaining a reasonable dose were fruitless. Numerous anode-cathode separations were tried and every

effort was made to ensure the spacing was uniform along the length of the blade. Preferrential emission was observed to occur from one or two areas which produced a fairly large dose (~250 mR measured at the source) whilst the emission from the other parts was virtually zero. Upon repetitive pulsing these 'hot spots' observed on the fluorescent screen would move around, concentrating in one area for a number of shots then switching to an adjacent region. Markings observed on the tantalum foil anode also indicated where strong emission had taken place though no irregularity in the anode-cathode positioning could be found which would account for this behaviour.

It became clear that the problem lay in the inability of the blade to 'light up' evenly along its extent. This phenomena was thought to be a consequence of a several of factors; the relatively low voltage at which the blade was operating, the risetime of the voltage pulse on the blade and the physical length of the blade. To achieve electron emission from a surface electric fields on the order of 10^7 Vcm^{-1} are required. For a typical anode cathode spacing of 4 cm and a 100 kV voltage pulse field enhancements on the order of 400 are needed, which although are not unreasonable may place the emitter close to the lower bound for effective field emission. The timescale on which emission sites form per unit length on the cathode is short [21] after which the impedance of the diode drops, lowering the available voltage and reducing the likelihood of further sites being produced. This implies a rapid dv/dt is required to ensure uniform formation of emission sites along the cathode. The 50 nsec risetime typical of the voltage pulses from the TLT supply (figure 3.4) coupled with the length of the blade, along which slight variations in position relative to both the anode and the clamping structure are likely to occur causing local variations in electric field conditions, add to the inability of the blade to produce uniform emission. Once localised emissions begin the particular site is favoured for subsequent emissions until a new area comes into effect resulting in the observed performance.

During the period experimenting with the blade numerous anode-cathode separations and blade mounting geometries were tried to little effect. It was, however, discovered that the output was sensitive to anode-cathode spacing uniformity and care had to be taken to set this accurately (± 0.5 mm) to eliminate its effects. One of the various mounting arrangements used included attaching the blade on pegs to hold it some 3 cm clear of the cathode structure to reduce any adverse shielding effects from the race track which affected

the performance. This, however, resulted in no improvement of the source. A number of different materials were used for the emitter in place of the blade. These included Metglass foil in one long length and in discrete strips and copper foil strips, all with little success. The best performance to date was achieved using an array of pins and the results using this cathode which are now discussed.

The pins were mounted in the cathode support spaced by 1 cm and projecting ~ 1 cm from it as shown in photograph 3.1. The best performance was obtained with an anode cathode spacing of 3.8 cm . Figure 3.5 shows the resulting increase in uniformity of the source observed using the fluorescent screen when the pins were used compared to that achieved with the blade cathode and in figure 3.4 a typical cathode voltage pulse achieved under these conditions is presented. In figure 3.6 the uniformity in air of X-ray emission at a distance of 25 cm from the front of the source is shown. This is the position at which the discharge region is situated when the laser and X-ray source are mated together. These measurements were made with the Vinten ionisation chamber placed at a number of points across the width of the source and the average value of a number of shots taken. The shot to shot variation at each position was ± 7% and cross checks using the quartz fibre dosimeters were carried out to good agreement. The low readings at positions 0 and 10 correspond to measurements taken at the extremes of the emitting area.

Although the uniformity obtained with this cathode (30 mR ± 25%) is far from ideal this was a vast improvement over previous results and proved adequate for preionisation of the laser. Further improvement of the uniformity in the cavity would be expected as the X-rays are scattered on passing through the window and the final preionisation electron production process discussed earlier will also lead to a more uniform spatial distribution. The elimination of 'hot spots' from the source appeared to be due to the ability of each of the pins to emit reliably and reproducibly. On inspection, markings on the pins indicated that they were indeed all contributing to the e-beam production. The increased emission observed towards one end of the source as shown in figure 3.6 could be due to non-uniform spacing of the pins from the anode, however this was not investigated as the X-ray source in this form proved capable of producing sufficient dose to preionise the laser. Measurements inside the discharge region, with the cavity in position adjacent to the X-ray source, recorded a dose of 5-8 mR, more than an order of magnitude greater than

Tallman and Bigio [5] and more recently Steyer and Voges [6] reported necessary for preionisation of an XeCl laser.

The variation in X-ray dose as a function of distance from the source is obviously an important parameter in this system where separation of the two units is necessary. The decrease due to divergence for this device is shown in figure 3.7 where the ratio of intensity of the source to the intensity recorded at a distance away is plotted against the distance from the source in a logarithmic graph. Two regions are identifiable, the first close in to the source where the observed intensity decreases approximately as $r^{-0.5}$, the second at distances greater than 15 cm where the decrease is approximately $r^{-1.2}$. In the first region X-rays diverging from parts of the source not colinear with the ionisation chamber contribute to the dose recorded keeping the rate of decrease with distance at a fairly moderate level, whilst at greater distances these contributions have less effect. In the limit of infinite distance the source becomes a point source from which the decrease would be expected to follow an r^{-2} dependance.

The variation in X-ray dose as a function of the voltage to which the Blumlein in the TLT system was charged to is shown in figure 3.8. The increase in dose is fairly linear with charge voltage as might be expected from the equations in the text, where the X-ray production efficiency is shown to increase with applied voltage in this linear fashion. As discussed in chapter 5 this variation with voltage is used to determine if the X-ray source is limiting the output from the laser and if increased performance could be expected with a better preionisation source. Temporal X-ray emission was not recorded but was expected to begin close to the peak of the cathode voltage and show similar characteristics (pulse length etc.) to the cathode voltage pulse thereafter [8].

In summary an X-ray source was built which produced a relatively uniform dose sufficient for effective preionisation of the laser as is discussed in chapter 5. The typical operating parameters of the source are shown in Table 3.1.

REFERENCES

1. S.C. Lin and J.I. Levatter, Appl.Phys.Lett. 34, 505 (1979).
2. International Tables for X-ray Crystallography Vol.3, The Kynoch Press. Birmingham, England (1962).
3. Stopping Powers For Electrons and Positrons, ICRU report no. 37.
4. O.R. Wood, Proc. IEEE 62, 355 (1974).
5. C.R. Tallman and I.J. Bigio, Appl.Phys.Lett. 42, 149 (January 1983).
6. M. Steyer and H. Voges, Appl.Phys.B. 42, 155-160 (1987).
7. J.I. Levatter and Z. Li, Rev. Sci. Instrum. 52, 1651 (November 1981).
8. M.R. Osborne, Ph.D. Thesis, University of London (1985).
9. S. Sumida, K. Kunitomo, M. Kaburagi, M. Obara and T. Fujioka, J. Appl. Lett. 52, 2682 (1981).
10. L.E. Kline and L.J. Denes, J. Appl. Phys. 46, 1567 (1975).
11. R.S. Taylor, Appl. Phys. B 41, 1-24 (1986).
12. A.S. Kozyrev, Yu.D. Korolev, G.A. Mesyats, Yu.N. Novoselov, A.M. Prokhorov, V.S. Skakun, V.F. Tarasenko and S.A. Genkin, Sov. J. Quantum. Electron. 14, 356 (1984).
13. Handbook of X-rays, ed. E.F. Kaelble, McGraw-Hill, New York (1967).
14. G.J. Hine and G.C. Brownell, Radiation Dosimetry (Academic New York 1956).
15. Rudolf Gerner, X-ray flash techniques, J.Phys.E. Sci. Instrum., Vol. 12, p. 336 (1979).
16. J.I. Levatter, R.L. Sandstrom and J.H. Morris, "The Corona Plasma Cathode" (unpublished).
17. L.P. Bradley, Inst. Phys. Conf. Ser. No. 29, 58 (1976).
18. F.S. Baker, A.R. Osborn and J. Williams, J. Phys. D 7, 2015 (1974).
19. H. Shields, R.L. Sandstrom and J.I. Levatter, Appl. Phys. Lett. 47, 680 (1985).
20. G.F. Erickson and P.N. Mace, Rev. Sci. Instrum. 54, 586 (May 1983).
21. G.K. Loda and D.A. Meskan, "Repetitively Pulsed Electron Beam Generator" Proceedings of the International Topical Conference on Electron Beam Research and

Technology, Albequerque,New Mexico (1975).

22. R.K. Parker, R.E. Anderson and C.V. Duncan, J.Appl.Phys. 45, 2463 (June 1974).

23. R.J. Noer, Appl. Phys. A28, 1 (1982).

24. I. Langmuir and K.T. Compton, Rev. Mod. Phys. 3, 191 (1931).

25. D.W. Forster, A.W.R.E. Report S.S.W.A. Note 733/398 (1973).

26. J.C. Martin, A.W.R.E. Report S.S.W.A. Note 759/193 (1975).

27. A. Watson, J. Appl. Phys. 38, 2019 (1967).

28. L.P. Bradley, Inst. Phys. Conf. Ser. No. 29, pp. 58-109 (1976).

29. M. Casey, Ph.D. Thesis, University of London. (1982).

30. P.W. Smith and H.R. Hutchinson, National Research and Development Council Report, Development Programme No. 109552. 'Gas Lasers for the Ultraviolet Wavelengths'.

31. C.R. Wilson and P.W. Smith, Proceedings 17th Power Modulator Symposium, Seattle (1986).

32. Dr.P.W. Smith, St. Andrews University, Private Communication.

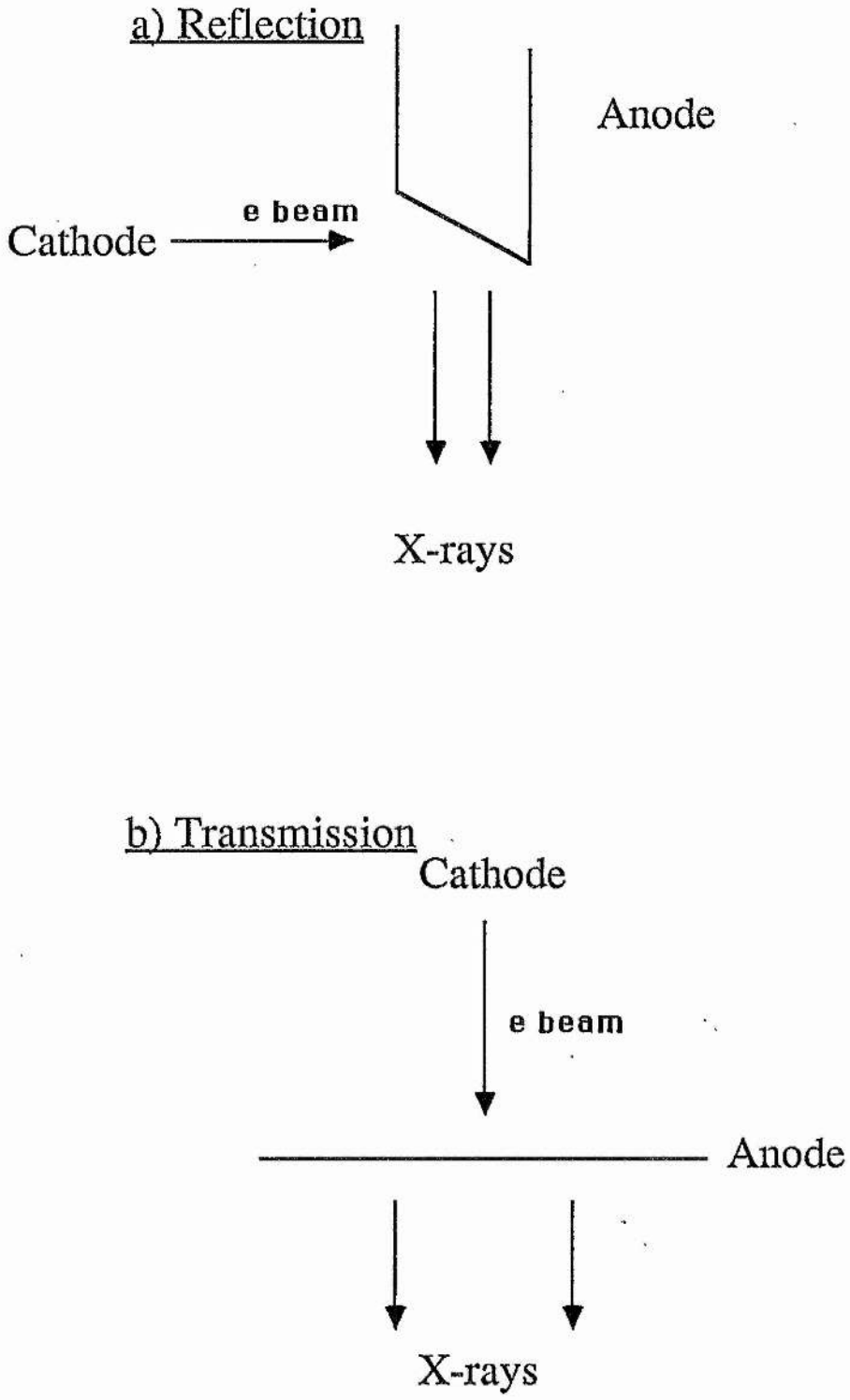

Figure (3.1):Target geometries for X-ray production

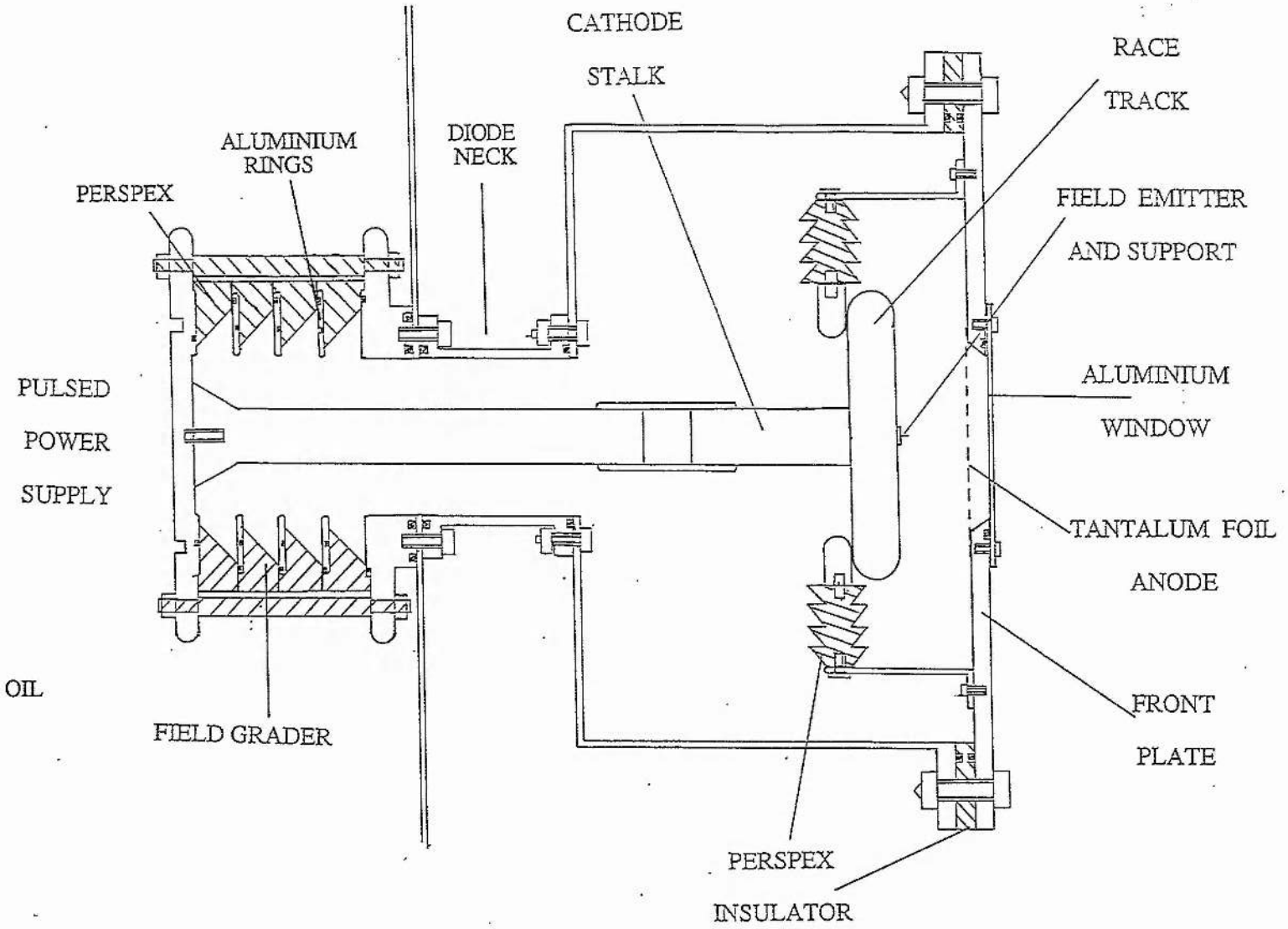

FIGURE (3.2) CROSS SECTION OF THE X-RAY SOURCE

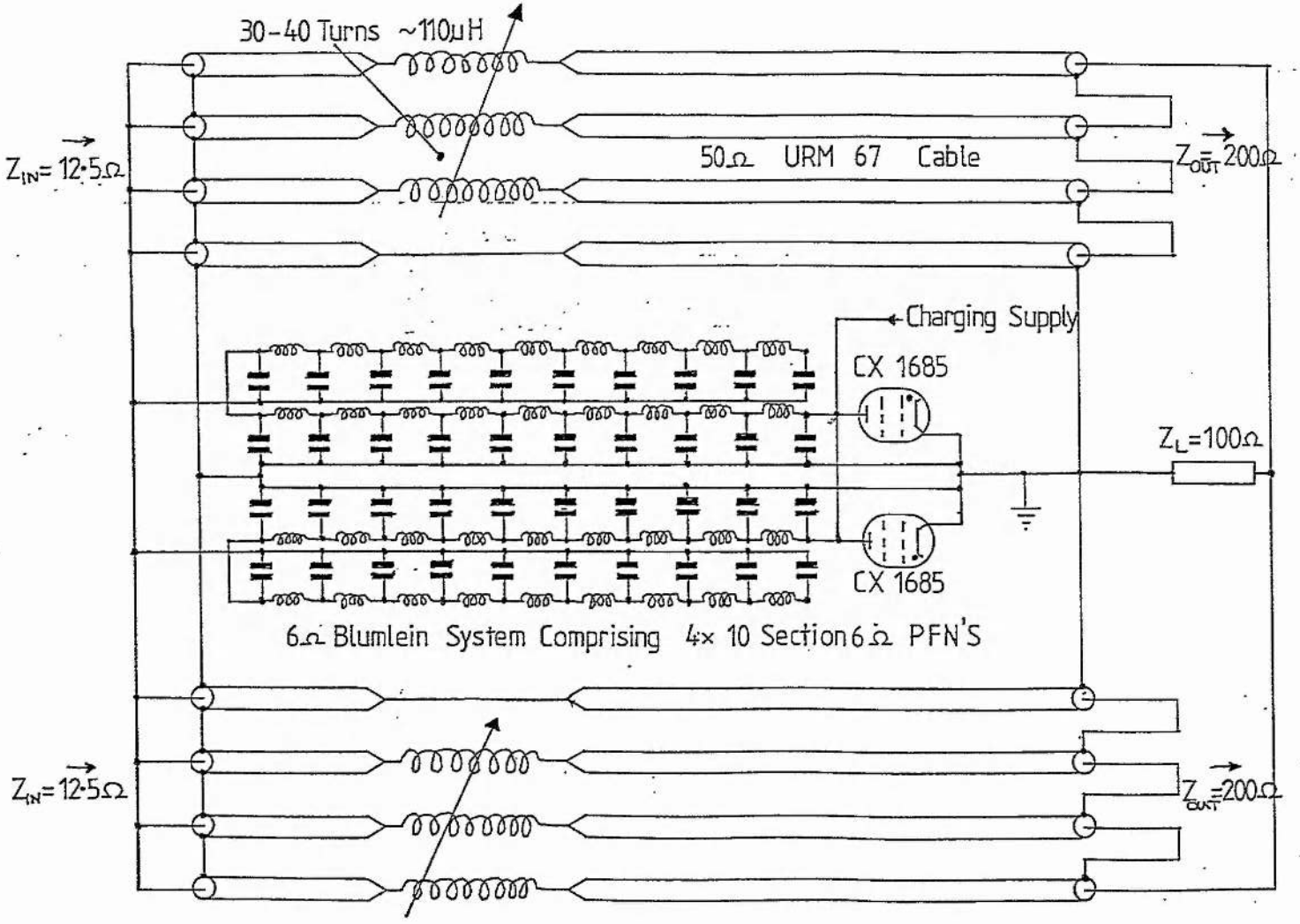

FIGURE (3.3) 100 kV 2 x 4 STAGE TRANSMISSION LINE TRANSFORMER PULSED POWER SUPPLY

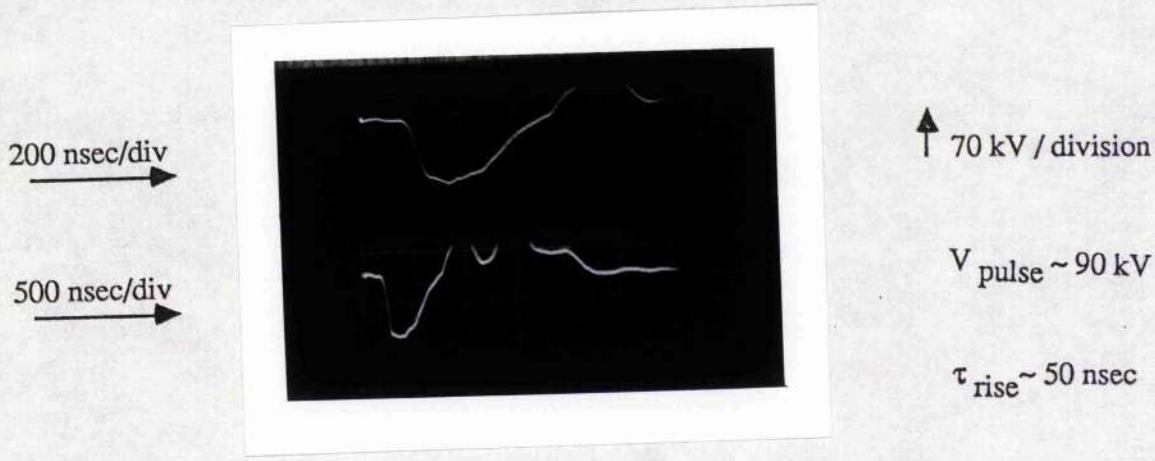

FIGURE (3.4) : Voltage pulse on e-beam cathode.
30 kV Blumlein charge voltage.
3.8 cm anode - cathode spacing.
Pin array cathode.

Table (3.1) : X-ray Source Operating Parameters

Window Size	100 cm by 8 cm
Anode Cathode Spacing	3.8 cm
Cathode Voltage	90 kV
Voltage Risetime	50 nsec
Pulse Length	320 nsec FWHM
Dose (at 25 cm from source)	30 mR (± 25%)
Dose (in cavity)	5 - 8 mR
Shot to Shot Reproducability	± 7%

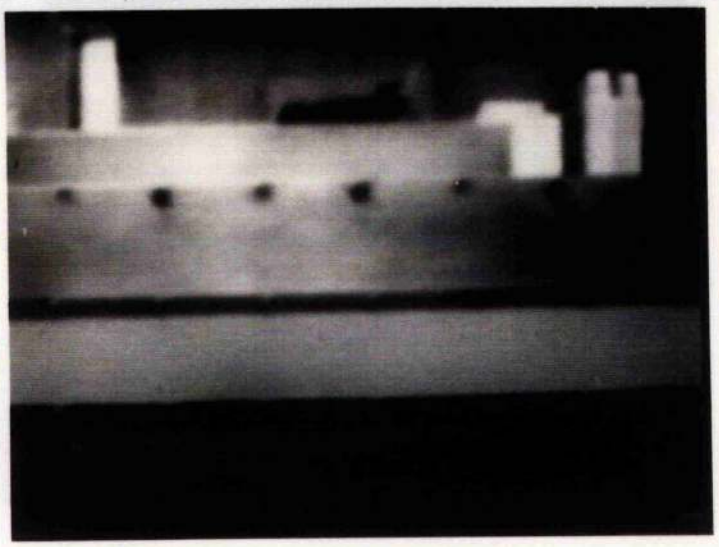

Front of the X-ray generator showing the position of the fluorescent screen.

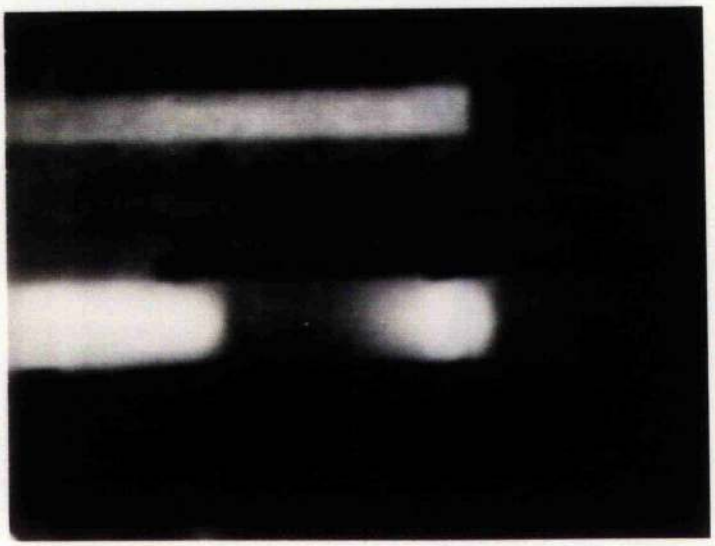

Fluorescence pattern observed with the blade cathode.

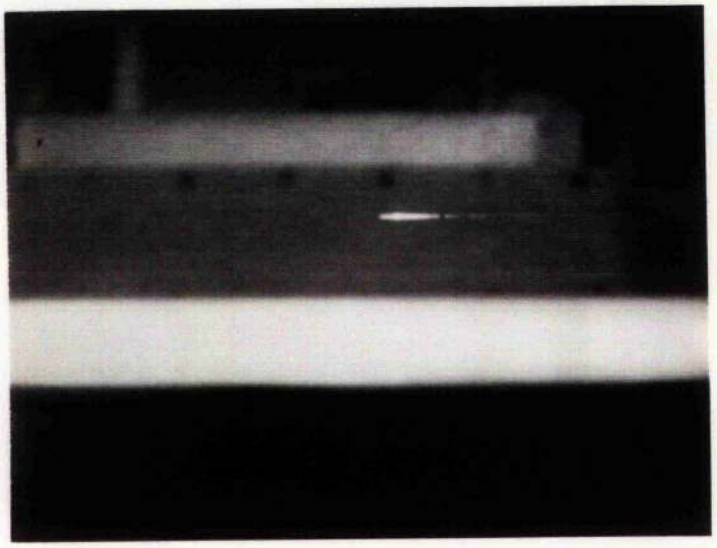

Fluorescence pattern observed with the pin array cathode.

FIGURE(3.5):Fluorescence patterns observed with the X-ray fluorescent screen placed in front of the source for different cathodes.

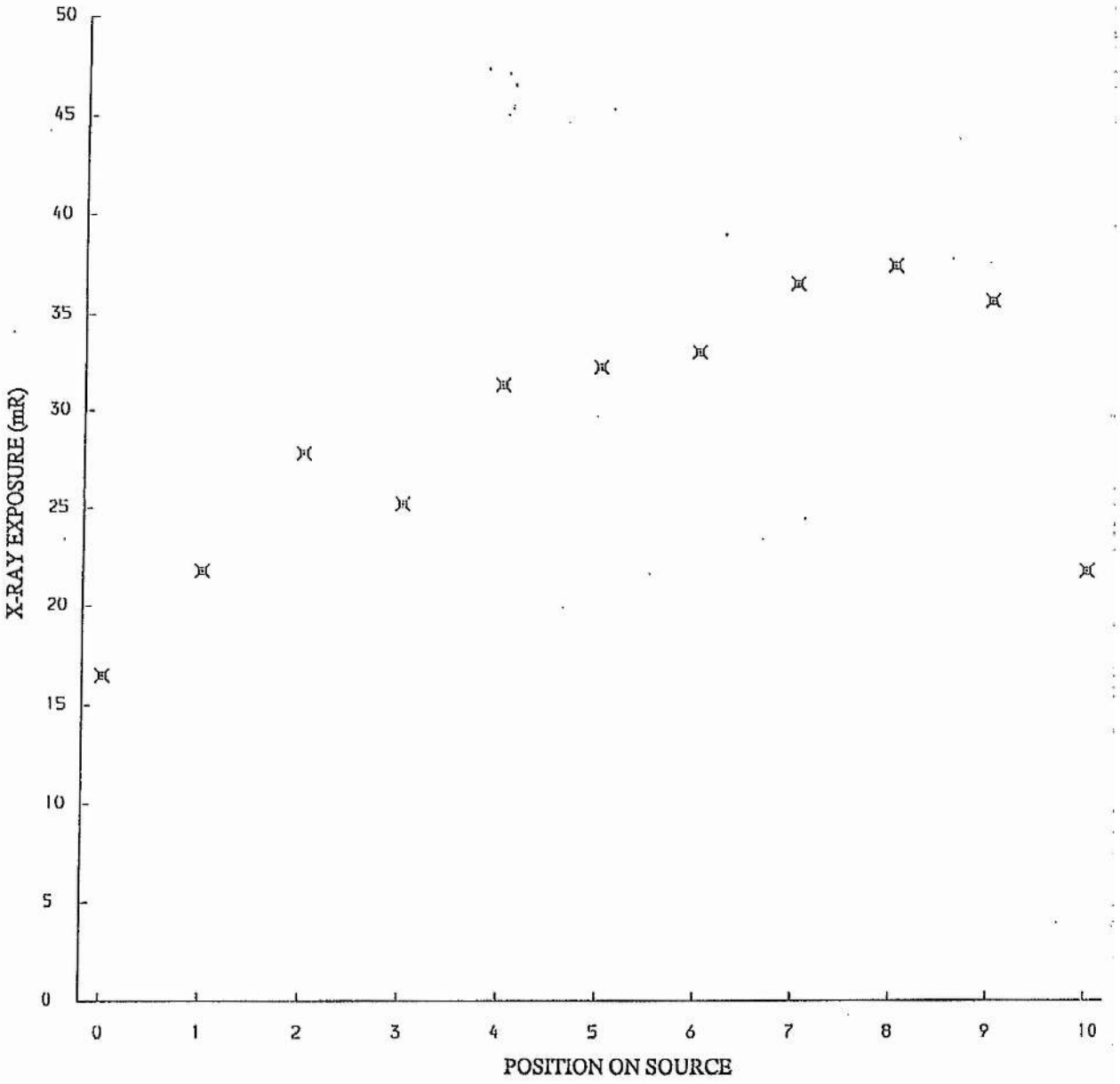

FIGURE(3.6):Flash X-ray source uniformity with pin array cathode.
Measured at a distance of 25cm from the source.

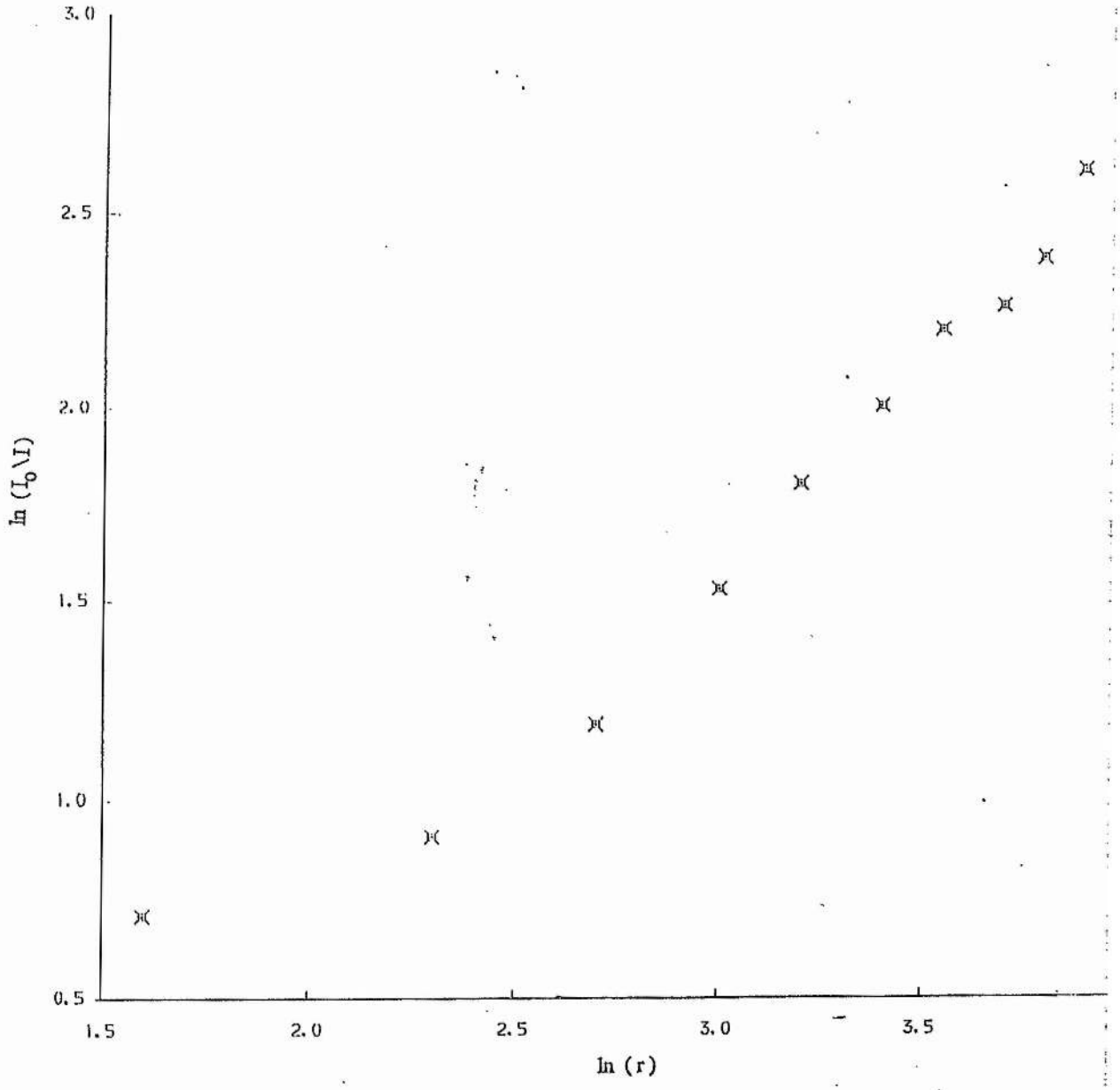

FIGURE(3.7):Logarithmic plot of ratio of incident X-ray intensity (I_0) to transmitted intensity (I) versus distance from the source (r).

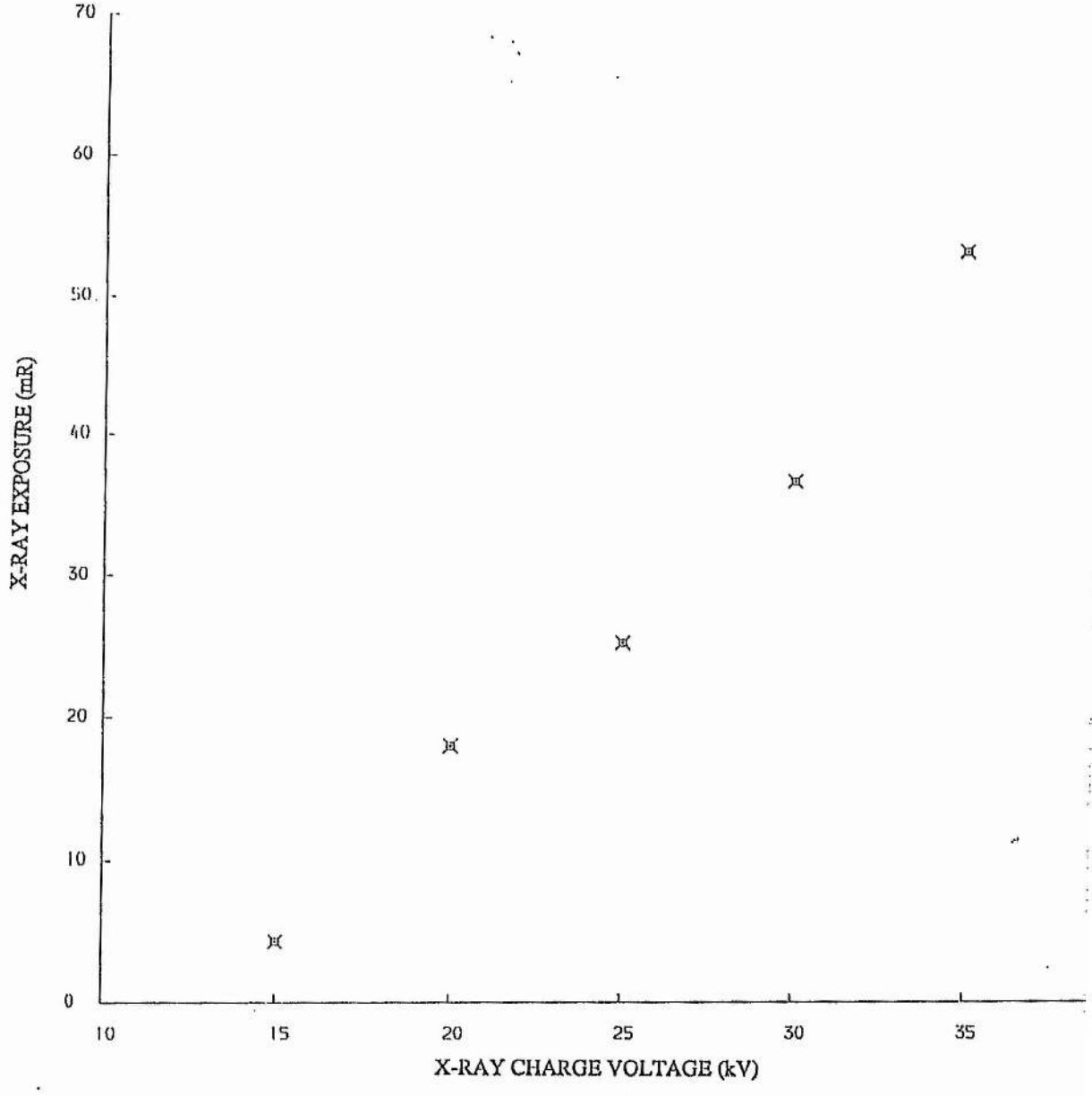

FIGURE(3.8):Variation of X-ray exposure with voltage.

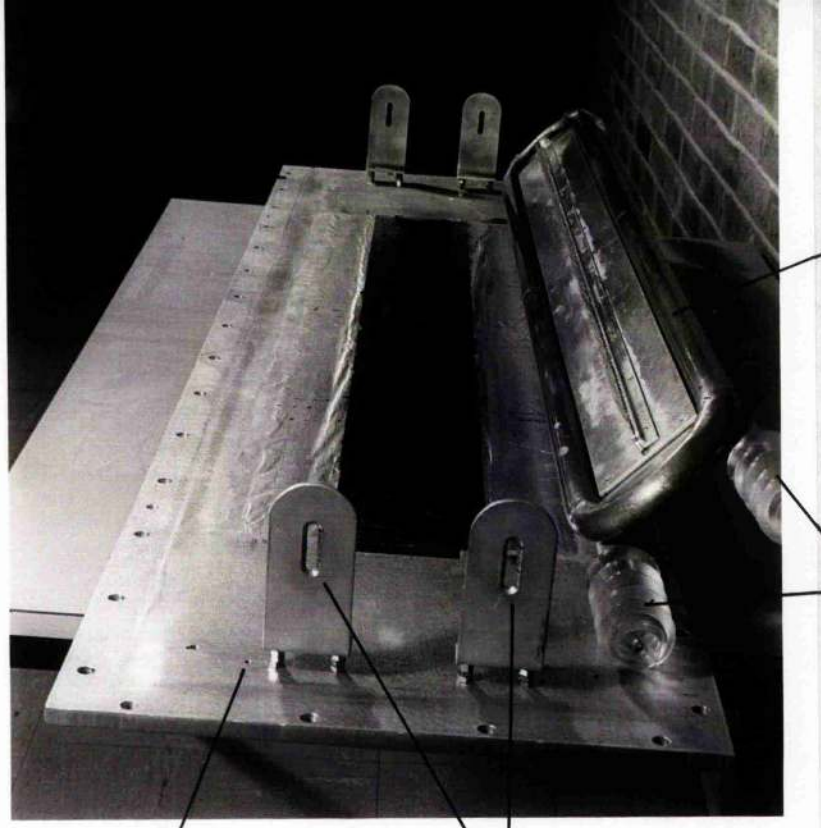

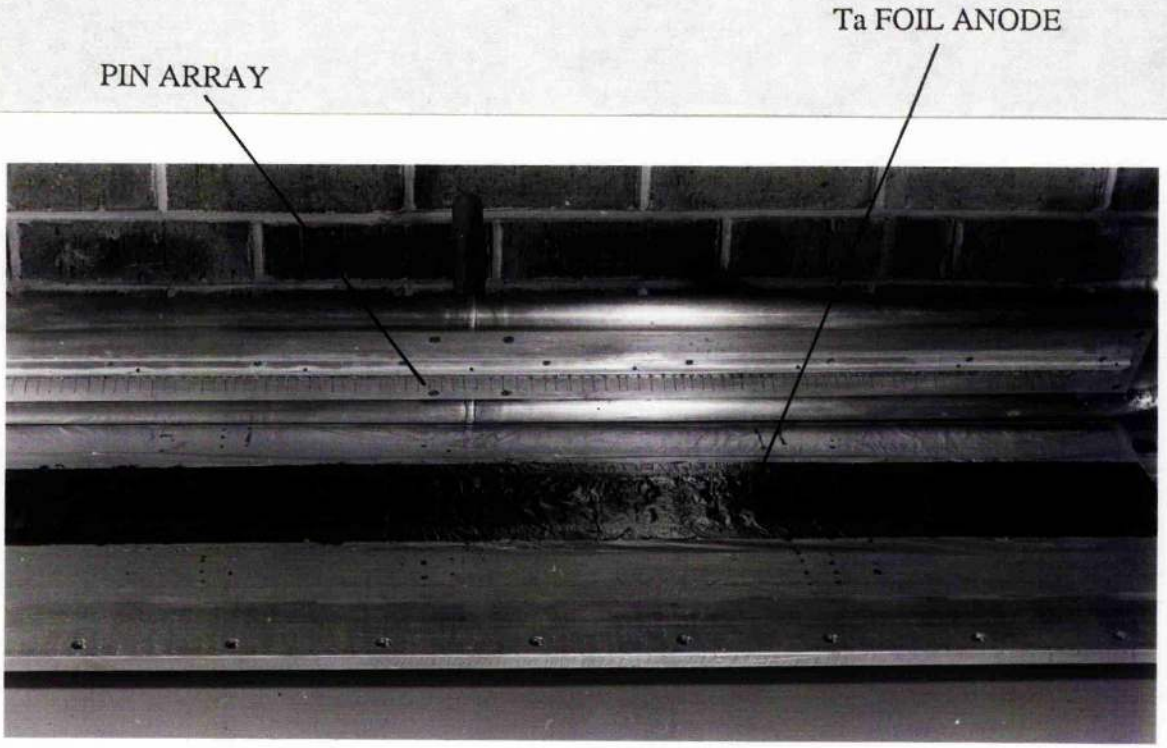

PHOTOGRAPH(3.1): The cathode support structure with the pin array and the front plate of the X-ray diode showing the tantalum foil anode and mounts for the cathode.

CHAPTER 4

LASER HEAD AND GAS FILL SYSTEM

4.1 Introduction

This chapter will describe in detail the design and construction of the laser head and associated elements such as the electrodes, electrical feeds and the gas filling system. Typically, mercury halide lasers operate at high temperatures, 140°C-180°C, necessary to maintain adequate vapour pressures of a few millibar (figure 4.1), and with high buffer gas pressures in the range 2-5 bar, utilising a transverse electrode geometry as for CO_2 TEA and excimer lasers. Together with these operating conditions of high pressure and temperature which must be addressed in the design, hot mercury bromide vapour being a halogen bearing compound is extremely corrosive, an important factor to be considered in a long life laser. Listed below are the design requirements of such a laser cavity followed by a discussion of how these were met in the device built, together with the problems encountered.

4.2 Requirements of the Laser Cavity

(i) High Temperature

As discussed, all components of the cavity must be able to withstand the high operating temperatures required and care must also be exercised in the choice of materials to avoid undesirable chemical reactions with the corrosive vapour. A major problem of high temperature operation is that of differential thermal expansion between various components which could lead to thermal stress and subsequent failure of the device. Expansion coefficients of materials must be closely matched and these components must also be able to withstand thermal cycling. It is also important to ensure that all parts of the cavity and gas filling system which are in contact with the vapour are heated uniformly to prevent

condensation in any cold spots.

(ii) High Pressure

In many high pressure gas discharge lasers the underlying trend is for the output energy to increase with buffer gas pressure [1] as either the discharge glow voltage increases improving energy transfer from the pulsed power supply or as the kinetic efficiency increases (or both). With this in mind the cavity must be designed to withstand buffer gas pressures of many atmospheres. A further structural requirement comes from the shock wave produced in the high pressure gas mixture as up to 100 Joules of energy are dissipated in each discharge pulse. The cavity must be physically robust to withstand this.

(iii) Electrical Considerations

The design of the cavity must isolate the main discharge electrode from parts of the chamber at earth potential to avoid tracking problems inside the cavity and ensure the discharge runs in the desired region between the electrodes. Typical track path to discharge path ratios in the region of 3:1 are used though by using a double electrical feed geometry to reduce the effects of field enhancement at the discharge electrode, which can initiate surface tracking, this has been reduced to as little as 1.2:1 [2]. One must also take care to minimize the head inductance to allow the fastest discharge current risetime to be achieved. These two requirements contradict each other in terms of the size of the laser head and care must be taken to comply with both.

(iv) Chemical Compatibility

The life limiting factor in a high repetition rate mercury bromide laser is that of undesireable chemical reactions of materials used in the construction of the cavity with $HgBr_2$ and discharge products such as HgBr, Hg, Br_2, and Br. These lead to consumption of the laser fuel and possible contamination of the gas subsequently reducing laser output and gas lifetime. As will be discussed such reaction products can produce a build-up of dust within the discharge region affecting the optical quality of the laser medium and resulting in a reduction in laser performance. Structural weakening of the cavity could ensue with the possible catastrphic failure of the device. In order to eliminate these reactions great care must

be taken with materials compatibility when designing mercury bromide lasers and several studies have been undertaken with this in mind. A brief review of some of this work is now presented.

From the outset of the development of the mercury bromide laser it was realised that chemically inert materials should be used in the design of the laser cavity. Small scale lasers were constructed which used quartz [3] and pyrex [4,5], which are inert to such chemical reactions, for the discharge cell whilst electrodes were constructed from stainless steel, tungston and nickel plated aluminium [6]. These chamber materials however limit the operational pressures of these devices. More robust chambers allowing higher buffer gas pressures to be used were constructed using stainless steel [7,8] whilst Parks [9] used an aluminium cell in his e-beam pumped experiments, though both these materials are now known to undergo chemical reactions in these lasers. An extensive experimental and theoretical study carried out at Mathematical Sciences Northwest Ltd. [8] indicated platinum plated stainless steel would make the best cavity wall material showing excellent resistance to chemical attack by the gas mixture and that platinum would be the most suitable electrode material. However their investigation also showed that a long life laser could be constructed from less exotic materials using unplated stainless steel as the chamber material. In a recent study by Liu and Liberman [10] in which they evaluate the suitability of materials for use in mercury bromide lasers using thermochemical calculations in conjunction with experimental observations, they also conclude that stainless steel is a suitable material to use as the chamber material. Following an initial reaction of the metal a protective layer is produced on the surface which retards further reactions. In the region of the discharge however such a protective layer would be readily ablated and a non reactive material such as gold or platinum should be used for the electrode materials.

Without the knowledge of these materials compatibility studies at its time of conception, the laser described here was designed using stainless steel for the chamber and the main discharge electrode. This had proven to be an acceptable material to use in other halogen bearing excimer lasers, however as is discussed later its use did affect the performance of this device. Although gold plating of the cavity was investigated, economic considerations prevented any steps towards this being taken and similarly no attempts were made to aquire platinum electrodes for the device. The design of the cavity is now discussed

in detail.

4.3 Cavity Design

A plan view and cross-section of the discharge cavity are shown in figure 4.2. The cavity is essentially constructed in three parts: (i) the metallic central body at each end of which the cavity windows are mounted, (ii) the front plate which houses the X-ray window, ground electrode and gas ports, and (iii) the Torlon insulator for the main discharge electrode. The main body is approximately 13 cm wide, 19 cm high and 124 cm long and constructed from 321 grade stainless steel. This material was chosen for the cavity because of its excellent corrosion resistance properties, high service temperature and low thermal expansion. However, as mentioned above and is discussed later, this has proven to be less than the ideal material for use in these lasers. Flanges on both sides of the central body house the O-ring groves which support the 0.210 inch cross sectional diameter o-rings used to give the vacuum/pressure seals when the cavity is assembled. A more detailed discussion of the O-rings used is given later. Circular flanges at the ends of the central body hold the 3 inch diameter, 1/2 inch thick, quartz windows in place. Slightly oversized O-rings are used for the window seals, the extra compressibility afforded by this allowing accurate alignment of the windows to be carried out to compensate for the two ends not being precisely parallel.

The front plate is also made of 321 stainless steel and bolts on to the central body. Access to the inside of the cavity when the laser is assembled is achieved by removing this plate. A slot of dimension 102 cm by 7.5 cm is milled out of the centre of this plate where the X-ray window, designed to transmit X-rays from the preioniser source into the discharge region, is positioned. This window must satisfy two conflicting requirements. It must be able to withstand a pressure differential of several atmospheres, thus it should be structurally strong, however it must also transmit the maximum X-ray flux possible into the cavity. Transmission of X-rays through material is governed by an exponential absorption rule [11]

$$I = I_0 \exp(-\mu x)$$

where I_0 - incident intensity

I - transmitted intensity

x - thickness of absorber

μ - linear absorption coefficient

the reduction in intensity being determined by the quantity of matter traversed by the beam. For a highly transmitting X-ray window a thin layer of low density material is desirable yet for the structural criteria a substantial thickness of material would be best.

Figure 4.3 shows the X-ray transmission properties of materials of various thickness over the range of photon energies of interest. Taking an energy of 50 KeV the best materials are found to be either aluminium (ρ = 2.7 gm cm^{-3}) or beryllium (ρ = 1.8 gm cm^{-3}). Beryllium has the advantage that a thicker, hence stronger window could be constructed whilst maintaining a high transmission > 80%, however the problems with handling this material detract from this. Aluminium is easy to handle, readily available, strong and a good material for plating (an important factor in the protection of the window from chemical attack) and thus made the preferred choice for the window material. Stainless steel foil is another commonly used window material [12] though this has to be very thin to achieve high X-ray transmission and is more suitable for preionisation sources of higher average photon energies than the one used as described in chapter 3.

One major disadvantage of aluminium over stainless steel is its lack of corrosion resistance. In order to protect the aluminium inside the cavity from chemical attack all areas exposed to the gas were plated with nickel. Several workers [6,13] had used nickel in other systems with no reported problems and H.N. Rutt [14] suggested nickel undergoes no attack in the presence of bromine in work done in connection with the hydrogen bromide laser. However, in a recent article [10] Liu and Liberman have reported that nickel along with aluminium and other metals are not suitable for use in HgBr lasers. Using thermochemical calculations they show the free energy change of the reaction between Ni and $HgBr_2$ is negative indicating a reaction between these will proceed to produce $NiBr_2$ and Hg. With the knowledge of materials compatibility available at the time of conception of the device described here an aluminium window plated with nickel was used in the laser and no visual signs of corrosion have been observed to date.

The nickel was applied to the 1 mm aluminium window by an electroless plating

technique to produce a 1.5 thou thick layer. It was essential to keep this layer thin to prevent excessive absorption of the X-rays by the nickel which has a linear absorption coefficient twenty times that of aluminium [15]. The ground electrode (figure 4.2) through which the X-rays must also pass to reach the discharge region was similarly made of 1mm aluminium and plated with nickel, forming a total thickness of 6 thou nickel and 2 mm aluminium through which the X-rays must traverse. The final transmission factor of 60% for 50 keV X-rays into the discharge region was felt adequate to allow effective preionisation of the laser gas mixture for the formation of a uniform discharge.

The X-ray window is supported by a Hibatchi type grid to prevent excessive distortion of the window during the vacuum/pressure cycles and is sealed to the front plate using O-rings. The ground electrode is attached to the front plate by bolts, its height above the plate adjustable using spacers allowing the separation between the two electrodes to be varied up to a maximum of 5.5 cm. As indicated in figure 4.2 stainless steel bars can be mounted inside the cavity to restrict the flux of X-rays to the desired region of the cavity. This affords control over the width of the discharge volume preionised which was found to be essential for the production of a homogeneous discharge and uniform output beam from the laser as discussed in chapter 5. The final detail of this part of the laser head are the two one inch gas ports close to each end, through which the laser is filled and evacuated. A full description of the gas filling system is given later.

The Torlon insulator forms the last part of the cavity and supports the high voltage electrode, isolating it from the earthed body of the laser. Torlon [16] is a high performance poly (amide - imide) thermoplastic which exhibits exceptional physical and chemical properties. It can withstand continuous exposures at temperatures in excess of 230^{o}C, is resistant to attack by many corrosive agents and is mechanically robust. The coefficient of linear thermal expansion of Torlon is 2.7 x10^{-5} cm/cm/^{o}C which is close to that of stainless steel ~ 2x10^{-5} cm/cm/^{o}C [17], eliminating possible problems of differential thermal expansion between the cavity materials. The main portion of the insulator is constructed from 1 inch Torlon plate through which numerous stainless steel feedthroughs pass, each sealed with its own o-ring, and which hold the main discharge electrode in position. The high voltage feed from the pulsed power supply is connected to these. Bonded to this plate are pieces of 1/4 inch Torlon which are non-load bearing but act to form a longer tracking

distance from the electrode to the earthed body of the cavity. As shown in figure 4.2 these fit inside the central body when the laser is assembled, a similar arrangement being used at the ends but shaped to keep clear of the window area. The insulator is held in place against the main body of the cavity by an array of bolts which themselves fit inside Torlon 'jackets' to increase the tracking length outside the cavity between them and the high voltage feed. The earth returns to the pulsed power supply are attached to the cavity by these bolts.

The main discharge electrode is fabricated from 316 grade stainless steel. The shape of this electrode is similar to that utilised in a large X-ray preionised XeCl laser constructed at Imperial College [18], which is a scaled up version of the electrodes found in commercial Lambda Physik excimer lasers. This electrode shape was found to work well in these laser systems and so was utilised in this device. It is shaped with a flat top 2.5 cm wide with radiused edges and is 100 cm long. The aluminium oversized ground electrode is 106 cm long and 8 cm wide. The field shaping electrode shown in figure 4.2 was added to the cavity after initial experiments revealed a surface tracking problem stemming from the edges of the electrode adjacent to the insulator surface. The role of this electrode in modifying the field at this point, hence removing the problem, is discussed more fully in chapter 5.

4.4 O-ring Materials

Viton [19] with its high maximum working temperature and excellent resistance to attack by many solvents was chosen as the O-ring material best suited for this laser. Moulded Viton O-rings are normally available 'off the shelf' but due to the large size of the cavity requiring an O-ring of internal diameter 42 inches, a complete moulded ring could not be obtained. Instead, extruded Viton chord was used cut to the appropriate lengths and bonded. At room temperature these seals worked well but failed after one or two thermal cycles to 200°C. Several factors were identified as being the cause of the failure. These O-rings were found to be prone to compression setting. Following a thermal cycle under compression the O-ring would change shape, effectively taking on the shape of the grove hence loosing the ability to form a seal. The chord was also prone to extrusion and splitting at corners of the O-ring grove. This latter problem could have been due to the sharp nature of the corners so these were modified slightly to reduce the strain on the O-ring at these points.

These problems all pointed to the inability of Viton O-ring chord to work under the conditions required which were within the manufacturers specifications. A test to compare the performance of a piece of O-ring chord with a piece cut from a moulded O-ring, under similar conditions to those of the laser cavity, was done. The results showed the O-ring chord was inherently inferior to the moulded O-ring, a result eventually confirmed by the manufacturers. Following this O-rings were constructed by using two of the largest available moulded O-rings, cutting and joining them to form one of the appropriate dimensions. Using this home-made moulded Viton O-ring the problem of failure after a few thermal cycles was cured and to date the original O-rings manufactured in this way are still in use in the system!

A search was conducted concurrently for other more specialised types of O-ring designed for high temperature operation with corrosive agents and which could be ordered to size. Teflon coated FEP encapsulated Viton O-rings [20] looked the most promising alternative without using metal seals which would require a re-design of the cavity. This type of seal was obtained, however, due to the successful operation of the home made ring the need has not arisen to test them in the cavity. PTFE O-rings were tested in parts of the system but were found to 'flow' on heating under compression thus losing the ability to form a seal. All O-rings finally used in the cavity and flow loop were made from moulded Viton O-rings and further problems were minimal.

4.5 The Oven and Heating Procedure

The cavity is heated by a home built fan assisted oven utilising three 2 kW heater elements and fans from a large domestic oven. The oven is constructed from stainless steel sheet and Pearlite is used as an insulator. Two circular holes in each end allow optical access to the discharge region, the mirrors which form the optical cavity are mounted close to these holes outside the oven. A slot in one side of the oven wall mirrors the X-ray window in the cavity and in the X-ray source allowing X-rays to be transmitted to the cavity. A thin sheet of Kapton film is fixed over this area to prevent excessive heat loss through it. The unfortunate consequence of surrounding the cavity with an oven in this manner is the distance placed between the X-ray source and cavity reducing the intensity of X-rays at the cavity through divergence of the beam. This point is discussed in more detail in Chapter 2.

To keep the pulse forming line system at room temperature and to keep the inductance low the electrical feeds to the laser are brought in through a short transition section (figure 4.2). This transition section is shaped and extends the full length of the electrode to minimize inductance and the oven is designed to fit around these feeds keeping heat loss from this area as low as possible. Electrical insulation between the high voltage feed, earth returns and oven walls is by Nomex aramid paper [21]. This high temperature insulator has advantages over others of its type (eg. Kapton) as it is very flexible, hence easy to shape around awkward objects, and is relatively inexpensive. However, its dielectric strength is lower and a larger number of layers have to be used. The edges of the electrical feeds and field shaping electrode were shaped as far as was possible to prevent field enhancement along them and only one failure due to insulation punch through occured during operation of the laser.

The temperature of the oven is controlled by three mercury microswitches which control the heating elements. The microswitches outside the oven are connected via capillary tubes to mercury reservoirs attached at intervals along the laser body and may be individually set. This affords reasonable control of the body temperature and with appropriate manipulation of the air flow from the fans uniform heating of the cavity is achieved. A number of thermocouples attached to the laser at various places gave accurate measurements of the temperature and were used to calibrate the microswitches and hence oven temperature. In operation the cavity temperature was maintained at 180^{o}C - 200^{o}C, well above the temperature of the mercury bromide reservoir ensuring no "cold spots" existed inside the cavity where condensation might take place.

Obviously with such a large mass of stainless steel to be heated the cavity requires some time to achieve the desired temperature. Owing to its position the stainless steel electrode receives no direct heating from the air circulating in the oven and relies mainly on heat transfer through conduction via the stainless steel feedthroughs (themselves poor conductors) or from gas inside the cavity heated at the walls. This electrode is thus the slowest part of the cavity to achieve its final temperature and so dictates the length of time heating must take place for before the laser can be operated. Figure 4.4 shows the temperature of this electrode, measured using thermocouples attached along its length, as a function of heating time with the oven temperature fixed at 180^{o}C. Typical operating

conditions for this laser require temperatures in excess of 150°C to be achieved to prevent condensation of mercury bromide vapour inside the cavity, thus under the conditions of figure 4.4 a minimum heating time of five hours is required prior to operation of the laser. This time may be reduced slightly by operating at a higher temperature and filling the cavity to a few atmospheres to increase heat transfer via the gas. In practice the cavity was filled with one or two atmospheres of Helium and the oven temperature maintained at a temperature of 200°C for a period of five hours to ensure adequate temperatures in the cavity were achieved.

4.6 The Gas Handling System

A schematic of the gas handling system is shown in figure 4.5. Two one inch stainless steel ports from the laser head pass through the oven and are connected to the pumping and filling systems. The pipework between the laser head, condenser and evaporator, external to the oven, is heated by heating tape and insulated with glass fibre strip. Temperature is monitored on the pipes using thermocouples and controlled by limiting the power to the heating tapes using variacs. All other parts of the system are free of mercury bromide vapour, as is discussed later and hence do not require heating.

A more detailed diagram of the evaporator is shown in figure 4.6. A twelve inch long chamber fabricated from stainless steel, fits inside the pipe connected to the laser head. This container is filled with glass wool impregnated with mercury bromide powder and designed to give maximum contact between gas flowing through the evaporator and the powder. A heating chord positioned in a spiralled grove cut in the pipe is used in conjunction with a proportional temperature controller to give accurate control over the evaporator conditions. This type of controller eliminates any time lag between the heater element and thermocouple sensor thus avoiding overshoot during the heating cycle and allowing the mercury bromide vapour pressure in the evaporator to be determined with reasonable accuracy. Gas from the filling rig, preheated to some extent by heating part of the pipework connected to the evaporator, flows through picking up saturated mercury bromide vapour pressure and transports it into the laser head. The pressure inside the cavity, buffer gas mixture and flow rate are all determined using the Leybold Heraeus and Budenberg gauges.

Typically a fill to three or four atmospheres buffer gas pressure using this technique

takes approximately 5 minutes and ensures a uniform distribution of vapour inside the cavity. An alternative technique used by other workers on smaller sealed off systems [22,23] where the mercury bromide powder is held in an independantly heated sidearm to the cavity relies on diffusion of the heavy molecules through the lighter buffer gases, a process which is slow under the operating conditions of the laser. For large volume systems as described here this is not a practical filling method as the timescale for producing a new laser mixture would be several hours making parametric studies extremely tedious. This technique also requires the cavity to be filled with the appropriate mixture of cold buffer gases, sealed and heated to the required operating temperature, the cavity eventually filling with saturated vapour at the source temperature. Any outgassed products from the laser chamber, eg. hydrogen, during the long heating period therefore contaminate the gas possibly impairing the operation of the laser or leading to the build-up of corrosive acids upon reaction with products of the discharge, eg. hydrogen bromide. In the system described here the internal surface area excluding electrodes is approximately one square meter from which the degree of outgassing could be considerable. During the initial attempts to achieve lasing in mercury bromide with this system such a static gas filling technique was used but without success as no lasing was obtained for the reasons outlined above.

To circumvent this problem of gas contamination a condenser is used on the pumping side of the system which allows the cavity to be evacuated whilst hot, any mercury bromide being trapped out of the gas in this unit, and the remaining buffer gas pumped away or possibly recirculated. The condenser is fabricated in the same manner as the evaporator except it is only heated at the input end to prevent a build-up of solid mercury bromide blocking the flow, the rest of the condenser is air cooled. Periodically the condenser must be emptied and the reservoir refilled, a process done by either exchanging the two containers or by manually emptying the condenser and replacing the powder in the evaporator. The more elegant technique used by Baker and Seddon [22] of reversing the gas flow whilst heating the condenser and cooling the evaporator would be time consuming here due to the thermal capacity of stainless steel making large temperature changes of these units a lengthy process. The advantage of this latter method is the cavity may be kept sealed preventing possible contamination also eliminating any contact with the poisonous mercury bromide. The valves used in the heated parts of the filling system for isolation are one inch ball valves with a

stainless steel body and PTFE ball seats. These were obtained from British Steam Services and required the minor modification of adding an o-ring seal to the ball stem to improve the vacuum performance of the valve to the level required.

The gas filling procedure begins with heating the cavity and associated pipework to the required temperature. Next the cavity is evacuated to ~ 10^{-2} mbar by the rotary pump, any condensibles such as water vapour being removed by the liquid nitrogen trap, then sealed from the vacuum system. The evaporator is then brought up to temperature and the desired buffer gases are flowed through filling the cavity with the gas/vapour mixture, the flow rate being controlled by Nupro needle valves upstream of the evaporator. Removal of the mixture commences with any overpressure in the cavity passing out through the Sodium Hydroxide trap to extract any impurities from the gas which has already been purged of its vapour content as it passed through the condenser. The chamber is then evacuated, the buffer gas mixture being pumped away by the rotary pump, in preparation for the next fill or for close-down of the laser. Typical filling and emptying times for this system are in the region of five to ten minutes.

A more economical system would include a gas recirculator with suitable traps to prevent build-up of any impurities allowing replenishment of the mercury bromide vapour. For this size of cavity a fill to three or four atmospheres of neon buffer gas costs in the region of £15 so considerable savings could be made by re-using the gas. Use of such a recirculation system would not only increase the gas lifetime and reduce the cost of operation but would also be pertinent in high repetition rate experiments where removal of the hot ionised gas in which a discharge has just taken place and its replacement with fresh gas prior to the subsequent discharge is essential to maintain effective laser operation. The 'used' gas can then be transported around a flow loop including heat exchangers to remove the effects of discharge heating and suitable traps to remove any impurities formed during the discharge. With these points in mind the design of a circulation system was undertaken, although to date it has not been incorporated into the system.

A longitudinal flow was chosen as the best suitable for the laser as it was the easiest to incorporate into the design of the system although this type of flow limits the maximum possible repetition rate due to the long clearance times (the time to completely replace the volume of gas between the electrodes) of the gas flowing in this direction. With transverse

flow directions kilohertz repetition rates are possible [24]. The envisaged flow system incorporated a gas circulator of some description situated between the two gas ports in the laser head extracting gas from one and replenishing with the fresh gas through the other. A search was carried out to find a commercial company who could supply us with a suitable pump to circulate the high pressure gas which would have the specifications of corrosion resistance, temperature compatibility etc. as for the cavity. This proved to be a difficult task and following an extensive period of detective work it became apparent that no company could supply us with a pump which could meet these specifications. To overcome this a circulator was designed and built 'in house'. This consisted of a stainless steel impeller, purchased from B.O.B. Fans Ltd., Derby, housed in a stainless steel casing and driven by a magnetically coupled motor which was adapted from a domestic central heating circulation system. Initial tests on this system in air proved successful but it has yet to be fully tested in the laser.

4.7 Materials Compatibility

A more important use of a gas circulation system would be the removal of a build-up of 'dust' observed suspended inside the laser cavity following discharge pulses, using suitable filters in the flow loop. This 'dust' which has also been reported by other workers [25,26] causes severe degradation of the optical quality of the laser medium to the extent that the beam from a HeNe alignment laser directed along the axis of the cavity is almost totally scattered. A quantitative elemental analysis of the dust using an electron probe microanalysis technique showed its constituents to be mainly bromine, iron, nickel and chromium with traces of manganese, silicon, chlorine, mercury and oxygen. The results of one such analysis are shown in figure 4.7. An accelerated beam of electrons impinges on the dust sample and X-ray crystal spectrometers are used to scan through the emitted X-ray spectrum to record identifiable emissions. The figure shows the scanned spectrum along the x-axis with intensity on the y-axis, the main peaks in the spectrum are identified. Aluminium is also possibly present in this spectrum but is hidden by the large bromine peak.

These results are what would be expected upon reaction of bromine with the constituents of stainless steel and materials ablated from the electrodes. Reactions of iron and bromine can form either iron (II) or iron (III) bromide, the former of these, $FeBr_2$, is greenish yellow in colour whilst the latter, $FeBr_3$, is dark red-brown [27]. The colouration

of the dust was consistent with the presence of both these products. Deposits on the walls of the container which were reddish-brown in colour - although not analysed - also pointed to the formation of $FeBr_3$. These results are not surprising as bromine was used to passivate the cavity in an attempt to prevent chemical reactions of the mercury bromide vapour with the cavity materials. However it is possible that reactions of the vapour or discharge products could also be taking place, especially in the region of the discharge electrode where any passivated layer will be ablated by the discharge, adding to the production of the dust. This is backed up by the fact that the cavity was 'cleaned up' on several occasions when most of the dust was removed. Yet on subsequent operation of the laser more dust was observed present in substantial amounts.

Consumption of bromine during the discharge through these chemical reactions in the formation of metal bromides, eg.

$$HgBr_2 + Fe \rightarrow FeBr_2 + Hg$$

implies the release of mercury vapour into the cavity which should then be detectable. The dust analysis showed possible trace amounts of mercury were present and a metallic deposit on the windows of the cavity was thought to be mercury. Also, as will be discussed in chapter 5, the presence of free mercury in the discharge was observed spectroscopically. Chemical tests were also used[28] in an attempt to discover the origins of the dust and in the first instance to find any possible reason for the lack of observed laser emission during the initial experiments with the device when the static gas filling technique was used, before the other pitfalls of this method were realised as discussed above. The various tests used are now summarised below, the first few are direct tests to show the presence of mercury bromide, whilst the latter ones may be used to show the presence of various reaction products.

1. Mercury bromide ($HgBr_2$) in its normal state is a white powder and is soluble in methanol.
2. The addition of mercury bromide to sodium hydroxide solution results in the formation of a reddish precipitate of the oxide in the reaction

$$HgBr_2 + 2NaOH \rightarrow HgO + 2NaBr + H_2O.$$

This may be converted into the yellow mercuric oxide in excess of the alkali.

3. In silver nitrate solution mercury bromide forms the pale yellow precipitate of silver bromide.

4. When Hg_2Br_2 reacts with NaOH a black precipitate of the mercurous oxide is formed which is insoluble in excess of the precipitant.

$$Hg_2Br_2 + 2NaOH \rightarrow Hg_2O + NaBr + H_2O.$$

5. $FeBr_3$ in ammonia solution results in the reddish-brown precipitate of ferric hydroxide

$$FeBr_3 + 3NH_3 + 3H_2O \rightarrow Fe(OH)_3 + 3NH_4Cl$$

whilst $FeBr_2$ in ammonia solution produces the green precipitate of ferrous hydroxide ($FeOH_3$).

The results from these tests and the dust analysis on the deposits formed in the cavity suggest that some reaction between discharge products and cavity material is taking place, though the overall effect on the laser performance due to fuel loss in this way is thought to be minimal. The shot to shot decrease in output energy, shown in figure 4.8 as, observed during operation of the laser is thought to be caused by the build-up of dust in the lasing medium. As the figure shows the output energy falls off fairly rapidly with the initial shots then becomes more constant after 6 or 7 discharges. Visual inspection of the discharge volume after each of the initial shots indicated that the concentration of dust did in fact increase, as observed by the scattering of the HeNe alignment laser. The origin of the dust being mostly due to corrosion products ablated from the surface of the electrodes is confirmed by the discontinuity in output energy shown in the figure after the tenth shot. At this point a discharge was initiated without the preionisation source turned on, the arc-like nature of this discharge between the electrodes causing more dust to be dislodged into the gas resulting in the observed decrease in output energy. The suspicion that dust formation and not fuel loss through the chemical reactions outlined above is responsible for the observed decrease in performance was confirmed by an increase observed in output energy when the laser was left for a short period to allow some of the dust to settle inside the cavity. Subsequent shots again showed a decrease in pulse to pulse energy as the discharge

produced shock wave disturbed the settled dust. Use of a recirculating system to control this dust build-up should dramatically improve the shot to shot reproducibility of the laser.

As previously mentioned a recent study by Liu and Liberman [10] on the chemical control of HgBr lasers has addressed very closely the materials problems in these lasers. Their final conclusions are that materials such as stainless steel, which will initially react with the mercury bromide to produce a protective layer on the surface inhibiting any further reaction, could be used in the cavity of a long life laser if situated at some distance from the discharge region. Electrode materials should be made form non-reactive materials such as gold or platinum to ensure no reactions occur which will leave a film on their surface subsequently ablated by the discharge. Other workers [8] have experimented with a number of materials in their cavity including platinum, gold, molybdenum and tungsten and shown excellent gas lifetimes ($> 10^8$ shots) are achievable with little build-up of corrosion dust. They attributed the formation of dust to corrosion induced by water vapour present in the cavity [29], highlighting the necessity of a clean vacuum tight system for a long life laser. Unfortunately financial and time constraints limited the materials tested in the laser described here but for a truly long life laser chemical compatibility must be assured and this point should be addressed in future work.

In summary, a cavity and gas filling system which gives reproducible results, designed using knowledge of materials compatibility at the time of conception has been built. The gas handling system allows changes in the gas composition to be carried out fairly rapidly enabling a full parametric study of the laser to be undertaken on a reasonable timescale. With the addition of a gas flow and clean up system long gas liftimes and excellent shot to shot reproducibility would be expected.

CHAPTER 4

REFERENCES

1. M.R. Osborne, Ph.D. Thesis: "An X-ray Preionised Excimer Laser". Imperial College, London (July 1985).
2. B.L. Wexler, A.P. Desoriers and J.D. Simpson: Paper TH Q4 Conference on Lasers and Electro-Optics, Baltimore (1985).
3. E.J.Schimitschek, J.E.Celto and J.A.Trias, Appl. Phys. Lett. 31, 608 (1977).
4. E.J.Schimitschek and J.E.Celto, Optics Lett. 2, 64 (1978).
5. F.Kvasnik and T.King, Optics Comm. 41, 199 (1982).
6. R. Burnham, Appl.Phys.Lett. 33, (2) (July 1978).
7. R.Burnham and W.T.Whitney, J. Appl. Phys. 52, 3849 (1981).
8. Mathematical Sciences Northwest Inc. : Final Report, 200 Watt Mercury Bromide Laser (June 1984).
9. J.H.Parks, Appl. Phys. Lett. 31, 297 (1977).
10. C.S. Liu and I. Liberman, IEEE J.Quant.Elect. QE 23, p. 245 (February 1987).
11. International Tables for X-ray Crystallography. Volume 3, page 157 (1962). (The Kynoch Press)
12. T.A.Znotins, C.H.Fisher, T.E.DeHart, J.P.McDaniel and J.J.Ewing Appl. Phys. Lett. 46, p. 228 (February 1985).
13. A. Feltham, private communication.
14. H.N. Rutt, J.Phys.D. 12, 345-353 (1979).
15. Kaelble, Properties of X-rays.
16. The Torlon was obtained from Polypenco Ltd.
17. Handbook of Materials Science volume 2 CRC press inc Florida.
18. P.W.Smith, Private Communication.
19. 'O' Rings Design Manual, George Angus & Co Ltd.
20. Teflon FEP encapsulated Viton o-rings supplied by Polytetron Ltd., Mönchengladbach, Germany.
21. Nomex aramid paper is manufactured by Du Pont and supplied by Kensulat Ltd., London.
22. H.J. Baker, N. Seddon, J.Phys.E : Sci. Instrum. Vol 18, p. 277 (1985).

23. E.J. Schimitschek and J.E. Celto, Opt.Lett. 2, 64 (1978).

24. M.Matera, R.Buffa, P.Burlamacchi, L.Fini and R.Salimbeni, Rev. Sci. Instrum.56, 205 (1985).

25. Scaling Studies for Mercury Bromide Lasers (March 1981). Report by Mathematical Sciences Northwest Inc., contract No. ONR : N00014-80-C-0245.

26. M. Stonefield, Manchester University, private communication.

27. Cotton and Wilkinson, Advanced Inorganic Chemitry Interscience Publishers (1962)

28. See for example: Macro and Semimacro Quantitative Inorganic Analysis by Arthur I. Vogel (Longmans).

29. J.J. Ewing, private communication.

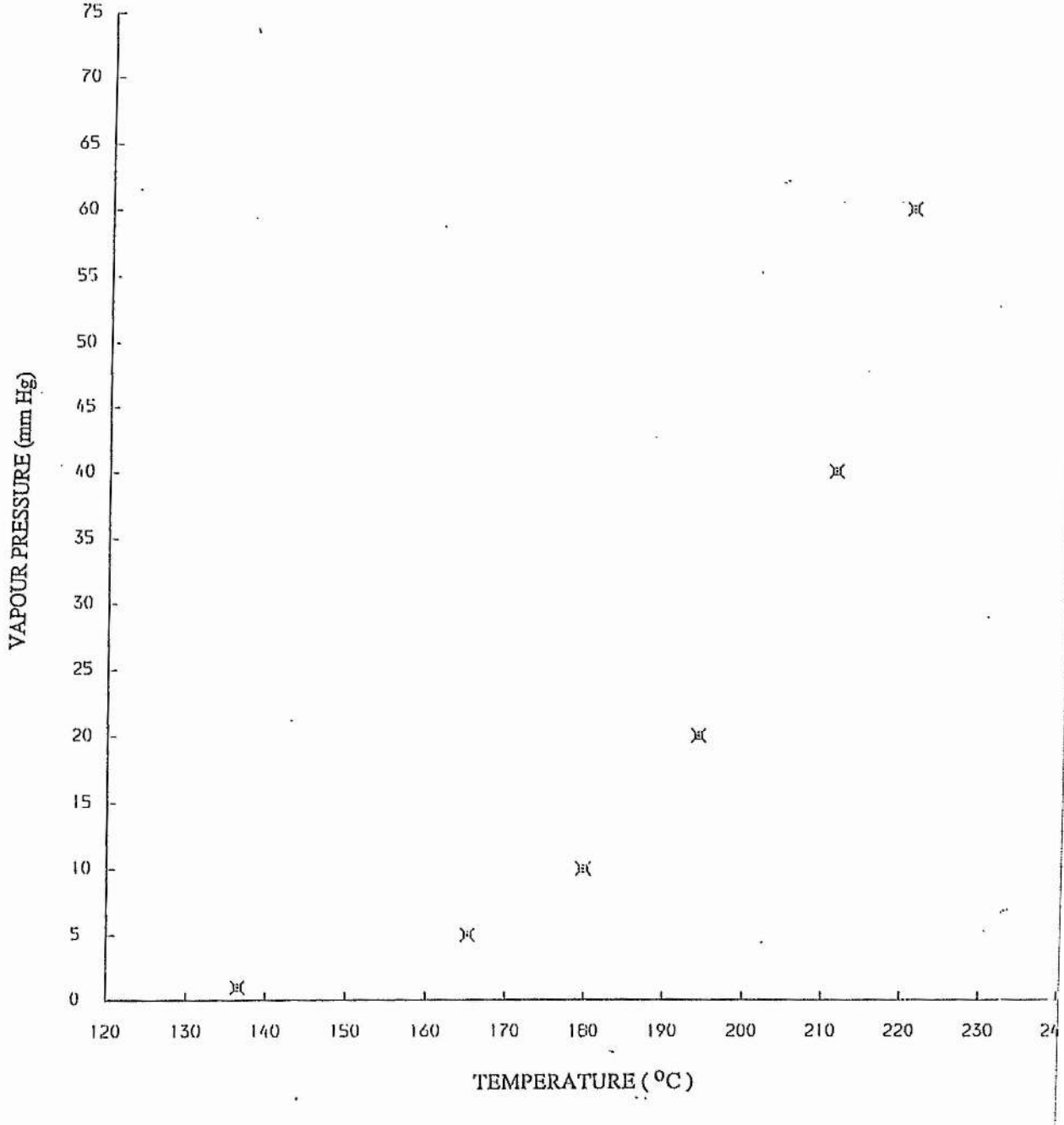

FIGURE (4.1): Mercury bromide vapour pressure as a function of temperature.

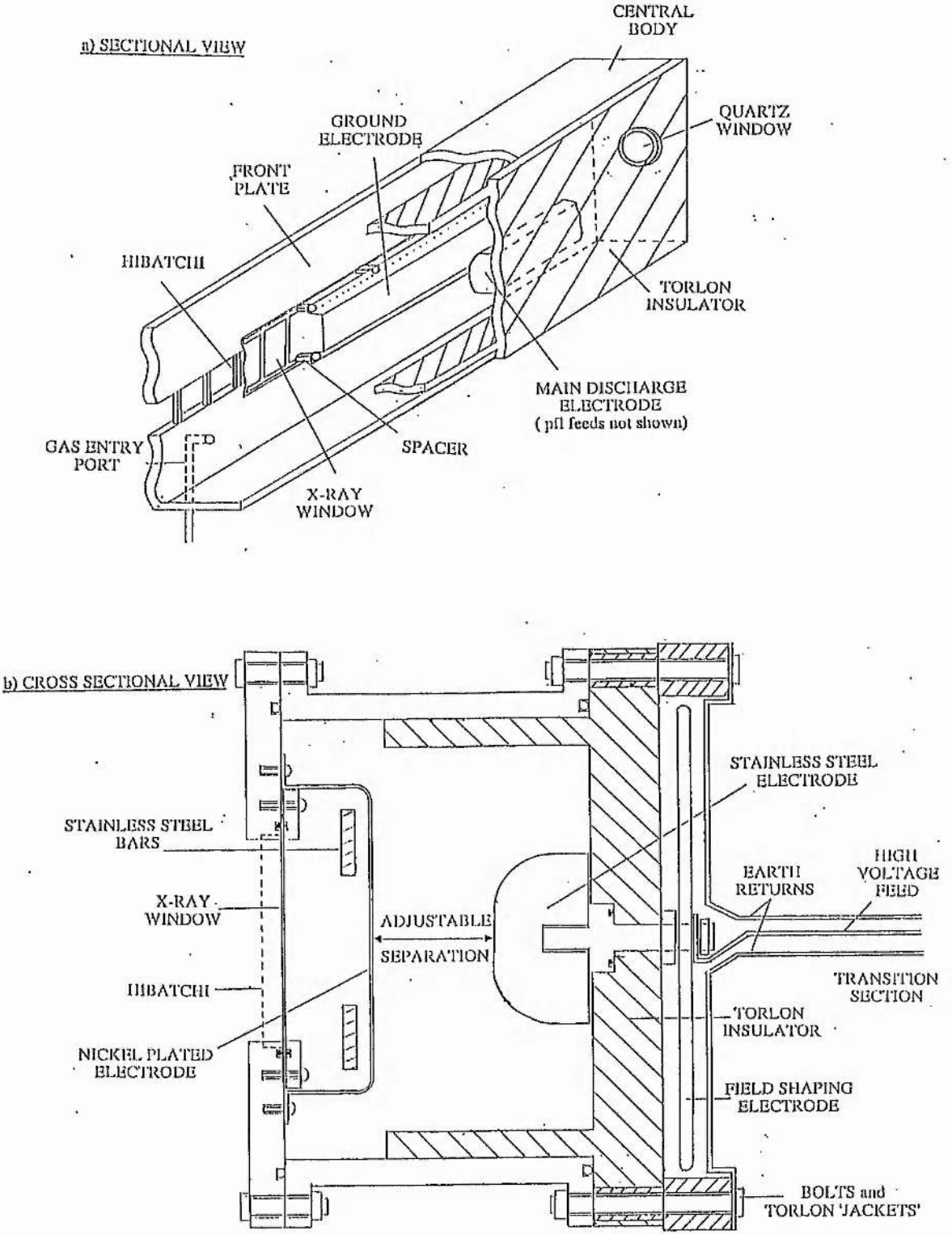

FIGURE(4.2):The design of the laser discharge cavity.

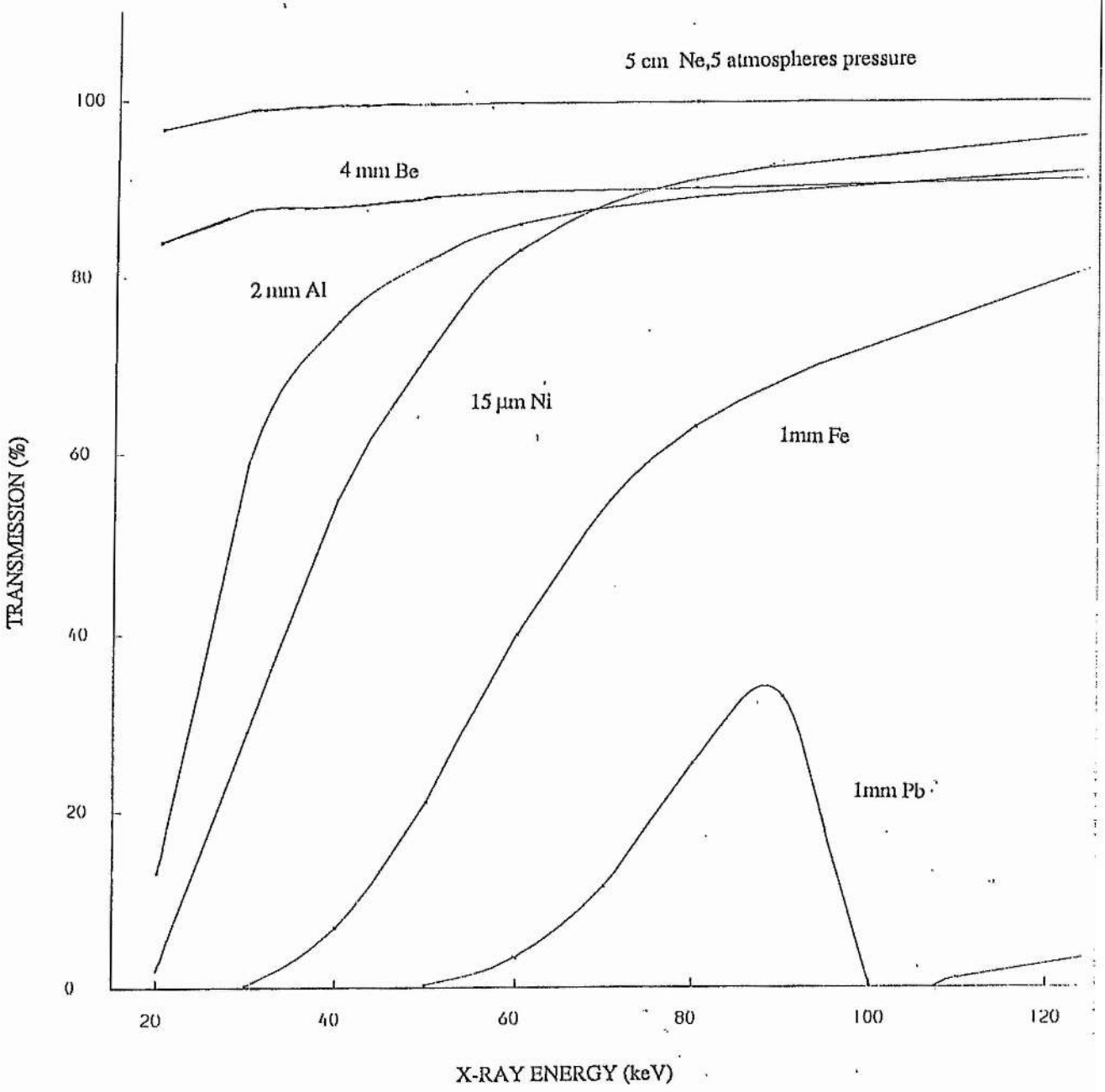

FIGURE (4.3) : X-ray transmission through various materials over the energy range 20 - 120 keV.

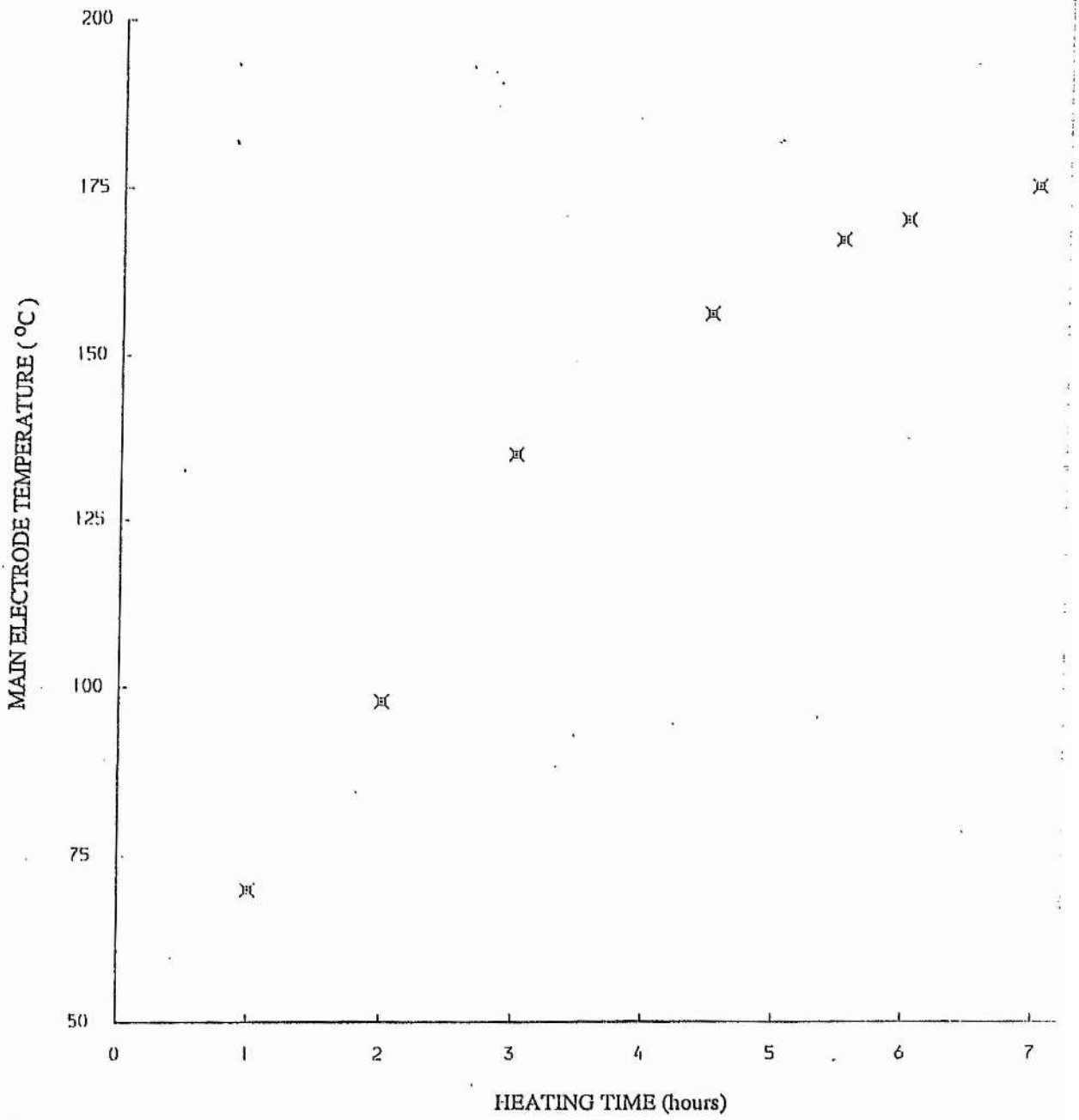

FIGURE (4.4) : Main electrode temperature versus heating time with oven temperature set at 180 ^{o} C.

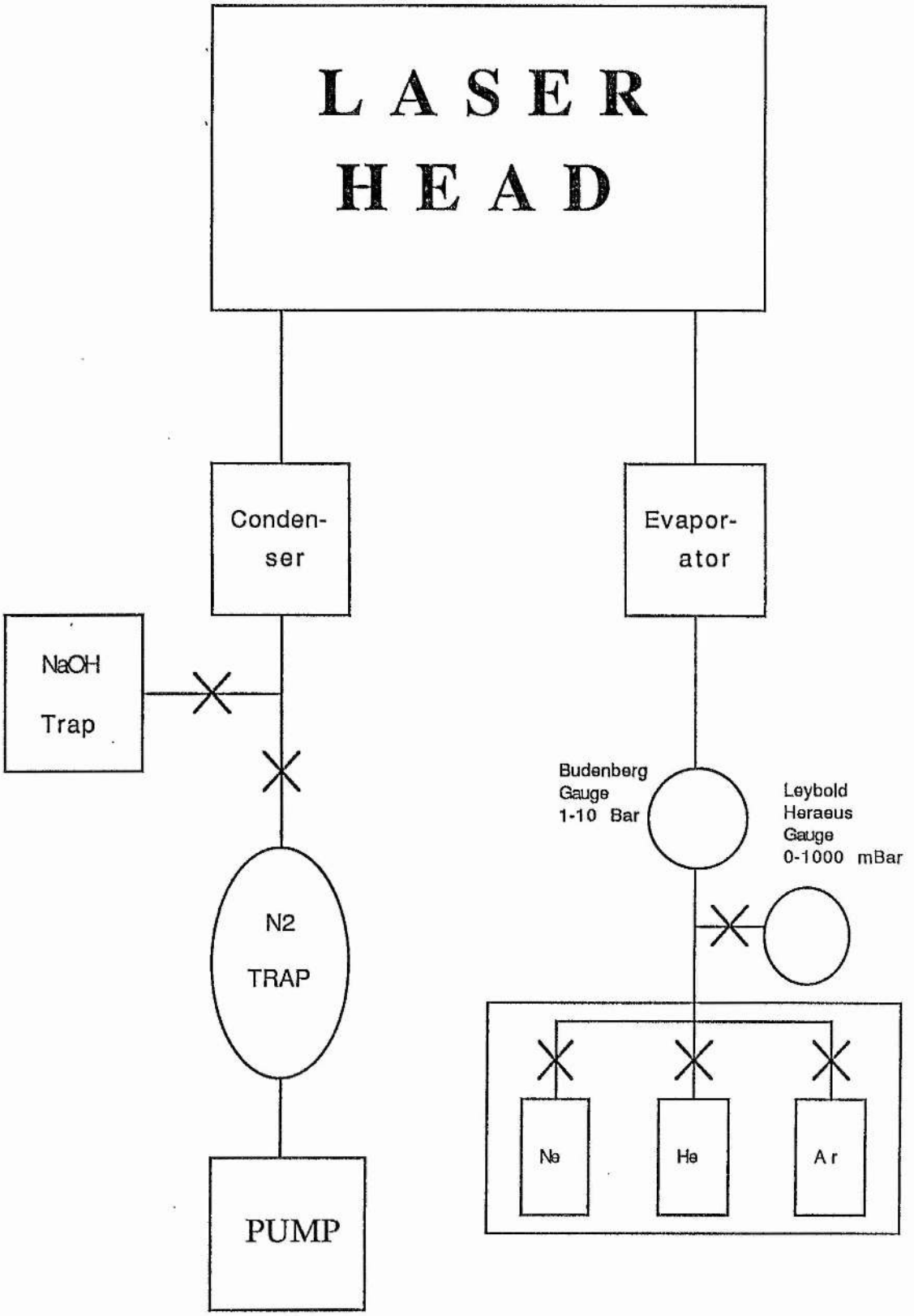

FIGURE (4.5): Schematic diagram of the gas handling system.

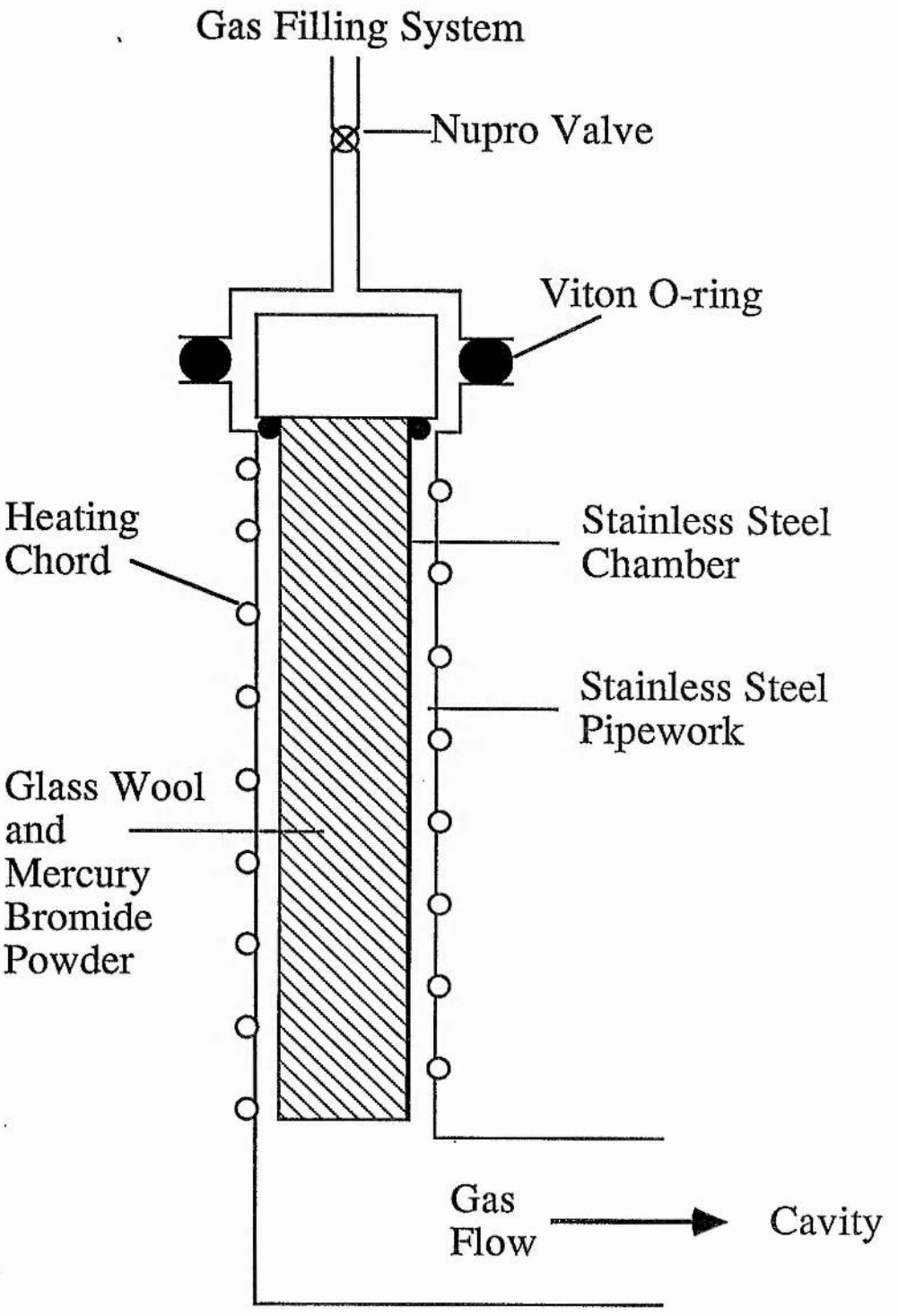

FIGURE(4.6): Schematic diagram of the evaporator. The condenser is similar but only the input end is heated.

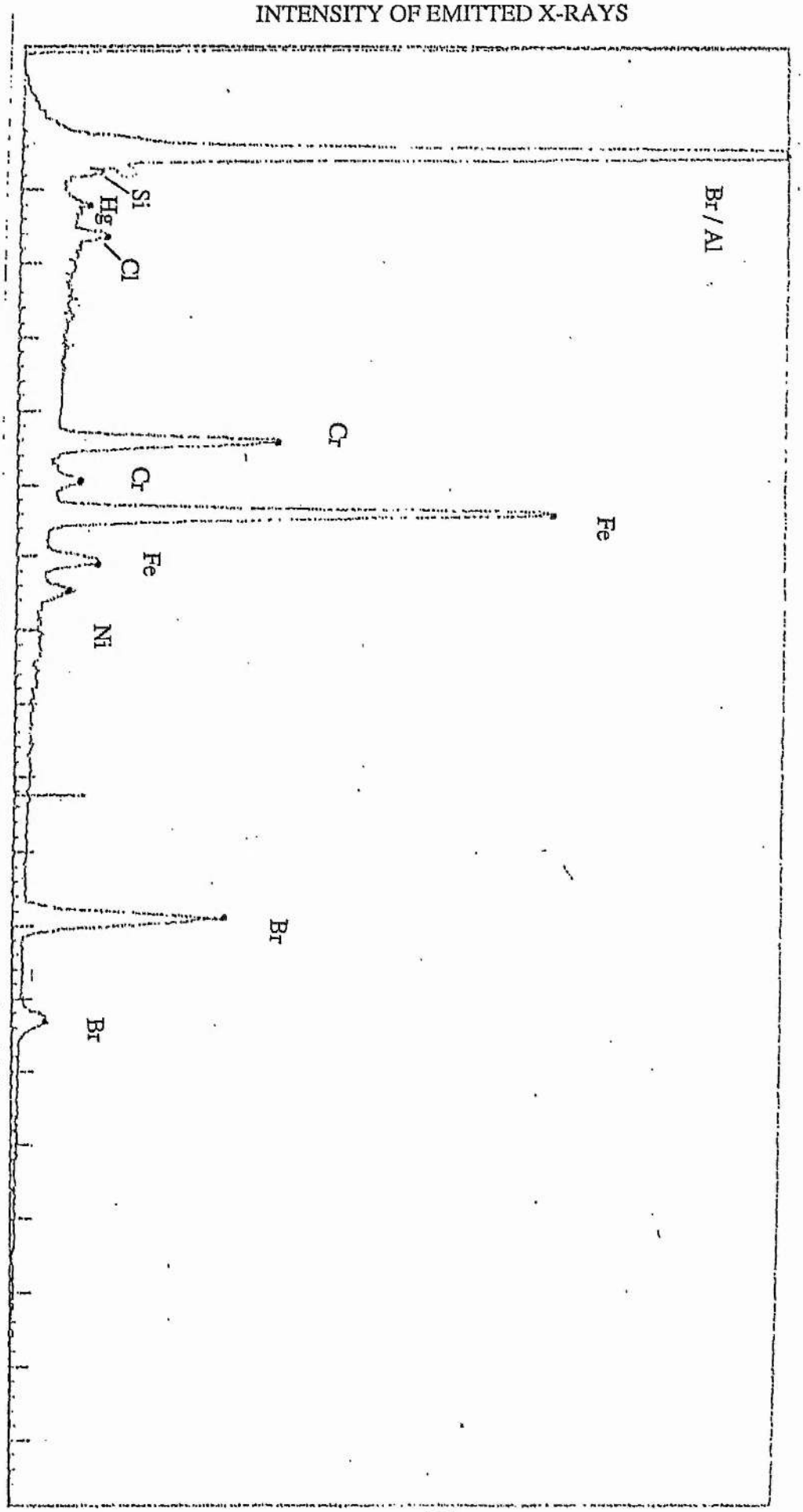

FIGURE (4.7) : Scan from an electron beam micranalysis

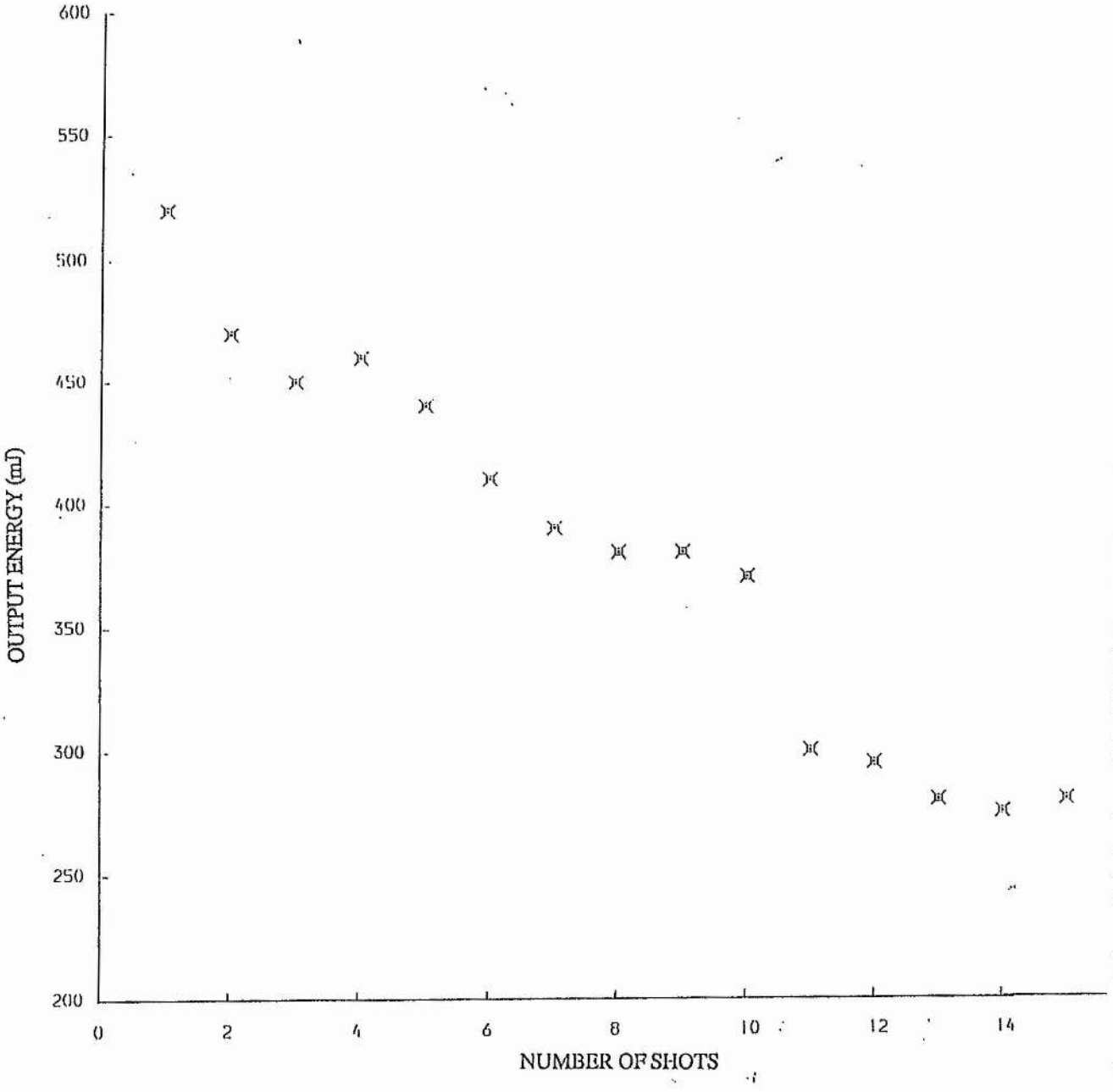

FIGURE (4.8) : Output energy with number of shots fired.
150 °C mercury bromide reservoir temperature.
2 Bar Ne buffer.

CHAPTER 5

Laser Operation and Optimisation

5.1 Introduction

A brief history of the problems encountered during initial attempts to achieve lasing from mercury bromide is now given with a discussion of how these were overcome. In the following sections results obtained during a parametric study to optimise the operation of the laser are presented and discussed. Unless otherwise stated these results were obtained with the ten parallel modules in the DPFL system, each of ten sections, charged to 30 kV and an X-ray source charge voltage also of 30 kV. The optical cavity used consisted of a flat 100% reflectivity multidielectric mirror and a 33% reflecting output coupler at the laser wavelength, separated by 1.5 metres. This plane-plane resonator configuration allows maximum utilisation of the discharge volume. Using only a quartz flat as an output coupler a decrease in laser performance of 5-10% was observed so the 33% output coupler was used in the optical cavity during all experiments described. Alignment of the optical cavity followed a routine procedure in which a HeNe laser beam directed along the discharge volume was used initially to align the windows of the cavity and then the external optical cavity. During operation of the laser it was found benefitial to adjust the mirrors occasionally, as the alignment was found to drift due to heating of the mirror mounts, resulting in a subsequent improvement in output.

Initial experiments with the laser indicated the maximum output and hence highest operating efficiency was achievable at the maximum possible discharge gap. To this end the majority of the experiments with the laser were carried out at an electrode separation of 5 cm and all the results presented in the following sections were obtained at this spacing. The output energy results presented are the values obtained from the initial shot from the laser following a fresh gas fill, thus eliminating any detrimental effects of dust in the cavity on the laser performance as discussed in chapter 4. For similar reasons the pulse length measurements were taken consistently after only a few shots with the new gas mix. Reproducibility of these results was confirmed by numerous operations of the laser under the same conditions of gas composition etc., the fill to fill variation was found to be within 10%. Following a number of repeated operations of the laser a deposit was observed to build up on

the windows of the cavity. The area on the window where this deposit formed followed that of the discharge and hence where the laser beam impinged on its surface leading to the conclusion that the deposit was formed during some photochemical reaction in the gas at the surface of the optic. The deposit could clearly be seen in the beam of a flashlight shone into the cavity and also as it scattered the beam from the HeNe alignment laser. To reduce the deterimental effects of this on the performance of the laser the windows were routinely cleaned with a solvent which easily removed the deposit. No attempts were made to analyse the deposit as it was produced in too small a quantity to enable a significant amount to be collected for testing.

5.2 Initial Laser Experiments

Figure 5.1 shows a schematic diagram of the laser system and photograph 5.1 shows the complete laser assembled and in position ready for operation. The X-ray source and DPFL system were DC charged from their respective charging units and discharged via the two thyratron trigger units. To ensure adequate preionisation existed in the gas prior to initiation of the main discharge a delay line, composed of a suitable length of coaxial cable, was inserted between the two thyratron trigger units affording control over the relative temporal positions of the voltage pulses from the X-ray source and discharge. These were monitored using copper sulphate potential dividers and, after suitable attenuation, the signals were multiplexed at the Tektronix 519 oscilloscope to show their temporal overlap. Multiplexing of the signals in this fashion ensures the signals are accurately synchronised in time. Sufficient delay was introduced between the two trigger units to prevent initiation of the discharge pulse until after the peak of the X-ray voltage pulse and figure 5.2 shows typical pulses multiplexed in this fashion. These results are discussed in more detail later. A cable length of 40 metres was found to give the required delay to produce a preionised discharge and this was used as standard on the majority of the experiments on the laser. With this length of cable the discharge pulse commenced after the preionisation pulse had reached its peak, as the figure shows. However varying this delay to introduce a significant time delay between the preionisation pulse and the discharge pulse led to some interesting results which are discussed in section 5.5.

The first experiments with the complete laser system involved attempts to produce a

uniform glow discharge in an inert gas such as helium or neon and these showed some problems existed. Using a T.V. camera and video to visually monitor inside the discharge region two effects were observed. The discharge was not a uniform glow discharge between the electrodes, instead a constricted or 'arcy' discharge was observed, also during these experiments a surface breakdown problem occurred as the discharged tracked across the surface of the Torlon insulator and did not form between the electrodes. These observations pointed to two problems of the system, the X-ray source was not producing sufficient preionisation inside the gas to enable a glow discharge to form and parasitic discharges under these low initial electron conditions were emanating from the corners of the main discharge electrode near the surface of the insulator causing flashover to occur. The first problem was overcome by work on the X-ray source to improve its output exposure and uniformity as discussed in chapter 3.

The surface tracking issue was tackled by the addition of a field shaping electrode [1] to the electrical feeds to modify the field lines produced in the cavity so as to minimize any enhancement effects at the electrode insulator interface. Illustrated in figure 4.2 of the previous chapter is the position of the field shaping electrode incorporated in the laser. The effect of this electrode on the field lines around the main discharge electrode is shown schematically in figure 5.3. Without the added electrode in position severe field enhancement occurs at the corners of the discharge electrode near the surface of the insulator due to the geometry of the electrical feeds connected to the cavity. Even though these corners were radiussed in anticipation of this, flashover problems were still encountered. Upon inclusion of the field shaping electrode the field enhancement is removed from the discharge electrode, the main area of enhancement then being moved to the edges of the added electrode external to the cavity. By careful shaping of the edges of this electrode and through effective insulation between it and the earth return feeds, subsequent problems of breakdown or flashover were reduced. After installation of this electrode the surface tracking problem inside the cavity was eliminated and only one breakdown problem occurred, due to electrical punchthrough between it and the earth return, which was easily overcome by the addition of extra insulation between them.

Following these modifications uniform glow discharges were obtained and figure 5.4 shows open shutter photographs of a preionised discharge in neon gas at one atmospere

pressure and for comparison a constricted discharge where the preionisation source is turned off when the discharge is initiated. In the discharge without preionisation numerous streamers are observed to form along the length of the electrodes primarily emanating from the corners of the main discharge electrode where any field enhancement effects are likely to be more pronounced. However some streamers are observed to form in the middle of the electrodes and these probably start from some non uniformity in the surface at that point. This situation is of course unsuitable for effective excitation of a laser gas mixture because of the low current densities and hence excitation rates in the areas outside the individual streamers. Indeed during operation of the laser if a non preionised discharge was initiated no laser output was observed. In contrast to this the uniform nature of the glow discharge produced with effective preionisation allows efficient excitation of the laser gas to take place and production of a high quality laser beam.

To ensure the system would operate as a laser a short time was spent in operating it as an XeCl laser. This allowed the successful demonstration of the preionisation source and DPFL system without the added complexities of heating the cavity and achieving the required concentration of mercury bromide vapour. Energies in excess of 1 Joule at 308 nm were obtained from the system and discharge gaps of 5 cm were successfully operated at presures up to 5 atmospheres. Some brief experiments with the X-ray source showed there to be adequate preionisation and no tracking problems were observed even at the largest electrode separation.

Following this successful demonstration, operation of a mercury bromide laser was attempted and once again problems were encountered. The repetitive failure of the cavity O-rings after one or two heating cycles and the initial use of the static gas fill system as discussed in chapter 4 made progress slow and tedious until these problems were eliminated. Once these were identified and dealt with successful lasing of mercury bromide was achieved and the remainder of this chapter discusses results obtained with this laser system.

5.3 Optimisation Experiments

Using the gas flow filling technique outlined in chapter 4, blue-green emission from the laser could be routinely obtained and optimisation experiments with respect to buffer gas, buffer gas pressure, mercury bromide vapour pressure, discharge gap etc. were undertaken.

Output energy was monitored by a calorimeter (Laser Instrumentation Ltd. Model 7AN) and temporal profile of the output pulse using a photodiode (ITL model TF1850 with S-20 photocathode). To prevent saturation of the photocathode and possible damage, the output beam was reflected off two glass slides and passed through a number of attenuating gauzes (normally 5 or 6) to reduce the beam intensity prior to illumination of the photodiode. Uniformity of the output beam was monitored visually through burn patterns recorded on blackened polaroid film exposed to the laser emission and by observing the laser beam irradiating a suitable target.

The initial experiments with neon and helium buffer gas identified effects which were detrimental to the quality of the discharge and hence the output beam. The discharges were observed to be 'arcy' in nature, an effect which was not present in experiments with the XeCl laser mix, producing two intense regions of emission emanating from the radiussed corners of the main discharge electrode. Figure 5.5(a) shows a typical burn pattern observed from this type of non-uniform discharge for a 5 cm electrode separation, the two constricted regions of emission are obvious. The burn patterns are reduced in size compared to the actual discharge dimensions as some focusing of the output beam was found necessary to produce reasonable images. At reduced electrode separations (~ 2 cm) good beam quality was observed but increasing the discharge width resulted in deterioration of the beam as the discharge became more susceptible to local variations in electric field. It appeared that, although profiled, field enhancement on the radiused corners of the main discharge electrode was promoting constriction of the discharge in these two areas. Upon opening of the cavity for inspection the main discharge electrode was found to be marked along its length near its radiused edges and directly opposite these on the ground electrode similar markings were observed. These results are indicative of arcing taking place during the discharge originating from these areas as the results of the burn marks indicated.

A similar effect was investigated by Kushner et al. [2] who used streak cameras to monitor the temporal evolution of their discharge and a theoretical model to predict the effect of electrode contours on the discharge. The influence of the electrode contours on the stability of the discharge is manifested through the local value of E/N. A significantly higher value of E/N in one region of the discharge resulting from the electrode shape will alter local excitation and ionisation rates. The degree to which these spatially varying rates result in one

area of the discharge becoming more conductive than another, leading to constriction, depends on the difference between local values of E/N. The model of Kushner et al. showed the cases with severely contoured electrodes resulted in more severely constricted laser pulses. In this laser the severe contouring of the electrode occurs at the profiled edges where the discharge is observed to constrict.

To overcome this instability problem the discharge had to be restricted to areas away from those responsible for promoting constriction. This was achieved by masking the flux of preionisation X-rays using stainless steel collimating bars placed behind the X-ray transmitting electrode. The position of these bars is shown in figure 4.2. These were positioned in such a way as to ensure the corners of the profiled electrode were not irradiated and the discharge was confined to the central area of the electrodes. Masking of the X-ray flux in this manner as an effective method of controlling the discharge width was established during the experiments when this system was operated as an XeCl laser mentioned earlier. This technique was used by Tallman and Bigio [3] to improve the discharge uniformity in their X-ray preionised device with impressive results. Similar experiments were carried out by Taylor [4] in a laser utilising laser induced preionisation where the width of the discharge could be controlled by using masks to restrict the width of the preionisation beam. A further benefit afforded by this masking process is the reduction in X-ray flux which falls upon the Torlon insulator subsequently reducing any preionisation of the surface and the possibility of surface flashover. During this initial experimental phase it was also observed that the discharge uniformity was dependent on the concentration of mercruy bromide vapour present. Even with the preionisation X-rays masked, if vapour pressures in excess of 4-5 mbar were used in the gas mix constriction of the discharge was again observed to take place. These low values of vapour pressure are approximately half those observed by other workers [5] to produce optimum laser performance. This feature appears to be device specific and is possibly a further effect of the main electrode profile and of the fairly low recorded exposures and hence preionisation electron density formed by the X-ray source in the discharge region. This point is discussed in more detail in chapter 6.

These initial experiments defined the operating regime of the laser in terms of electrode spacing, discharge width (determined by collimation of the preionisation X-rays) and mercury bromide vapour pressure, within which a uniform discharge and good output beam

quality could be produced. Figure 5.5(b) shows burn patterns obtained under operating conditions of 5 cm electrode gap, 3 cm X-ray flux, 3.5 mbar mercury bromide vapour pressure and 3 bar neon buffer gas. The improvement in beam quality over the output before the above restrictions were imposed is obvious. A typical set of device waveforms for this mix is shown in Figure 5.6(a) corresponding to an output energy in excess of 700 mJ and an efficiency of ~ 0.8 % defined as laser output energy divided by energy stored on the DPFL. The voltage is measured at the short transmission section before it passes through the oven wall. For this particular case the breakdown voltage is ~30 kV and the discharge self sustaining voltage is ~ 9kV which is lower than the value at which optimum energy transfer from the DPFL supply takes place. As will be discussed, closer matching is achieved at higher buffer gas and mercury bromide vapour pressures. The laser pulse duration is 75 nsec full width at half-maximum and laser oscillations initiate some 40 nsec after breakdown of the gas. As the electrical length of the DPFL is 240 nsec, as described in chapter 2, this implies a large proportion of the energy stored on the line is being deposited after the termination of the laser pulse. Use of a shorter pump pulse duration should then result in increased efficiency and this point is dealt with in section 5.5.

Another important parameter of the discharge which can be measured is that of the current passing through the laser. Knowledge of the magnitude and temporal behaviour of the current pulse along with the voltage pulse can give information on the rate of power deposition into the gas and can lead to a large amount of information pertaining to the operational characteristics of the laser. It is however important in making such current measurements to do so in a manner which results in the observation of the true current pulse passing through the laser head. One widely used technique requires the use of extremely low impedance current viewing resistors (CVR's) placed in the earth return from the laser in close proximity to the laser head to eliminate any inductive effects which may affect the pulse shape. Another incorporates Rogowski coils, which measure the current passing through the conductor which it encircles, placed around the electrical feeds near to the cavity. Although some current measurements were undertaken on the laser using T and M Research Products CVR's these results were not felt to be representative of the true current pulse in the discharge and are not presented here. This was because of the obtrusive nature of the oven surrounding the cavity and the high operational temperatures resulting in the subsequent

inability to place the current probe in the vicinity of the laser head.

Once the initial operating parameters had been established as discussed above a full parametric study of the laser was undertaken. The results of this study are now presented and unless otherwise stated they were recorded with a 5 cm electrode gap, a collimated X-ray flux 3 cm wide and a neon buffer gas pressure of 3 bar.

Figures 5.7-5.9 show the effect of mercury bromide vapour pressure on the performance of the laser. The vapour concentration is given in terms of the mercury bromide reservoir temperature, the vapour pressure specific to the reservoir temperature may be determined by reference to figure 4.1. Although these results are pertinent to a neon buffered mixture at 3 atmospheres, similar trends were observed at other pressures and for other buffer gases. The peak in output energy corresponds to the peak in the observed pulse width and these both decrease of reservoir temperatures in excess of 150^{o}C. Constriction in these lasers has been shown to be a function of several factors including mercury bromide concentration and discharge products [2] which contribute to a large extent in the constriction process, primarily through the multistep ionisation processes of excited states of mercury as discussed in chapter one. The severe degree to which the presence of mercury bromide affects the discharge was observed experimentally upon running the laser following the operation of an XeCl laser discharge in the same system which showed no effects of discharge constriction as observed in the latter case. As the mercury bromide vapour pressure is increased, more mercury is formed during the discharge and more rapid constriction occurs. The observed turnover in output energy and pulse length is then a direct consequence of the deteriorating discharge stability at higher mercury bromide concentrations which is also reflected in the decrease in output beam quality observed through the burn patterns.

Figure 5.9 shows the variation in the discharge self-sustaining voltage as a function of mercury bromide concentration. The dominant electron loss process involving the parent compound in these laser discharges is through recombination with the mercuric bromide ion [2]

$$e^{-} + HgBr_2^{+} \rightarrow HgBr + Br\,.$$

An increase in the mercury bromide concentration results in an increase in the formation of

these ions during the discharge and increased electron attachment. To restore the balance between ionisation and attachment for sustained discharge operation the discharge operates at a higher value of E/N where ionisation rates are increased. This shows up directly through the value of the self sustaining voltage.

Figures 5.10-5.12 show the effect on the laser performance of various buffer gases over the range of operating pressure with the mercury bromide concentration fixed at the optimum value determined by the 150°C operating temperature of the reservoir. The maximum output energy is observed with neon buffer at a pressure of 4 bar and is a factor of two greater than that for helium or argon. Other authors have also reported improved laser performance using neon buffer gas not only for mercury bromide discharge lasers [5] but also for other discharge excited excimer lasers [6]. The improved performance with neon buffer is a direct consequence of the much longer pulse lengths typical of this mixture. However, comparison of figures 5.10 and 5.11 show the peak in output energy and hence laser efficiency occurs at 4 bar whilst the maximum pulse length occurs at 3 bar and decreases at higher pressures. The observed peak in output energy is due to the combined effect of the pulse length being close to its maximum value and the increase in discharge self-sustaining voltage with pressure as shown in figure 5.12. This results in a more efficient transfer of electrical energy from the DPFL to the gas as the discharge operates closer to the matched condition. At higher gas pressures discharge instabilities onset with subsequent constriction and more rapid termination of the laser pulse reducing laser output.

Shorter output pulses at lower buffer gas pressures are typical of helium based mixtures leading to lower output energies. The higher self-sustaining voltage observed when using helium buffer gas, as shown in figure 5.12, means the laser operates at higher E/N values than for neon buffered mixtures, where ionisation rates are increased promoting constriction of the discharge even at low pressures. An analysis by Cravath [7] of the rate of energy loss from electrons of mass m moving through a gas of molecules of mass M shows that the fractional energy loss per collision is given by

$$f = \frac{8}{3}\frac{mM}{(m+M)^2}\left(1-\frac{T_m}{T_e}\right)$$

where T_m and T_e are the molecular and electronic temperatures. Under normal discharge conditions $T_e >> T_m$ so the term in parenthesis approaches unity and as M >> m the equation may be simplified to

$$f = \frac{8m}{3M}$$

From this we see that when the lighter helium buffer gas is used the fraction of energy transfer during elastic collision processes is much higher than that for the heavier neon atom. This in turn lowers the electron temperature in the gas and forces the discharge to operate at a higher E/N to sustain the glow discharge, which is reflected in the observed increase in self sustaining voltage with the lighter buffer gas.

Argon based mixtures were, in general, difficult to break down and resulted in poor laser performance in contrast to the e-beam sustained results of Hsia et al. [8]. Figure 5.6(c) shows a typical set of device waveforms for argon buffer gas at a pressure of 1.5 bar. In comparison to the results of the neon mixture shown in the same figure the long avalanche time before the glow discharge is established is obvious. This results in the late onset of lasing observed with this buffer gas and corresponding short laser pulses. As the argon buffer pressure was increased this breakdown time also increased resulting in a reduction in the length of the laser pulse, as shown in figure 5.11, until at pressures in excess of 2.5 bar the gas would no longer break down. This behaviour with Ar buffer has also been noted elsewhere [9] and could be due to the existence of a significantly lower threshold for the excitation of argon [10] than for neon [11] in the electron energy range of interest, resulting in a competitive excitation process with that of electron impact ionisation of $HgBr_2$ [12]. This in turn would lead to the longer formative phase time of the discharge through the slower increase in electron density from ionisation of mercury bromide, resulting in the observed behaviour [13].

The results of this parametric study of buffer gases established that neon was the optimum gas to use with this laser resulting in highest output energies and maximum efficiency. In all subsequent experiments on the laser presented here this was used as the

preferred buffer gas. However in the interests of preserving neon supplies (the cost of a typical fill being ~ £15!) the laser was usually operated at 3 bar pressure and an increase in output energy of 10-15% as shown in figure 5.11 would be expected at 4 bar.

5.4 Effects of Additives

Numerous authors have reported improved performance with small scale mercury bromide lasers when additives such as N_2, Xe and SF_6 were introdced into the gas mixture [14,15,16]. The consequences of using such additives have been extensively studied and, as will be discussed, two trains of thought currently exist for their observed effects on laser performance. Figures 5.13-5.15 show the results obtained with this laser when various amounts of additives were introduced to the gas mixture. None of these showed any improvement in output energy and even small amounts of Xe and SF_6 had catastrophic effects on laser performance. With nitrogen a slow decline in output energy was observed as the percentage of additive was increased. However an extension of the pulse length to the maximum obtained with this laser of 92 nsec FWHM at a concentration of 1.5% occurred. This effect was, in part, thought to be due to the stabilising effect nitrogen has been shown to have on discharges in mercury bromide lasers [9,17]. Fisher et al. [9] observed, using streak cameras, a more uniform discharge lasting for a longer period of time when nitrogen was added to the mixture. An effect attributed to a reduction in multistep ionisation processes and subsequent discharge constriction through changes in kinetic processes following the addition of nitrogen.

Other authors have reported substantial performance improvements upon addition of nitrogen to small scale, preionised discharge, mercury bromide lasers [14,15]. In these devices two possible reasons have been established for the observed effects. Nitrogen increases the self-sustaining voltage of the discharge, as figure 5.15 shows, resulting in improved matching of the discharge local to the pulsed power supply, depositing more energy in the gas and increasing laser efficiency. For lasers where the match is not optimum, as is typical of devices with small discharge dimensions, this effect in part explains the observed improved behaviour. However in the device described in this thesis the matching between the discharge load and DPFL is fairly close and any improvement in energy transfer

through the addition of nitrogen is offset by excitation processes in the additive, which compete during the discharge, with those of upper laser level production. Figure 5.6(b) shows device waveforms for a gas mix including 1.5% nitrogen. Comparison with the traces for the neon buffered mix shown in the same diagram, under the same excitation conditions, shows the resulting pulse length extension and increase in discharge self sustaining voltage with the additive. Also evident in these waveforms is a delay in the onset of lasing observed upon the addition of nitrogen. An effect attributed to electronic and vibrational excitation of the additive competing with upper laser level excitation and increasing the required pumping time for the laser to achieve threshold conditions.

Energy transfer from metastable states of nitrogen to mercury bromide resulting in formation of the upper laser level has also been proposed [18] and extensively studied [15] as an explanation for the improved performance of small scale lasers using this additive. However, as discussed above, no beneficial effects on laser output energy directly attributable to this process were observed during experiments on this device although the resulting increase in pulse length upon the addition of nitrogen may, in part, also be explained by this scheme. The existence of these metastable states results in a storage mechanism in the medium whereby, following the collapse of the discharge, pumping of the upper laser level can still continue through this energy transfer process. Although this effect was not examined in great detail it is certainly an area worthy of further investigation as it may give an insight to the possibility of producing longer pulses from these lasers. A similar upper laser level excitation route by energy transfer from excited metastable states of xenon additive, proposed by Chang and Burnham [19] was also investigated. The observed decrease in performance with Xe additive, shown in figures 5.13- 5.15, is in part due to the reduction in discharge self-sustaining voltage through the low ionisation potential of this additive, resulting in less efficient energy transfer from the pulsed power supply to the gas. Absorption in the blue/green region by Xe_2^* species formed in the discharge [8] may also contribute to lower optical extraction efficiency in mixtures containing Xe again leading to a reduced output.

Recently, substantial improvements to the operation of a UV preionised mercury bromide discharge laser were reported upon addition of SF_6 to the gas [16]. These results

are attributable to the improved matching between the discharge and the pulsed power supply. The addition of electronegative SF_6 to the gas mixture in the device described here resulted in a rapid increase in the discharge self-sustaining voltage as the concentration was increased and a decrease in the output energy and pulse length. The major effect of SF_6 is due to the attaching nature of the additive which affects the balance between electron production in the discharge through ionisation, and loss through attachment. This forces the discharge to operate at a higher value of E/N increasing the rates of ionisation to restore the balance between electron loss and production, which is observed as an increase in the discharge self sustaining voltage. The higher operational E/N of the discharge also promotes the runaway multi-step ionisation process in mercury, discussed earlier, resulting in more rapid constriction of the discharge observed during these experiments through the deterioration in uniformity of the output beam, with subsequent pulse shortening and decrease in output energy. Other effects of this additive are to diminish the effective preionisation density prior to the initiation of the discharge, the effect of such a reduction is discussed in the following section, and to lower the electron temperature following vibrational excitation of the molecule through electronic collisions. At concentrations of the additive in excess of 0.5% a glow discharge could no longer be sustained in the device and no laser emission was observed.

In summary, no additives were observed to have any beneficial effects on the output energy and efficiency of this laser although an improvement in output pulse length with nitrogen occured.

5.5 X-ray Source Effects

In order to establish the exposure produced by the X-ray source and subsequent preionisation electron density in the discharge region was sufficient for optimum performance of the laser, an investigation into the effect of reducing the X-ray exposure was undertaken. This was achieved simply by altering the X-ray supply charge voltage, the effect of which on the produced exposure is shown in figure 3.7. In figure 5.16 the result of this on the performance is plotted in terms of the relative output from the laser. Because of the presence of copious amounts of 'dust' inside the discharge volume, as discussed in

chapter 4, and the resulting variation in shot to shot laser output, it is necessary to observe the effect of altering this parameter on the relative output. This is the average of several shots under 'normal' operating conditions of a 30 kV X-ray supply charge, relative to the average of a similar number of shots (usually five, the results being taken alternatively with those under 'normal' operating conditions) with the parameter adjusted. In this way the variations caused by the 'dust' are reduced and the true effect of the parameter being varied is reflected in the results.

Figure 5.16 shows that the exposure produced by the source under 'normal' operating conditions is indeed sufficient for optimum laser operation. However the level produced is close to the lower limit, and at supply charge voltages of 25 kV and below, the relative output decreases. Several factors can contribute to the decline in laser performance. At reduced preionisation electron densities (PED) the discharge takes a longer time to avalanche, during which localised instabilities may grow leading to constriction with rapid termination of the laser pulse and reduced output. Formation of parasitic discharges outside the electrode region but acting in parallel to the main discharge during this extended formative phase can reduce the discharge E/N and hence excitation rates and thus represent an energy loss mechanism. A reduction in active volume as the discharge is confined to the area between the electrodes where maximum exposure occurs may also result with the consequence of reduced output. In contrast, under conditions of much higher PED discharge formation time would be reduced [20] minimising the detrimental effects of these other processes affording the possibility increased laser output. This effect has been observed elsewhere [9] where a decrease in laser performance of ~50 % was observed following a reduction in preionisation electron density of two orders of magnitude. This is one area of investigation the author feels would be beneficial to the future performance of this device.

One further preionisation effect investigated was the required overlap of the flash of X-rays and the discharge pulse for effective operation of the laser. By introducing varying lengths of co-axial cable between the two thyratron trigger units, as discussed in section 5.1, the relative overlap of the discharge pulse and that of the X-ray diode could be controlled. Figure 5.2 shows typical waveforms of the multiplexed signals, suitably attenuated at the oscilloscope, from the X-ray and discharge voltage pulses and the effect of additional delay on these. As previously discussed a cable delay length of 40 metres, corresponding to

initiation of the discharge pulse shortly after the peak of the preionisation pulse, resulted in uniform preionised discharge formation. With shorter delay lengths, less than 20 metres, no laser output was obtained as insufficient preionisation of the gas had occured prior to initiation of the discharge to ensure formation of a uniform plasma. However added cable delays of up to 420 metres in length representing temporal delays of over 2 μsec between the peak of the X-ray pulse and the onset of the discharge pulse were used with no discernable decrease in the performance of this device. The main attaching process in mercury bromide gas mixtures under conditions of no applied discharge field [12] is that of dissociative attachment to $HgBr_2$ resulting in the formation of the Br^- ion. Nighan et al. [12] measured the cross section for this process and found it to be resonant in character with a significant value for electron energies between 3.1 eV and 4.5 eV. In a preionised gas the energy of the preionisation electrons is only a few eV [21] so this process has little effect on the initial electron density. In their analysis of preionisation electron decay processes in XeCl avalanche discharge excited lasers, much of which is applicable to the case of the mercury bromide laser, Chengen and Lo [21] show that in laser gas mixtures of several atmospheres pressure, containing mostly Ne as the diluent, the electron temperature is cooled through elastic collision processes between the electrons and buffer gas atoms to 0.1 of its original value within only 50 nsec. This further reduces the probability of dissociative attachment reactions taking place at significant time delays after the termination of the preionisation pulse. Kushner et al. [2] investigated the effects of diffusion of charged species in their kinetic study of the mecury bromide discharge laser and found it to be negligible on a timescale of 200 nsec. It is therefore unlikely that diffusion will play a significant role in the decay of the preionisation density even on the longer timescale of microsecond durations. In the light of this diccussion the results of the above experiment are understandable.

In contrast to this for fluorine based rare gas halide lasers, the large dissociative attachment rate of the halogen [22] results in a substantial reduction in the preionisation electron density on the timescale of a few nsec and it might be expected that such long delays could not be tollerated in this system. However it has been observed experimentally [23] that the effect of preionisation in such systems can last for 10-20 μsec. Hsia [23] proposed a preionisation model to explain this observed behaviour where F^- ions, formed following

dissociative attachment of the preionisation electrons, act as an electron reservoir which following electron detachment can replenish the preionisation electron density. The lifetime of these ions is long explaining the long timescale effect of the preioniser. For the case of the XeCl rare gas halide laser the dissociative attachment rate of the halogen donor, HCl, is much smaller than that of F_2 [21] and the timescale for decay in the preionisation electron density is microseconds. Such long delay times between the preionisation and discharge pulses have been realised in a carefully prepared and passivated system by Shields et al. [24] and by Zheng et al. [21] showing that dissociative attachment to HCl is not a major electron loss process in this laser system as for the mercury bromide laser. The results of [21] show that the maximum delay time that can be tolerated whilst still resulting in a uniform discharge decreases with the number of discharges, an effect attributed to the production of Cl_2 through dissociation of HCl during the discharge. In an analagous fashion it is likely that the maximum delay time tolerable in the mercury bromide laser will also be dependent on the number of discharges as free bromine is produced as a result of dissociation of $HgBr_2$. This effect, however, was not investigated during the experiments described here as the maximum delay between the X-ray pulse and the discharge pulse tolerable for the formation of a uniform discharge was never observed , even following a significant number of shots. Similar results to those observed above were reported recently for the case of the mercury bromide laser by Stonefield and King [25] where delays of up to 0.5 μsec resulted in little decline in performance observed from their 2 cm x 2 cm discharge laser. The importance of these results in mercury bromide laser design, showing precise overlap of preionisation and discharge pulses is not critical, is to relax the operational conditions of these lasers in this respect.

5.6 Effects of DPFL Characteristics

The effect of altering the DPFL charge voltage and hence the gas energy loading on the relative output from the laser is illustrated in figure 5.17. The relative output is used here for similar reasons to those discussed in the previous section. As the voltage is increased the relative output increases but at a decreasing rate as the maximum charge voltage used of 30kV is approached. Although laser performance improves with increased energy loading it

does so at the expense of efficiency. The stored electrical energy is proportional to the square of the charge voltage. As the rate of increase in laser output decreases with chage voltage then the efficiency of the laser also decreases. Kushner et al. [2] showed that discharge constriction occurs after a critical amount of energy is deposited in the gas. As the energy loading is increased one would expect to see this reflected in a reduction in the duration of the pulse length. However, due to the effects of dust accumulation in the discharge this effect was not addressed during these experiments and is an area where the author thinks a more detailed study should take place.

An alternative method of changing the energy loading on the gas is to alter the number of modules in the DPFL system and hence the impedance of the pulsed power supply. The results of this experiment are shown in figure 5.18, for a constant DPFL charge voltage of 30 kV. As the stored energy is increased by running more modules in parallel, the relative output increases, but at a decreasing rate, to its value with 10 modules. This again implies laser efficiency is decreasing with increased energy loading. Throughout these experiments the discharge self-sustaining voltage remained constant, independant of the impedance of the DPFL implying its sole effect was on the discharge current. This eliminates the possibility of changes in discharge E/N and subsequent rate constants being in part responsible for the observed effects.

The effect of reducing the energy loading on the gas through a reduction in pump pulse duration was also investigated. Results presented in section 5.3 show the maximum pulse duration achieved in a neon buffered mixture to be 82 nsec FWHM. From the waveforms of figure 5.6 the delay in onset of laser emission following gas breakdown is approximately 40nsec implying that after 120 nsec the discharge has constricted and any further pumping of the laser medium is ineffective. However, the DPFL system is designed with an electrical length of ~ 240 nsec, resulting in almost half the energy stored on the line being utilised inefficiently. A substantial increase in laser efficiency would then be expected by reducing the length of the discharge pulse, achieved through a reduction in the number of sections used in the DPFL modules. The results of this experiment are presented in figures 5.19-5.20.

As the number of sections in the DPFL is decreased to five, halving the stored energy, the output energy decreases by only 15% and laser efficiency, defined as laser output energy

divided by stored electrical energy, almost doubles to nearly 1.5%. Figure 5.20 shows the output pulse length stays constant until the pump pulse duration becomes comparable to the time from breakdown of the gas to the end of laser emission, corresponding to five sections in the DPFL. Fewer sections in the line result in a decrease in pulse length determined by the reduction in pump pulse duration and correspondingly the output energy also falls off more rapidly. The seemingly short pulse observed for the case of five sections in the DPFL, as the figure shows, is a result of the windows in the cavity requiring cleaning. The build up of a deposit on the optics, as discussed in chapter 4, increases the losses hence the laser takes more time to achieve threshold and shorter pulses are produced. These results are not surprising following the above discussion and similar though less detailed observations were made by Znotins et al. [5] who used lines of two electrical lengths.

In conclusion for efficient pumping of mercury bromide discharge lasers pump pulse lengths on the order of 120 nsec have been shown to be optimum. This corresponds to the time between initiation of laser oscillations following gas breakdown and termination of the laser pulse through constriction of the discharge.

5.7 Spectroscopy

A 1 metre Hilger and Watts spectrometer and a Chelsea Instruments Ltd. S100 grating spectrometer were used to spectroscopically analyse the discharge. The spectrum from the Hilger and Watts spectrometer was recorded on 35 mm negative film which, following development, was analysed visually or with the use of a Joyce, Loebl and Co. Ltd. double beam recording microdensitometer. Output from the grating spectrometer was recorded directly on type 667 polaroid film. Figure 5.21 shows a typical fluorescence spectrum observed with neon buffer gas, recorded by the microdensitometer over the wavelength range 440 nm - 520 nm. This figure also shows the spectrum over a wider band from 400 nm - 600 nm recorded by the grating spectrometer. The observed spectrum is characteristic of emission from discharges in mercury bromide with numerous bands visible to the blue side of the double peaked fluorescence maxima centred around 502-504 nm associated with the $v' = 0 \rightarrow v'' = 22,23$ vibrational transitions. The structure corresponds to transitions from other upper vibrational, v', levels to $v'' = 22$ or other vibrational levels of

the ground state ($X^2\Sigma^+$). The appearance of these transitions indicates a distribution of v' levels in the electronically excited B state, populations of levels up to v'=10 have been reported by other authors [26]. The tentative assignments to the various observed bands follow those of Liberman and Leslie [27], a detailed analysis of the results was not undertaken due to the non linear calibration of the spectrometer making precise measurements of the various transitions difficult. Furthermore, the spectrum is likely to consist of the overlapping transitions from the numerous naturally abundant isotopes of HgBr making spectroscopic identification of the transitions a difficult task.

In the wider band spectrum from the grating spectrometer various lines corresponding to transitions of mercury atoms are visible, spectroscopically confirming its presence in the discharge. As discussed earlier the accumulation of mercury in the discharge promotes the tendency towards constriction due to ease with which its excited states are ionised. This evidence confirms earlier speculation that this process is responsible for the behaviour of and relatively short output pulses obtained from the laser. The spectrum of laser emission was also observed and consisted of two lines of linewidth ~ 1 nm FWHM, corresponding to the two peaks in the fluorescence spectrum, the strongest line again being towards the blue.

Fluorescence measurements have been used to measure the small signal gain in lasers using the single pass/double pass ASE method [28]. Here the peak intensity of the spontaneous emission amplified through a single pass of the gain medium is compared with that allowed to traverse the gain medium a second time following reflection from a mirror, to assess the magnitude of the small signal gain. However, under conditions of optimum gas mixture, the stimulated emission produced by the laser could not be suppressed even with no mirrors and the cavity windows misaligned, making this method no use in this particular case. The measurement of sidelight fluorescence in many lasers has enabled observations to be made on the discharge and laser properties, however this technique is again inappropriate with this particular device, due to the dust produced in the discharge. Stimulated emission along the axis of the laser would be scattered off the dust particles and affect the fluorescence measurements. Renton and Piper [29] used an optically pumped mercury bromide laser to perturb the inversion of a short pulse UV preionised avalanche discharge mercury bromide laser, whilst monitoring the gain along the discharge dimensions by a counter-propagating probe beam at 501.7 nm from a CW Ar^+ ion laser. This is one technique which may be

applicable to this laser for a more detailed study of its operational characteristics, even in the presence of corrosion dust.

5.8 Repetition Rate Experiments and Gas Lifetime

Only a few experiments were carried out at significant rep rate, mainly because of the deterimental effects of dust build-up in the discharge region on the laser output as shown in figure 4.8. The limited results obtained however did show that laser output stabilised after a short period of operation and remained steady for the remainder of the test period. Repetition rates up to 10 Hz, limited by the available capacitor charging unit, were run for periods of several minutes during which no problems were encountered with the pulsed power supply or X-ray source. In stationary gas mixtures such as those considered here it has been noted [30] that density gradients produced in the previous discharge limit the repetition rate to a few Hertz in order to prevent arcing. A detailed study of discharge stability was not undertaken during the experiments discussed here but it is an area where the author thinks more work should be carried out. Recirculating the gas mixture inside the laser chamber is the obvious method used to remove any perturbations produced by the previous discharge pulse and with this in mind a magneically coupled blower was constructed for use with this system. The details of the proposed circulation scheme and design of the blower were outlined in chapter 4. However, to date, this has not been tested in the device. An added benefit of the inclusion of such a circulating system, as discussed previously, would be in the removal of dust from the discharge region improving laser performance and shot to shot reproducibilty.

No lifetime tests were undertaken with this laser but during the experimental period single gas fills were used for periods of up to five hours with the final output energy being 50% of the initially recorded value. During this period the gas was subject to several hundred discharge pulses. As previously discussed the primary cause for this decrease in output energy is the buildup of corrosion dust in the laser medium following reactions with the stainless steel parts of the cavity, the limiting factor in the useful lifetime of this laser. Through careful choice of cavity materials it has been shown that extensive gas lifetimes, in excess of 5×10^8 shots [9], can be achieved with these lasers proving their potential for extremely long life operation.

5.9 Summary

A full parametric study of the laser covering gas composition and pressure, X-ray source effects, energy loading and other pulsed power supply effects was carried out. The optimum buffer gas was found to be neon and the peak output energy of 710 mJ in a pulse length of 82 nsec was obtained at a pressure of 4 bar with 3-4 mbar mercury bromide vapour pressure. The use of additives in the gas mixture had no benefitial effects on the output energy although nitrogen was observed to produce an extension in the output pulse length. Efficiences in excess of 1.5% were achieved by matching the temporal duration of the discharge pulse to the maximum useful for pumping the discharge prior to the onset of constriction. A summary of the laser performance is given in Table 5.1. The effect of E/N on the discharge parameters is briefly discussed in Appendix 5.

CHAPTER 5

REFERENCES

1. The author is grateful to Dr. R.C.G. Killean, Departments of Physics and Astronomy, University of St. Andrews, for his helpful discussions regarding the effect of the field shaping electrode.
2. M.J. Kushner, A.L. Pindroh, C.H. Fisher, T.A. Znotins and J.J. Ewing, J.Appl.Phys. 57, 2406 (1985).
3. C.R.Tallman and I.J.Bigio, Appl. Phys. Lett. 42, 149 (1983).
4. R.S.Taylor, Appl. Phys. B 41, 1-24 (1986).
5. T.A. Znotins, C.H. Fisher, T.E. DeHart, J.P. McDaniel and J.J. Ewing, Appl.Phys.Lett. 46, 228 (February 1985).
6. Robert C.Sze, Appl.Phys.Lett. 33, 4596 (1978).
7. Austin M.Cravath, Phys. Rev. 36, 248 (1930).
8. M.W. McGeoch, J.C. Hsia and D.E. Klimek, J. Appl. Phys. 54, 3723 (1983).
9. Mathematical Sciences Northwest Inc. Final Report. 200 Watt Mercury Bromide Laser (1984).
10. N.T.Padial, G.D. Meneses, F.J. da Paixao and Gy. Csanak, Phys. Rev. A 23, 2194 (1981).
11. P.J.O.Teubner, J.L. Riley, M.C. Tonkin, J.E. Furst and S.J. Buckman, J. Phys. B 18, 3641-3652 (1985).
12. W.L.Nighan, J.J.Hinchen and W.J.Weigand, J. Chem. Phys. 77, 3442 (1982).
13. The author is indebted to Miles Turner for pointing out the possibility of this process.
14. R. Burnham, Appl.Phys.Lett. 33, 156 (1978)
15. H.J. Baker and N. Seddon, Appl.Phys.B. 36, 171 (1985).
16. M. Sugii and K. Sasaki, Appl.Phys.Lett. 48, 1633 (1986).
17. C. Fisher, Spectra Technology Ltd. Private Communication.
18. William L. Nighan, Appl.Phys.Lett. 36, 173 (1980).
19. R.S.F.Chang and R.Burnham, Appl.Phys.Lett. 36, 397 (1980)
20. Cheng-En Zheng, Dennis Lo and Shao-Chi Lin, Appl.Phys. B. 41, 31-37 (1986).

21. Zheng Chengen and Dennis Lo, Chinese Physics-Lasers 14, 232 (1987).

22. K.J.Nygaard, S.R. Hunter, J. Fletcher and S.R. Foltyn, Appl. Phys. Lett. 32, 351-353 (1978).

23. J. Hsia, Appl. Phys. Lett. 30, 101 (1977).

24. H.Shields, A.J.Alcock and R.S.Taylor, Appl.Phys. B 31, 27-35 (1983).

25. M. Stonefield and T. King, Paper 31P - Eighth National Quantum Electronics Conference, St. Andrews, Scotland (1987).

26. W. Luthy, R. Schmiele and T. Gerber, Phys.Lett. 88A ,450 (1982).

27. I. Liberman and S.G. Leslie, Advanced Laser Technology and Applications, SPIE Vol. 335, p. 48 (1982).

28. M. Casey, Ph.D. Thesis, University of London (1982).

29. B.J. Renton and J.A. Piper, Paper TUH3, CLEO 1986, San Francisco, California.

30. E. Schimistchek, AGARD Conference Proceedings No. 300, Monterey, CA, USA (1981).

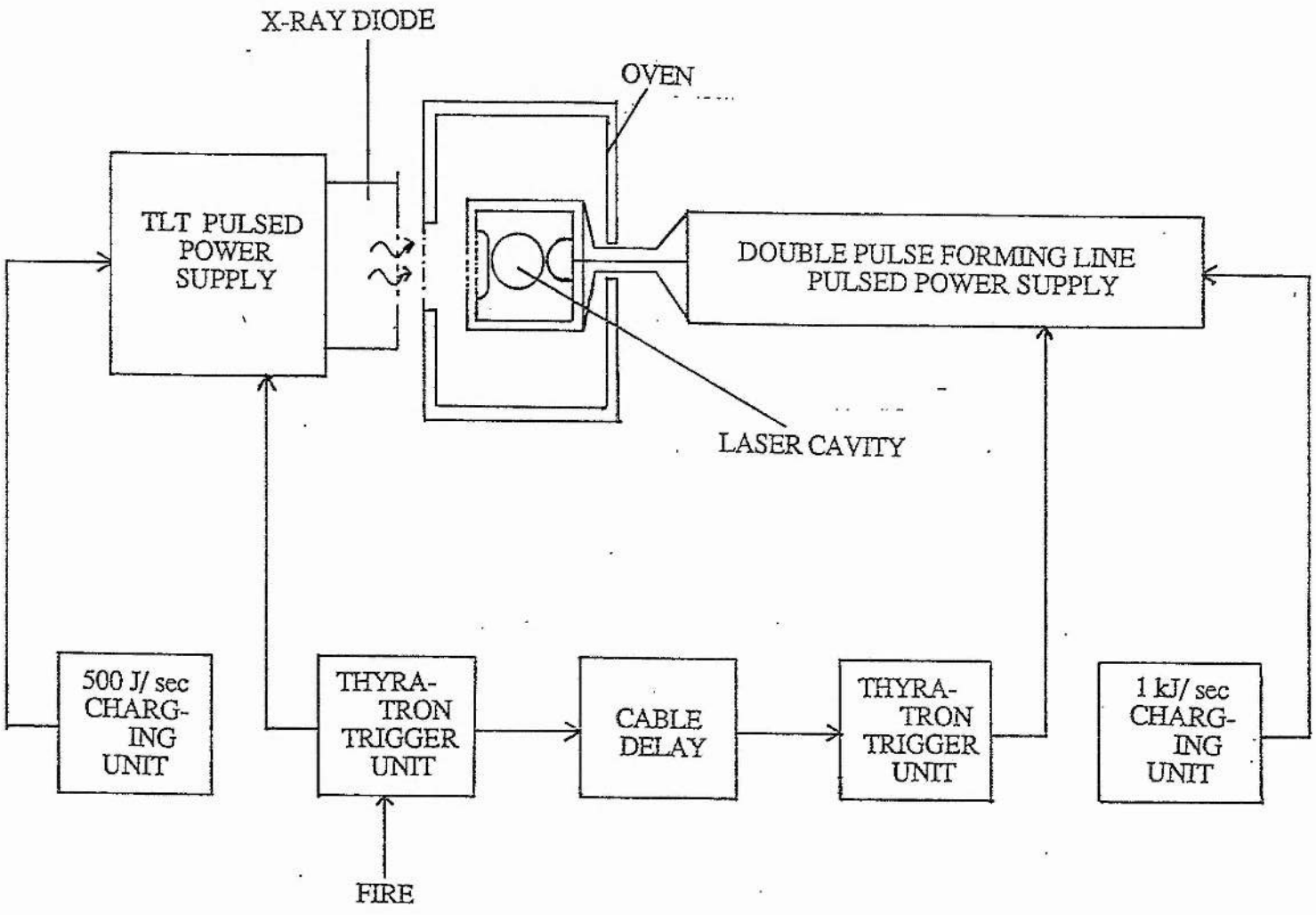

FIGURE (5.1) :DIAGRAM OF THE COMPLETE LASER SYSTEM

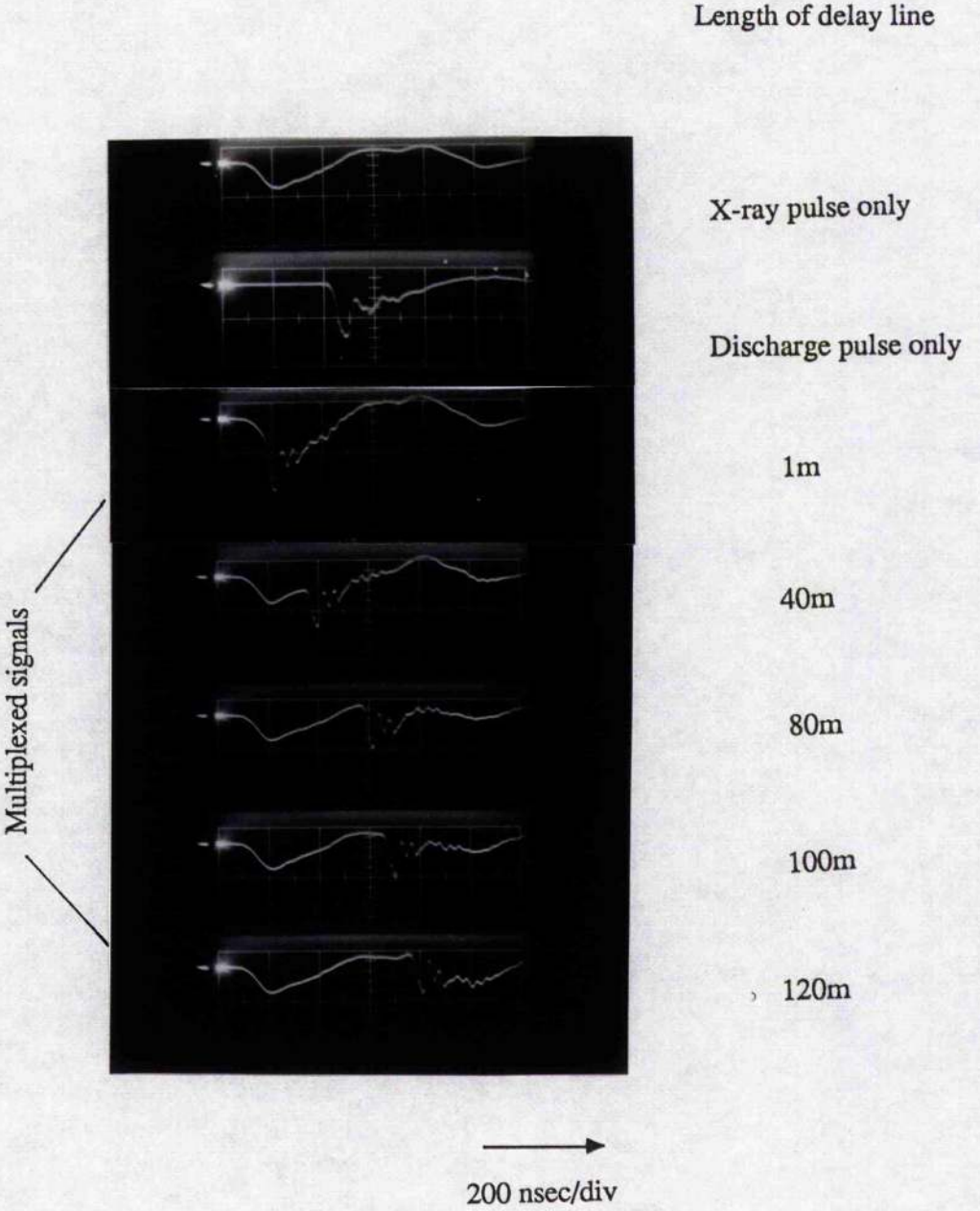

FIGURE(5.2): Effect on the temporal overlap of the X-ray diode and discharge voltage pulses of different lengths of delay line between the two thyratron trigger units.

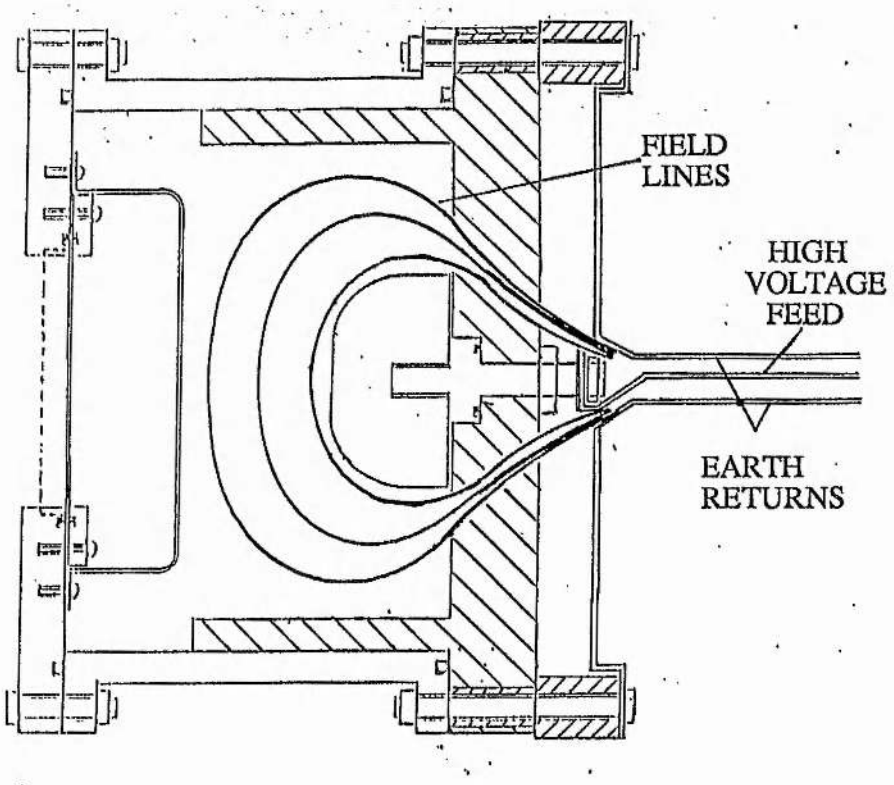

(a) No electrode - field enhancement takes place at the corners of the discharge electrode.

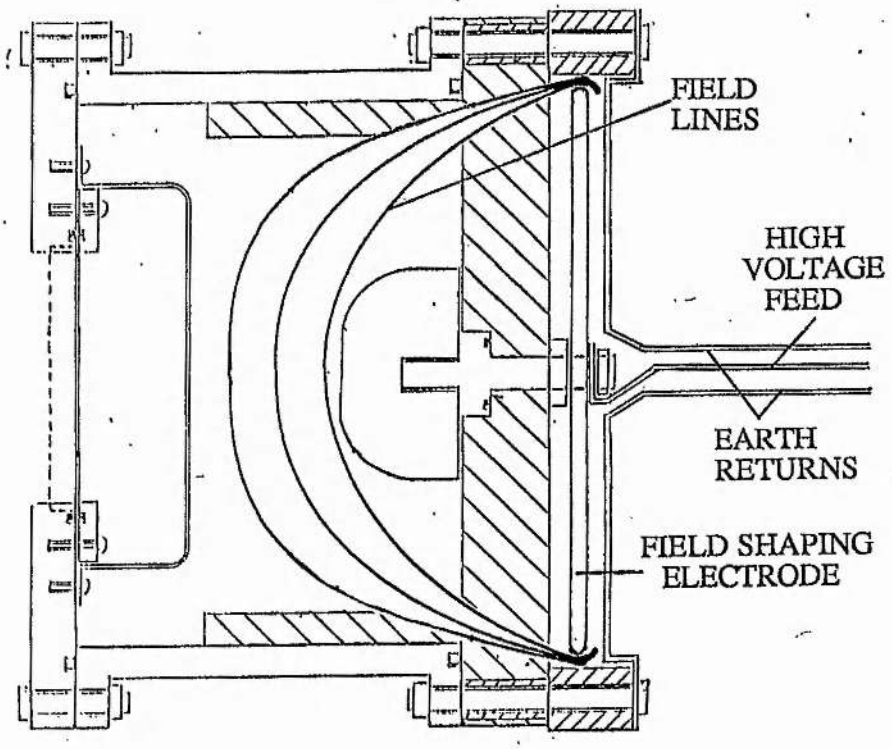

(b) With electrode - the field is removed from the corners of the discharge electrode.

FIGURE (5.3): Schematic diagram showing the effect of the field shaping electrode on the lines of equal potential around the main discharge electrode.

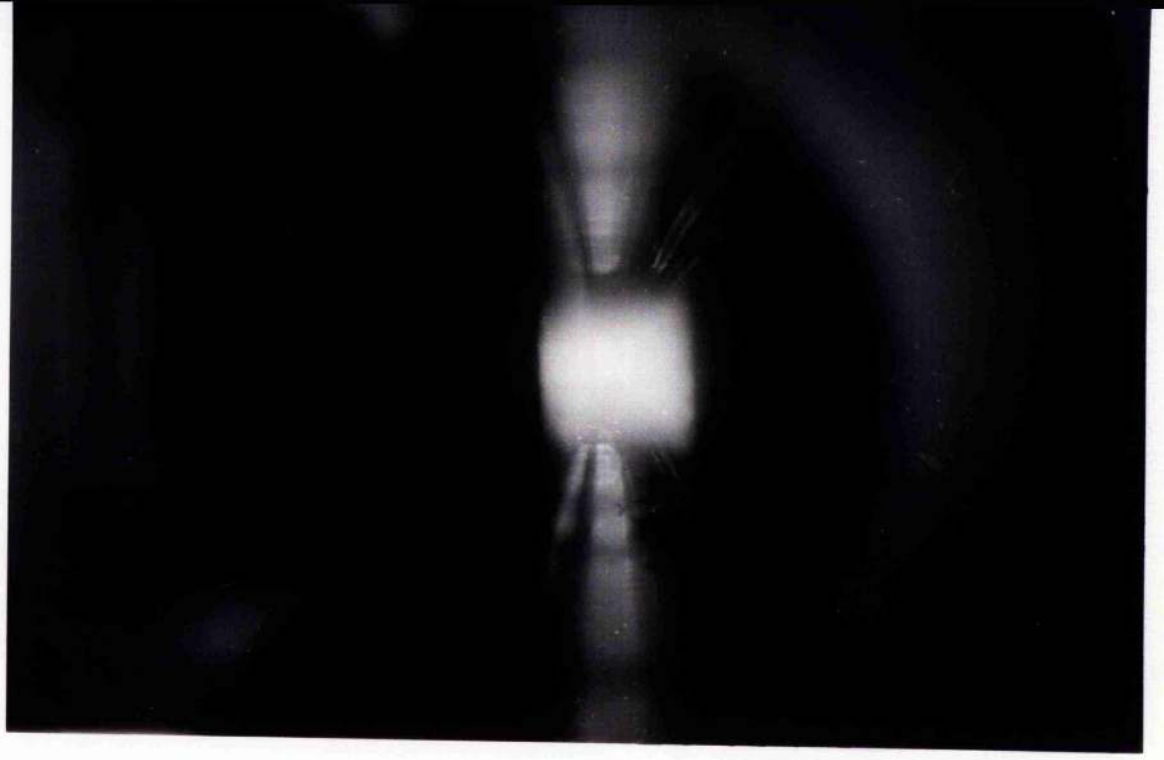

(a) Preionised glow discharge

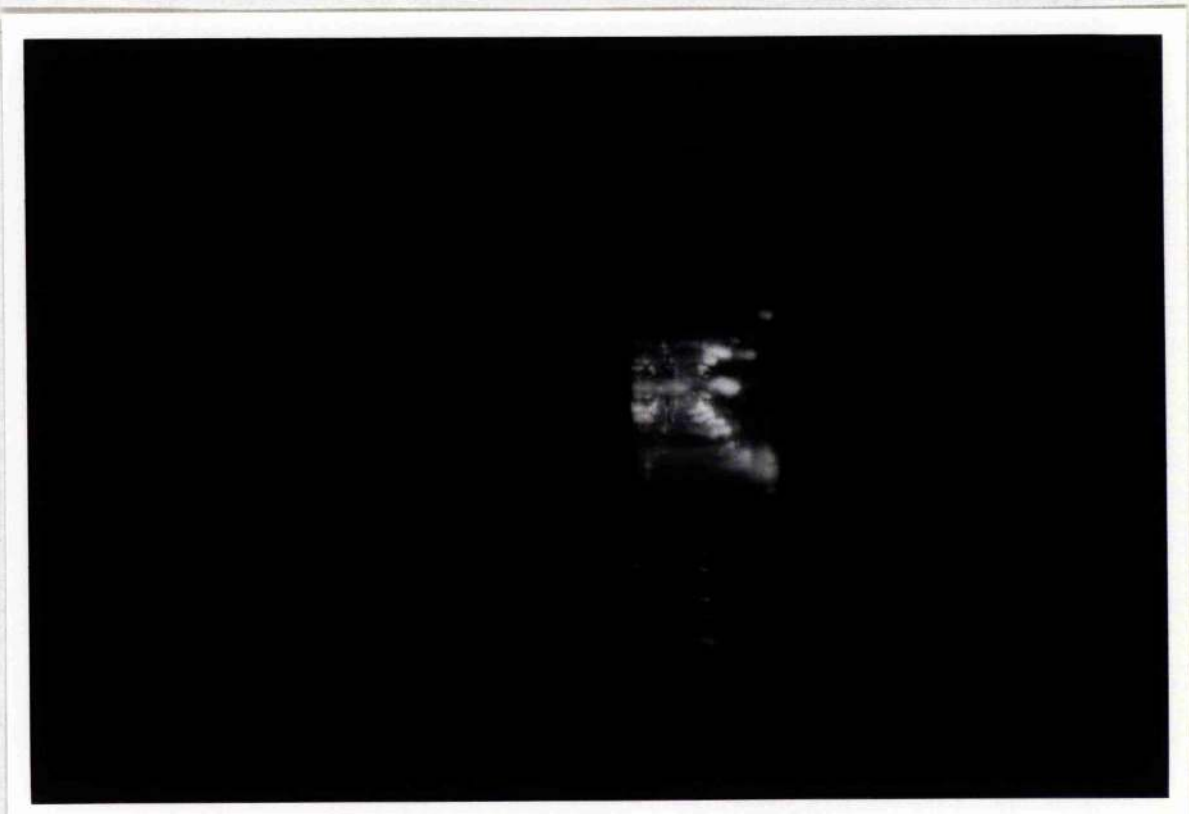

(b) Non preionised constricted discharge

FIGURE(5.4):Open shutter photographs of discharges in neon at one atmosphere pressure with and without preionisation.

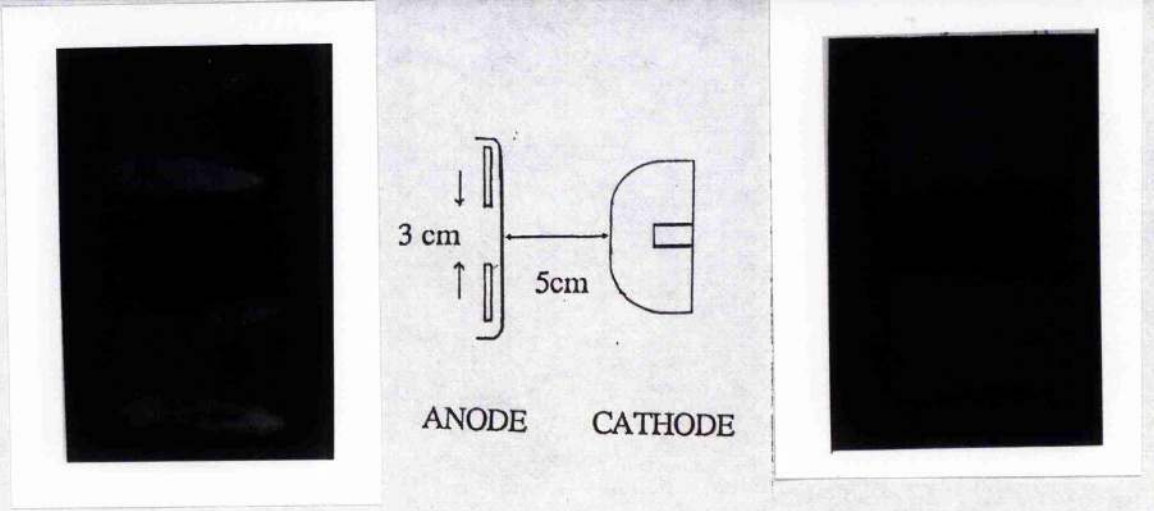

(a) No X-ray collimation

(b) With collimation

FIGURE(5.5):Burn patterns produced on blackened polaroid film after some focussing of the output beam, with and without collimation of the X-rays.
Gas mixture; 3 Bar neon buffer, 150 ^{o}C $HgBr_2$ reservoir temperature.

TABLE(5.1):LASER PERFORMANCE SUMMARY

WAVELENGTH	502-504 nm
MAXIMUM OUTPUT	710 mJ
MAXIMUM PULSE LENGTH	82 nsec FWHM Ne buffer
	92 nsec FWHM 1.5% N_2 additive
BEAM SIZE	5 cm by 3 cm
BEAM UNIFORMITY	Visually good
PEAK PUMP POWER DENSITY	400 kw cm^{-3}
EXTRACTION	0.5 J $litre^{-1}$
GAS MIX FOR OPTIMUM OUTPUT	4 bar Ne ~4 mbar $HgBr_2$
OPTICAL CAVITY	100 % plane mirror 33 % R plane output coupler Separation 1.6m
GAIN LENGTH	100 cm
PREIONISATION WIDTH	3 cm

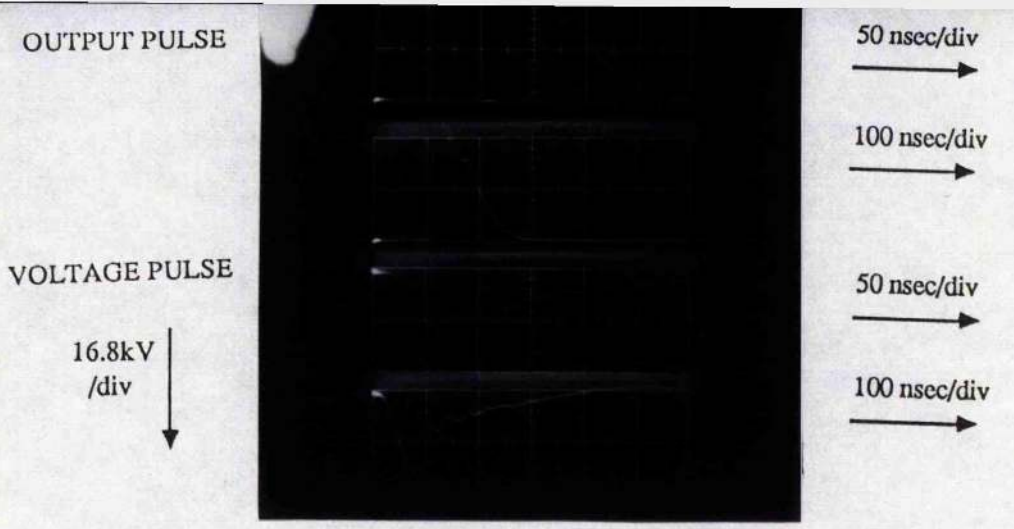

(a) 3 Bar neon buffer

(b) 3 Bar neon buffer plus 1.5% N_2 additive

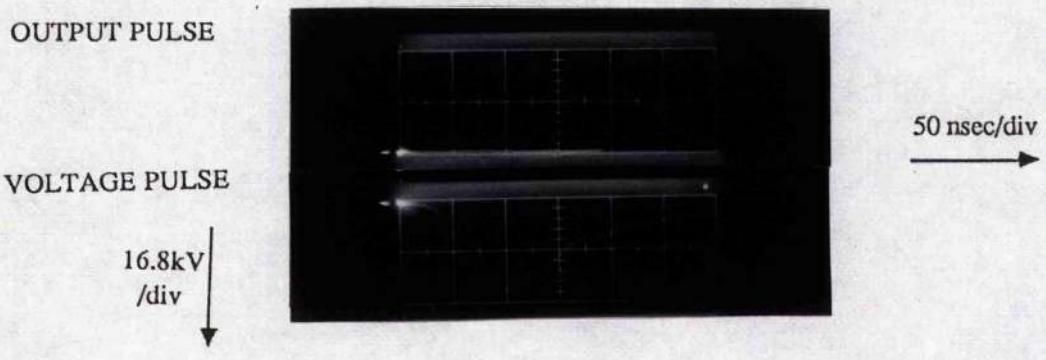

(c) 1.5 Bar argon buffer

FIGURE(5.6):Device waveforms for Ne and Ar buffered mixtures and Ne plus 1.5% N_2 additive.
Mercury bromide reservoir temperatue 150°C.

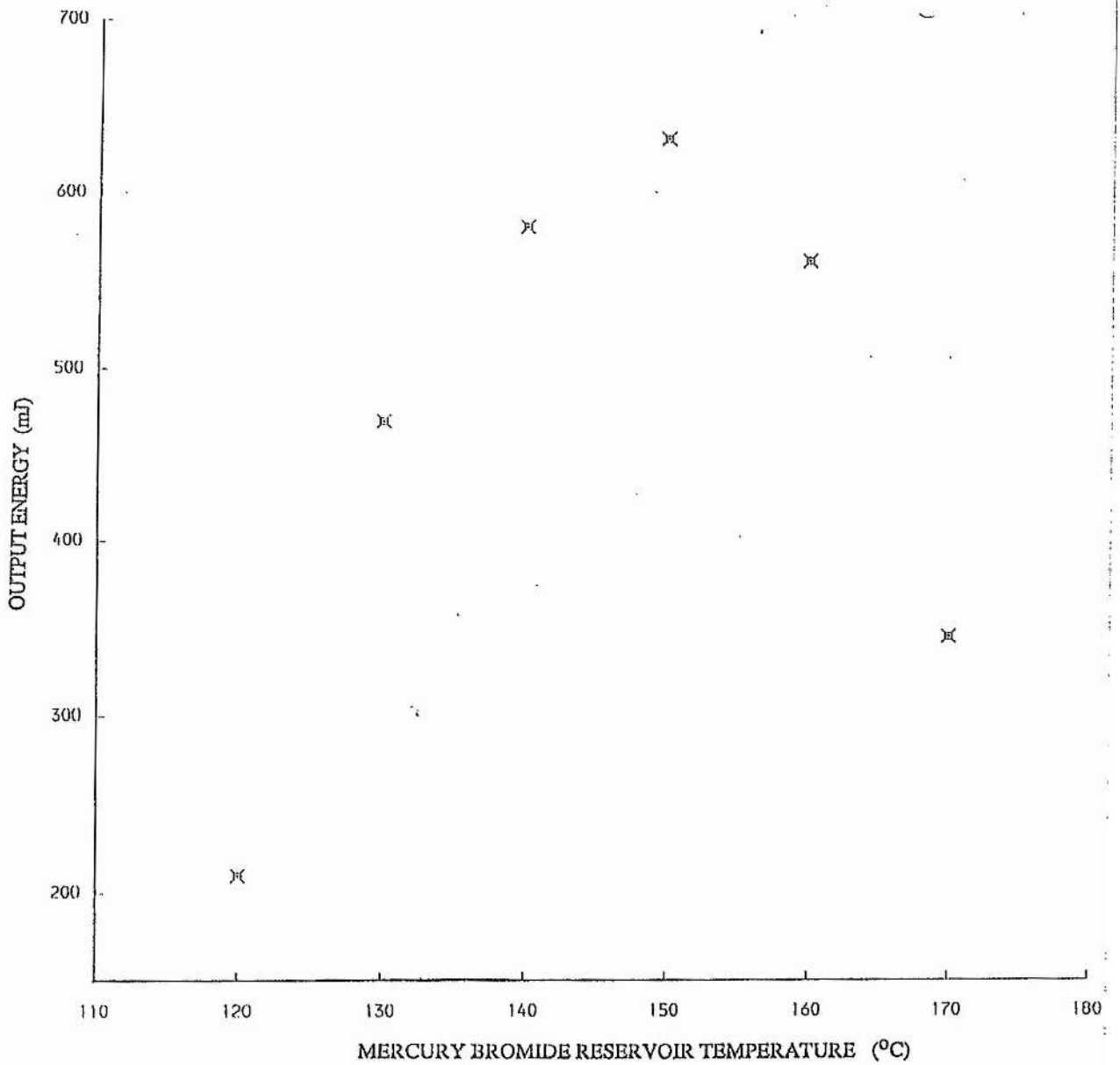

Figure(5.7):Output energy versus mercury bromide reservoir temperature.
3 Bar Ne buffer, 3 cm X-ray collimation, 5 cm electrode gap.

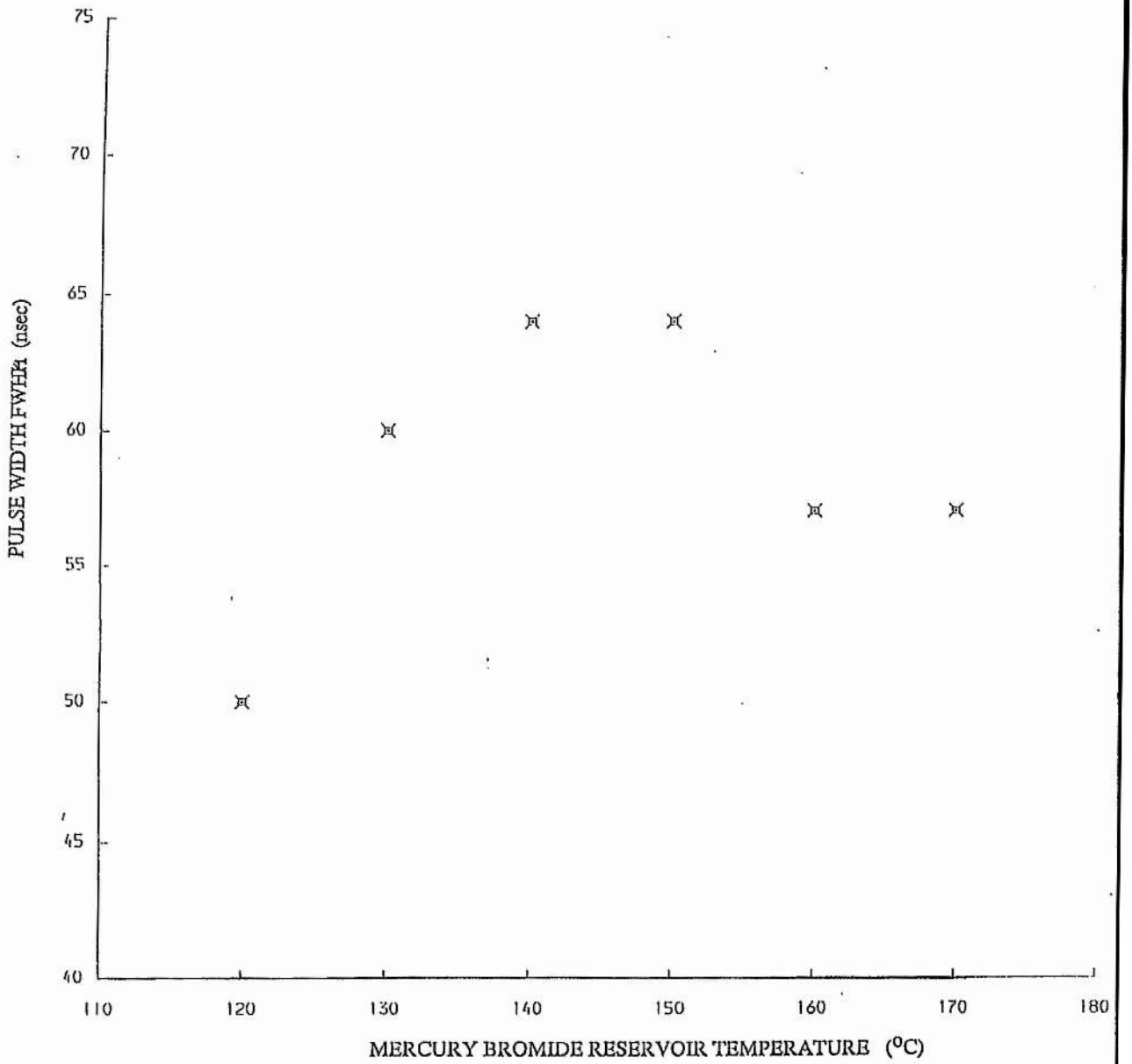

Figure(5.8):Output pulse width versus mercury bromide reservoir temperature. 3 Bar Ne buffer, 3 cm X-ray collimation, 5 cm electrode gap.

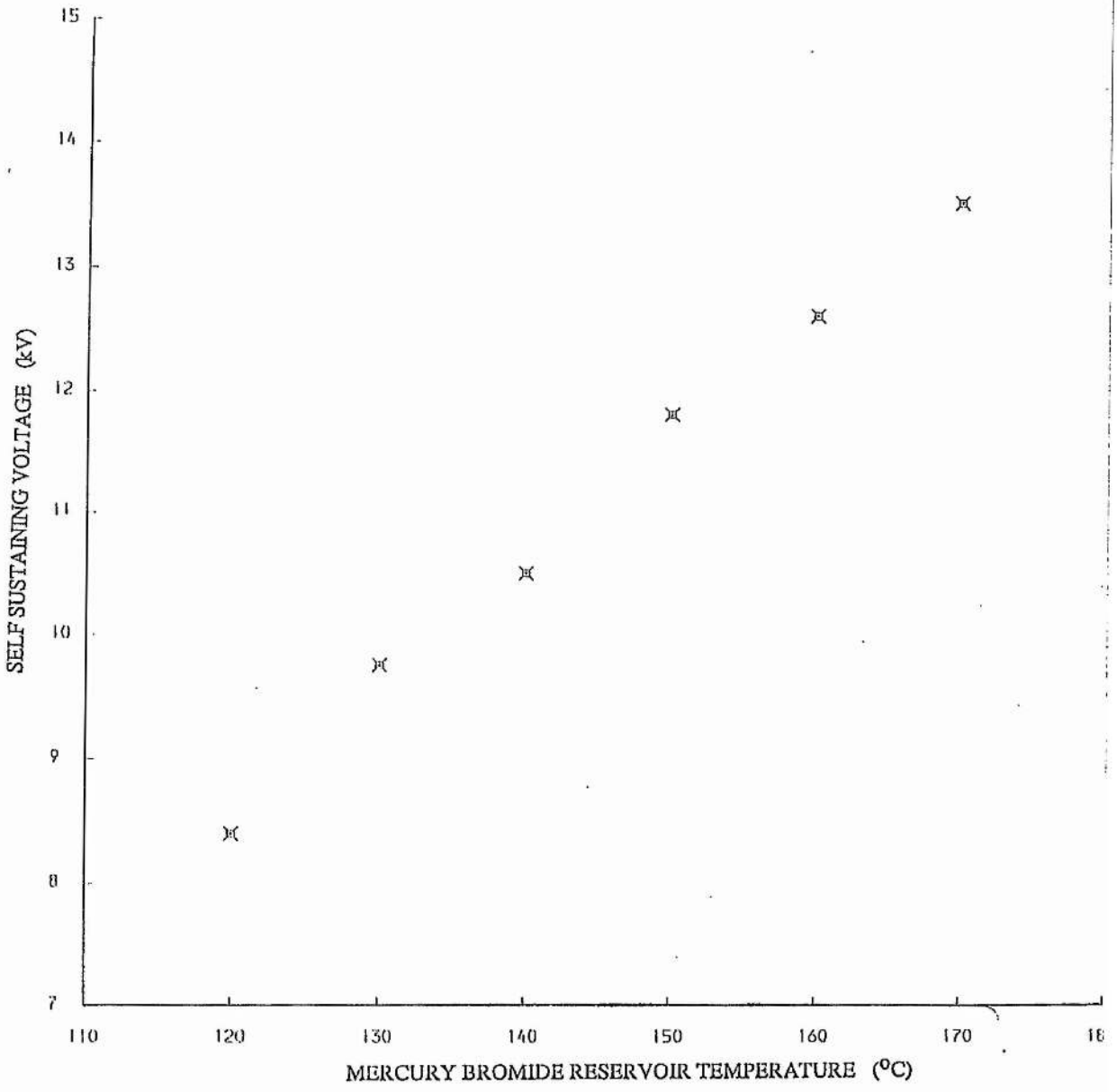

Figure(5.9):Self sustaining voltage versus mercury bromide reservoir temperature. 3 Bar Ne buffer, 3 cm X-ray collimation, 5 cm electrode gap.

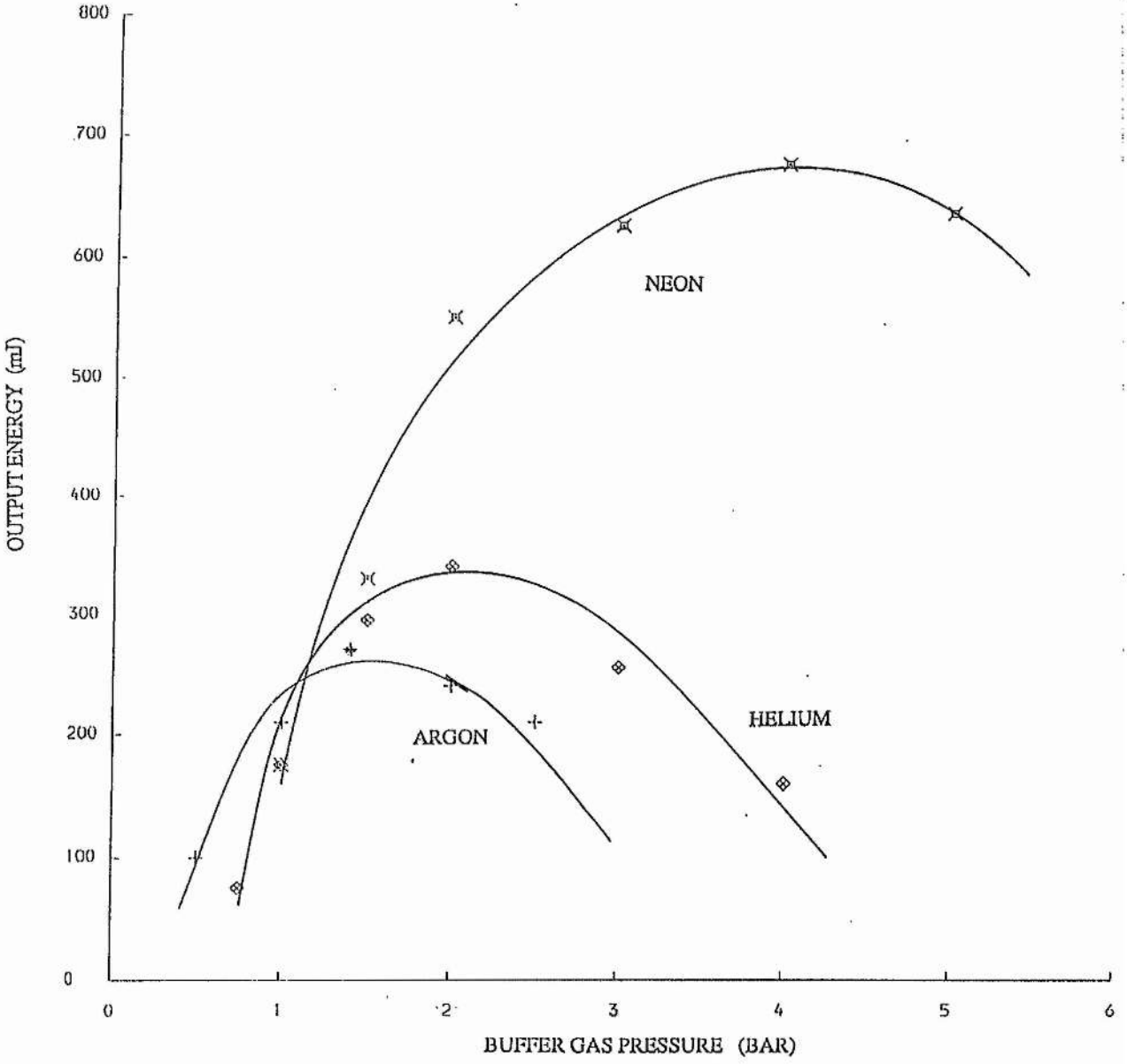

FIGURE(5.10):Output energy versus buffer gas pressure for various gases. 150 °C $HgBr_2$ reservoir temperature, 3 cm X-ray collimation, 5 cm electrode gap.

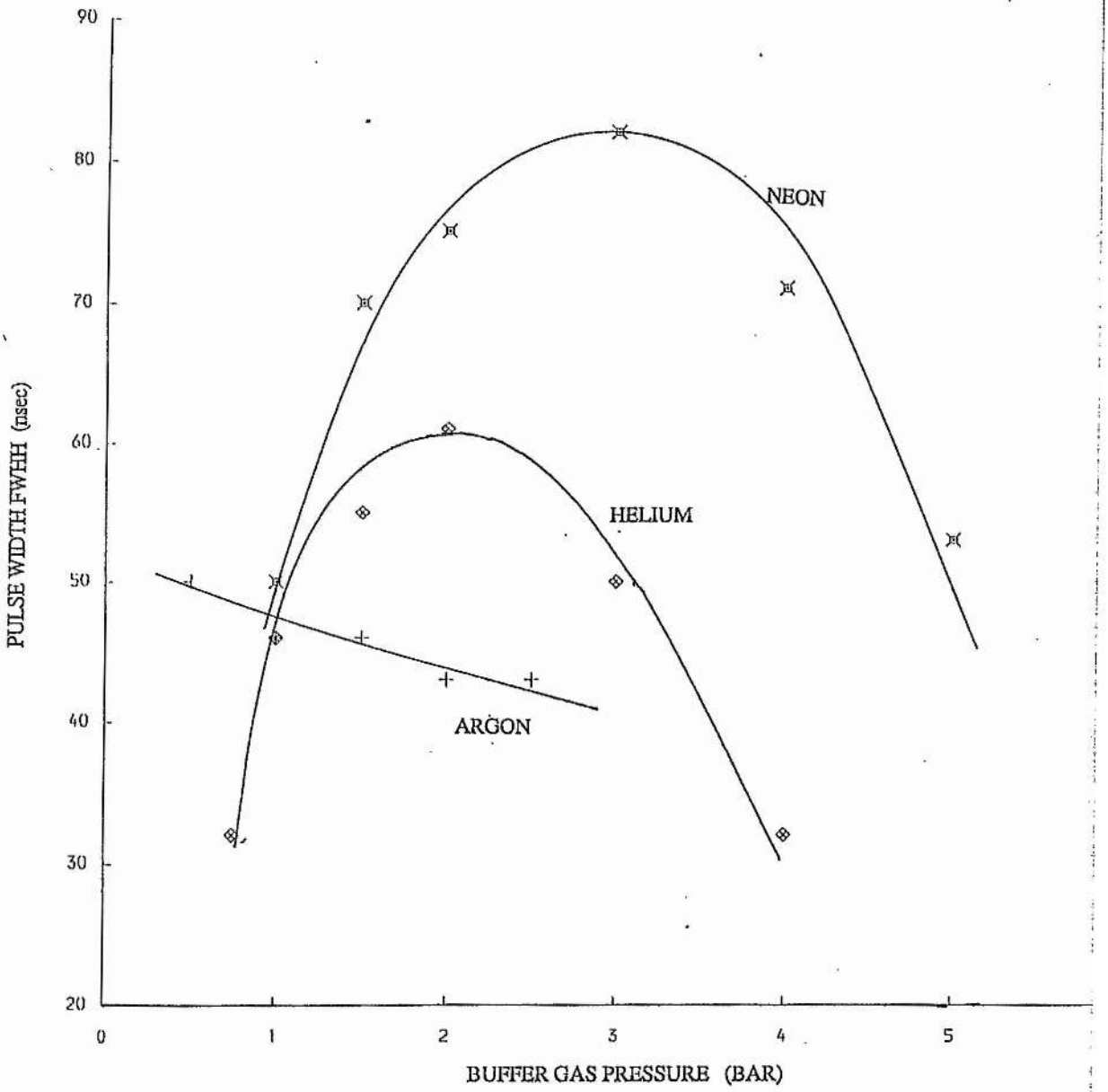

FIGURE(5.11):Output pulse width versus buffer gas pressure for various gases. 150 °C $HgBr_2$ reservoir temperature, 3 cm X-ray collimation, 5 cm electrode gap.

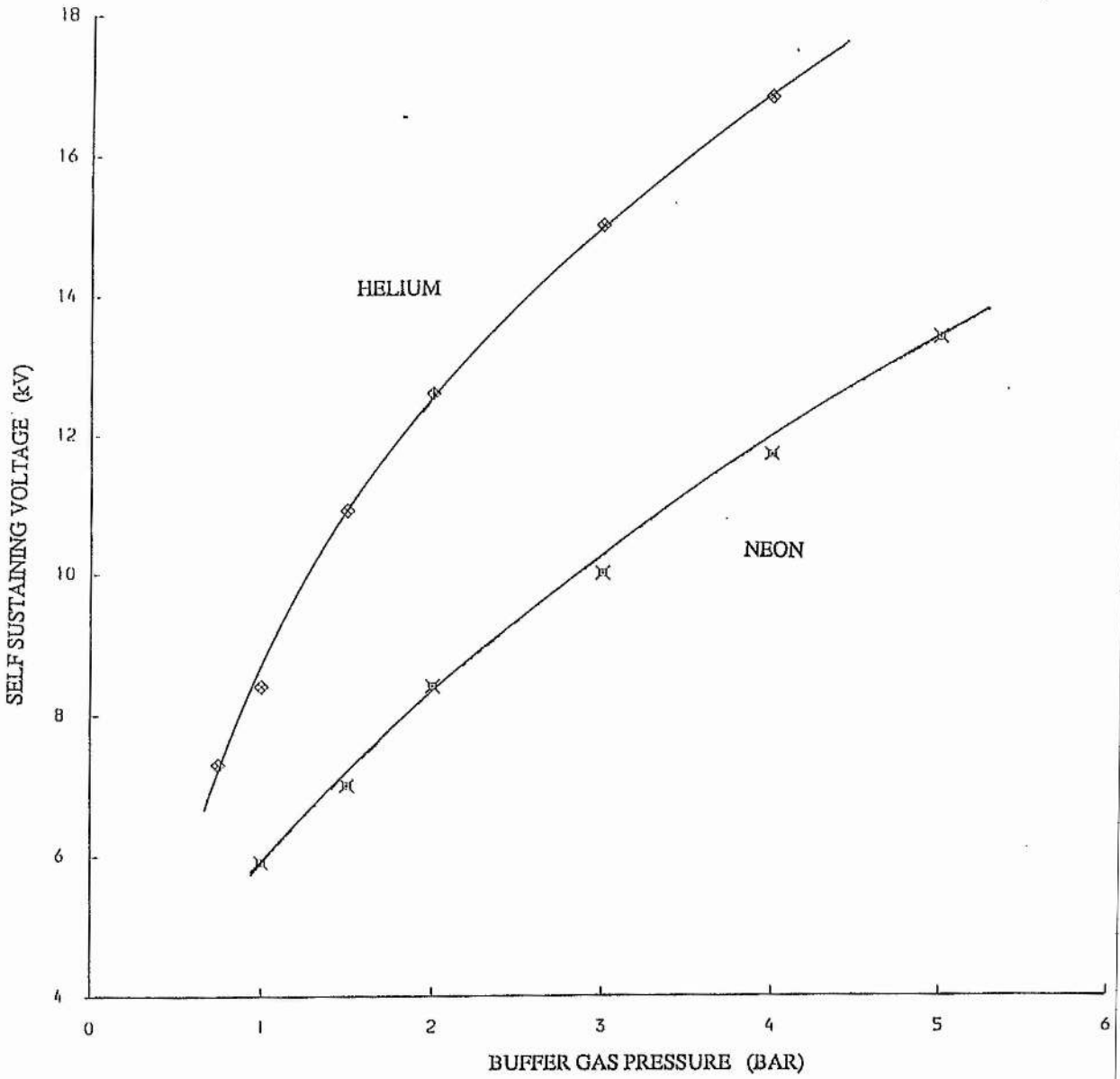

FIGURE(5.12):Self sustaining voltage versus buffer gas pressure for various gases. 150 ^{o}C $HgBr_2$ reservoir temperature, 3 cm X-ray collimation, 5 cm electrode gap.

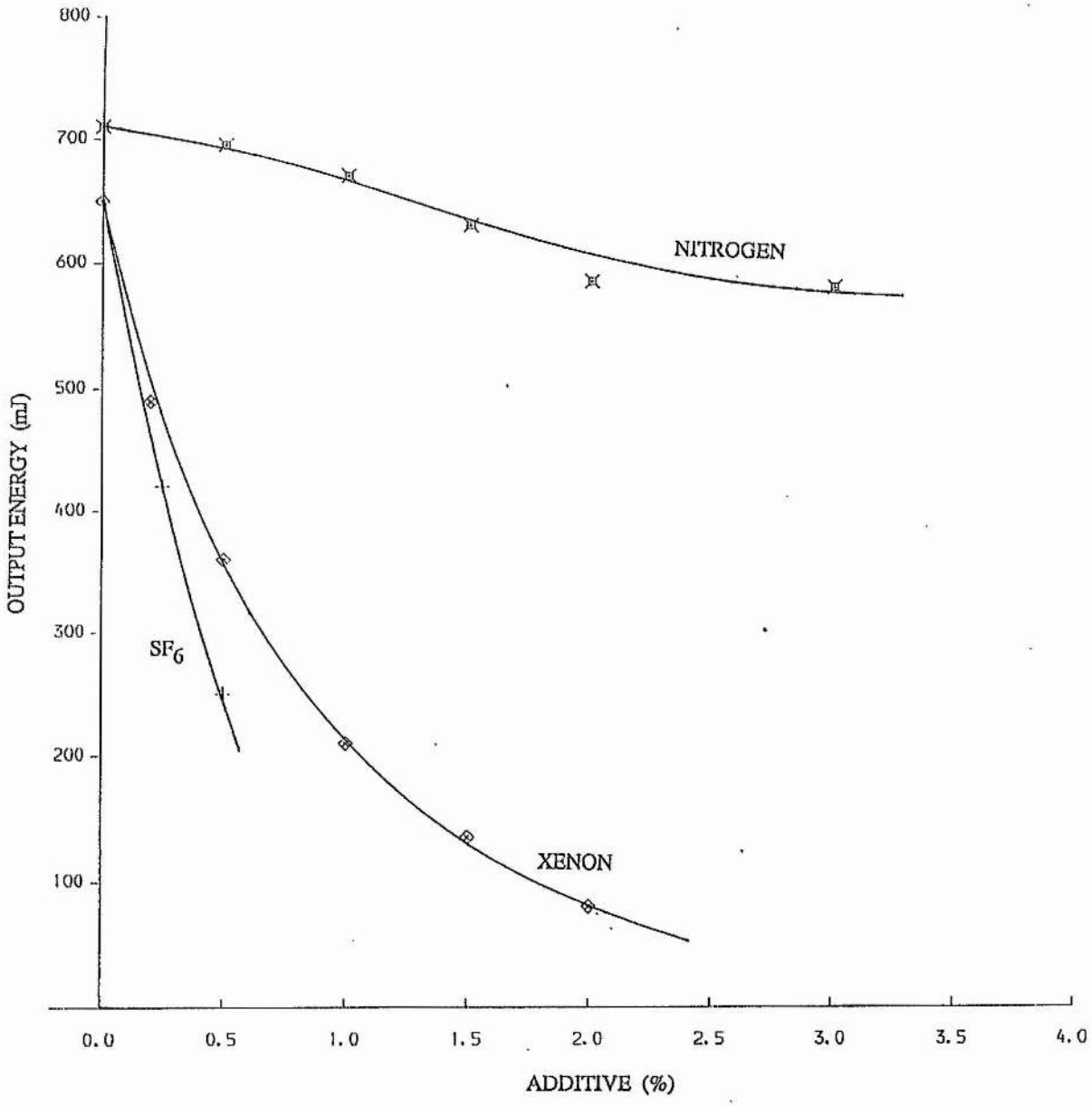

FIGURE(5.13):Output energy versus percentage of additive.
3 Bar Ne buffer, 150 ^{o}C $HgBr_2$ reservoir temperature,
3 cm X-ray collimation, 5 cm electrode gap.

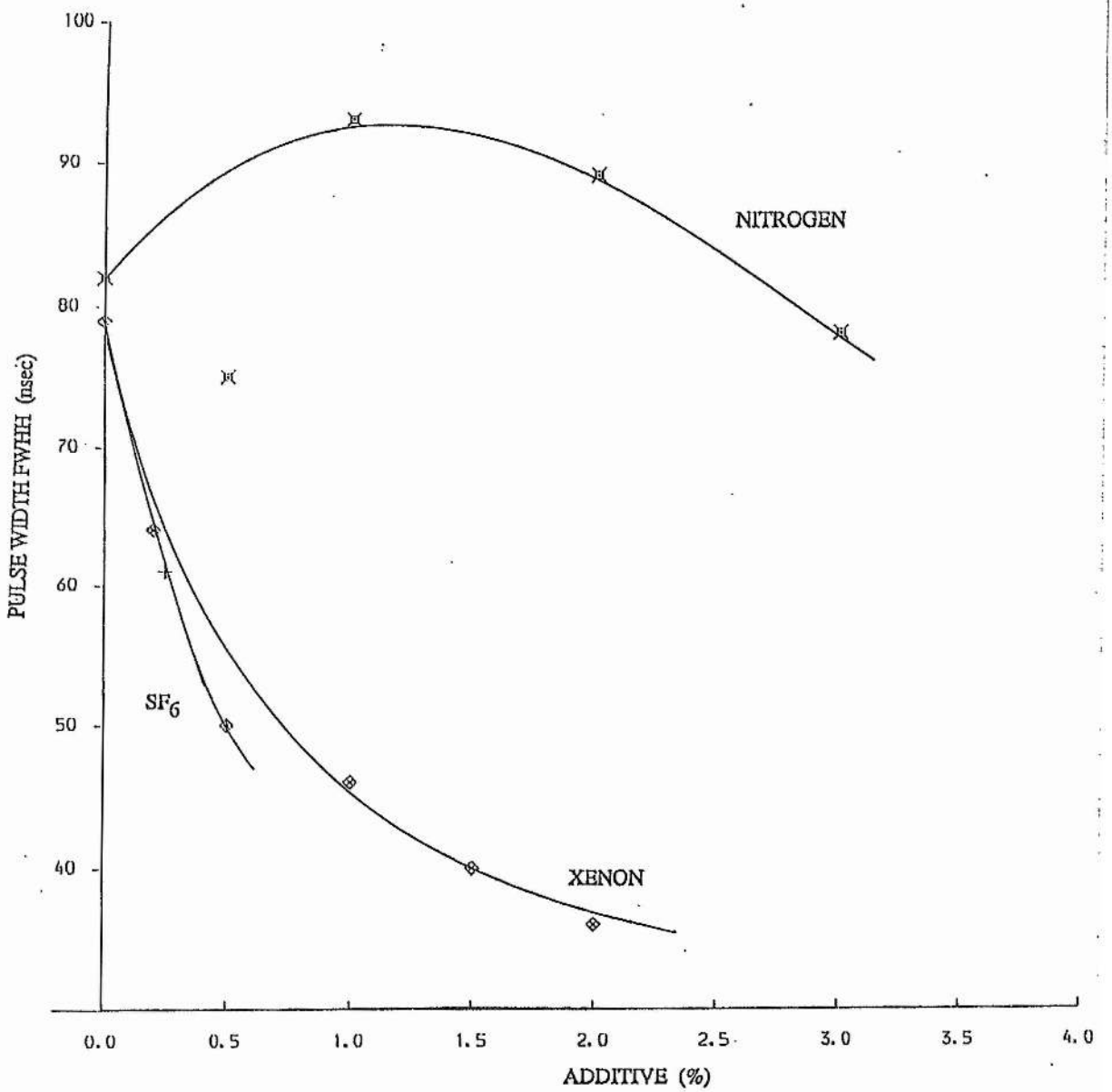

FIGURE(5.14):Output pulse width versus percentage of additive.
3 Bar Ne buffer, 150 ^{o}C $HgBr_2$ reservoir temperature,
3 cm X-ray collimation, 5 cm electrode gap.

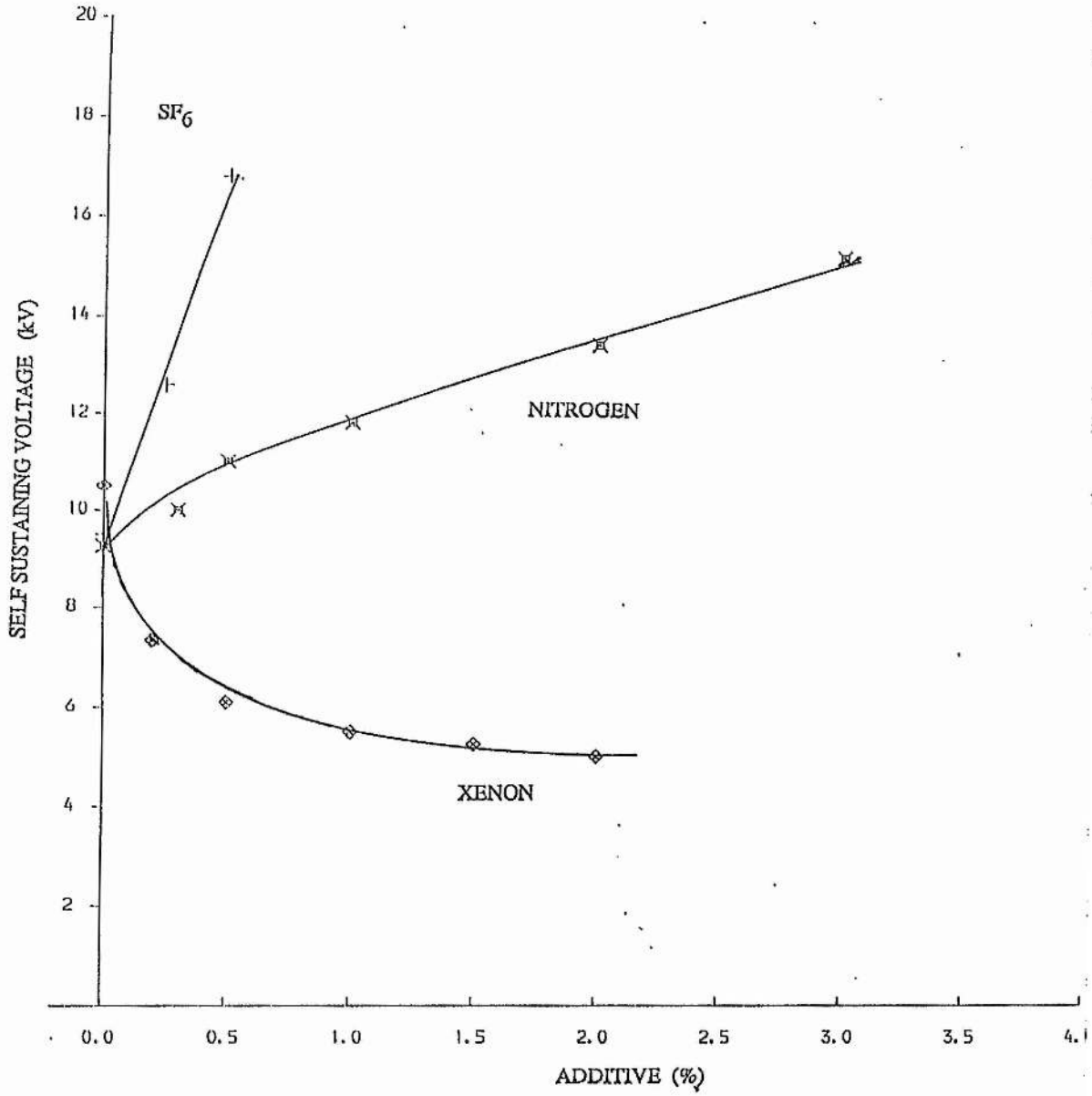

FIGURE(5.15):Self sustaining voltage versus percentage of additive.
3 Bar Ne buffer, 150 ^{o}C $HgBr_2$ reservoir temperature,
3 cm X-ray collimation, 5 cm electrode gap.

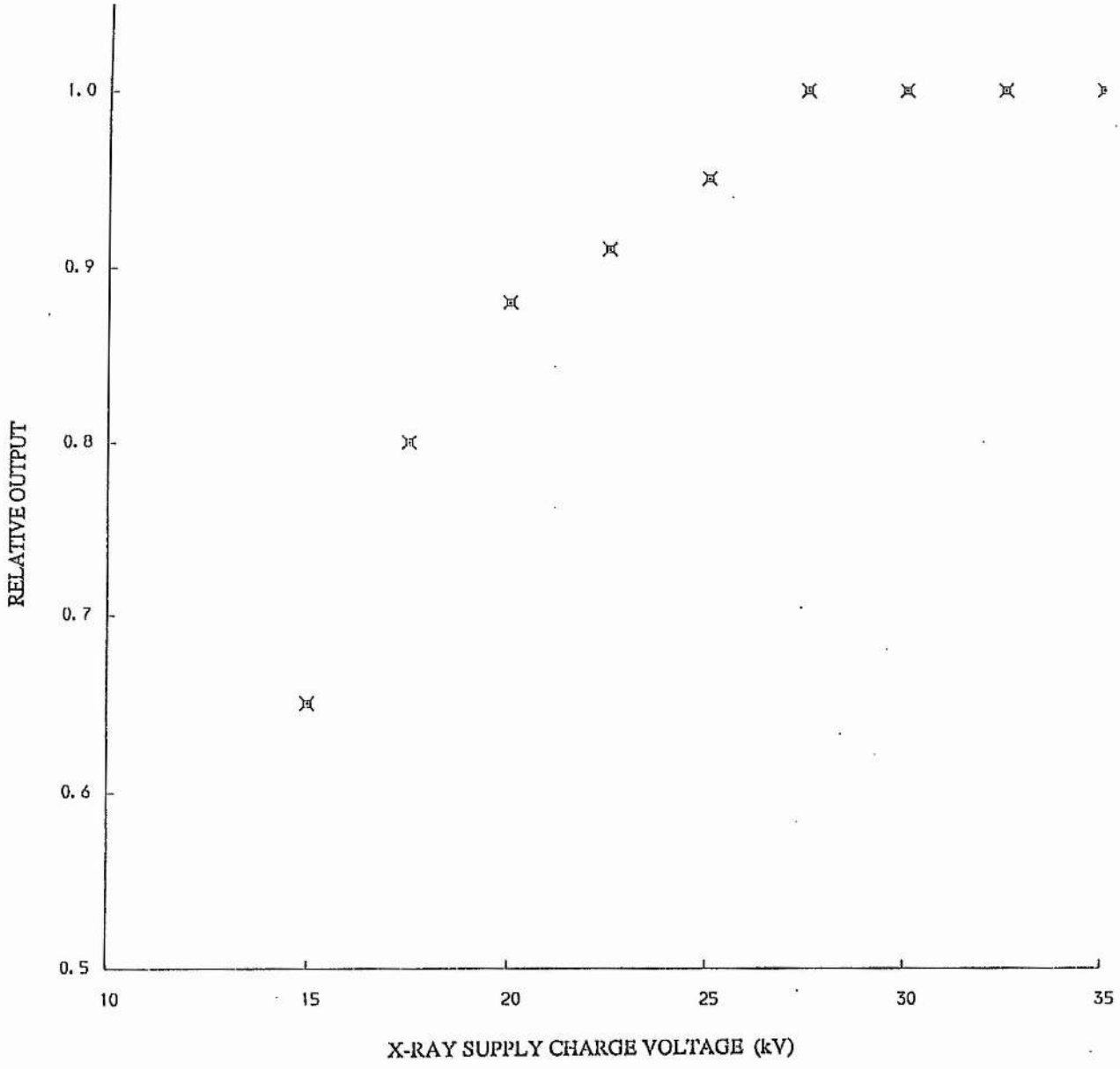

FIGURE(5.16):Relative laser output versus X-ray supply charge voltage.

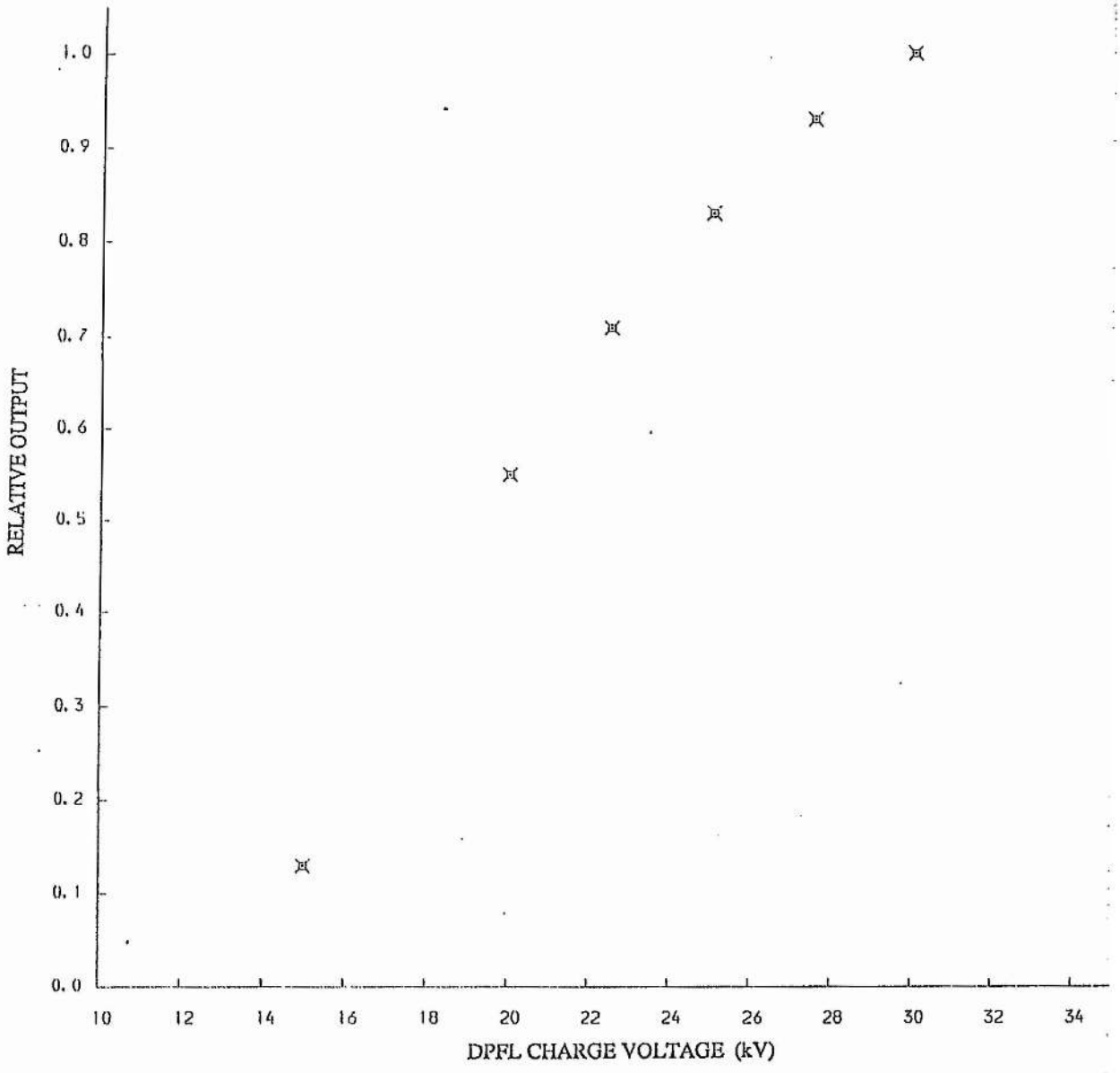

FIGURE(5.17):Relative laser output versus DPFL charge voltage.

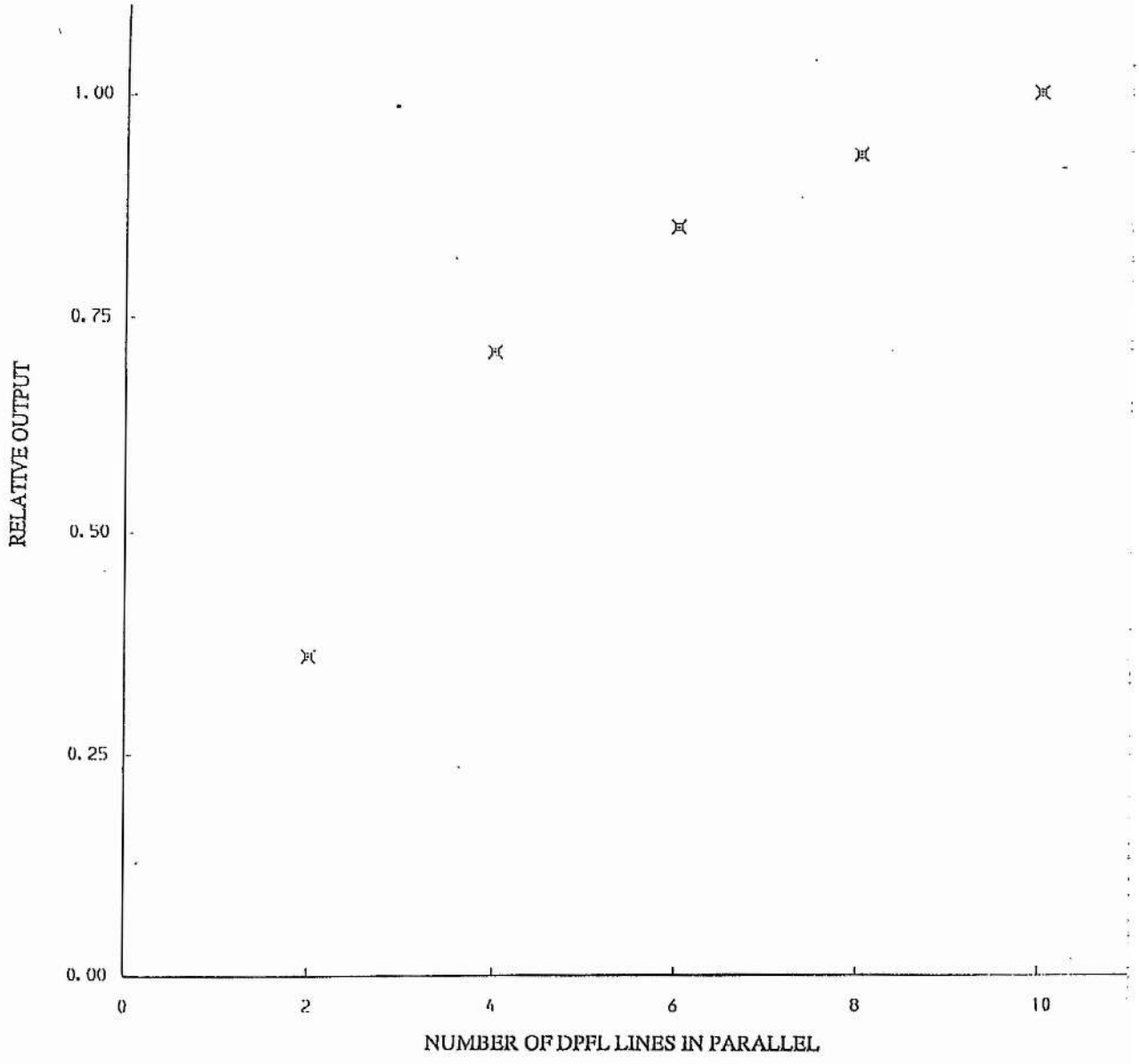

FIGURE(5.18)Relative laser output versus number of DPFL modules in parallel.

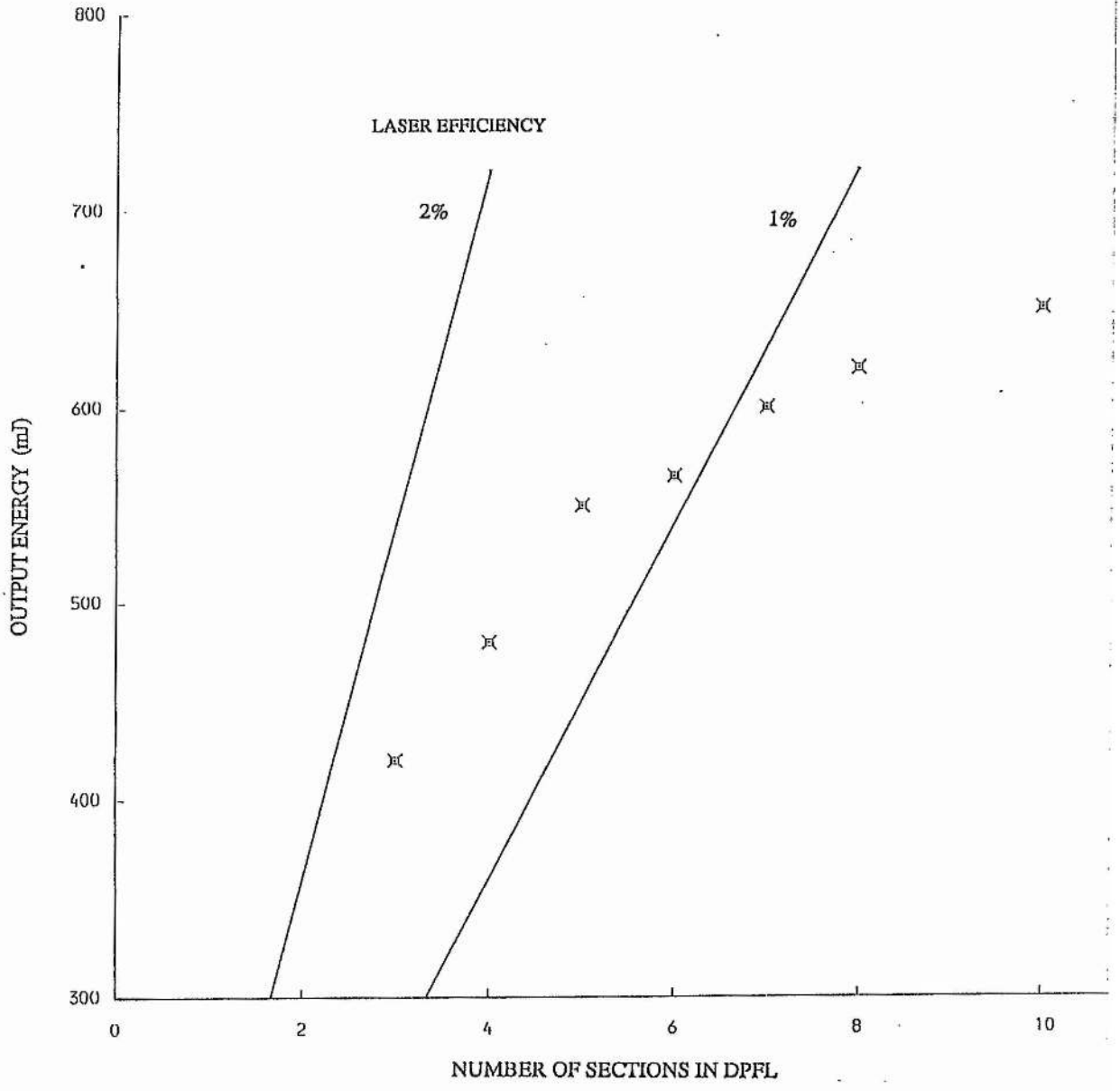

FIGURE(5.19):Output energy versus number of sections in the DPFL modules. 3 Bar Ne buffer, 150 ^{o}C $HgBr_2$ reservoir temperature, 3 cm X-ray collimation, 5 cm electrode gap.

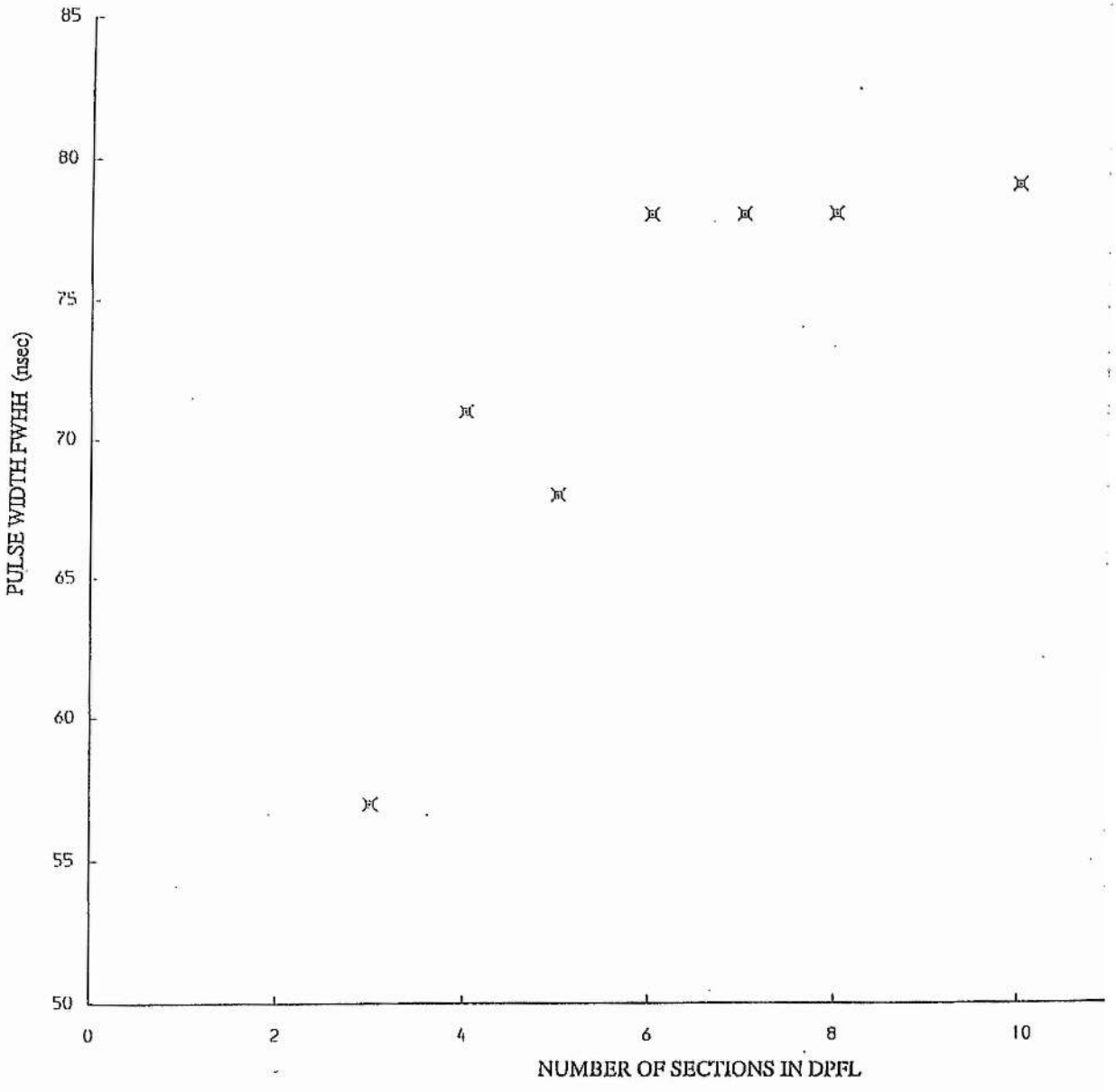

FIGURE(5.20):Output pulse length versus number of sections in the DPFL modules.
3 Bar Ne buffer, 150 ^{o}C $HgBr_2$ reservoir temperature,
3 cm X-ray collimation, 5 cm electrode gap.

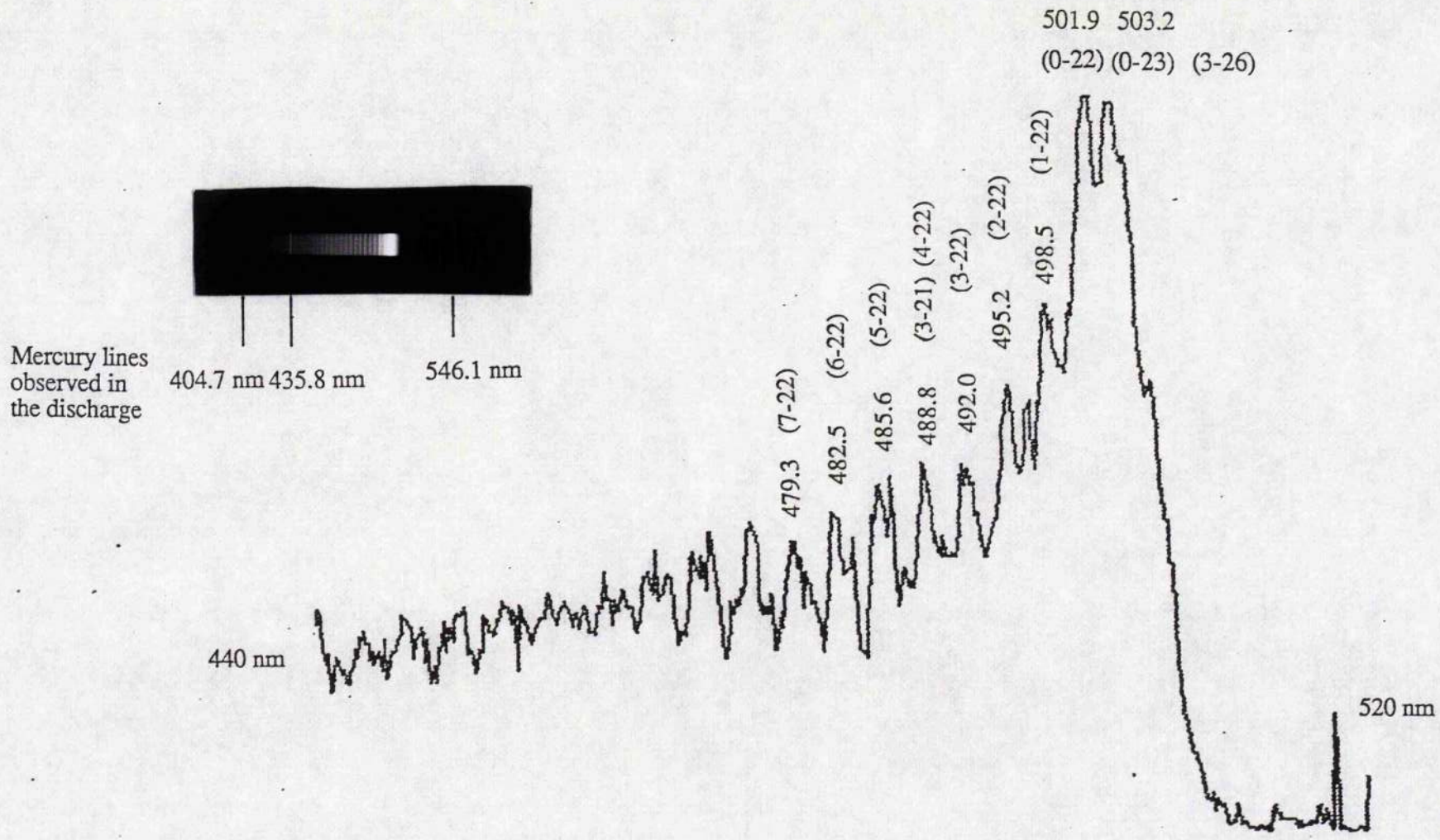

FIGURE(5.21):Fluorescence spectrum from the laser observed using a 1 metre Hilger and Watts spectrometer and a Joyce, Loebl and Co. double beam microdesitometer. The assignments to the bands follow those of ref [27]. The inset shows a similar spectrum recorded using a Chelsea Instruments Ltd. S100 spectrometer.

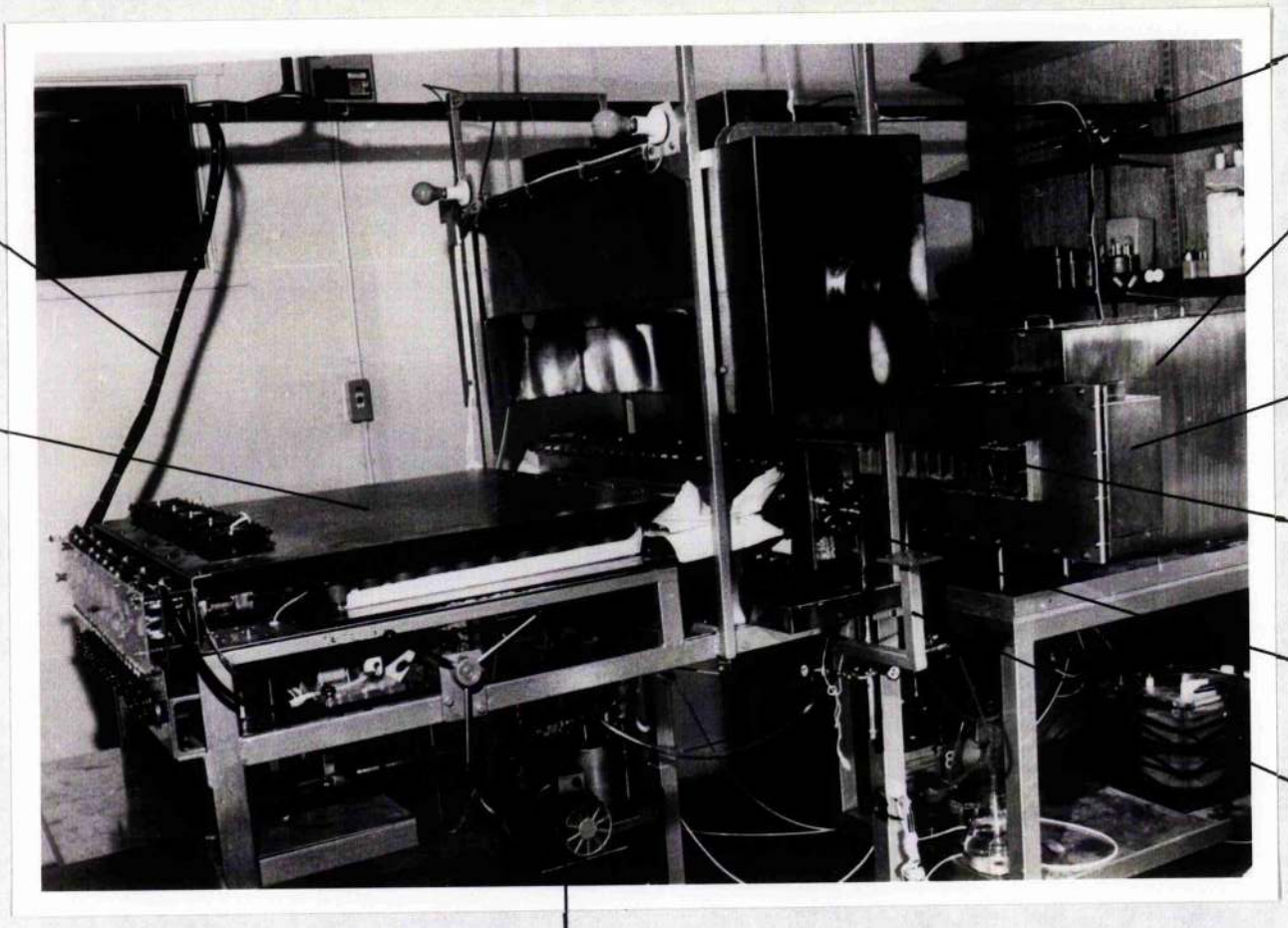

PHOTOGRAPH(5.1):The complete laser system in position for operation.

CHAPTER 6

CONCLUSIONS AND FUTURE WORK

6.1 Introduction

This chapter briefly reviews the accomplishments of the work detailed in this thesis. The main results achieved are summarised and the limitations of the laser are discussed. Areas where further investigation and development of this device may prove interesting and worthwhile will be elucidated. Finally, potential ideas for future work will be discussed.

6.2 Performance Review

The double pulse forming line system described in chapter 2 has demonstrated the feasibility of using multiple paralleled thyratrons in the production of a reliable and fairly compact pulsed power supply with a high repetition rate capability for driving laser discharges. The modular construction of the supply enables its output impedance to be varied from 3.6 Ω to 300 mΩ simply by altering the number of these modules run in parallel. Also, any faults which develop in the system such as capacitor failure can rapidly be attended to without dismantling the whole device, thus minimising down time. A simple alternative to the spiker/sustainer excitation technique [1,2] is offered by the 'spike line'. This forms an integral part of the DPFL and automatically produces a high voltage transient at the beginning of the discharge pulse to help initiate gas breakdown. The 'spike line', being a passive component of the system, requires no extra switches or charging and trigger circuitry [1]. It also eliminates the need to reset any magnetic materials used in such circuits to provide isolation between the spiker pulse and the main pulse forming line [2].

The low measured jitter (~2 nsec), repetition rate capability and reliability of the supply described here are features characteristic of thyratron switched devices. At present the repetition rate of this supply is limited to 10 Hz by the available charging unit, but with this technique kilohertz repetition rates should be achievable through the use of ceramic thyratrons. In practice the DPFL supply performed well with only minor problems and the ease with which its characteristics (pulse length, output impedance etc.) could be altered proved extremely useful during the experimental period with the laser.

Whilst existing technology was used in the development of the X-ray diode, the TLT

pulsed power supply developed by C.R. Wilson and P.W. Smith [3] proved to be another novel piece of pulsed power engineering used in this laser system with exceptional reliability. Although the final uniformity of the X-ray source was far from ideal, it proved adequate for effective preionisation of the laser. The X-ray exposure measured in the cavity whilst still fairly low (~5 mR), is more than an order of magnitude greater than that reported [4,5] for effective stabilisation of rare gas halide lasers. However, substantial performance improvements have been obtained in mercury bromide [6] and XeCl lasers [7] upon increasing the preionisation electron density. This observation is discussed in more detail in the following section with respect to increasing the performance of this device.

The optimum operating conditions for the laser were 4 bar neon buffer gas, ~3.5mbar $HgBr_2$ vapour pressure with a 5 cm electrode gap and the preionisation X-rays collimated to irradiate a 3cm wide area. Output energies in excess of 700 mJ were achieved in pulse lengths of ~80nsec (FWHM). These are comparable to the longest pulse lengths reported for discharge pumped mercury bromide lasers [8]. The optimum value of $HgBr_2$ vapour pressure is low in comparison to that found elsewhere, an effect attributed to two characteristics of this device. The relatively low X-ray exposure hence preionisation electron density and the shape of the main discharge electrode. A discussion of how these features may be improved with a view to increasing laser performance is also presented in the following section.

The effect of additives in the gas mixture showed no improvements in output energy as observed with smaller scale lasers [9]. However, with nitrogen added to the discharge an increase in output pulse length was observed, the maximum achieved being 92 nsec (FWHM) at 1.5% concentration. An effect in part attributed to the stabilising effect N_2 has been shown to have on these discharges [6]. Table 5.2 summarises the performance of the laser.

6.3 Possibilities for improving the Laser Performance

Numerous features have already been indicated which may lead to improvements in the performance of the laser. Increasing the preionisation electron density (PED) by upgrading the X-ray source is likely to improve laser performance for two related reasons. Zheng et al.

[7] have reported large improvements in the output performance of a small discharge volume XeCl laser by increasing the preionisation electron density. This is attributed to the reduced avalanche time during formation of the discharge when higher initial preionisation levels are used. Increasing the preionisation electron density shortens the time for which the avalanche process must proceed to achieve the final, steady state, electron density of the discharge. This allows a larger fraction of the useful discharge pulse to be utilised for excitation of the laser gas. As discussed in section 5.6 the useful pulse duration for mercury bromide lasers is determined by the onset of constriction in the discharge. A shorter formative phase would then result in the laser achieving threshold more rapidly and an extension in the pulse length.

The second benefit of a reduction in discharge formation time comes from the diminished time in which parasitic discharges can form outside the discharge volume. These compete with the main discharge for power delivered by the pulse forming network, thus act to reduce the laser output. It has been observed [6] that these parasitic discharges are enhanced at lower preionisation electron densities. It is also noted in [6] that at lower preionisation levels discharge stability can only be achieved by reducing the mercury bromide vapour pressure to a level substantially below that at which optimum laser performance occurs at higher PED's. This results in a decrease of 50% in the observed output energy when the preionisation electron density is reduced by two orders of magnitude. In chapter 5 the effect of increasing mercury bromide vapour pressure on the discharge stability in this laser was described. The optimum performance being achieved with a vapour pressure of ~3.5 mbar, less than 50% of the value at which the maximum laser output was observed elsewhere [6,8]. An estimate from the measured exposure in the gas places the preionisation electron density produced by the X-ray source at ~5 x 10^6 cm^{-3}. A figure which is at the lower end of those used in [6] where the reduced output was observed and the laser optimised at low mercury bromide vapour pressures. From this discussion it is therefore likely that a significant improvement in laser performance would result from an increase in PED. This would enable higher $HgBr_2$ vapour pressures to be used whilst maintaining a stable discharge allowing a new operational regime to be investigated with possible increase in output energy. The possible reduction in discharge formation time afforded with increased preioniation electron density could also result in longer pulse lengths.

A number of possible options exist to enhance the effectiveness of the X-ray source.

As discussed previously the large distance between the X-ray source and the discharge volume substantially reduces the X-ray flux in the cavity due to divergence. Reducing this gap would result in increased utilisation of the X-ray source. In other X-ray preionised lasers [10], the design is such that the laser head and X-ray diode are mated together. This minimises the loss through divergence and also eliminates one of the extra X-ray windows required by having the laser head and X-ray diode seperate, again increasing the effectiveness of the source. However, due to the obtrusive nature of the oven, reduction of this gap is not possible with this laser and would require a complete re-design of the system. Also, integrating the X-ray diode with the laser head might introduce further problems due to the high operating temperatures of the device. A more feasible approach to the problem would be to increase the output from the X-ray source.

A further investigation of cathode materials than that already undertaken, as discussed in chapter 3, may result in improved X-ray source performance. The main alternative to the blade or pin structures, not yet tried, would be to use carbon fibre emitters [11]. However, modifying the pulsed power supply may prove a better approach to increasing the effectiveness of the X-ray source. This could be achieved by stacking more cables in the TLT system [12] enhancing the gain of the supply to produce a higher voltage. As discussed in chapter 3 the diode current density is space charge limited and proportional to $V^{3/2}$. Any increase in voltage then results in a substantial increase in current density. Also, as the efficiency of X-ray production scales linearly with applied voltage, an increase in the conversion efficiency will also occur at higher voltages. However, the higher accelerating voltages will also cause a shift in the emitted X-ray spectrum to shorter wavelengths where the mass absorption coefficients are reduced, see figure 4.3. Although this increases the intensity of X-rays passed through the X-ray window into the cavity, any benefits afforded by this may be offset by the reduced absorption in the gas. Kozyrev et al.[13] have shown that the beam utilisation efficiency, defined as the ratio of the X-ray energy absorbed per unit volume in the gas to the energy of the beam electrons incident per unit surface area of the target, is a weak function of accelerating voltage above 50keV.

The penalty to pay for stacking more lines in the TLT system is the reduction in Blumlein PFN output impedance required to drive the system. This may result in an increase in current risetime at the switched end of the line which could be detrimental to the source

performance. Faster risetimes could be achieved by replacing the thyratrons in the TLT system with a low inductance spark gap although this would remove the repetition rate capability and low jitter, characteristic of thyratron switched supplies. The results of chapter 5, however, show that precise timing of the X-ray pulse and discharge pulse is not necessary in these lasers, relaxing the jitter requirement. These results also indicate that no process exists in the gas whereby the preionisation electron density is significantly reduced on timescales in excess of 1 μsec. Thus extending the X-ray pulse length, by introducing more sections into the Blumlein PFN driving the TLT supply, should result in an increased accumulation of preionisation electrons. The diode current density may also be increased by reducing the anode cathode spacing. This again may result in increased performance of the X-ray source but with reduced diode impedance. A design change in the TLT supply would be required to reduce the output impedance of the pulsed power supply in order to ensure adequate voltage was produced at the cathode.

It is useful to make a comparison between the laser system built by Mathematical Sciences Northwest Inc. (MSNW) and this one to see where any major differences occur which may lead to identifying a method of increasing the efficiency or output energy (or both) of the laser. Table 6.1 summarises the main characteristics of the two lasers for the condition of maximum output. The main difference is in the pump power density, due to the shorter pump pulse duration and higher pump energy density used by MSNW. An increase in the pump energy density of the device described in this thesis could be achieved by running more lines in parallel in the DPFL system. The resulting lower output impedance of the pulsed power supply and the consequent higher discharge currents could result in increased laser performance. Asside from the practical problems of achieving this in terms of the design of the DPFL system, Kushner et al.[14] have shown that discharges in these lasers constrict after a critical amount of energy is deposited in the gas. Whilst there is no doubt that increasing the pump power density in this laser would result in improved performance, there would be a limit to the benefits afforded by this due to the onset of constriction. Other differences between the two lasers, some of which have been mentioned previously, include the higher preionisation density (PED) and optimum $HgBr_2$ vapour pressures of the MSNW device. Their laser also optimises at 5 bar neon buffer gas pressure. Under the conditions of increased PED affording operation at higher mercury bromide

vapour pressure, as discussed above, higher buffer gas pressures may also show promise for enhanced performance in our device.

An increase in laser performance could possibly be achieved by altering the shape of the main discharge electrode. As discussed in section 5.3, the electrode contours can result in one area of the discharge having a higher value of E/N than another. This leads to enhanced excitation and ionisation rates and eventual localised constriction of the discharge in these areas. By using an electrode with a larger flat area than that described in chapter 4, and restricting the discharge to the desired area through confinement of the preionisation X-rays, an increase in useable discharge volume should be achievable. A further benefit afforded by the use of flatter electrodes is a more uniform deposition of energy in the discharge volume. This would tend to increase the possible energy loading, hence pump pulse duration before constriction of the discharge ensues, with a resulting increase in pulse length.

Scaling the discharge dimension, by means of enlarging the electrode gap in this device, is limited to 5 cm by the physical size of the cavity. During the initial laser experiments, discussed in chapter 5, the optimum laser performance was observed at the largest possible gap. A similar result was also observed in [8] where an electrode gap of 5cm, comparable to the maximum in this laser, gave a lower output energy and efficiency than the maximum electrode separation in that device of 6.5 cm. It is therefore likely that better laser performance would be achieved by scaling the discharge dimensions in this way. The maximum useable gap would, however, be restricted by the voltage pulse required from the PFN to break the gas down. In [8] a charge voltage of 58 kV was used with the 6.5 cm gap, whilst the DPFL supply with a 30 kV charge voltage can only achieve a 45 kV peak output.

Scaling to a larger electrode separation would require a re-design of the cavity. This could result in a larger, hence more inductive cavity and care would be required in the design to prevent any degredation in the current ristime by this affecting laser performance. An increase in the DPFL charge voltage above the 30 kV maximum used in the experiments discussed here could be achieved and, as the results of section 5.6 show, would result in larger output energies although possibly at the expense of efficiency. This would entail replacing the thyratrons in the pulsed power supply, which have a maximum anode voltage of 35 kV, with a multichannel rail gap for operation at higher voltages. This, however,

would require the line to be pulsed charged and triggering problems could result. An advantage of using a multichannel rail gap would be in the improved current risetime from the supply, through the reduction in inductance of the switch. Improved laser performance may result due to the increased time during the discharge, proir to constriction, when significant current exists and this may be another factor in the lower outputs obtained than those reported in [8]. At higher voltages, the conductors would have to be removed from the air to prevent flashover problems and corona losses by either submerging the system in oil or enclosing it in an atmosphere of Freon. Without revising the design of the pulsed power supply and the discharge cavity it appears that upgrading the X-ray source is the route by which increased laser performance could be achieved. A result which requires experimental confirmation.

As for the chemical compatibility of the cavity materials with the laser mixture, discussed previously, little can be done to improve this in the present system and reduce production of corrosion dust. The theoretical and experimental results reported elsewhere [6,15] have shown that for a long life laser materials selection is extremely important. Platinum, gold, molybdenum, glass and ceramics are suitable materials for use in the construction of mercury bromide lasers. Stainless steel has proven to be too reactive leading to the formation of corrosion dust and both aluminum and nickel are known to be incompatible with mercury bromide vapour. The installation of the gas circulation system discussed in chapter 4 should improve the shot-to-shot laser performance by clearing the dust from the discharge region. However, this would only be a short term solution. For a truly long life laser a complete re-design of the cavity, taking into account the materials compatibility studies now at our disposal, would be required.

6.4 Future Work

With the comments of the previous section in mind, the laser is fully operational, reliably produces energies well in excess of 0.5 J and is, as far as is known from published results, the largest existing X-ray preionised mercury bromide discharge laser. A large number of experiments remain to be undertaken to provide further information on the laser. The possibility also exists of enhancing the laser performance with the system in its present form through injection locking. These points are now discussed in more detail.

Time and spatially resolved gain and absorption measurements in the discharge would provide an insight into the kinetics of the laser. This would include investigating the possible limitations, aside from discharge stability, of long pulse operation due to self-absorption by mercury bromide or excited species formed in the discharge. On the timescale typical of discharge pulses no efficient process exists for the depopulation of the lower laser level. Thus a significant X state number density can build up resulting in absorption during the laser pulse, introducing a serious loss channel. Such absorption measurements could lead to an estimation of the X state density which would be useful for comparison to computer models of the discharge.

Spatial inhomogeneities have been shown in this work and elsewhere [6] to be of great importance to discharge stability in these lasers. Measurements of spatial variations in the gain would provide information on the local excitation rates in the discharge, again useful for comparison with multidimensional computer simulations of the laser. With these and other experiments in mind a thyratron triggered, flashlamp pumped dye laser was constructed [16] with a tuning range covering the laser gain spectrum and other regions by use of the appropriate dyes. Time limitations, however, have so far prevented its use as a diagnostic in this system.

Measurements of the population density of excited states of mercury in the discharge would be of great importance in the investigation of discharge constriction. Kushner et al. [14] used Hook method interferometry[17] to measure the density of excited Hg atoms under typical discharge conditions in their device. They also predicted the temporal and spatial variation of mercury ions in their multidimensional model. Such measurements, spatially and temporally resolved, would be useful in the analysis of this laser to investigate these populations in areas where variations in discharge E/N occur due to the electrode shape. This would enable an investigation to be undertaken of the kinetics of the constriction process. It would also be of great interest to carry out these measurements with nitrogen in the gas mixture. This would help clarify the effect of the additive on the performance of the laser in terms of pulse length and discharge stability. As far as is known this has never been attempted.

Injection locking experiments on mercury bromide lasers have been reported with enhanced laser performances of up to 30% observed [18]. By injecting a narrow linewidth

seed pulse into the laser cavity the broad band laser output can be considerably spectrally reduced. Other techniques of line narrowing by introducing gratings or prisms into the optical cavity result in a reduction of laser output due to the losses these introduce. The narrowband injected pulse, in this technique, essentially reduces the time for the laser to achieve threshold at that wavelength, increasing the energy extraction from the discharge. Injection locked laser emission shows spectral characteristics of wavelength and linewidth similar to that of the seed pulse. The narrow bandwidth and tunability achievable with this technique are essential for some of the potential applications of mercury bromide lasers mentioned in chapter 1. Coupled with the potential improvement in output energy this makes an attractive if not essential experiment to undertake with this system. Further ,the low jitter characteristic of the DPFL supply means these experiments may be undertaken without the problems associated with triggering of the seed and laser discharge pulses, ensuring the required temporal overlap of the pulses may be achieved.

The dye laser discussed above was also designed with these experiments in mind and is tunable over the free running laser spectrum. Further it has been mode-locked in this spectral region. This offers the opportunity to use the mercury bromide discharge to amplify pulses of picosecond duration. The high peak powers of these blue/ green pulses could have uses in spectroscopy and biophysics. One potential application of these is in the investigation of DNA molecules[19]. These absorb at wavelengths around 250 nm, accessible by frequency doubling the output from a mercury bromide laser. The fluorescence of these molecules could then be observed using nanosecond excitation pulses to monitor average effects whilst shorter, picosecond pulses, would be useful for transient effects. Further possible applications of mercury bromide lasers in general include underwater pulsed holography, of interest to oil rig manufacturers to monitor the submerged structure and in medicine. Numerous medical applications utilise lasers operating in the visible region of the spectrum. Argon ion and dye lasers are used in opthalmic surgery [20] to photocoagulate retinal tissue and argon lasers have uses in treating Glaucoma patients. Both these lasers also have applications in treating portwine stains [21]. The pulsed nature and operational wavelength of the mercury bromide laser may be of use in this area.

Mode-locking of the laser itself offers the opportunity to produce very short optical pulses directly. Although the output pulse length of 80 nsec is short limiting the number of

cavity round trips to produce pulse narrowing. For this reason the technique of producing picosecond pulses by amplifying the modelocked output from a dye laser would be more appropriate. However, active and passive [22] mode-locking of excimer lasers with comparable pulse lengths has been achieved. No published work has been previously reported on mode-locking of $HgBr_2$ lasers and this may prove an interesting exercise to undertake. Once again time limitations have prevented progress being made in any of these experiments.

6.5 The Future for Mercury Bromide Lasers

At the present time funding on mercury bromide laser development, which was mainly defence orientated, has been reduced to minimal amounts. This appears mainly due to the lack of a suitable detector for operation at the laser wavelength in connection with an underwater communications system. The technical problems and long life issues of this laser system having been overcome making a truly long lived, space based laser a practical reality with the technology available at present [23].

Attention has recently turned to the development of other systems, some of which were mentioned in chapter 1, for the production of laser emission at a wavelength suitable for use with available detectors. Raman shifting in lead vapour of the output from an XeCl laser [24] and the C to A laser transition in XeF [25] fall into this category. The operational wavelengths of these systems make them attractive for underwater applications as they lie in the absorption minimum of sea water. They also overlap with the operational wavelength of atomic vapour resonance filters based on caesium [26] which have shown to be capable of quantum efficiencies greater than 95%. However, the Raman shifting technique limits the efficiency of such systems and adds complexity to the device whilst the XeF C to A laser still requires much development to reach the performance levels achieved with mercury bromide lasers.

Ongoing work at Los Alamos National Laboratory by Chung et al. [27] has shown promising results using optical filters based on semiconductor diode laser pumped rubidium vapour which may see a revival in interest in mercury bromide lasers. These filters have a wide field of view, relatively high quantum efficiency, sub-microsecond response times, narrow bandwidth and low diode laser power requirements. Their discrete operational

wavelengths cover the range from 487.3 nm to 776.2 nm with transitions within the output spectrum of the mercury bromide laser. Should these filters prove effective, coupled with the large database of knowledge accumulated over the past decade on this laser, a space based submarine communications system founded on these technologies may emerge.

Aside from the development of a deployable communications system a number of other interesting features of mercury bromide lasers would also be worthy of further research. Recently [28] experiments on the $X^2\Sigma_{1/2}^+ \rightarrow B^2\Sigma_{1/2}^+$ absorption band of HgBr centred at 350 nm have shown that optical pumping of the upper laser level directly from the ground state is feasible. Following the initial B state formation, through excitation and dissociation of the parent compound, and emission of a laser photon, the HgBr molecule is left in the ground state and is available for re-excitation to the upper laser level. The quantum efficiency of ~ 70% for this process is much greater than that for excitation directly from the parent molecule. This offers the possibility of continuously re-using these molecules in an efficient laser system which could be flashlamp pumped.

Direct optical pumping of $HgBr_2$ using an ArF laser was utilised to demonstrate the first mercury bromide laser [29]. A pumping technique using a wideband optical source formed from a surface discharge has also been reported [30]. Results of these and experiments on other mercury halide [31] and excimer lasers [32] have shown pulse lengths of microsecond duration are possible. No limitations are imposed on this technique of pulse length through discharge stability. Such long pulses could result in the production of very short (picosecond) pulses from mode-locking experiments. This technique also enables higher mercury halide vapour pressures (several tens of millibar) to be used in the gas mixture allowing an experimental regime, not possible with discharge excited lasers due to stability problems, to be investigated. The pump power densities achievable with these surface discharges are much greater than those possible at present with discharge excited devices. Again this enables new experimental areas to be investigated which are of interest not only to mercury bromide but other laser systems too.

Multicolour lasers have also been demonstrated by this optical pumping technique using mixtures of mercury halides to produce laser emission at two and three wavelengths simultaneously [33]. Small scale discharge excited lasers operating on two or three

wavelengths using mixtures of mercury halides have also shown promise as possible candidates for multicolour lasers with reasonable efficiency and output [34]. Such lasers may have applications in spectroscopy and photochemistry where it is often desirable to use two or more wavelengths simultaneously or to rapidly change the operational wavelength. Scaling of these studies to larger X-ray preionised discharge lasers may prove interesting and would be worthy of further investigation.

Recent advances in the search for more volatile mercury halide bearing compounds such as the alkyl mercury bromides [35] have resulted in some success. Such compounds would enable these lasers to operate at lower temperatures than presently required to produce the necessary vapour pressure. This would substantially reduce the technical problems associated with the high operating temperatures of these devices. Significant luminescence emitted by HgBr molecules in mixtures based on C_2H_5HgBr and C_4H_9HgBr molecules, following discharge excitation, was observed at temperatures below 100°C and laser action has also been reported. Again this is an area where large advances may be made in the future, simplifying the design of mercury bromide lasers.

Finally an area of interest which is currently being addressed in St. Andrews is that of operating a liquid mercury halide laser. In aqueous solution mercury halide exist almost exclusively (99%) as the HgX_2 molecule [36]. Under optical excitation at the appropriate wavelength formation of the HgX(B) level may be possible followed, in a manner similar to the gaseous phase, by emission of a blue-green photon upon relaxation of this level to the ground state. A system which is somewhat analogous, although the formation kinetics are different, is that of excimer laser emission in cryogenic liquids as discussed in reference [37]. In this case stimulated emission on the B→X band of the XeF* molecule in the liquid phase was observed following optical excitation. The observed wavelength of emission of 404 nm was shifted by ~ 0.5 eV to the red with respect to the corresponding gas-phase emission under these operating conditions. By comparison, then, it might be expected that the emission from mercury bromide in solution would be red shifted. At present the experiments are in their infancy. Under illumination by the 308 nm emission from an XeCl laser (the shortest wavelength laser available at the time of the experiment) some faint blue-green emission has been observed (possibly due to some two photon absorption

process). More information is required on the absorption and emission spectra of the mercury halides in solution. This type of 'liquid laser' lends itself to the technique of optical pumping and some experiments using a surface discharge as the optical source have also been undertaken [38].

CHAPTER 6

REFERENCES

1. W.H. Long Jr, M.J. Plummer and E.A. Stappearts, Appl.Phys.Lett. 43, 735 (1983).
2. C.H. Fisher, M.J. Kushner, T.E. DeHart, J.P. McDaniel, R.A. Petr and J.J. Ewing, Appl.Phys.Lett. 48, 1574 (1986).
3. C.R. Wilson and P.W. Smith, Proceedings 17th Pulsed Modulator Symposium, Seattle (1985).
4. C.R. Tallman and I.J. Bigio, Appl.Phys.Lett. 42, 149 (1983).
5. M. Steyer and H. Voges, Appl.Phys. B42, 155 (1987).
6. Mathematical Sciences Northwest Inc. 200 Watt HgBr laser - Final Report.
7. Cheng-En Zheng, Dennis Lo and Shoo-Chi Lin, Appl.Phys. B41, 31 (1986).
8. T.A. Znotins, C.H. Fisher, T.E. DeHart, J.P. McDaniel and J.J. Ewing, Appl.Phys. Lett. 46, 228 (1985).
9. R. Burnham, Appl.Phys.Lett. 33, 156 (1978).
10. M.R. Osborne, P.W. Smith and M.H.R. Hutchinson, Opt.Commun. 52, 415 (1985).
11. G.F. Erickson and P.N. Mace, Rev.Sci.Instrum. 54, 586 (1983).
12. C.R. Wilson and P.W. Smith, Seventeenth Modulator Symposium, Seattle (1986).
13. A.V. Kozyrev, Yu.D. Korolev, G.A. Mesyats, Yu.N. Novoselov, A.M. Prokhorov, V.S. Skakun, V.F. Tarasenko and S.A. Genkin Sov. J. Quantum. Electron. 14,356 (1984).
14. M.J. Kushner, A.L. Pindroh, C.H. Fisher, T.A. Znotins and J.J. Ewing, J. Appl. Phys. 57, 2406 (1985).
15. C.S. Liu and I. Liberman, IEEE J.Quantum Electron. QE23, 245 (1987).
16. M. Padgett, M.Sc. Thesis, University of St. Andrews (1986).
17. I. Smilanski, L.A. Levin and G. Erez, Optics Letters 5, 93 (1980).
18. T. Shay, F. Hanson, D. Gookin and E.J. Schimitschek, Appl.Phys.Lett. 39, 783 (1981).
19. Professor W. Sibbett, St. Andrews University, private communication.

20. Lasers and Applications, pages 42-44 December 1985.

21. Lasers and Applications, page 28 June 1986.

22. S. Watanabe, M. Watanabe and A. Endoh, Appl.Phys.Lett. 43, 533 (1983).

23. J.J. Ewing, Private Communication.

24. H. Reiger, IEEE J.Quantum Electron. QE22, 405 (1986).

25. C. Fisher, R.E. Center, G.J. Mullaney and J.P. McDaniel, Appl.Phys.Lett. 35, 901 (1979).

26. J.B. Marling, J. Nilsen, L.C. West and L.L. Wood, J.Appl.Phys. 50, 610 (1979).

27. Y.C. Chung, J.D. Dobbins and J.M. Shay, Paper submitted to IEEE J.Quantum Electron. (October 1987).

28. D.P. Green, K.P. Killean and J.G. Eden, Appl.Phys.Lett. 48, 1175 (1986).

29. E.J. Schimitschek, J.E. Celto and J.A. Trias, Appl.Phys.Lett. 31, 608 (1977).

30. S.P. Bazhulin, N.G. Basov, V.S. Zuev, Yu S. Leonov and Yu Yu Stoilov, Sov.J.Quantum Electron. 8, 402 (1978).

31. S.P. Bazhulin, N.G. Basov, S.N. Bugrimov, V.S. Zuev, A.S. Kamrukov, G.N. Kashnikov, N.P. Kozlov, P.A. Ovchinnikov, A.G. Opekan, V.K. Orlov and Yu.S. Protosov, Sov.J.Quantum Electron. 16, 836 (1986).

32. V.S. Zuev, G.N. Kashinikov, N.P. Kozlov, S.B. Mamer, V.K. Orlov, Yu.S. Protosov and V.A. Sorokin, Sov.J.Quantum Electron. 16, 1665 (1986).

33. S.P. Bazhulin, N.G. Basov, S.N. Bugrimov, V.S. Zuev, A.S. Kamrukov, G.N. Kashnikov, N.P. Kozlov, P.A. Ovchinnikov, A.G. Opekan and Yu.S. Protosov, Sov.J.Quantum Electron. 16, 990 (1986).

34. M. Stonefield, Private Communication.

35. A.D. Klenrentov, I.S. Lakoba, E.A. Petrukhin and A.S. Podsosonnyi, Sov.J.Quantum Electron. 16, 1560 (1986).

36. Advanced Inorganic Chemistry, Cotton and Wilkinson (2nd edition), Interscience London (1962).

37. M. Shahidi, H. Jara, H. Pummer, H. Egger and C.K. Rhodes, Opt.Lett. 10, 448 (1985).

38. G.A. Erickson, St. Andrews University, Pulsed Power M.Sc. Report (1987).

	Discharge Volume (L)	Stored Energy (J)	Output Energy (J)	Efficiency (%)	Pump Energy Density (JL^{-1})	Extracted Energy Density (JL^{-1})	Preionisation Electron Density (cm^{-3})	$HgBr_2$ Vapour Pressure (mbar)	Pump Power Density (MWL^{-1})	Pump Pulse Length (nsec)	Ne Buffer Pressure (bar)	PFL Impedance (mΩ)
St. Andrews	1.5	90	0.71	0.8	60	0.5	$5x10^6$	3.5	250	240	4	360
MSNW	2.5	250	3	1.25	100	1.25	10^9	10	830	120	5	600

TABLE (6.1): Comparison of the conditions for maximum output from the Mathematical Sciences Northwest Inc laser [8] and the one constructed in St. Andrews.

APPENDIX 1

Units of X-ray Exposure and Dose

In the majority of work published on X-ray preionised lasers the quantity of X-radiation is expressed in terms of exposure. The unit of exposure is the roentgen (R) and is a measure of the X-radiation to which a body is exposed. It is equal to the total charge collected of ions of one sign liberated by photons in air.

By definition

$$1\ R = 2.58 \times 10^{-4}\ C\ kg^{-1}$$

which is equivalent to ~ 10^9 electrons cm^{-3}. The exposure may be determined by measuring the ionisation caused by the radiation with an ionisation chamber or quartz fibre dosemeters.

Another unit which appears in the literature is the rad. This is a measure of the energy absorbed per unit mass and is termed the dose.

By definition

$$1\ rad = 10^{-2}\ J\ kg^{-1}$$

although this unit has now been superseded by the Gray (Gy)

$$1\ Gy = 1\ J\ kg^{-1}.$$

This may be measured using thermoluminescent detectors.

Finally, the equivalent dose, which is used for radiation protection purposes, is related to the dose by a quality factor (QF) for the particular type of radiation in question. The unit is the rem and is defined by

$$1\ rem = 1\ rad \times QF.$$

For X-rays QF = 1 and so these are equivalent. The SI unit of the equivalent dose is the sievert (Sv)

$$1\ Sv = 100\ rem.$$

The exposure X(R) in air is related to the absorbed dose D(rad) by

$$D(rad) = X(R)\ W\ \frac{2.58 \times 10^{-4}}{e}$$

where W is the mean energy required to produce an ion pair in eV (~ 33.7 eV in air) and e

the electronic charge.

Hence

$$D(rad) = X(R) \times 0.87$$

and hence for materials where W ~ 33 eV these two are numerically similar. Converting to sieverts using the above definitions

$$X(mR) = D(Sv) \times 1.15 \times 10^{-5}$$

this conversion factor was used to generate some of the results presented in this thesis.

Reference

A. (1) International Commission on Radiation units and measurements, Report 33.

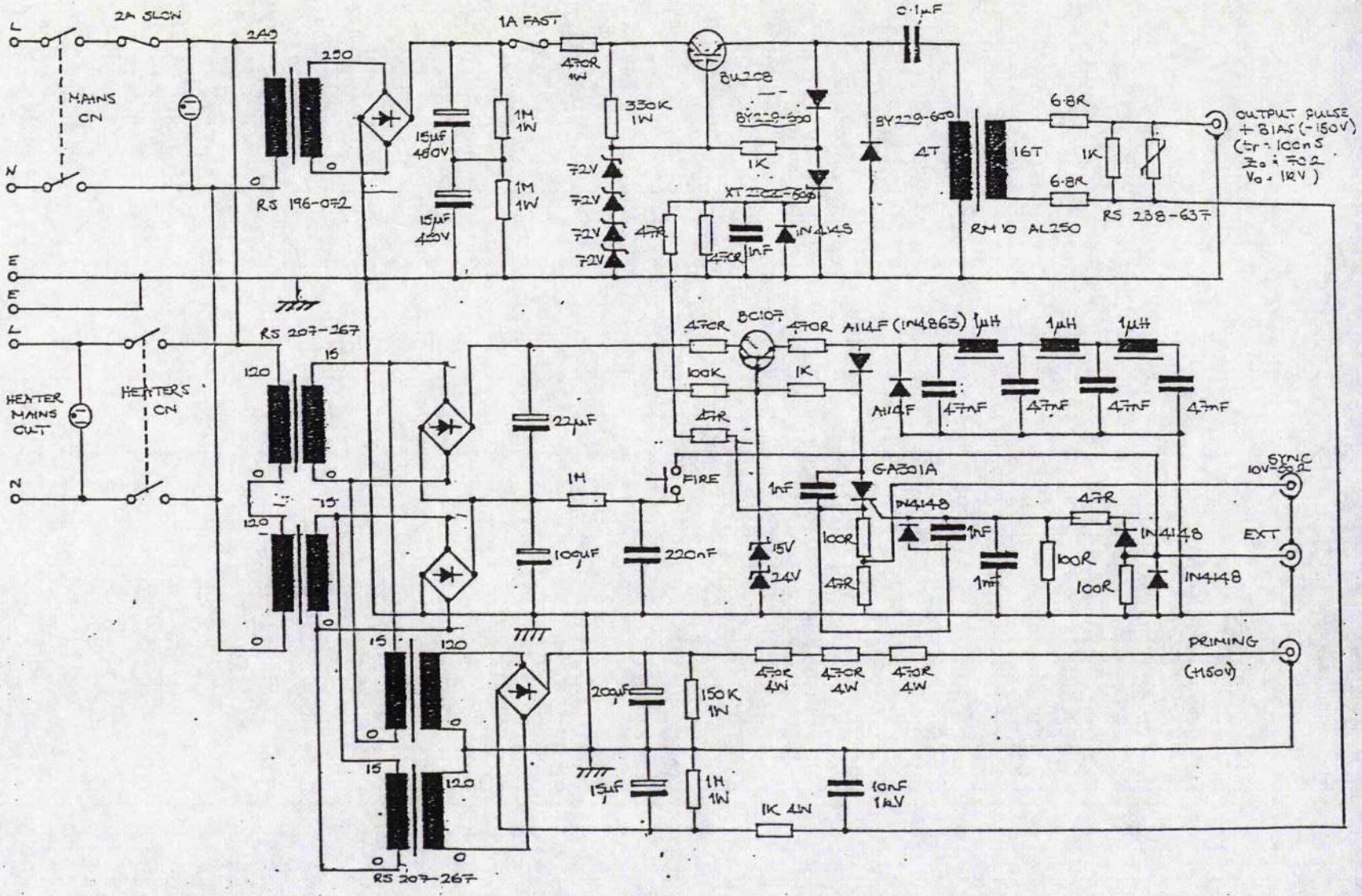

APPENDIX (2):Circuit diagram of the trigger unit for the thyratrons in the DPFL supply.

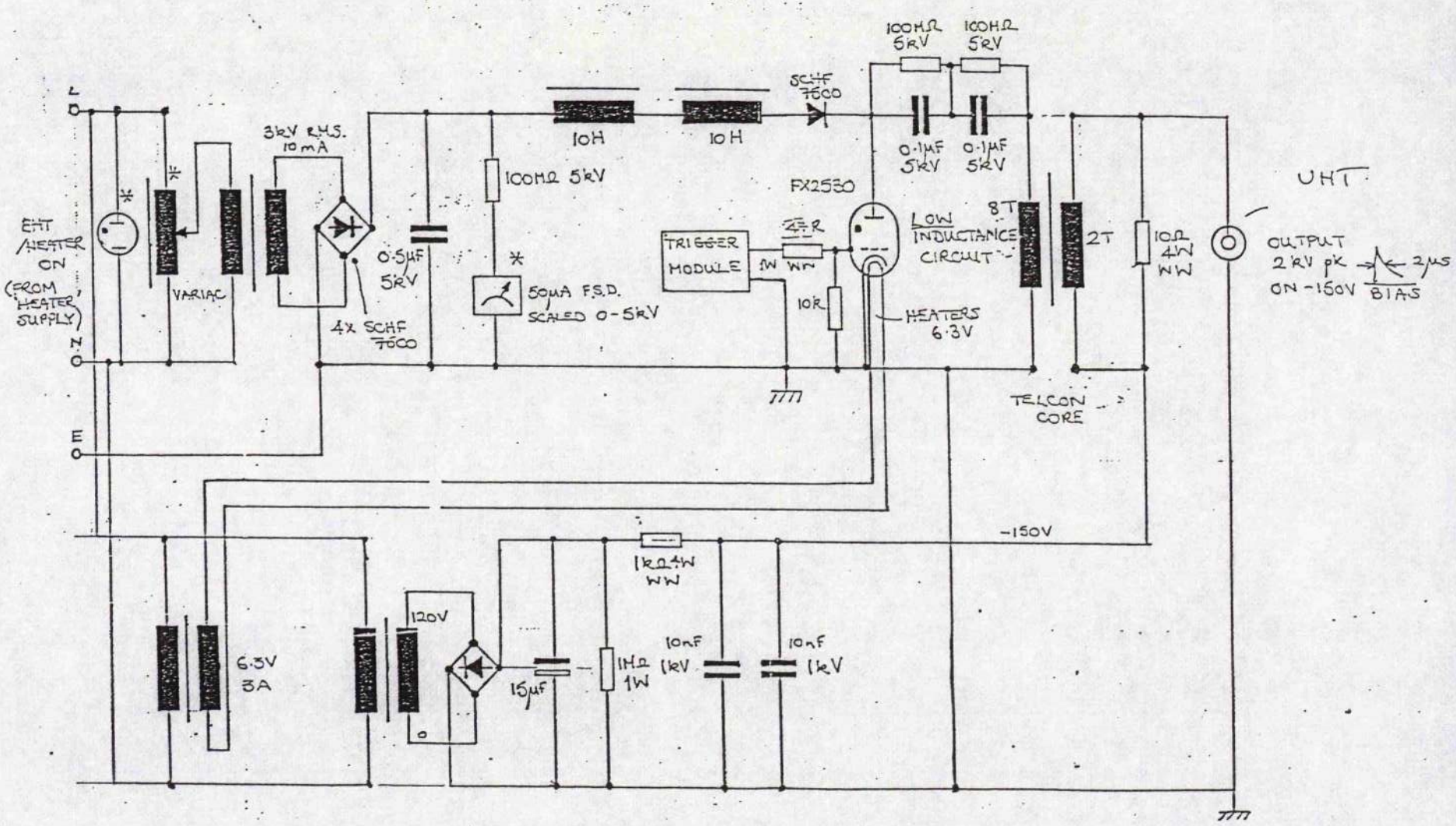

APPENDIX (3): Circuit diagram for the trigger unit for the pulsed power supply in the X-ray generator.

APPENDIX 4

Publications

1. 'A Multi-Paralleled Thyratron, Repetitively Pulsed, Power Supply for High Power Gas Lasers', A.J.W. Brown and P.W. Smith, Proceedings of the Seventeenth Modulator Symposium, Seattle, June 1986. Also published as EEV Technical Reprint 161.

Technical Reprint 161

A Multi-Paralleled Thyratron, Repetitively Pulsed, Power Supply for High Power Gas Lasers

by A. J. W. Brown and P. W. Smith

Reprint of a paper presented at the Seventeenth Modulator Symposium, Seattle, June 1986

EEV
Chelmsford, Essex, CM1 2QU, England
Telephone: Chelmsford (0245) 261777 Telex: 99103
Telegrams: Enelectico, Chelmsford Facsimile: 0245 250424
Subsidiary of The General Electric Company, p.l.c. of England

A MULTI-PARALLELED THYRATRON, REPETITIVELY PULSED, POWER SUPPLY FOR HIGH POWER GAS LASERS

A J W Brown and P W Smith
Department of Physics
The University of St Andrews
St Andrews
Fife KY16 9SS
Scotland

Introduction

There is growing interest in the construction of high repetition-rate, high average-power visible and ultraviolet pulsed gas-discharge lasers, such as the rare-gas halide and mercury halide lasers, for applications in isotope separation and optical communications. The pumping requirements of these lasers place considerable demands on the performance characteristics of the pulsed power supplies used to drive them. These demands are exacerbated when the lasers are required to operate at significant repetition rates. Apart from the obvious requirement that energy must be deposited in the gas at a rate sufficient to maintain the population inversion, a number of other conditions must be satisfied. These include:

1. The initial amplitude of the electric field between the two discharge electrodes, before gas breakdown, must be at least three times that of the field which results when self-sustained discharge conditions have been established. The electric field required to break-down the gas is always higher than the self-sustained discharge field and recent work has shown that this is one of the conditions necessary for the establishment of a stable high pressure glow discharge in a preionised laser gas mix [1].

2. The rise-time of the electric field between the two discharge electrodes must be fast (≤ 50 ns). This is a further condition for the establishment of a stable high pressure glow discharge.

3. The impedance of the pulsed power supply must be matched, as closely as possible, to that of the electrical discharge to ensure good efficiency in the transfer of electrical energy from the pulsed power supply to the discharge plasma. This is a difficult constraint to meet in practice, because the impedance of typical plasmas is often less than an ohm and is also time dependant. Care must therefore be taken to minimise the inductance of the feeds from the pulsed power supply to the discharge cavity and the cavity inductance, and hence prevent loss of current rise-time at these low impedance levels.

4. The components used to construct the pulsed power supply must be capable of operation at high repetition rates without failure from excessive wear or heating due to loss. In addition, it is often necessary to synchronise the laser output pulse to another event. Therefore, the jitter in the time delay between the receipt of an external trigger command, by the laser system, and the start of laser action must be minimised.

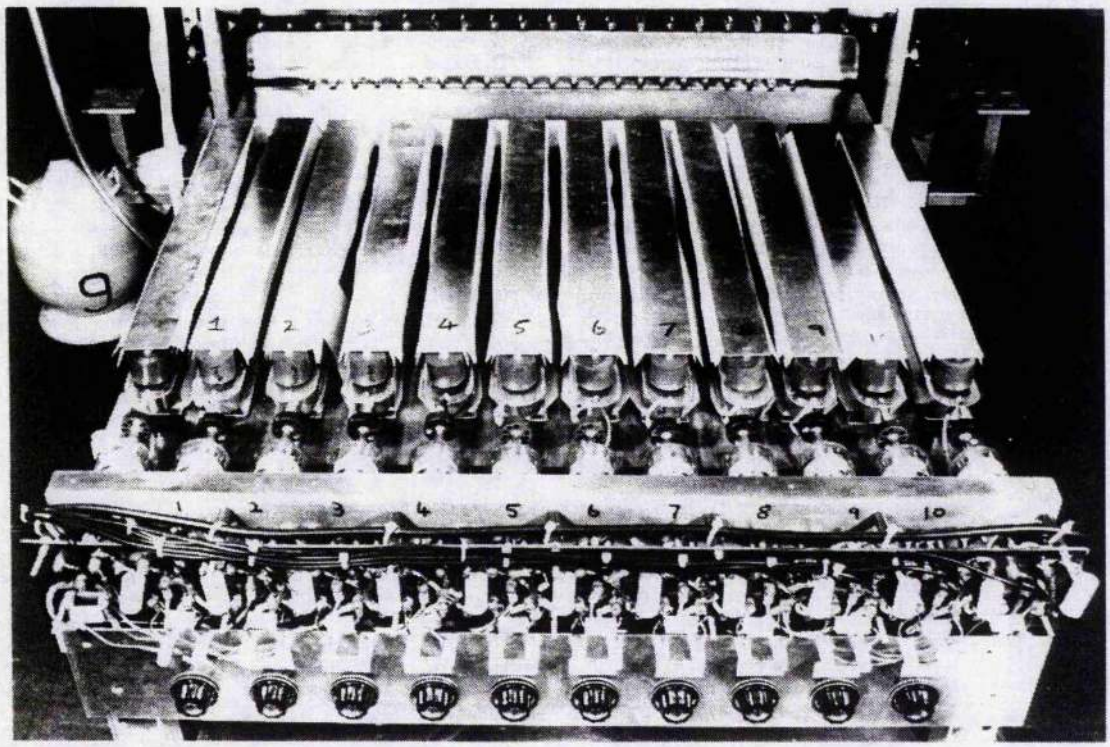

Figure 1 Photograph of the Pulsed Power Supply with the top cover removed

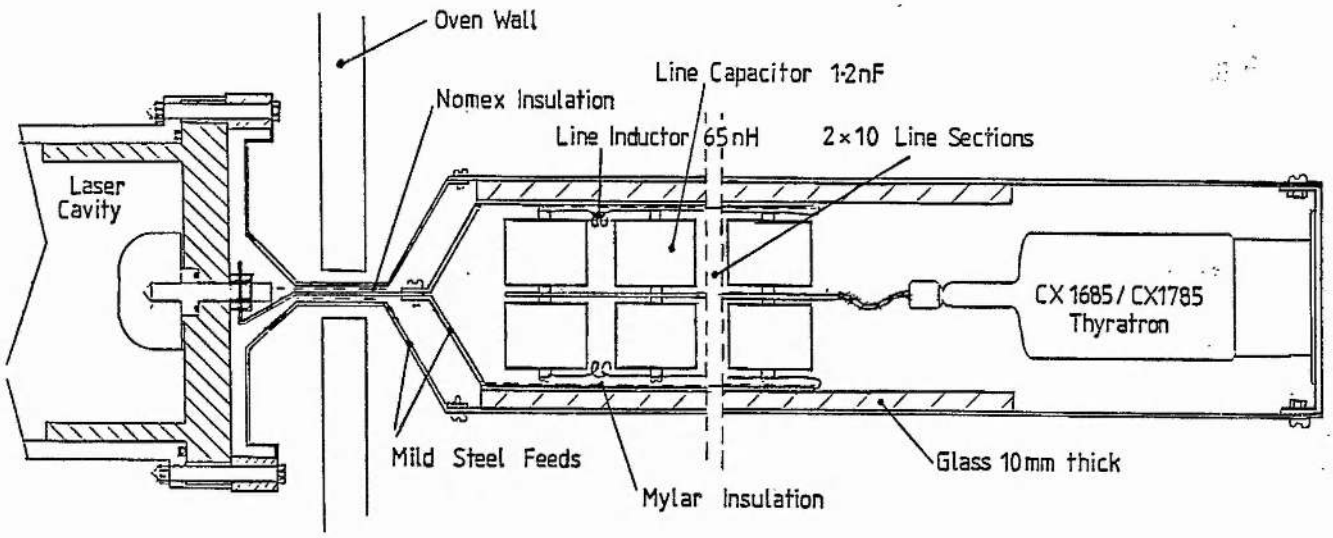

Pulse Forming Line System Construction

Figure 2

These requirements have been applied to the design of a repetitively pulsed power supply constructed to drive an X-ray preionised discharge mercury bromide (HgBr) laser (λ=502-504 nm), which is currently under development. The power supply comprises a modular double pulse forming line built from discrete inductors and ceramic "door-knob" capacitors, which is switched by up to twelve thyratrons operating in parallel. Thyratrons are the obvious choice as switches for this type of pulsed power supply because they have long-life capability, low jitter, high power gain (compared to spark gaps) and do not require external flowing gas supplies.

Construction

A diagram of the construction of the power supply together with a photograph of the supply with the top cover removed is given in figures 2 and 1 respectively. The double pulse forming line system comprises up to twelve, modular, double pulse forming networks. Each network has ten sections and is constructed from $BaTiO_3$ ceramic "door knob" capacitors (40 kV, 1.2 nF) and discrete 65 nH inductors. The output impedance of each module is 3.6Ω and the minimum pulse duration (FWHM) delivered into a matched load is 220 ns. Each pulse forming line module is switched by its own thyratron and the modules are connected in parallel after the thyratrons. Thus with twelve modules the minimum output impedance achievable is 300 mΩ. The total capacitance of the line system is 288 nF which provides a maximum stored energy of 130 J at a line charge voltage of 30 kV. Capacitors with a maximum voltage rating of 40 kV were chosen not only for reasons of reliability, but also to minimise the effect of the reduction in capacitance of $BaTiO_3$ capacitors with applied voltage caused by the ferro-electric nature of the dielectric material. At a line charge voltage of 30 kV, manufacturers data suggests that the capacitors should change their value by no more than 5% due to the dielectric stress incurred at this applied voltage.

Initially, type CX 1685 glass thyratrons were used to switch the pulse forming line modules. These tubes have a peak forward anode voltage of 35 kV and a peak anode current of 5 kA. They also have the advantage of being cheaper than comparable ceramic types. This is an important consideration when large numbers of tubes are to be operated in parallel. At the full 15 kV output potential of the line, when operating into a matched 300 mΩ load, each tube conducts a maximum current of 3.75 kA. This is significantly less than the peak anode current rating which will ensure satisfactory tube lifetimes. Furthermore, the 70 kA μs^{-1}, dI/dt rating of these tubes, as measured by the manufacturers (E.E.V. Ltd.), suggest that the design goal of a total dI/dt = 1000 kA μs^{-1} could almost be reached using twelve tubes in parallel. Current sharing between tubes is automatic because each thyratron switches its own pulse forming network. Whilst it is possible to use paralleled thyratrons to switch a common energy storage system in low inductance discharge circuits[2], the modular approach was chosen because it has an added advantage. Since it is difficult to predict accurately the impedance of a given laser discharge load, it is important that the impedance of the power supply should be capable of being altered with the minimum of inconvenience. In the system described the impedance can be adjusted simply by removing or adding modules, without changing the output pulse characteristics.

A low output impedance (4Ω) trigger generator was constructed to fire the paralleled tubes. The output circuit of this generator comprised a 0.2 μF capacitor, charged to 8 kV, which is discharged through an FX 2530 thyratron into the primary of a 4:1 turns-ratio, step-down autotransformer. This produces a pulse with a maximum amplitude of 2 kV rising in 100 ns which is superimposed on a bias of -150 V. Individual 50Ω coaxial cables are run in parallel from the trigger generator to the grid drive circuits of each of the thyratrons shown in figure 3. The priming grid of each tube is pulsed (current driven). Since the anode delay

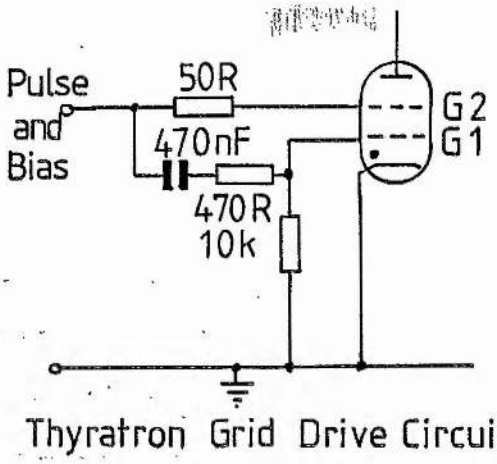

Thyratron Grid Drive Circuit

Figure 3

times of each of the tubes is different and can be as long as 250 ns for CX 1685 thyratrons, the length of the trigger cables to each tube is adjusted to ensure that all the tubes fire in synchronism. It is very important that the reservoir voltage of each tube is set just below the point at which the tube fails to hold-off the maximum applied voltage. This ensures that the rate of current rise through the tube is maximised. Therefore, after the reservoir voltage of each individual tube is set, the anode delay time is measured. Working from the tube with the maximum delay time, extra cable is added in series with the trigger cables to the other tubes so that the effective anode delay times of all the tubes are matched to within 10 ns. In practice it was found that the maximum tube-to-tube variation in anode delay time was 65 ns. A constant voltage transformer was used to supply the heater and reservoir mains transformers to prevent any variation in the mains supply from upsetting the synchronisation of the thyratrons. An alternative way of adjusting the anode delay times is to vary the negative bias on the control grids of each of the tubes. However, this method was rejected for reasons of cost as each tube would require its own control grid bias supply.

In order to meet condition 1, two, glass insulated, secondary transmission lines in a fold-back configuration are used to connect the output from the double pulse forming line system to the laser cavity. This arrangement allows the thyratrons to be operated with their cathodes at ground potential. The impedance of the secondary lines (see figure 1) is three times that of the double pulse forming line system and comprise what is best described as a "spike line". The transit time of a pulse along these lines is 10 ns and analysis of the performance of the complete line system (see figure 4), using a lattice diagram, shows that a short high voltage transient of approximately 20 ns duration is produced at the start of the output pulse. Under ideal conditions the amplitude of this transient is 1½ times the line charge voltage, when the system is discharged into an infinite load, simulating the behaviour of a laser gas mix before break-down.

Performance

The output pulse from an individual line module and thyratron, charged to 30 kV, is shown in figure 5(a). The peak output voltage is 15 kV and the 10-90% voltage risetime is seen to be approximately 50 ns

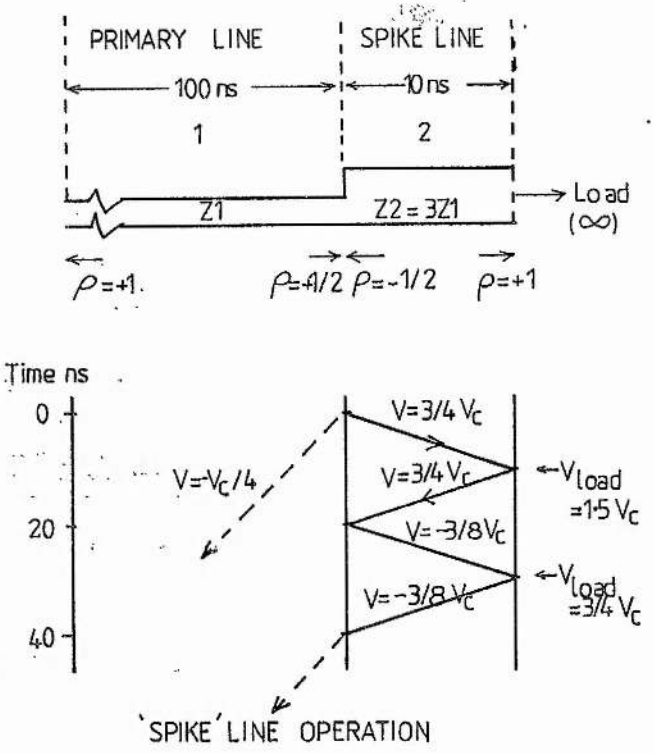

Figure 4

into a matched 3.6Ω load which represents a dI/dt of 83 kA μs^{-1}. Careful "fine-tuning" of the values of the line inductors was carried out to set the line impedance as close as possible to 3.6Ω. The absence of any significant reflection suggests that the line modules after trimming have a characteristic impedance very close to the design target. It is interesting to note that although the peak output voltage is 15 kV, which would be expected under matched conditions, the pulse duration is much longer (240 ns FWHM) than anticipated due to a long tail on the pulse. An explanation for this observation is given in the next section.

The output pulse from the complete line system comprising twelve modules charged to 30 kV and discharged into a matched 300 mΩ load is shown in figure 5(b). It can be seen that there is some degradation in pulse rise-time (tr = 55 ns) and the pulse is broadened to 290 ns FWHM which is probably due to slight performance variations from tube to tube, which cannot be completely removed. However, the pulse shape and amplitude are similar to that given by a single module. The rate of rise of current is calculated to be 9.09×10^{11} A s^{-1}.

To test the "spike-line", the pulsed power supply was discharged into a high impedance load (70Ω) which simulates the behaviour of the laser gas mix during its formative phase. The resulting output pulse is shown in figure 5(c). The amplitude of the spike is less than anticipated which is thought to be due to the thyratron rise-time being significantly longer than the spike duration. This hypothesis has been subsequently tested on a line module with a 45 ns "spike line" and the amplitude of the voltage transient was found to be close to the theoretical value i.e. 1½ times the line charge voltage.

The time jitter in the firing delay of the system

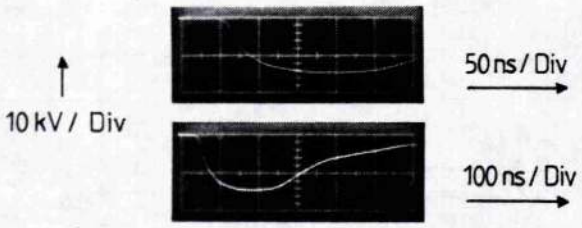

Figure 5(a) Output of a single line module into a matched 3.6Ω load

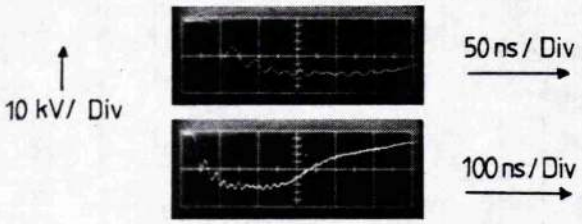

Figure 5(b) Output of DPFL system (12 modules) into a 300 mΩ load

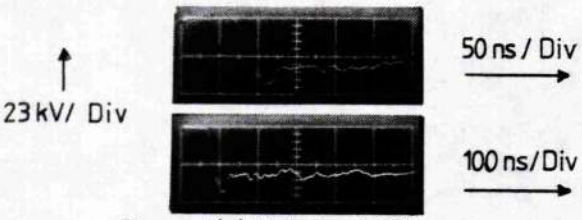

Figure 5(c) Output of DPFL system into a 70Ω load

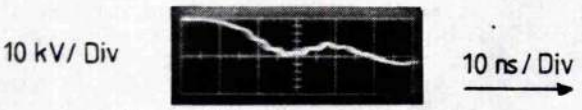

Figure 5(d) 100 overlaid output pulses from DPFL system (rising edge)

was also measured and in figure 5(d) a trace of 100 overlaid shots of the rise of the output voltage pulse is displayed. The observed jitter is 2-3 ns.

Since it is very difficult to predict the impedance characteristics of a given laser discharge plasma, an assessment of the behaviour of the power supply when operated into undermatched loads was investigated. An undermatched load causes a voltage reversal at the anode of the thyratrons, at the end of the pulse. The size of the reversal depends on the degree of undermatching. An important problem was discovered as a result of these tests. It was observed that under low load conditions a number of the thyratrons broke down and an arc was visible in the vicinity of the anode and anode stem. On closer investigation it was found that this was caused by the anticipated anode voltage reversal. Although the CX 1685 thyratrons will withstand a peak inverse anode voltage of 25 kV, this reverse voltage must not be applied too quickly otherwise tube break-down results. Our measurements showed that the tubes were failing at relatively low reverse voltages (~5 kV) because of the rate of rise of the reverse voltage (t_r = 50 ns). To overcome this problem the CX 1685 thyratrons have been replaced by ten CX 1785 hollow anode thyratrons which can conduct current in a reverse direction should the polarity of the voltage

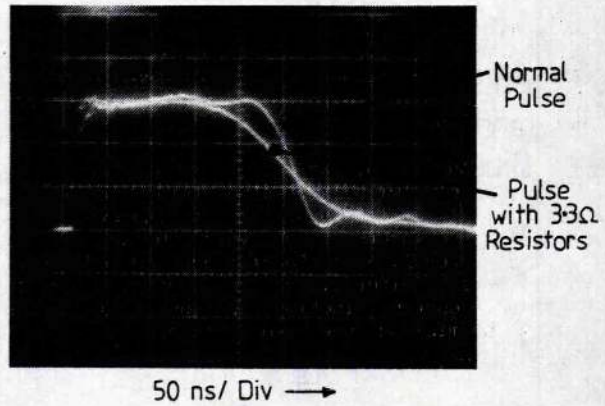

Figure 6 The effect of adding 3.3Ω resistors in series with the line capacitors

at the anode reverse. The performance characteristics of the system using these tubes is otherwise identical to the performance using the CX 1685 thyratrons.

The power supply is limited to a maximum repetition rate of 10 Hz only because of the size of the capacitor charging unit available for charging the line system. There is, however, no apparent reason why such a power supply should not be operated at much greater repetition rates (≲1 kHz) limited only by such factors as capacitor loss, thyratron recovery, and anode dissipation.

Pulse Shape Considerations

An interesting feature of the complete pulsed power supply is the shape of the output pulse. Whilst the rise-time of the pulse is predictable on the basis of the current rise-time characteristics of the thyratrons, the long tail on the pulse (300 ns) was not expected. Indeed when the line modules were tested at low voltages (30 V) to determine their characteristic output impedance, the tail was found to be very much less (50 ns) than that observed at the full operating voltage. To account for this tail a theoretical investigation of the propagation characteristics of lumped component pulse forming networks was carried out. As a result it was discovered that the observed behaviour could be accounted for if the ceramic capacitors have a small, but finite equivalent series resistance (E.S.R.). Parallel loss in the capacitors or series resistance in the line inductors can be shown to attenuate the propagation of a voltage pulse along a discrete component network, but will not affect the rise-time of the pulse. Because of the mechanism by which pulse forming line action occurs rise-time loss along a network does not effect the rise-time of the pulse produced, but will cause a lengthening of the pulse fall-time. This hypothesis was checked using the computer programme ECAP [3] to investigate the theoretical transient behaviour of a ten section pulse forming network in which the capacitors had E.S.R. values of 1-5Ω. As expected the tail of the pulse lengthened as the E.S.R. was increased. This effect was also demonstrated using a low voltage, ten section network, constructed from inductors and capacitors of identical values to that of the full-scale double pulse forming line modules. It was found experimentally that the tail could be lengthened to 180 ns by adding 3.3Ω resistors in series with each of the line capacitors. A photograph showing the line behaviour with and without the 3.3Ω resistors is given in figure 6. These observations imply that the capacitors used in the pulsed power supply have an E.S.R. which is dependant on the voltage

or current at which the line is operated. This effect could be important as it could lead to excessive heating in the capacitors at high repetition rates. Further investigation of this behaviour is currently being carried out.

In conclusion, we have demonstrated a pulsed power supply with the parameters required for reliable, long life operation of high average power gas discharge lasers. The system characteristics can be satisfactorily accounted for and the modular design facilitates alterations in output impedance. Impressive current risetimes approaching 10^{12} Amps/sec into a 300 mΩ load have been achieved.

References

1. Rothe, D E, Levatter, J I, and Sandstrom, R L, "Efficiency Optimisation of a Discharge-Excited XeCl Laser" Helionetics Inc. Technical Report on ONR Contract N00014-82-C-0087, December 1982.
2. McDuff, G, "Parallel Operation of Thyratrons in Low Inductance Discharge Circuits", 3rd I.E.E.E. Pulsed Power Conference Proceedings, 308, Albuquerque 1981.
3. ECAP is described in the IBM Manual "1620 Electronic Circuit Analysis Programme (ECAP) Programme No 1620-EE-02X; Manual number. GH20-0170-2".

Acknowledgements

Financial support for this work is gratefully acknowledged from the Royal Signals and Radar Establishment, Malvern U.K. The authors would also like to thank H Menown and his team at EEV Ltd for encouragement and helpful discussions on the parallel operation of thyratrons.

APPENDIX 5

The Effect of E/N on Discharge Parameters

The role of the discharge E/N (electric field/number density) on the kinetic processes in the $HgBr_2$ laser has been studied for the case of the e-beam controlled discharge by Nighan and Brown [1] and McGeoch et al [2], and more recently for an X-ray preionised self-sustained discharge laser by Kushner et al [3]. Figure 1 shows some of the results calculated by Nighan and Brown which may be used to illustrate a number of points regarding the effect of E/N on discharge parameters. Although these results are pertinent to an e-beam controlled discharge, information applicable to self sustained discharges may be obtained from them. Self sustained discharges operate at an E/N value determined by the gas mixture and pressure, where electron production through ionisation and loss through attachment and/or recombination processes are equal. In the case of the mercury bromide laser the dominant loss process is by dissociative attachment through the reaction

$$e + HgBr_2 \rightarrow HgBr + Br^-.$$

Under these conditions no growth or decline of the electron density takes place and the discharge is stable, at least for a period of time until some instability process ensues. In the mercury bromide laser this instability process is the multistep ionisation of mercury formed during the discharge leading to its collapse. Under e-beam controlled discharge conditions the operating E/N can be set at a value at which the rates of ionisation and attachment are not equal. The electron beam is used to increase the electron density to balance the electron loss and production rates. Under the conditions of figure 1 the operational E/N for a self sustained discharge would be ~4.5 Td, however the optimum production rate of the upper laser level may occur at an E/N other than that set by self sustained discharge operation. The figure indicates that the peak in discharge power into B state formation for the conditions of this mixture occurs at an E/N of ~3.5 Td. Electron beam controlled operation affords control over the discharge E/N enabling the operational conditions to be chosen for maximum upper laser level production. Such flexibility is not

possible under self sustained discharge conditions.

Figure 1 also shows the fractional discharge power which goes into various other processes in the discharge. At low values of E/N, vibrational excitation dominates electron energy loss whilst at E/N values in excess of ~1.5 Td electronic excitation becomes the dominant process as the electron energy distribution extends to higher energies where the thresholds for electronic exctitation occur. The fractional discharge power into HgBr (B) state production under these conditions shows a fairly broad peak around 3-4 Td which falls off rapidly below 2Td and also decreases at higher E/N. Similar results were obtained in a model of a self sustained discharge by Fisher et al [4] as shown in figure 2. They observed a similar peak in B state formation efficiency decreasing at higher and lower E/N as more discharge power is chanelled into other processes such as ionisation, electronic excitiation and vibrational excitation. The results of figure 2 also show that the B state production efficiency is fairly insensitive to the concentration of HgBr increasing only slowly with increased concentration and that the peak in formation efficiency moves to a higher value of E/N with increased concentration.

Nighan and Brown [1] analysed the results of experiments involving several laser gas mixtures focusing on the factors effecting discharge characteristics and upper laser level production in their device. These include attachment and ionisation rates, discharge current density, small signal gain, fluorescence and electron collision processes. They found experimentally that under operating conditions of E/N ~ 4.3×10^{-17} V cm^2 a stable uniform discharge could be maintained. However at increased E/N ~ 6.1×10^{-17} V cm^2 the discharge terminated prematurely due to ionisation instabilities which led to discharge current runaway. At lower E/N values charged particle production is dominated by the electron beam source whereas direct and multistep ionisation by discharge electrons becomes increasingly important at higher E/N values leading to the observed current runaway. In order to model the laser/discharge kinetics Nighan and Brown used a set of self consistent cross sections for electron/$HgBr_2$ attachment, ionisation, vibrational and electronic excitation which resulted in satisfactory agreement between measured and computed results. For a mixture of 0.35% $HgBr_2$ in neon buffer they show that the net attachment (the difference between the attachment rate and ionisation rate) decreases rapidly at E/N values greater than 5×10^{-17} V cm^2 leading to current runaway. For a similar laser mixture they investigate the

electron fractional power transfer (FPT) in the discharge (see figure 1) showing that at an E/N ~ 4 x 10^{-17} V cm^2 the FPT associated with HgBr (B) has its maximum of 7-8% and decreases at lower and higher E/N values. Vibrational excitation of $HgBr_2$ represents about 10% energy loss at this value, increasing rapidly at lower E/N whilst electronic excitation represents 75% of the FPT in the discharge and increases with increasing E/N.

McGeoch et al [2] developed a kinetic model of the Ar/$HgBr_2$ sustained discharge laser based on numerous experimental results. Their initial experiments indicated that argon buffer gas gave the highest laser efficiency and best energy loading, a result which has not been observed with self-sustained discharge lasers as previously discussed in this thesis. In their model, in a similar fashion to Nighan and Brown [1], they used cross-sections for the formation of $HgBr_2$ excited states with threshold energies of 5 eV, 6.4 eV and 7.9 eV. The processes associated with these cross-sections are discussed in Chapter One of this thesis, the 6.4 eV process leading to B state formation. They computed the discharge fractional power into each of the $HgBr_2$ excited states as a function of E/N for conditions typical of their laser. These show that in the E/N range of interest (2-8 x 10^{-17} V cm^2) a large fraction of the power is channelled into the 5 eV process resulting in HgBr X or A state formation. As the A state is dissociative (see figure 1.2 of chapter 1) this may lead to formation of mercury in the discharge which, as has been discussed previously, leads to discharge constriction. This 5 eV process also tends to curtail the electron energy distribution and take much of the discharge power, inhibiting the higher energy processes and hence limiting HgBr (B) formation. The computed discharge fractional power for B state production is less than 10% in the E/N range of interest in agreement with the results of Nighan and Brown [1].

Kushner et al [3] used a multidimensional model of an X-ray preionised, self-sustained discharge laser to study the performance of a mercury bromide laser. Again this model used cross-sections for the three electronic excitation processes in $HgBr_2$ in a similar fashion to the models discussed above, although modified to give satisfactory agreement between the model and experiments. They calculated the electron impact rate constants for excitation and ionisation and, as discussed in Chapter One, found those for ionisation collisions from the excited states of mercury formed in the discharge have the highest rate

constants of any process in the discharge. Thus any processes leading to the formation of mercury or its excited states in the discharge contributes heavily to the ionisation rate and subsequent collapse of the discharge.

It is useful to make a comparison between the results obtained with the laser discussed in this thesis and those of the experiments and models mentioned above. The operational E/N for this laser for optimum laser performance falls in the range 2-2.5 x 10^{-17} V cm^2 whilst Kushner et al report an E/N on the order of 4 x 10^{-17} V cm^2. The lower E/N value for our device is a factor of the lower $HgBr_2$ concentration used in the gas mixture. McGeoch et al showed in their model that the formation efficiency of HgBr (B) peaks at lower values of E/N for lower $HgBr_2$ concentrations. A similar result was obtained in reference[4] the results of which are shown in figure 2 and discussd above. Also at lower $HgBr_2$ concentration the attachment rate will be decreased hence a stable discharge will operate at lower E/N where electron production and the ionisation rate is reduced to balance electron gain against loss. This was observed experimentally in this laser as a decrease in the discharge self sustaining voltage as the mercury bromide concentration was reduced as discussed in chapter 5.

Refering to the results of figure 2 for a mercury bromide concentration of 0.1%, typical of the mixture used in our device, the B state production efficiency has its maximum value at an E/N of ~2.5 Td, close to the optimum operating conditions of our laser. From this analysis it would appear that the laser is running close to the optimum E/N for B state production under the conditions for which maximum laser output was obtained. Figure 3 shows the laser output from our device as a function of E/N for a mercury bromide concentration of 0.1%. The variation in E/N was obtained by utilising different neon buffer gas pressures over the range 2-5 bar. The peak in output is observed to occur at an E/N of ~2.1 Td, close to that predicted for the peak in B state production efficiency in figure 2. From this analysis it would appear that for the mercury bromide concentrations used in our device, which were restricted to low values because of the discharge stability problem encountered as discussed in this thesis, the laser is operating close to its optimum value of E/N for upper laser level production. As discussed above, figure 2 shows the HgBr(B) state production efficiency is fairly insensitive to mercury bromide concentration in the gas

mixture. In the experiments conducted with this laser efficiences approaching 2% were achieved, close to the maximum observed by Fisher et al [4], even at the lower mercury bromide concentrations used. These results and those presented in figure 2 show that the intrinsic efficiency of these lasers is not strongly dependent on $HgBr_2$ concentration.

REFERENCES FOR APPENDIX 5

1. W.L. Nighan and R.T. Brown, J.Appl.Phys 53, 7201 (1982).
2. M.W. McGeoch, J.C. Hsia and D.E. Klimek, J.Appl.Phys 54, 3723 (1983).
3. M.J. Kushner, A.L. Pindroh, C.H. Fisher, T.A. Znotins and J.J. Ewing, J.Appl.Phys. 57, 2406 (1985).
4. Mathematical Sciences Northwest Inc. Final Report: 200 Watt Mercury Bromide Discharge Laser, June 1984.

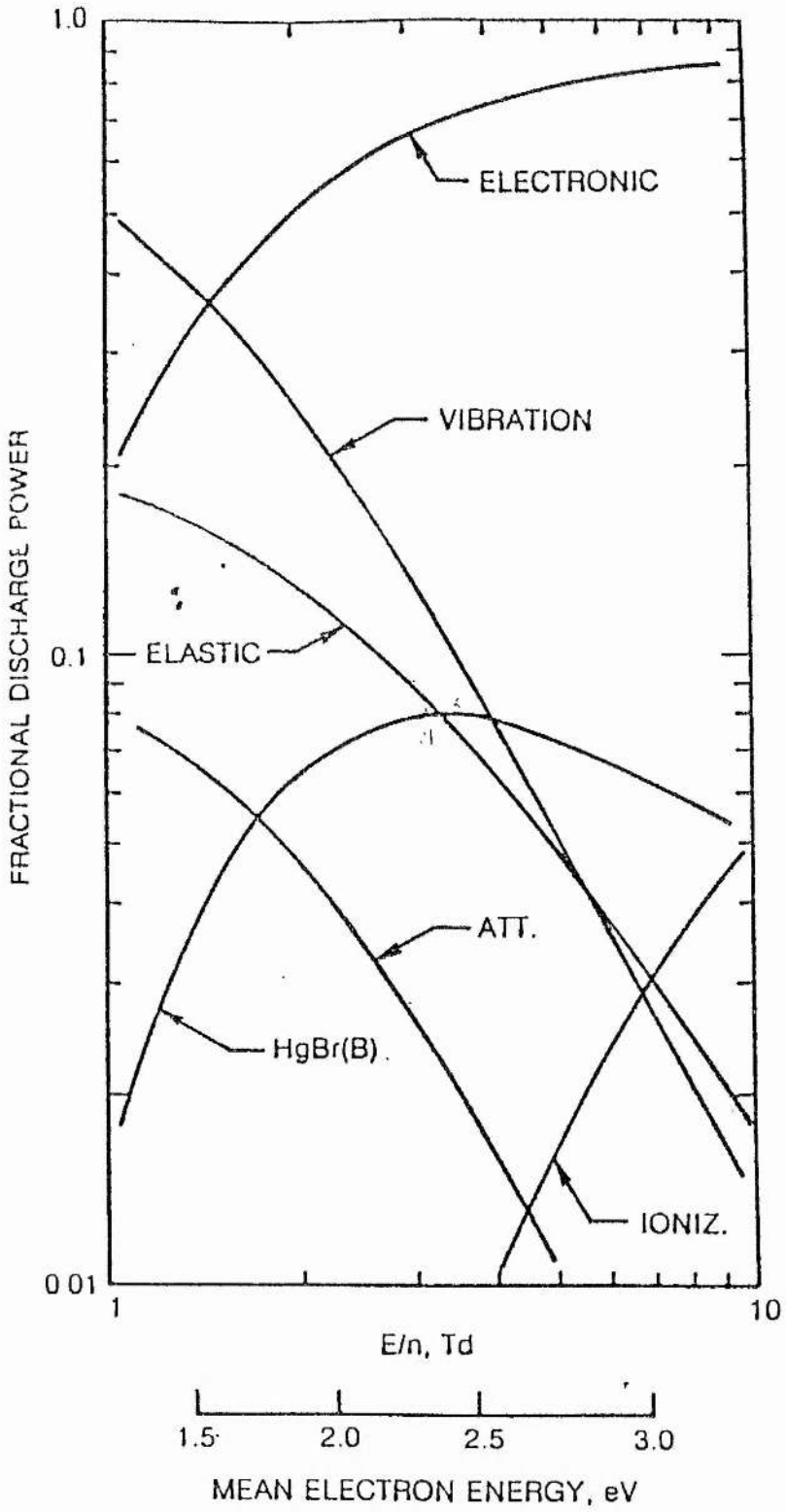

Figure 1: Fractional discharge power as a function of E/N for a mercury bromide concentration of 0.35% in 2 bar neon buffer. Taken from reference [1].

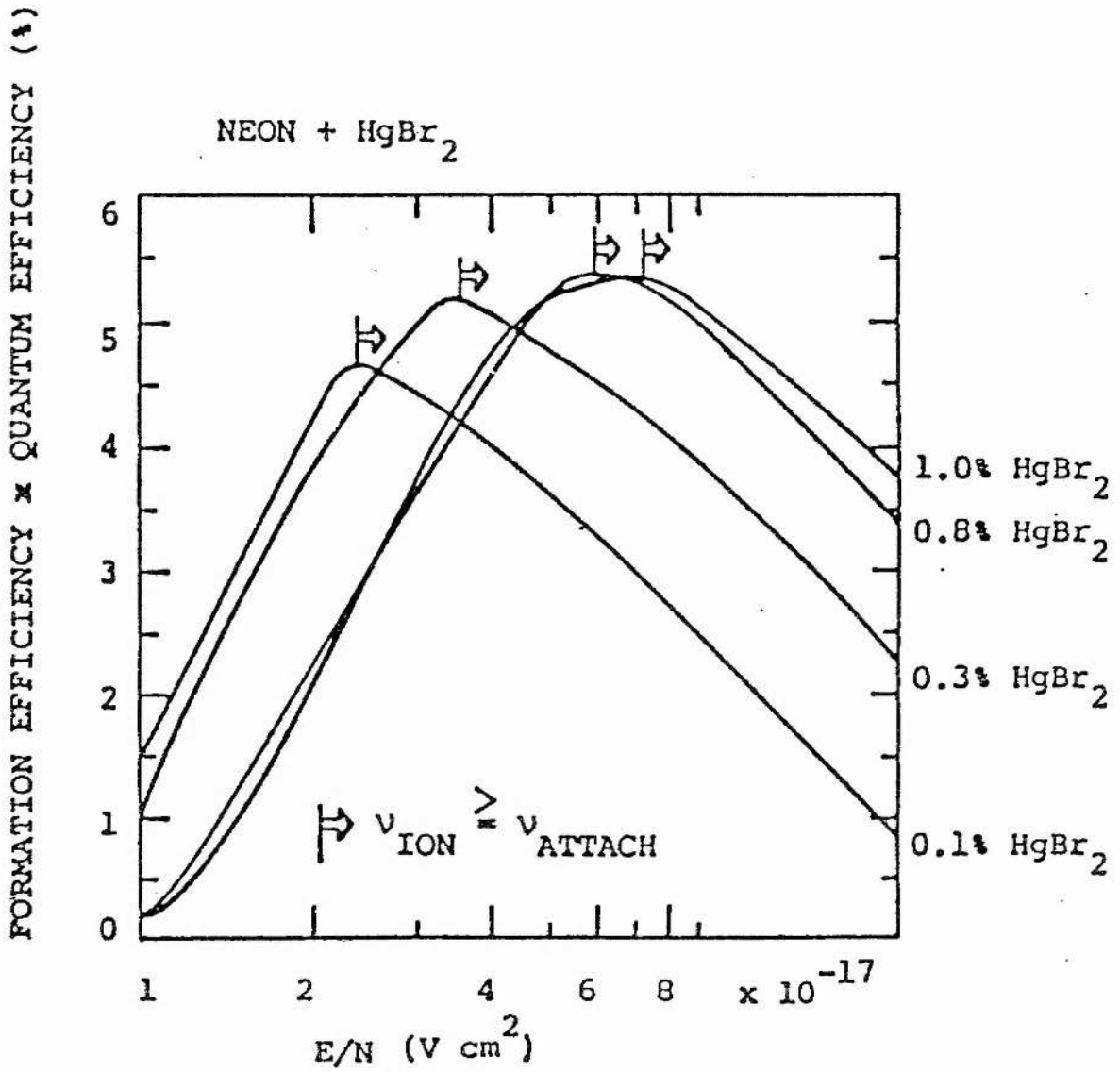

Figure 2: HgBr(B) state production efficiency as a function of E/N for various $HgBr_2$ concentrations.
Taken from reference[4].

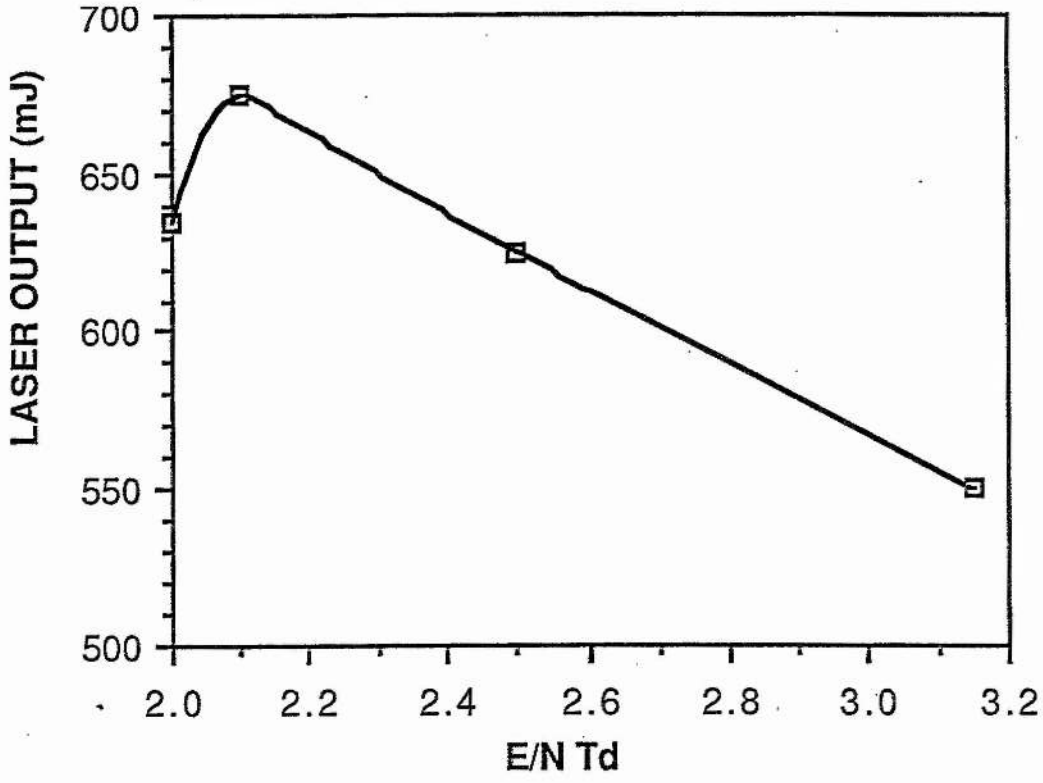

Figure 3: Plot of laser output versus E/N for a mercury bromide concentration of 3.5 mbar and discharge gap of 5cm.